Durham University

Durham E-Theses

A search for TeV gamma ray emission from X-ray binary stars

Christopher Charles Geoffrey Bowden

How to cite:

Bowden, Christopher Charles Geoffrey (1993) A search for TeV gamma ray emission from X-ray binary stars. Doctoral thesis, Durham University.

Use policy

The full-text may be used and/or reproduced, and given to third parties in any format or medium, without prior permission or charge, for personal research or study, educational, or not-for-profit purposes provided that:

- a full bibliographic reference is made to the original source
- a https://etheses.durham.ac.uk/id/eprint/5631/ is made to the metadata record in Durham E-Theses
- the full-text is not changed in any way

The full-text must not be sold in any format or medium without the formal permission of the copyright holders.

Please consult the full Durham E-Theses policy for further details.

Academic Support Office, The Palatine Centre, Durham University, Stockton Road, Durham, DH1 3LE
e-mail: e-theses.admin@durham.ac.uk Tel: +44 0191 334 6107
https://etheses.durham.ac.uk

A Search for TeV Gamma Ray Emission from X-ray Binary Stars

by Christopher C.G. Bowden

Ph.D. Thesis, University of Durham, 1993

ABSTRACT

This work is concerned with the detection of pulsed TeV gamma ray emission from a number of X-ray binary systems by the use of the atmospheric Cerenkov technique. Chapters 1 and 2 give an overview of the development of gamma ray astronomy, with emphasis placed on progress made in the detection of TeV gamma rays by their Cerenkov radiation in the atmosphere. Chapters 3 and 4 describe the University of Durham atmospheric Cerenkov telescopes, which were used to make the observations reported in this work, and the standard data processing and analysis procedures adopted.

The main part of the thesis deals with the application of these techniques to observations of five X-ray binaries. After a review of the properties of such objects in Chapter 5, Chapters 6 and 7 deal specifically with the results for two of the systems considered to be among the most likely candidates to give a detectable TeV photon flux; Centaurus X-3 and Vela X-1. A study of all data recorded on Cen X-3 over the course of six years suggests the presence of a weak gamma ray flux pulsed at the X-ray period. Previous reports of stronger emission near the ascending node of the orbit are confirmed here. For Vela X-1, the analysis of a dataset recorded during a single dark moon interval reveals evidence for two short outbursts of pulsed TeV gamma ray emission. Chapter 8 reports the series of observations made of SMC X-1, 4U1626-67 and XO021-72, and upper limits are placed on the TeV gamma ray emission from each.

Finally, the results reported here are compared with the predictions of a number of theoretical models, some of which are found to give good agreement with the limits and detections derived in this work. A discussion of the status of this field and future observational prospects is also given.

A Search for TeV Gamma Ray Emission from X-ray Binary Stars

by

Christopher Charles Geoffrey Bowden, B.Sc.

The copyright of this thesis rests with the author.
No quotation from it should be published without
his prior written consent and information derived
from it should be acknowledged.

A thesis submitted to the University of Durham in accordance with the regulations for admittance to the degree of Doctor of Philosophy

**Department of Physics,
University of Durham**

September 1993

UNIV DURHAM
14 JAN 1994

TABLE OF CONTENTS

PREFACE

The observations described and analysed in this thesis were carried out using the University of Durham Mark 3 and Mark 4 atmospheric Cerenkov telescopes at Narrabri, New South Wales. The author participated in the collection of data using these instruments for a total of five dark moon intervals. He also assisted with the construction and testing of the recently deployed Mark 5 telescope, and investigated the potential use of a Cerenkov pulse timing facility in this telescope. He was part of the team responsible for the routine pre-processing of the data collected from each of the telescopes on its return to Durham.

The author has made detailed studies to search for evidence of pulsed TeV gamma ray emission in the data recorded on a number of X-ray binary systems and pulsars, and was wholly responsible for the analyses of the five X-ray binaries presented in this thesis. He carried out a full reanalysis and updating of the large set of observations recorded on Centaurus X-3. This included the first application of the technique previously developed to search for a site of gamma ray emission displaced from the X-ray source in a binary system. He also made a detailed study of the data recorded on Vela X-1 in 1991 February which led to the discovery of two bursts of pulsed gamma ray emission from this object. The Durham databases on SMC X-1, 4U1626-67 and X0021-72 were all updated and reanalysed by the author in order to enlarge and improve upon previous results. Where necessary, the author has tested and modified the software used in these analyses, and was responsible for the comparison of the results with the theoretical predictions given in Chapter 9.

None of the work presented in this thesis has previously been submitted as part of the fulfilment of a degree course in this or any other university.

ACKNOWLEDGMENTS

I would first like to thank Professor A.D. Martin for the provision of the facilities of the Department of Physics at the University of Durham during the course of my studies, and the Science and Engineering Research Council for the award of my research studentship. I also sincerely thank my supervisor, Professor Ted Turver, for his advice, guidance and encouragement during the course of this work.

Respect and thanks are due to all members of the Durham group for their help and friendship over the last three years - Stella Bradbury, Karen Brazier, Alberto Carraminana, Paula Chadwick, Ed Dickinson, Nigel Dipper, Pete Edwards, Susan Hilton, Eric Lincoln, Vince Mannings, Lowry McComb, Keith Orford, Steve Rayner, Ian Roberts, and Ken Tindale. Special thanks to Ross Bingham and Trish Thomas for their great hospitality during my time in Australia, which was much appreciated, and to Joy Turver for her fine cooking.

Thanks to Steve Fullerton, Rodger Manning and Graeme Oldham for three years of deep and meaningful discussions on the important things in life. Thanks also to Mike Comerford, Duncan Lowe, Dave Reid and Stuart Thomas.

I am very grateful to my parents and Kath, Phil and Paul for their support. Finally, thanks to Allan Langer, Hugh Morris, Paul Ramsey, Jason Perry, Damon Searle, Carl Dale, Eddie Newton, Nathan Blake and Cohen Griffith. Adar Glas am byth.

CHAPTER 1 - INTRODUCTION

1.1. The Origins of Astrophysical Gamma Rays

1.1.1. Gamma Radiation as an Astrophysical Tool

In all astrophysical disciplines, the basic aim is to investigate how the laws of physics apply to situations involving extremes in temperature, pressure and density only found in celestial objects. High energy astrophysics in particular allows the study of processes which are completely beyond the reach of laboratory measurements. Despite the low flux of gamma ray photons as compared with those of lower energy, the high energy content of each photon means that a large proportion of the total energy emitted by a source may be contained in this range of its spectrum. Thus a vast amount of information directly related to the basic mechanisms powering an astrophysical object may be gathered from observation of its gamma ray emission.

Situations of particular interest and relevance to the field of gamma ray astronomy include the study of massive black holes in active galactic nuclei, observations of high energy emission influenced by the intense gravitational and magnetic fields of compact objects, and the origin of the ubiquitous cosmic rays. The latter problem has existed since the discovery of the cosmic radiation during the balloon flights of Hess (1912), and may be solved by observations of the sources of the highest energy gamma rays which are produced by interactions of relativistic charged particles. These gamma rays provide unique information on the processes which are involved in cosmic ray production since only they are undeflected in the magnetic fields of interstellar space, and hence preserve directional information on their emission site. This thesis is concerned with an attempt to discover such sources via their gamma ray production in the TeV energy range.

1.1.2. Gamma Ray Production Processes

1.1.2.1. Nuclear Collisions

The emission of gamma rays from nuclear collisions arises from the decay

of the unstable neutral pi mesons, which along with their charged counterparts are produced in such interactions. Many other strange particles result from these energetic collisions but the pions are by far the most abundant. The decay of the neutral pion results in the production of two gamma rays, each with energy W_o=68 MeV, i.e. half the pion's rest energy. Since in the observer's rest frame the initial pion may have any velocity, the resultant gamma rays may have energies between

$$W_o\left[\frac{(1-\beta)}{(1+\beta)}\right]^{1/2} \quad \text{and} \quad W_o\left[\frac{(1+\beta)}{(1-\beta)}\right]^{1/2}$$

where the initial pion velocity was βc (e.g. Garmire and Kraushaar, 1965). The pions will be produced with a large range of velocities,and hence the gamma ray energy spectrum from such a process will show a peak at W_o.

In the context of astrophysics, this process may occur anywhere where protons accelerated to high energies are incident on a target material, and hence the gamma rays produced may act as a good tracer of the cosmic ray or matter density. Pion production may also result from the annihilation of a nucleon with an antinucleon, a process which results in a more sharply peaked gamma ray energy spectrum as the pion produced is usually at rest in the centre of mass frame. A considerably less important process is the production of neutral pions in proton - photon collisions, due to the low flux of particles with sufficient energy to enable such a process to occur.

1.1.2.2. Bremsstrahlung

The passage of an electron near a charged particle results in the emission of electromagnetic radiation of energy up to that of the electron's initial value. For relativistic electrons traversing an ionised region of space, this can result in the production of high energy gamma rays if the deflection caused by the interaction is of sufficient magnitude. The intensity spectrum of relativistic bremsstrahlung photons is independent of energy up to the value where all of the electron's kinetic energy is given up in the

interaction, i.e. $E=(\gamma-1).m_e c^2$ where γ is the relativistic factor. The overall energy spectrum will show the same power law dependence as that of the electron energy spectrum.

1.1.2.3. Synchrotron Radiation

Synchrotron radiation, or magnetobremsstrahlung, occurs when a relativistic electron is deflected in the presence of a strong magnetic field. The electron loses energy by spiralling around a field line and the resultant emission is strongly beamed in the direction of the forward component of its motion. In the case of a non-uniform magnetic field, the emission is also known as curvature radiation.

The magnetic field required to produce gamma rays by this process is at least 10^{12} Gauss, which is commonly achieved in pulsar magnetospheres. However, in such intense fields, the resultant photon flux is likely to be very strongly absorbed by electron-positron production (see Chapter 5). Thus synchrotron emission has more importance to gamma ray astronomy as an indicator of the presence of relativistic electrons in weaker fields. The detection of this emission at lower energies indicates that other gamma ray production processes involving these high energy electrons are viable.

1.1.2.4. The Inverse Compton Effect

Relativistic electrons which may produce only low energy electromagnetic radiation in weak magnetic fields via the synchrotron process described above have an alternative means of producing high energy gamma rays. This effect arises from their imparting energy in a Compton scattering interaction to a photon with an energy of as low as a few eV, such as a starlight photon. An incident photon with energy of this order may be scattered in this inverse Compton process by an electron of energy 10 GeV to produce a photon with energy 1 GeV (Felten and Morrison, 1963). The resultant differential energy spectrum from this process has a power law form, resembling that arising from bremsstrahlung.

1.1.2.5. Gamma Ray Line Emission

Gamma ray line astronomy is possible in the MeV range through the radioactive decay of isotopes such as ^{56}Ni, ^{57}Co and ^{60}Fe, which are important in the study of nucleosynthesis in supernovae. The 0·511 MeV line arising from electron-positron annihilation has yielded valuable evidence on the production of positrons in active galactic nuclei, and the presence of relativistic electrons in these objects.

Schematic illustrations of some of these production processes are given in Figure 1.1.

1.1.3. Gamma Ray Absorption Processes

1.1.3.1. Pair Production in Charged Particle Collisions

Just as gamma rays may be produced as a result of electron-positron annihilation, so they may also be absorbed as a result of pair production in a collision with a heavy nucleus. This process has a threshold gamma ray energy of $2m_ec^2$, rising to $4m_ec^2$ in the case of a collision with an electron. Fortunately, the mean free path for a gamma ray between such collisions is of the order of Mpc for typical intergalactic densities, and ≥10 galactic radii for typical intragalactic densities. Hence absorption by this means is only significant in localised regions of much higher density.

1.1.3.2. Compton Scattering

Gamma rays may lose energy in collision with interstellar electrons. However, this interaction is characterised by the Thomson cross-section, and the probability of interaction decreases with increasing electron energy. Even for typical galactic and intergalactic electron densities of non-relativistic electrons, the mean free path of this process is of such magnitude as to render it unimportant.

1.1.3.3. Pair Production in Photon-Photon Collisions

Two photons of energies E_1 and E_2 are capable of pair production in a head-on collision if the total energy E_1E_2 in the centre of mass frame exceeds $2m_ec^2$. For a photon of energy 100 GeV, this process can occur in a collision

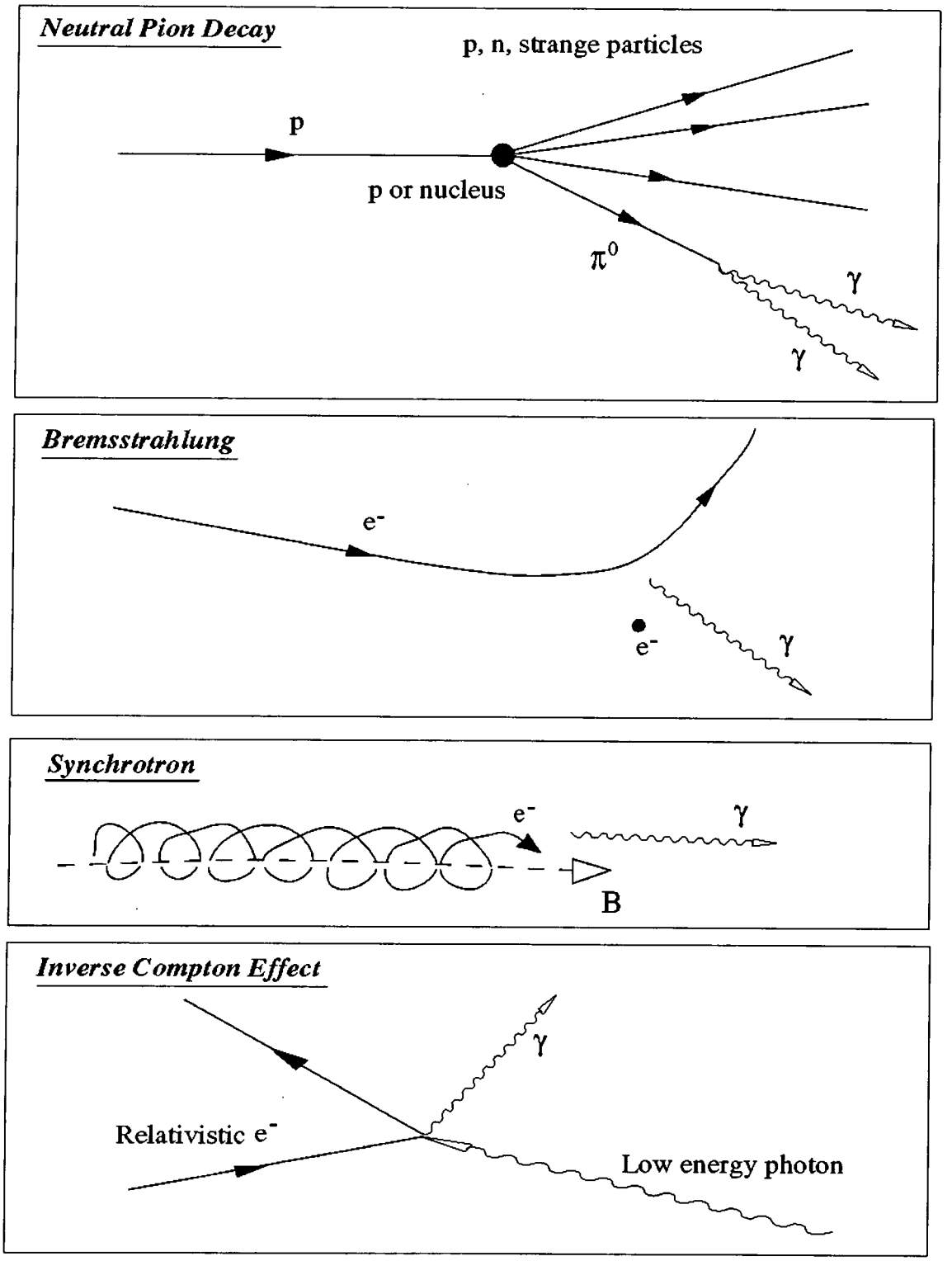

Figure 1.1 : Illustration of processes relevant to the production of high energy gamma rays in astrophysical sources.

with a starlight photon. It is also predicted that gamma rays with energies of ≥10 TeV may pair produce on collision with the ubiquitous photons of the cosmic microwave background. This is an important consideration in TeV gamma ray observations of distant active galactic nuclei (e.g. Punch et al., 1992) when an absorption dip may be detectable given sufficient telescope/detector sensitivity .

The typical mean free paths for a gamma ray in the absorption processes described above are shown graphically in Figure 1.2 (from Ramana Murthy and Wolfendale, 1986). This clearly shows the penetrating nature of astrophysical gamma rays, and underlines their usefulness in gaining information on sources obscured by the absorption processes which are most significant at lower energies.

1.2. Interaction of Cosmic Gamma Rays with the Atmosphere

1.2.1. The Cerenkov Effect

The radiation emitted by a charged particle traversing a medium with a velocity greater than the phase velocity of light in that medium can be thought of as an electromagnetic counterpart of acoustic and mechanical shock waves. This first detailed experiments conducted into this effect were those by Cerenkov (1937). The classical electromagnetical theory interpretation of this was provided by Frank and Tamm (1937). Subsequent quantum treatments of the process showed that only trivial modifications were required (e.g. Cox, 1944). An excellent qualitative explanation of the effect was presented by Jelley (1967) and is summarised here.

The simplest explanation of Cerenkov radiation relates to the concept of retarded electric potential. Consider an electron at a point e_1 travelling through a dielectric medium. At a point S, away from the electron path, the local polarisation vector P will be directed towards a point e_1', and a brief time later when the electron has travelled to a point e_2, the polarisation vector at S will point to a position e_2' (see Figure 1.3a). By resolving the

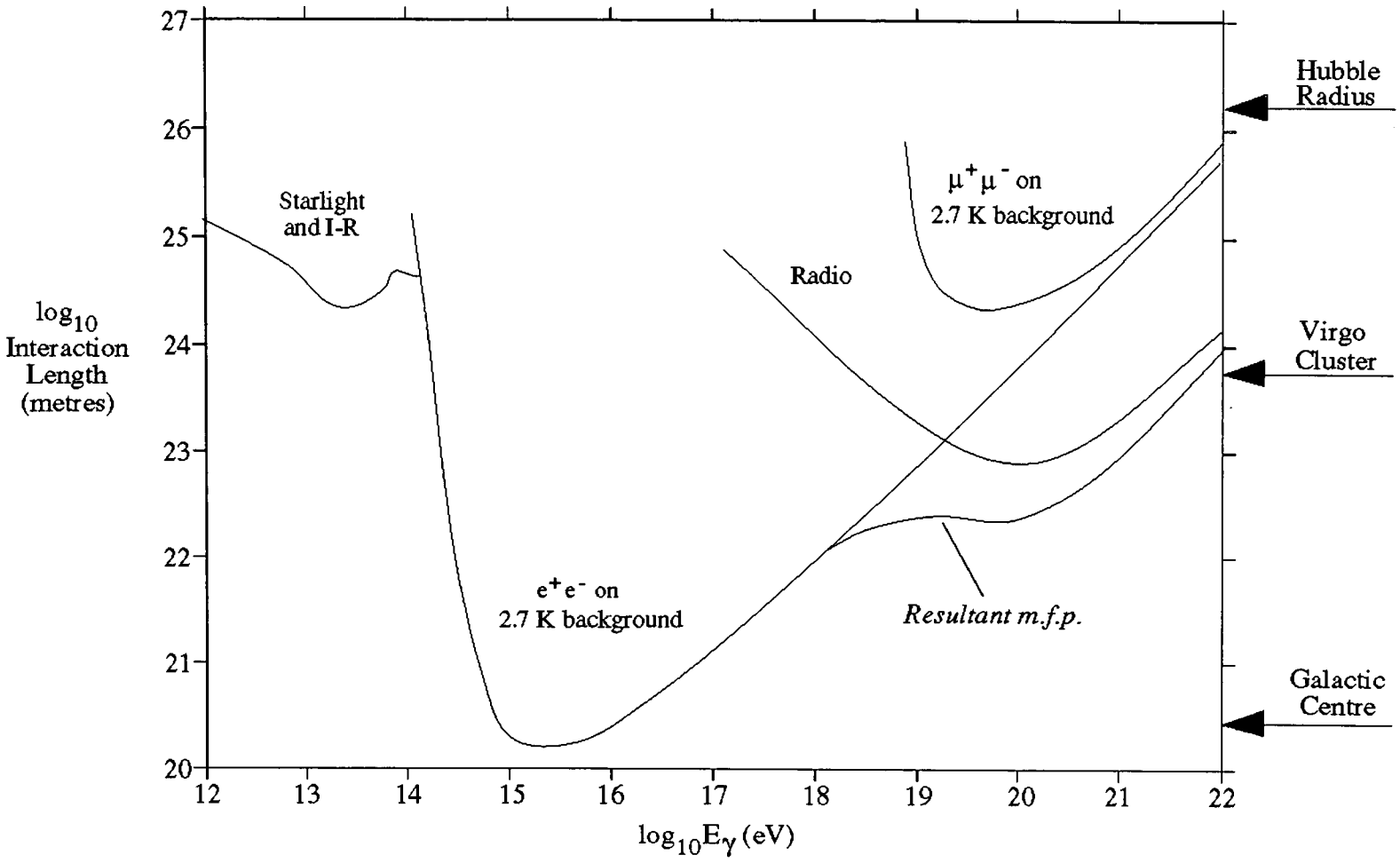

Figure 1.2 : Mean free path for a gamma ray against absorption on background photon fields as a function of energy. The right hand scale enables visualisation of the distances involved.

(after Ramana Murthy and Wolfendale, 1986)

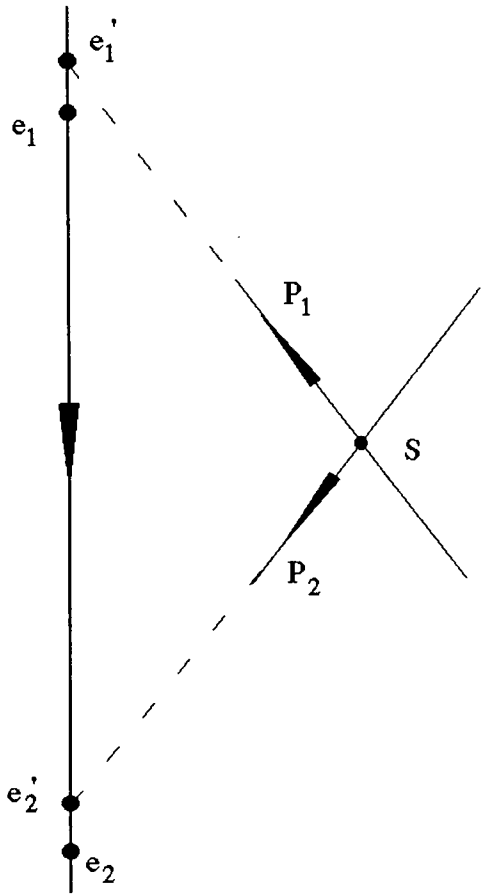

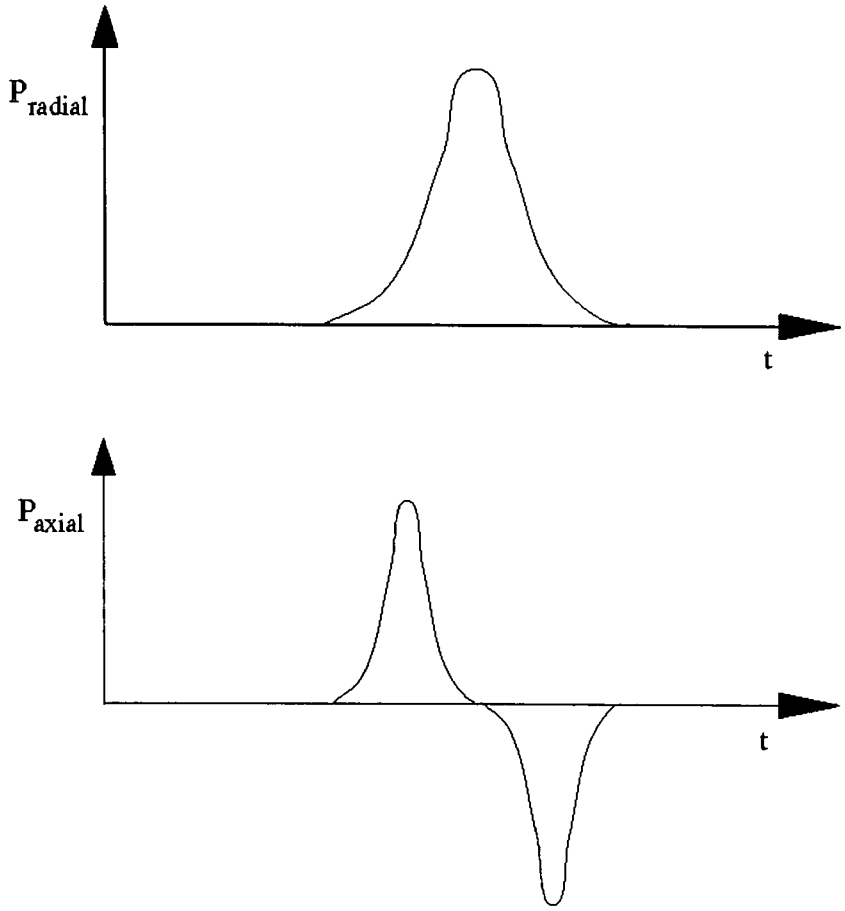

Figure 1.3a : Polarisation caused by the passage of a superluminal particle.

Figure 1.3b : Axial and radial components of the polarisation vector.

(both figures after Jelley,1967)

polarisation vectors axially and radially with respect to the electron track, it can be seen that whilst the radial components cancel at distances much greater than that of S, the axial components will not, and their variation with time at a given point is the first derivative of a delta function (see Figure 1.3b). The axial dipole so created will give an angular distribution of radiation related to $\sin^2\theta$, where θ is the angle between the axis of the track and the axis on which radiation is detected.

By considering a Huygens' construction of the 'wavelets' created by all elements of the track, it is seen that since the particle travels faster than the phase velocity of light on the medium, constructive interference will only occur at a certain angle to its path (see Figure 1.4). This corresponds to the plane wavefront BC, where the particle has travelled from A to B in the time taken for light to travel from A to C. If the particle has a velocity βc and the refractive index of the medium is n, then it is simple to show that the Cerenkov angle θ_c is defined by

$$\theta_c = \cos^{-1}(1/\beta n). \qquad (1.1)$$

Thus for a given refractive index n, there is a threshold β below which Cerenkov radiation will not occur, and radiation will in any case only occur at frequencies for which $n>1$. By axial symmetry, the radiation will be spread over the surface of a cone of half-angle θ.

Cerenkov's initial experiments were carried out using solids as the light-producing media, but the detection of similar radiation in liquids and gases is also possible, the only difference being the increased threshold energy and the smaller Cerenkov angle due the lower refractive index. Instruments using solids, liquids or gases to detect the passage of a single particle all have uses in particle physics. More important to the present work is the use of the atmosphere itself as a detector of Cerenkov radiation from the passage of high energy cosmic rays. Experiments designed to detect such radiation are briefly discussed in Chapter 2.

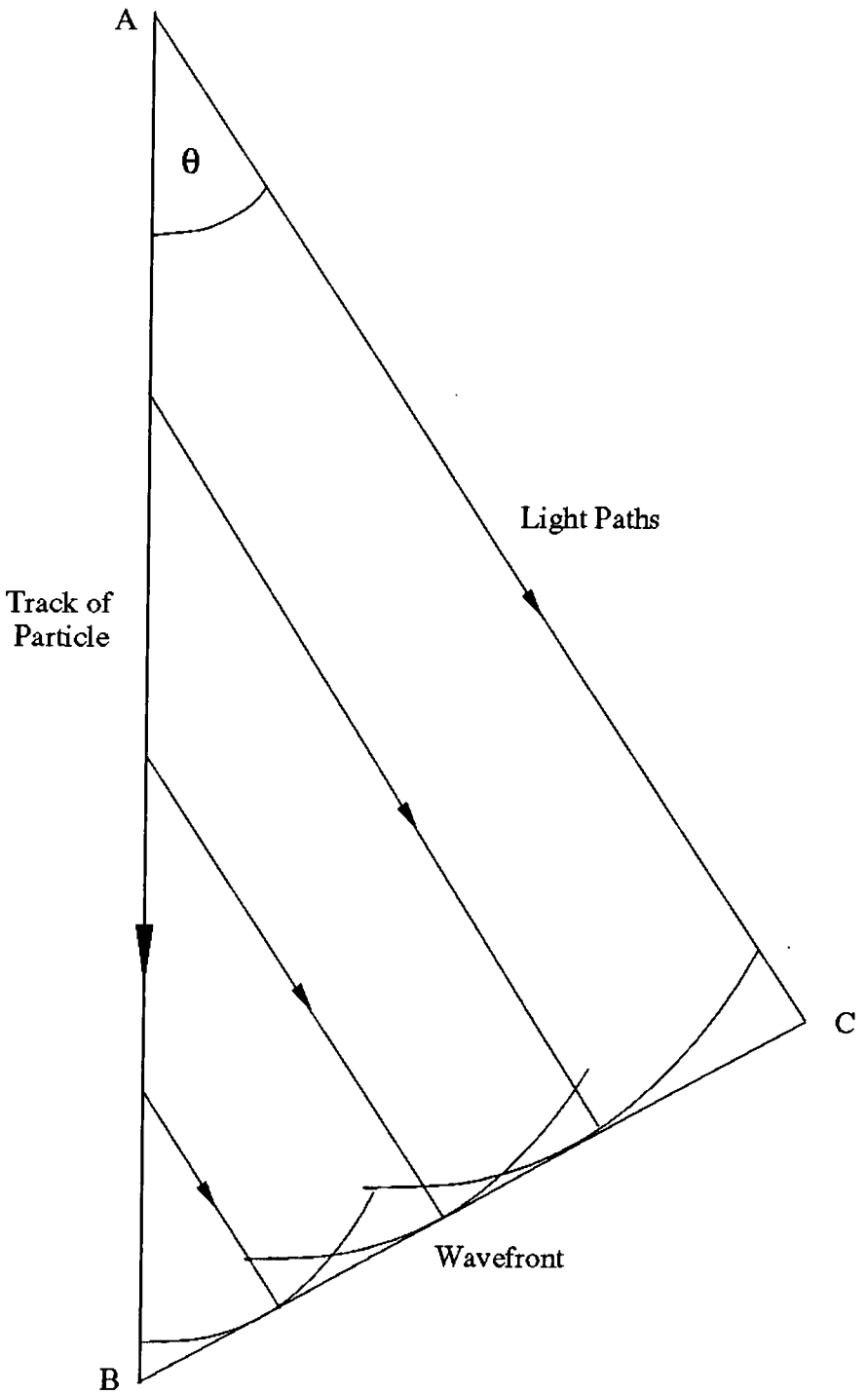

Figure 1.4 : Demonstration of coherence of Cerenkov radiation by the use of Huygens' construction.

1.2.2. Cosmic Ray Induced Air Showers

To understand the phenomenon of Cerenkov radiation from cosmic rays, the interactions of a high energy particle in the upper atmosphere must be discussed. Cosmic ray protons and photons will produce somewhat different showers, but the Cerenkov emission from each share many important features (e.g. Longair, 1992).

A gamma ray incident on the top of the atmosphere will rapidly undergo an encounter with an atomic nucleus resulting in the production of an electron-positron pair. Each of this pair may emit high energy photons by bremsstrahlung, which may themselves produce another electron-positron pair, and so the electromagnetic cascade of electrons and photons develops.

For ultra-relativistic particles, the interaction lengths for pair production and bremsstrahlung are very similar. For an initial gamma ray energy E_0, the first pair produced will each have energy $E_0/2$, whilst one interaction length later each of the resultant electrons and photons will have energy $E_0/4$, and so on. Therefore, at an atmospheric depth of n interaction lengths, the total number of photons and electrons is 2^n with an average energy $E_0/2^n$. The cascade development ceases when the electron energies drop below a critical value E_c where ionisation losses dominate. The maximum development of the shower thus occurs when the average energy per particle has this critical value. The total number of photons and electrons is then $\approx E_0/E_c$, and no mesons or other nuclear debris are produced.

A shower produced by a primary nucleon is initiated by a nuclear collision, producing a cascade of secondary nucleons and mesons, particularly charged pions. Successive nuclear collisions may continue the development of the cascade until the average energy per particle drops below that required for multiple pion production ($\approx$1 GeV). The neutral pions have a very short lifetime against gamma ray decay in the atmosphere and thus initiate secondary electromagnetic cascades. The majority of the charged pion flux decays to produce charged muons with accompanying neutrinos. The lower energy component

of the charged muons can decay to produce electromagnetic cascades at a greater atmospheric depth, whilst much of the higher energy content survives to at least ground level. Thus the number of electrons produced in the hadronic shower increases exponentially before a rapid decline, and the low energy muon flux varies in a similar way. In contrast, the high energy muon content decreases much more slowly.

The overall picture is therefore one of a shower consisting of a large number of secondary showers, the central nucleon and meson core being surrounded by a more scattered electron/photon component, continually replenished by meson decay. Nevertheless, due to the high energies involved, all of the shower components will travel in a well defined group around the central axis.

1.2.3. Cerenkov Radiation from Cosmic Ray Air Showers

It has already been shown that the characteristics of the Cerenkov radiation produced by the passage of a charged particle in a medium will depend very largely on the physical properties of that medium and in particular the refractive index. For Cerenkov radiation in the atmosphere, the effects of the exponential increase in density with atmospheric depth must also be allowed for.

Air at S.T.P. has a refractive index of 1·00029, and thus for ultra-relativistic particles, for which $\beta \approx 1$, the maximum Cerenkov angle θ_{max} is very small, about 1·3°. Expressing the refractive index n as $(1+\eta)$, then since $\eta << 1$ it is related to the maximum Cerenkov angle as

$$\theta_{max} \approx (2\eta)^{1/2} \text{ radians} . \qquad (1.2)$$

The refractive index of the atmosphere is proportional to the local density and hence pressure. Since the pressure varies exponentially with height h, measured from sea level, the refractive index will vary as

$$\eta = 0.00029 \exp(-h/h_o) , \qquad (1.3)$$

where h_o is the atmospheric scale height (≈7·1 km). The refractive index will

also vary with wavelength. The Cerenkov angle varies with density ρ as

$$\theta(\rho) = \theta(\rho_0) \, (\rho/\rho_0)^{1/2} \, , \qquad (1.4)$$

whilst the threshold kinetic energy E_{min} for Cerenkov radiation varies with density as

$$E_{min}(\rho) = E_{min}(\rho_0) \, (\rho_0/\rho)^{1/2} \, . \qquad (1.5)$$

The variation of E_{min} can also be expressed by relating it to the local value of η from equation 1.2, i.e.

$$E_{min}(\eta) = m_0 c^2 \, ((2\eta)^{-1/2} - 1) \, , \qquad (1.6)$$

where m_0 is the particle's rest energy. At sea level, the threshold energy for Cerenkov emission by an electron is 21 MeV, by a muon 4·4 GeV and by a proton 39 GeV. All of these values are well above the particles' rest energies and hence Cerenkov emission will only be expected from an ultra-relativistic particle ($\beta \approx 1$). However, given the required energies and the number spectra of each, the majority of the Cerenkov emission will arise from the electrons in the shower (Boley, 1964).

The expression of Frank and Tamm (1937) for the rate of energy loss by Cerenkov radiation may be expressed in terms of photon production N per unit length x given by

$$\frac{dN}{dx} = 2\pi\alpha \left[\frac{1}{\lambda_1} - \frac{1}{\lambda_2} \right] \sin^2\theta_{max} \, , \qquad (1.7)$$

where $\alpha = 1/137$, and λ_1 and λ_2 (in cm) are the limits of the wavelength band being considered. Approximating $\sin \theta_{max}$ as θ_{max}, and taking the wavelength range 350–500 nm, then the photon yield is

$$\frac{dN}{dx} \approx 390 \, \theta^2 \approx 780 \, \eta \text{ photons cm}^{-1} \, , \qquad (1.8)$$

for an ultra-relativistic particle. By substituting for η from equation 1.3, the photon yield can be related to height h above sea level as

$$\frac{dN}{dx} \approx 23 \exp(-h/h_0) \text{ photons m}^{-1} \, . \qquad (1.9)$$

Another useful quantity is the path length L traversed by the particle

in the atmosphere, expressed as a column density. This is calculated by integrating the exponential decrease in density with height above sea level from infinity to a height h. Thus the dependence of the Cerenkov angle with L is the same as that with density, i.e. $\theta_{max} \propto \rho^{1/2} \propto L^{1/2}$. The total path length of the atmosphere is about 10^4 kg m^{-2}.

Figure 1.5 shows the variation of electron threshold energy for Cerenkov emission, photon yield and Cerenkov angle with atmospheric height and path length. It can be seen that the threshold energy decreases as the particles penetrate further and with it the photon yield and hence intensity of the radiation. The overall intensity will therefore depend on the state of development of the electron-photon cascade. For a gamma ray of energy 300 GeV, the maximum development is reached at a depth corresponding to about 8 radiation lengths (Longair, 1992) where ionisation losses begin to dominate bremsstrahlung losses, as governed by the critical energy of air, 83 MeV. Since the radiation length in air is 365 kg m^{-2}, this situation occurs at an atmospheric depth of about 3000 kg m^{-2}, i.e. a vertical height of 10 km.

The Cerenkov light will penetrate to ground level, while the electrons of the cascade are totally absorbed, and for a 300 GeV photon primary, several million visible photons will be produced in a wavefront with a temporal thickness of approximately 10 ns. The precise form of the Cerenkov emission as viewed from ground level will however be affected by several factors inherent to the use of the atmosphere as a source of emission. Only small effects are induced by factors such as absorption, refraction, and dispersion (Jelley, 1967), leaving the single most important contribution to scattering of the Cerenkov light to be that arising from the Coulomb interactions of the charged particles in the shower with those in the atmosphere. This effect is also modified and enhanced by the influence of the geomagnetic field (Browning and Turver, 1977).

Rossi and Greisen (1941) showed that the mean Coulomb scattering angle θ_s

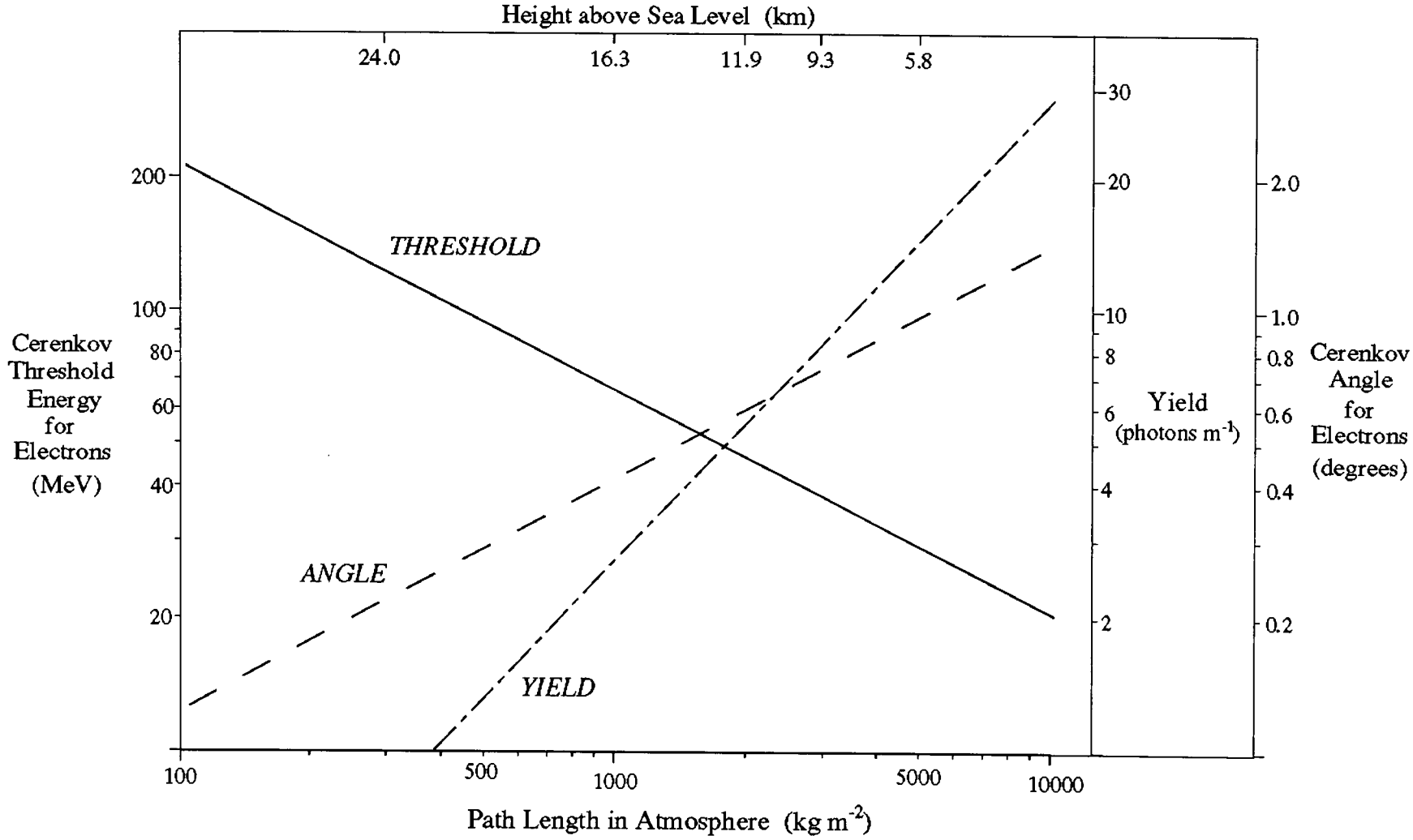

Figure 1.5 : Properties of Cerenkov radiation produced by electrons and positrons in the atmosphere. (after Ramana Murthy and Wolfendale, 1986)

for electrons with momentum p can be expressed as

$$\langle\theta_s^2\rangle = (E_s^2 / p^2\beta^2)t \ , \qquad (1.10)$$

where E_s is a constant 21 MeV, p is the electron momentum and t the path length measured in units of radiation length. For typical relativistic shower electrons, this expression can be reduced over a single radiation length to

$$\langle\theta_s\rangle_{rms} \approx E_s/E \ \text{ radians} \ . \qquad (1.11)$$

For an electron with energy 100 MeV, the scattering angle is $\approx 12^o$. Fortunately, at higher energies, the Coulomb effects are not so important, e.g. for electron energies of a few GeV at the height of maximum cascade development, the Cerenkov angle is almost identical to the typical Coulomb scattering angle. The net effect is to produce a set of contributions from many scattered electrons at various small angles to the shower axis, all directing some proportion of their Cerenkov emission into the solid angle viewed by a detector on the ground.

The overall result is the spreading of the light over the shower wavefront, producing a diffuse and almost uniform lateral photon distribution out to a radius of ≈150 m from the shower axis (for a vertically incident shower) corresponding to the front surface of the cone of Cerenkov emission with half-angle 1-2°. Beyond this radius, the intensity rapidly decreases due to the various contributions from the electrons scattered further away from the shower axis. This distribution on the ground is generally referred to as the Cerenkov light pool. In the central regions of this light pool for the 300 GeV photon primary discussed above, the photon density is about 10 m^{-2}. This will increase for a higher energy primary since more electron-positron pairs will be produced before the maximum shower development is reached, and this maximum will be at a greater atmospheric depth.

Although such a small light flux at first seems difficult to detect against the background flux of visible photons from the night sky, which is about 10^{12} $m^{-2}s^{-1}sr^{-1}$, a number of factors work in the favour of a potential observer. The key to observation of the Cerenkov light from individual air

showers lies in the large area of the Cerenkov light pool, $\approx 10^4$ m^2, which is equivalent to the effective area of a detector placed anywhere within this region on the ground. Further aid comes from optimal reduction of the angular acceptance of the detector, and selection of a gate time matched to the duration of the brief Cerenkov "flash". The practical techniques of gamma ray astronomy via the atmospheric Cerenkov technique are described in the next chapter (section 2.3).

CHAPTER 2 - GAMMA RAY ASTRONOMY

2.1. Early Proposals

The importance of the detection of astrophysical gamma rays arises from the fact that they combine the directional and temporal information on their point of origin with a close relation to the processes ultimately responsible for the production of radiation over a wide range of energies. This enables researchers to come as close as possible to some of the raw mechanisms of energy production in the universe.

The practical possibility of gamma ray astronomy was first outlined in a speculative paper by Morrison (1958). He concentrated on the energy range from ≈0·2-400 MeV, pointing out that lower energies would be less penetrating and less directly related to their origin, whilst higher energies would largely result from secondary interactions of cosmic ray particles. Measurements from the top of the atmosphere had already indicated that only about 1% of the particle flux above 0·5 GeV was due to gamma ray quanta.

The gamma ray flux due to an elementary volume with source strength S at a distance r is simply expressed as S/r^2. If r is measured in cm, S has the dimensions $cm^{-3}s^{-1}sr^{-1}$. The directional flux J for a detector of solid angle Ω is then the integral of the source flux over the volume intercepted by Ω, i.e.

$$J = \int d\Omega \int \frac{S}{r^2} r^2 \, dr \, . \qquad (2.1)$$

Since most astrophysical objects will have an apparent angular size well below the solid angle of practical detectors, the received flux becomes

$$J = \frac{1}{r^2} \int S \, dV \, , \qquad (2.2)$$

with V corresponding to the entire volume of the region of observation. J is thus expressed in photons $cm^{-2}s^{-1}$. This usually has to be folded with the detector's angular response function to give an instrument-dependent directional flux (Garmire and Kraushaar, 1965).

Estimates of photon fluxes in the range 10-100's of MeV for the Crab Nebula and several extragalactic sources were in the range of $\approx 10^{-2}$ $cm^{-2}s^{-1}$, a level believed to be detectable given the application of then-existing technology in high altitude balloon flights. Unfortunately, as Morrison himself had the foresight to warn, these estimates turned out to be greatly optimistic and orders of magnitude too large, but the seed was sown to spur effort in the field.

In the light of early experimentally derived limits, revised flux estimates were later published. For example, Garmire and Kraushaar (1965) surmised that the majority of the gamma ray flux from the Crab Nebula would arise from meson decay, with an estimated flux above 100 MeV of $\approx 10^{-5}$ $cm^{-2}s^{-1}$.

2.2. Advances Through Satellite Experiments

2.2.1. The Need for Space-based Observations

Almost a decade of frustration followed the initial estimates of astrophysical gamma ray fluxes. Despite the great effort put into employing scintillators, nuclear emulsions and spark chambers in high-altitude balloon flights, no substantiated sources were detected (for a review see Fazio, 1970).

After the realisation of the inadequacy of these techniques in the face of a gamma ray flux which was both much lower than predicted and heavily contaminated by the atmospheric background, effort was directed into the construction of more sophisticated instruments which could be operated above the Earth's atmosphere. These would have the benefits of a greatly reduced gamma ray background and a greatly increased exposure time. An early satellite flight, that of Explorer XI in 1961, had measured the total cosmic gamma ray flux as $(3{\cdot}3 \pm 1{\cdot}2) \times 10^{-4}$ $cm^{-2}s^{-1}$ in the range 300-700 MeV (Kraushaar et al., 1965). With a keener eye on the gamma ray sky, the determination of discrete sources of this flux would soon become a reality.

2.2.2. OSO-3: Detection of a High Energy Cosmic Background

The first experiment to yield positive results was a package contained in the Third Orbiting Solar Observatory (OSO-3), which was in use in 1967/68 (Kraushaar et al., 1972). This consisted of a multilayer CsI/plastic scintillation detector counter, a directional Cerenkov counter and a NaI energy detector. The instruments were operated in coincidence together, but in anti-coincidence with a shield of scintillation detectors in order to reduce the effects of the isotropic cosmic ray background. This discrimination technique revealed that cosmic ray induced events were $\approx 10^4$ times more common than gamma ray events. A total of 621 gamma ray events were recorded in the energy range ≈50-1000 MeV which showed a marked concentration in the galactic plane. Most of the sky was scanned and no evidence was found for any discrete sources with a flux greater than a few x 10^{-5} cm^{-2} s^{-1}.

2.2.3. SAS-2 : Identification of Discrete Sources

The Second Small Astronomical Satellite (SAS-2) was in orbit for 8 months in 1972/3 and carried the first satellite-borne gamma ray telescope capable of determining discrete source positions (Kniffen et al., 1977). The hub of the experiment was a digitised spark chamber which was triggered by four scintillation detectors. This was sufficient to give an angular resolution of 2-3°. The energy threshold was about 30 MeV.

During the course of the observations, about 60% sky coverage was achieved, and ≈8000 gamma ray events recorded. In addition to the detection of diffuse emission from the galactic plane, six localised (≥35 MeV) gamma-ray sources were identified, summarised as follows :

(i) The Crab Pulsar - a pulsed 33 ms signal was found with a flux above 35 MeV of ≈8 x 10^{-6} $cm^{-2}s^{-1}$. The unpulsed flux was about 60% of this, decreasing at higher energies. A strong interpulse was also noted and the overall light curve was consistent with those seen at other wavelengths.

(ii) The Vela Pulsar - this was the strongest source seen with a total flux above 35 MeV of ≈3 x 10^{-5} cm^{-2} s^{-1}. A clear double-peaked lightcurve was

recorded, out of phase with radio and optical results, implying a different production mechanism.

(iii) Two other radio pulsars - PSR's 1747-46 and 1818-04 - were detected at a flux level of $\approx 2 \times 10^{-6}$ cm^{-2} s^{-1} above 35 MeV,just above the threshold of detection. Like the Vela pulsar, both light curves showed an offset from the phases of the radio peaks.

(iv) Cygnus X-3 : a 4·8 hour light curve was identified in keeping with that seen at X-ray energies. The flux above 100 MeV was $\approx 4 \times 10^{-6}$ cm^{-2} s^{-1}, similar to the Crab pulsar at these energies. An assumed distance of ≥ 10 kpc gave an estimated luminosity of $\geq 10^{36}$ erg s^{-1}.

(v) γ195+5 - this was the first identification at any energy of the mysterious source later to become known as Geminga (Thompson et al., 1977). A 7σ signal was found near the galactic anticentre, consistent with a point source origin.The flux above 100 MeV was $(4{\cdot}3 \pm 0{\cdot}9) \times 10^{-6}$ cm^{-2}s^{-1}, and the spectrum appeared harder than any other known source.

2.2.4. COS-B : First Extragalactic Source Identification

After the short but successful flight of SAS-2, a similar satellite was required to reap the additional benefits that a longer exposure time would bring. The COS-B satellite achieved this by keeping an orbiting gamma ray telescope active for over 6 years after launch in 1975. The experiment consisted of a 16-level spark chamber, triggered by a stack of scintillation and Cerenkov counters (Taylor and Wills, 1981). The energy threshold was ≈70 MeV with energies measurable up to 300 MeV, though events were detected up to ≈5 GeV. The angular resolution was ≈2°. Over 2×10^5 celestial gamma rays were recorded over the course of the mission, vastly improving our view of the universe at these energies.

25 discrete sources found were detected, most lying very near the galactic plane, clearly indicating their intra-galactic nature (Bignami, 1984). Many of the discrete sources were correlated with large HI complexes

such as the rho Ophiuchi cloud. A knowledge of the amount of material contained within these clouds, obtained from other wavelengths, could be combined with the knowledge of their gamma ray emission to give an idea of the cosmic ray distribution in the Galaxy. Apart from rho Oph itself, which required a significant local enhancement of the cosmic ray flux, the cosmic ray density throughout the Galaxy was found to be remarkably uniform. The was an important result, suggesting an extragalactic origin of cosmic ray protons.

Of the other discrete sources, only the Crab and Vela pulsars were identified with known galactic objects. The gamma ray fluxes and pulsed light curves for these pulsars were virtually identical to the results obtained by SAS-2. No source was located at the position of Cygnus X-3 (e.g. Bennett et al., 1977). The source seen there earlier by SAS-2 was attributed to interstellar gas in the Cygnus region although this interpretation has been refuted (Fichtel, Thompson and Lamb, 1987).

Two further interesting discrete sources were detected. Firstly, Geminga (2CG195+04). The advance made in locating the position of the source enabled the discovery of a counterpart at both X-ray and optical wavelengths (Bignami, Caraveo and Lamb, 1984; Caraveo et al., 1984). This paved the way for later important discoveries about the nature of the object (see Section 2.2.5.2).

The most surprising result was the discovery of the first extragalactic gamma ray source, the quasar 3C273 (Swanenburg et al., 1978; Bignami et al., 1981). The gamma ray flux recorded from this object, $0{\cdot}6 \times 10^{-6}$ cm^{-2} s^{-1} above 100 MeV, implied an intrinsic luminosity of 2×10^{46} erg s^{-1}. This importance of this detection then was related to the fact that the gamma ray emission constituted the vast majority of the information available on the energetics of this distant source .

2.2.5. The Compton Observatory

2.2.5.1. Instrumentation

The Compton Observatory (previously the Gamma Ray Observatory, GRO) was proposed as the second component of NASA's Great Observatories programme. The

aim was to provide greater sensitivity to discrete sources, diffuse emission and gamma ray line emission than any previous experiments. It was realised that it was not possible in a given range of the wide gamma ray spectrum to improve energy and angular resolution without losing overall sensitivity, and so a set of complementary instruments were designed to provide optimal coverage, (Gehrels, Chipman and Kniffen, 1993 and refs. therein). It was also considered advantageous to use different detection techniques best suited to a particular part of the energy range. Four self-contained instruments were finally included in the spacecraft. The gamma ray spectrum was spanned from 50 keV to 30 GeV, almost six decades in energy, and continuity between the four experiments was achieved by overlapping of their energy thresholds (see Table 2.1). The Compton Observatory was launched in 1991 April and is still fully operational at the time of writing. The mission lifetime is currently expected to be at least 3 years.

(i) Oriented Scintillation Spectrometer Experiment (OSSE)

Operating in the range 0·1-10 MeV, this instrument consists of four identical large area NaI scintillation detectors. These are used as coaxial pairs, one of each pair observing the source, the other monitoring the background, interchanging at short time intervals so as to minimise background variations. The primary purpose is to obtain high resolution energy spectra of sources, but some resolution can be sacrificed to enable fast timing of pulsar signals.

(ii) Imaging Compton Telescope (COMPTEL)

This instrument was designed to produce a detailed sky survey of gamma ray sources in the range 1-30 MeV.The experiment comprises two detector arrays. In the upper detector, gamma rays are Compton scattered in a liquid scintillator, and the scattered photons are absorbed 1·5 m below in a 14-element NaI crystal detector. This can be compared to an optical camera, the upper detector replacing the lens, the lower replacing the film. The energy

	OSSE	COMPTEL	EGRET	BATSE	
				Large area	Spectroscopy
Energy Range (MeV)	0.10 - 10.0	1.0 - 30.0	20 - 3 x 10^4	0.03 - 1.9	0.015 - 110
Energy Resolution (FWHM)	4.0% at 5.0 MeV	6.3% at 4.4 MeV	20%	20% at 0.66 MeV	5.8% at 1.2 MeV
Effective Area (cm^2)	2013 at 0.2 MeV	29.4 at 4.4 MeV	1600 at 500 MeV	1800 at 0.1 MeV	127 at 0.2 MeV
Resolution (Strong Source)	10 arc min square error box	8.5 arc min	5-10 arc min	1 degree	———
Field of View	3.8 x 11.4 degrees	1 sr	0.6 sr	All sky	All sky
Source Sensitivity for 10^6 sec exp.	2 x 10^{-7} $cm^{-2} s^{-1} keV^{-1}$	5 x 10^{-5} $cm^{-2} s^{-1}$	1.5 x 10^{-8} $cm^{-2} s^{-1}$ > 1000 MeV	6 x 10^{-8} erg cm^{-2} (10 s burst)	———

Table 2.1 : A summary of the Compton Observatory instrument characteristics.

loss and position of each interaction are measured, enabling good angular and energy resolution.

(iii) Energetic Gamma Ray Experiment Telescope (EGRET)

EGRET operates in the energy range 20 MeV to 30 GeV. Like several previous satellite-borne gamma ray experiments it is based around a multi-layer spark chamber which detects gamma rays via their electron-positron pair production. An NaI energy counter is placed beneath the spark chamber. Strong sources can be located to within less than 10 arc minutes at GeV energies. This is the best angular resolution of any gamma ray experiment of its type, and arise from its large effective area, 1600 cm^2 at 500 MeV (c.f. COS-B maximum effective area of 50 cm^2 at 500 MeV) as shown in Figure 2.1. Sources may be detected to a threshold two orders of magnitude below the flux from the Crab.

(iv) Burst And Transient Source Experiment (BATSE)

The purpose of BATSE is to provide continuous all-sky coverage of gamma ray bursts and other transient sources. The experiment consists of 8 identical instruments mounted on each corner of the spacecraft. Each contains a large-area NaI scintillation detector, optimised for sensitivity and directional response, and a smaller,thicker NaI scintillation calorimeter to give good energy resolution over a wide range. Detection of a burst in the field of view of the other onboard experiments triggers them to record more detailed data. A valuable secondary capability is its ability to record virtually continuous data on strong pulsed sources from any part of the sky.

2.2.5.2. Highlights of Results

Before its launch, the Compton Observatory was expected to provide an unparalleled quantity and quality of information on the gamma ray universe. In its 2 years of operation to date, this has proven to be the case, with many important discoveries having been made. For an overview of the results, the reader is referred to the proceedings of the Compton Observatory Workshops. In

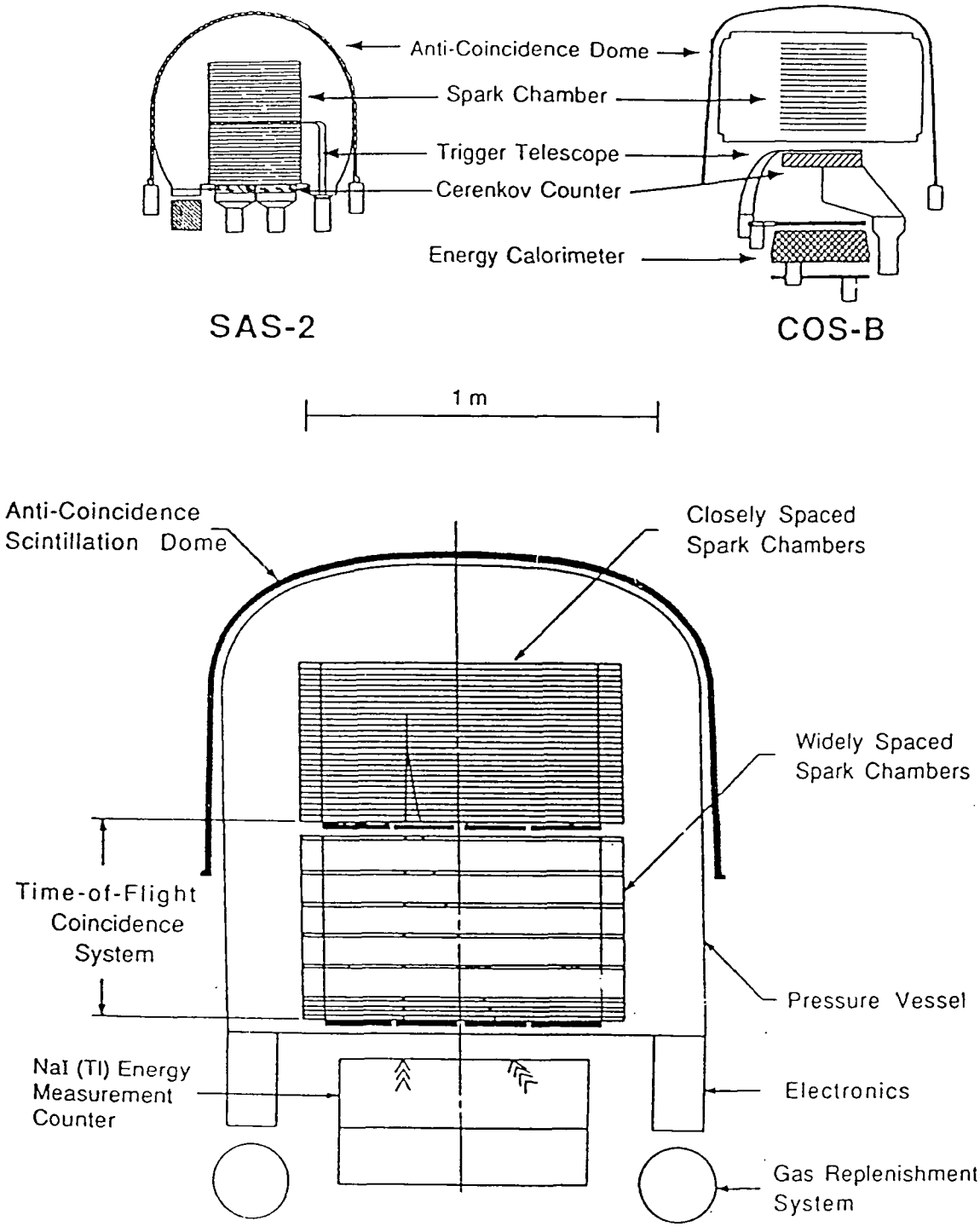

Figure 2.1 : A scale diagram showing the relative dimensions of SAS-2, COS-B and EGRET. All three share the same detection principle and the extra sensitivity offered by EGRET is clear.

(from Kanbach et al. 1990)

this section, three results of particular interest are mentioned.

(i) Geminga - Measurements using the soft X-ray satellite ROSAT eventually revealed the existence of pulsations from the X-ray source identified as the counterpart to Geminga (Halpern and Holt, 1992). The pulsar period was found to be 237 ms with a probability of $\approx 10^{-4}$ for chance occurrence. This enabled a search of the EGRET gamma ray database to be made. A sample of data in the energy range 100-500 MeV, recorded only 60 days after the ROSAT observations, yielded an unambiguous signal of negligible chance probability at 237 ms (Bertsch et al.,1992). Unlike the X-ray light curve, the ≥300 MeV light curve was found to be double-peaked. The flux ≥100 MeV was $\approx 4 \times 10^{-6}$ $cm^{-2}s^{-1}$, which combined with measurements of the spin-down rate showed that the source distance was around 100 pc making this one of the closest neutron stars known. Subsequent reanalyses have shown that the 237 ms periodicity could also be identified in the databases of SAS-2 (Mattox et al., 1992) and COS-B (Bignami and Caraveo, 1992).

(ii) New Gamma Ray Pulsars - Among the most important discoveries made to date by the Compton Observatory are those of two previously unseen gamma ray pulsars, which have been identified with the radio sources PSR 1509-58 and PSR 1706-44 (Wilson et al., 1993a; Thompson et al., 1992). These pulsars were first discovered by BATSE and EGRET respectively - the COMPTEL instrument has only detected the former (Bennett et al., 1993). Both have been found to have a light curve consisting of a single broad peak, and display energy spectra harder than that of the Crab. These were also two of the sources predicted to be detectable as gamma ray pulsars due to their high magnetic fields and relatively young ages.

(iii) QSO's - After the COS-B detection of 3C273 as a high-energy gamma ray source, it was hoped that the Compton Observatory would provide more evidence of extragalactic sources. EGRET has done this by detecting not only 3C273, but also discovering emission from many more radio-loud QSO's including 3C279 (Hartman et al., 1992). The intensity of this source was

$(2{\cdot}8 \pm 0{\cdot}4) \times 10^{-6}$ cm^{-2}s^{-1} at energies above 100 MeV, which indicated that this source could have been detected by SAS-2 or COS-B. The fact that neither did implies significant source variability. Its great distance makes it the most luminous gamma ray source known with a luminosity of $\approx 10^{48}$ erg s^{-1} between 100 MeV and 10 GeV.

2.3. Astronomy using the Atmospheric Cerenkov Technique

2.3.1. Extending the Gamma Ray Spectrum

The merits and positive results gained from satellite-borne gamma ray detectors have now been reviewed. Various celestial sources have been found to emit gamma rays up to energies of tens of GeV. However, at higher energies the flux of gamma rays diminishes to an extent whereby the constraints on the size of an orbiting detector make observations impracticable. In addition, the spark chamber technique is difficult to implement at such high energies as the electron-positron pair separation angle becomes very small. Fortunately, the very thing which made space-based telescopes desirable, namely the Earth's atmosphere, becomes a detector itself at these high energies via the Cerenkov radiation produced by the flux of cosmic particles (see Chapter 1). Cerenkov astronomy in the region of 10^{12} eV primary photons is often referred to as TeV or Very High Energy (VHE) gamma ray astronomy. It is defined simply by the primary gamma ray energy range ($\approx 10^{11}$ to 10^{14} eV) within which Cerenkov light showers are detectable using specially designed large aperture optical telescopes at ground level.

This is distinct from PeV or Ultrá High Energy astronomy where the primary particles are sufficiently energetic ($\geq 10^{14}$ eV) to produce secondary shower particles which are directly detectable by extensive air shower arrays. The primary energy threshold accessible by this technique decreases with height above sea-level since the lower the energy of the particle, the shorter will be its path length in the atmosphere. For recent reviews of this interesting field, the reader is directed to Yodh (1992) and Protheroe (1987).

2.3.2. Origins of Cerenkov Astronomy

It was first suggested by Blackett (1948) that the background light of the night sky as viewed from the surface of the Earth should contain a contribution arising from the visible Cerenkov radiation produced by cosmic particles. The proportion of the background due to this process was estimated to be about 10^{-4}. The first measurements of this light were made by Galbraith and Jelley (1953). Based on the assumption that the temporal and spatial properties of the Cerenkov light pool would have some similarities with those already measured for extensive air showers (Cranshaw and Galbraith, 1954), they used fast electronics in conjunction with a small light collector and photomultiplier to detect the brief pulses of light at a rate of several per minute (Jelley, 1987). Later work showed that the lateral extent of the light pool at ground level was $\geq$100 metres for a primary particle of energy 10^{15} eV, and the typical duration of a pulse was $\approx$10 ns (Galbraith and Jelley, 1955).

The application of this technique to detect gamma ray induced air showers as distinct from those induced by hadronic primaries was first suggested by Zatsepin and Chudakov (1962). The great advantages offered by the technique are the large effective collecting area afforded by the size of the Cerenkov light pool (at 10^4 m^2, much larger than any single detector) and the relative simplicity and cost-effectiveness of the equipment. The disadvantages are the difficulties in distinguishing between photon or proton primaries, and the requirement for a clear, moonless observation site, to avoid the hindrances of poor clarity and sky noise.

Much effort was put into attempts to detect the photon element of the cosmic ray flux by the use of Cerenkov telescopes. Perhaps the most exhaustive studies in the early days of the 1950's and 1960's were carried out by the AERE/UCD group in both the Republic of Ireland and Malta (see Fruin et al., 1964; Fegan et al., 1968) and by the Lebedev Institute group in the Crimea (Chudakov et al., 1965). Many prospective discrete source positions were

observed in an effort to locate an enhanced Cerenkov flux due to an excess of gamma ray showers. No significant fluxes were detected. For the Crab Nebula, the Lebedev group derived an upper limit of 5×10^{-11} $cm^{-2}s^{-1}$ for energies above 5 TeV. A number of other supernova remnants and radio sources were selected as candidate targets, again with nothing more than an upper limit resulting. Despite the lack of positive results in this direction, much information was gained on the nature of Cerenkov shower development and on the optimisation of the equipment used.

2.3.3. Detectors of Atmospheric Cerenkov Light

Although the photon density from an individual Cerenkov light shower is low, typically 50 m^{-2} within 100 m of the shower axis for a 1 TeV primary, it is the very brief duration of the observed flash which enables its detection. The average night sky background photon flux is about 10^{12} $m^{-2}s^{-1}sr^{-1}$, and a light detector with a time constant or gating pulse matched to the $\approx$10 ns duration of a Cerenkov flash can easily measure the enhancement due to such an event. The most obvious technique is also the simplest and most commonly used, i.e. employing a light collector (invariably a large mirror) to focus light onto a photomultiplier tube connected to electronic equipment for measurement of the anode current variations (see Figure 2.2). On such a short timescale, the only background fluctuation will be the random change in night sky brightness. This, however, will be a function of mirror size, field of view, the photomultiplier tube's quantum efficiency and the integration time of the system. If a Poissonian distribution is assumed, the night sky noise N is then

$$N \alpha (B.r.e.t.A)^{1/2} , \qquad (2.3)$$

where B is the intensity of the background, r is the solid angle viewed, e the quantum efficiency, t the gate time, and A the area of the mirror (Weekes, 1988). The actual air shower signal is proportional to the product of A and e, so the ratio of signal S to noise N is given by

$$S/N \alpha (Ae / Brt)^{1/2} . \qquad (2.4)$$

The energy threshold for shower detection is inversely proportional to S/N,

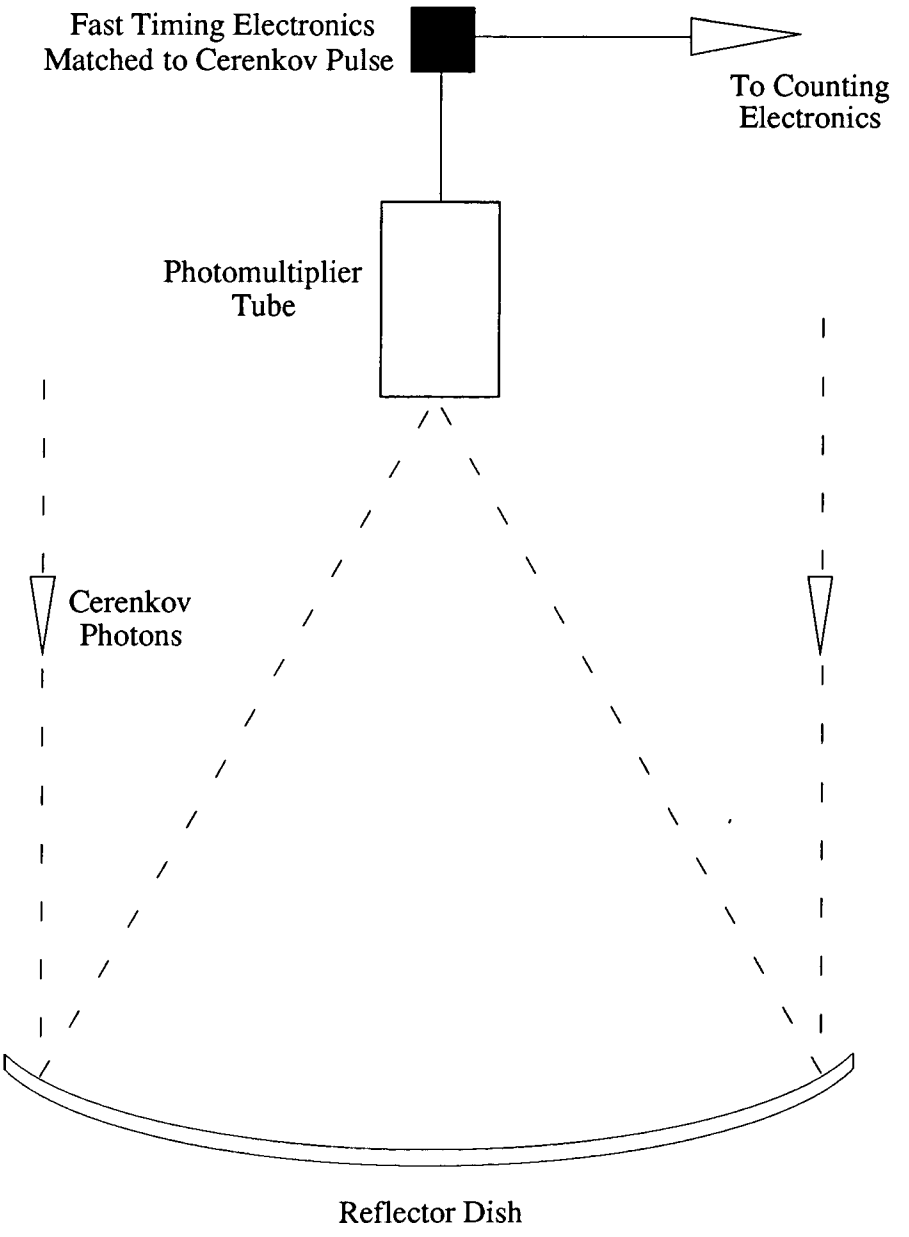

Figure 2.2 : Illustration of the basic atmospheric Cerenkov telescope system. At least 2 systems are usually operated in fast coincidence in order to reduce the background of night sky noise.

and thus to achieve the minimum threshold the value of Ae/rt must be maximised.

(i) Mirror area, A.

In the early days of Cerenkov astronomy in the 1950's, a large supply of war surplus searchlight mirrors was available, as used in the initial experiments of Jelley and Galbraith. Since the Cerenkov light flash has a typical angular spread of 1-2°, the resolution of these mirrors was quite adequate, but their diameter (1·5 m) too small for anything more than preliminary investigations. Increasing the mirror area can then be done in two ways. The first is to co-mount an array of small mirror elements, and the second to produce a large single reflector. In practice, the former has been more commonly used, due to the relaxed resolution criterion and the relative simplicity of obtaining or producing a large number of small mirrors (0·5-2 m diameter).

There are two other ways of increasing the effective collecting area and hence reducing the threshold energy. The first is to place more than one telescope dish/detector on the same mount (within ≈10 m of each other) and accept only events which are seen by all components within ≈10 ns. This reduces the background caused by instrumental effects and sky noise considerably. It has been shown that the background reduces with an increasing number of dishes, but three together offer the greatest efficiency before an effective plateau in the increased rejection is reached (Brazier et al., 1989). For a figure of merit Q defined as S^2/N where S is the rate of photon triggers and B the total background rate, three dishes offer a Q value of up to 10 compared with a single dish (Patterson and Hillas, 1989). A second method is to increase the number of independent telescopes sampling the Cerenkov light pool. Although n independent telescopes do not offer as great an increase in efficiency as n co-mounted telescopes, they do offer further possibilities in background rejection

techniques.

(ii) Photomultiplier quantum efficiency, e.

The Cerenkov spectrum has its intensity proportional to λ^{-2}, and the most suitable photomultipliers will therefore be those with peak response in the blue or near-UV regions of the spectrum. Bialkali phototubes are commonly employed and have a peak response at 3900 Angstroms where e≈30%.

(iii) Field of view, r.

The primary requirement of the field of view is that it must be large enough to gain maximum information on the observed Cerenkov light flash. However, widening the field of view has the effect of increased acceptance of unwanted background light, so that most detectors used have field widths optimised to ≈0·5-1°. This means that the response of the reflector to a point source at infinity should be of a similar order. The effects of coma can also be significant for larger fields of view. In practice, the field of view is defined by the size of photomultiplier tube used and the focal ratio of the reflector.

(iv) Integration time, t.

It is obviously beneficial to keep the integration time as short as possible in order to reduce the acceptance of background noise, and simulations have suggested that photon induced showers have shorter timespans than those induced by hadronic primaries. Thus the gate time should be matched closely to the predicted 3-5 ns duration of a photon induced shower, but in practice 5-10 ns is a more common figure due to limitations imposed by the high frequency performance of the electronics and the physical size of the detector.

Based on these broadly defined detection principles, the telescopes used for Cerenkov astronomy have become gradually more sophisticated and sensitive. This progress can be divided into three major generations of experiments, as summarised in Table 2.2.

TABLE 2.2 - The development of the techniques of Cerenkov astronomy	
1st Generation	1953 - late 1970s Characterised by simple Cerenkov telescopes, often a small array of 1.5 m mirrors, operated in simple drift-scan mode. No sophisticated rejection of the hadronic background. Searched for classical sources, e.g. Crab, Cas A, Cyg A, M87.
2nd Generation	Mid 1970s - early 1990s Spurred by the detection of gamma ray sources from satellite measurements. Characterised by improved hadronic background rejection, based on fast timing or crude measurement of the light distribution. Energy threshold reduced by building larger arrays. More targeted observations, especially COS-B sources, X-ray binaries and AGN's. Development of the imaging technique culminated in the Crab Nebula detection.
3rd Generation	Early 1990s - ? Emphasis on imaging following its successful implementation. Construction of arrays of N large imaging telescopes to exploit stereoscopy. Primary aims include the reduction of energy thresholds to 10s of GeV and follow up of Compton Observatory discoveries.

2.3.4. Simulations of Cerenkov Radiation from Air Showers

The aim of simulations of the Cerenkov light produced in a shower is to predict the expected lateral and angular distributions of the resultant photons which will help define the required parameters of the detectors used. Factors which must be taken into account include the primary energy, the impact parameter, Coulomb scattering of the electrons, geomagnetic effects and fluctuations between individual showers.

Early analytical simulations of the Cerenkov showers produced by particles with energies in the TeV range, such as those of Zatsepin and Chudakov (1962) and Sitte (1962), revealed several noteworthy features of the radiation distribution. As interest developed in this field, the possibility of using the atmospheric Cerenkov technique to detect gamma rays was of great interest but these early simulations were pessimistic about the possibility of discriminating between showers initiated by photon or proton primary particles.

In later simulations, the Monte Carlo technique has dominated. This is well suited to calculating the angular and lateral distributions of light in individual showers by considering the propagation of many individual photons. Discrepancies between different treatments can result from assuming different atmospheric models and different penetration depths for a given primary energy (e.g. Rieke, 1969; Castagnoli et al., 1972) Such techniques have been able to provide promising channels for discrimination between showers produced by primary photons or hadrons (Turver and Weekes, 1978).

In general, the lateral photon density distribution for a gamma ray shower at ground level is predicted to show a relatively flat shape up to about 100 m from the main shower axis, with a substantial drop further away (see Figure 2.3). An important effect to consider is that of the geomagnetic field. The electron cascade in the early stages of shower development is broadened by the field interaction, and this has greatest significance at high altitudes (hence low densities) where the electron mean free path is longest

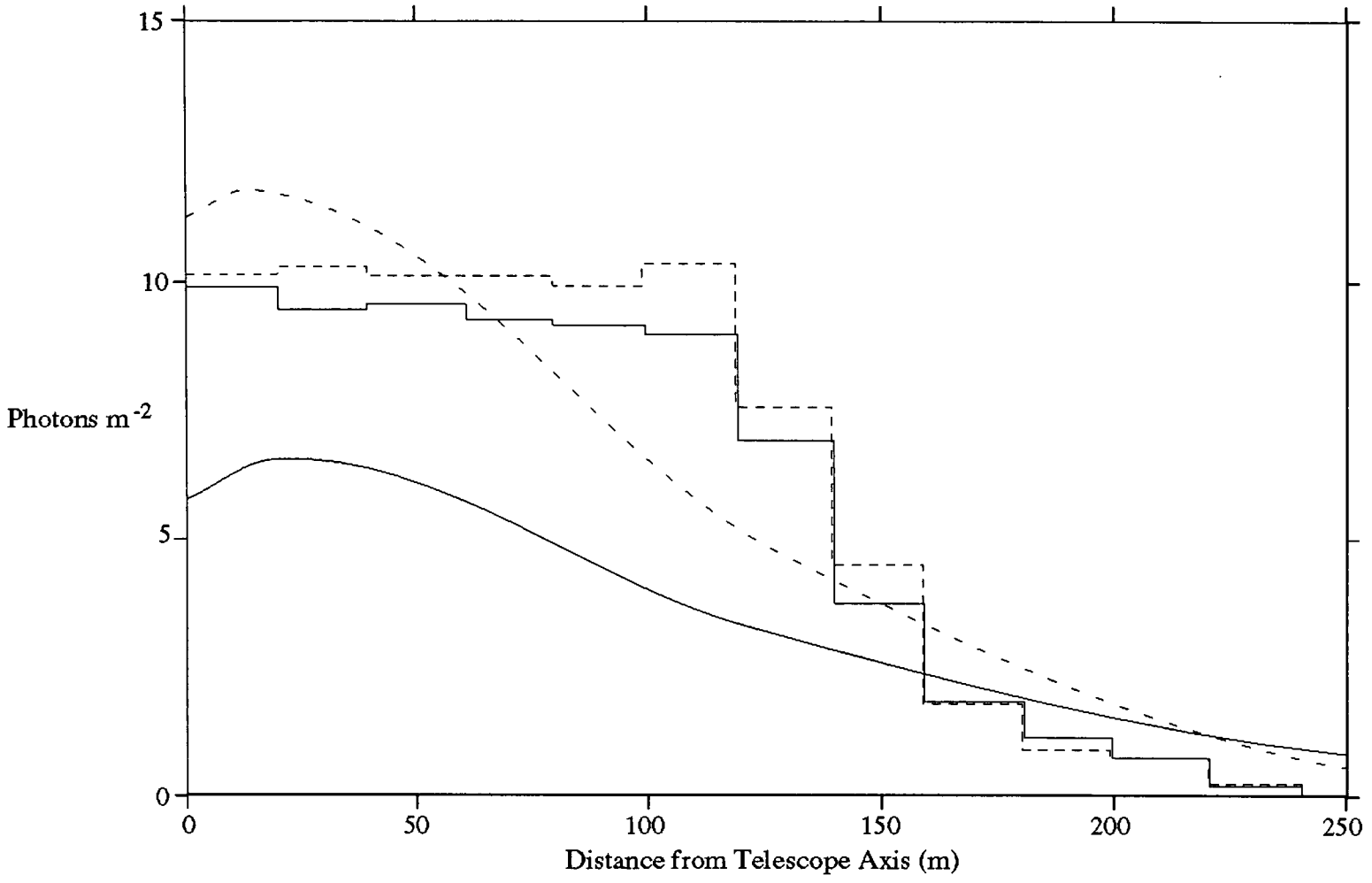

Figure 2.3 : Simulations of the lateral distribution of a Cerenkov light pool. The primary particle is assumed to be a gamma ray vertically incident on the axis of the Whipple reflector (alt. 2.32 km) Data calculated with (————) and without (- - - - - - - -) effects of geomagnetic field. Histogram data from Plyasheshnikov and Bignami, 1985. Curve data from Browning and Turver, 1977.

(Porter, 1973; Browning and Turver, 1977). The fluctuations in individual showers are increased by this effect, being most prominent at large distances from the shower axis. This can have the effect of requiring an increased field of view and hence raising the threshold energy (Bowden et al., 1992a).

The relationship of the shape of the shower to the impact parameter as measured from the axis of the detector has been found to be fairly consistent. All simulations indicate that a shower landing on and parallel to the detector axis will produce a concentric circular intensity profile, becoming more elongated as the displacement from the axis increases as shown in Figure 2.4 (Rieke, 1969). The shower core location is generally not coincident with the position of maximum intensity in the light pool.

2.3.5. Observational Modes

2.3.5.1. Drift Scans

The drift scan technique is one of the simplest tools in Cerenkov astronomy, and has been widely used, particularly in the early days of source searches (e.g. Jelley, 1967). It relies on the detection of an overall excess of Cerenkov showers coincident with the position of a candidate source. The operational method is straightforward. The detector attitude is maintained at a constant zenith and azimuth angle for a suitable period of time whilst the source position transits through the field of view. An equal angular distance either side of the source is usually observed, the full width of the scan being dependent upon the angular response function of the detector. A disadvantage of this technique is that it relies implicitly on stable atmospheric and instrumental conditions. This dependence may be reduced by using a similar detector, offset in azimuth by several degrees to provide a check on external effects (e.g. Stepanian et al., 1975). In addition, further background rejection techniques, similar to those detailed in the following sections, may be implemented to reduce the hadronic background and improve the likelihood of detecting a gamma ray signal.

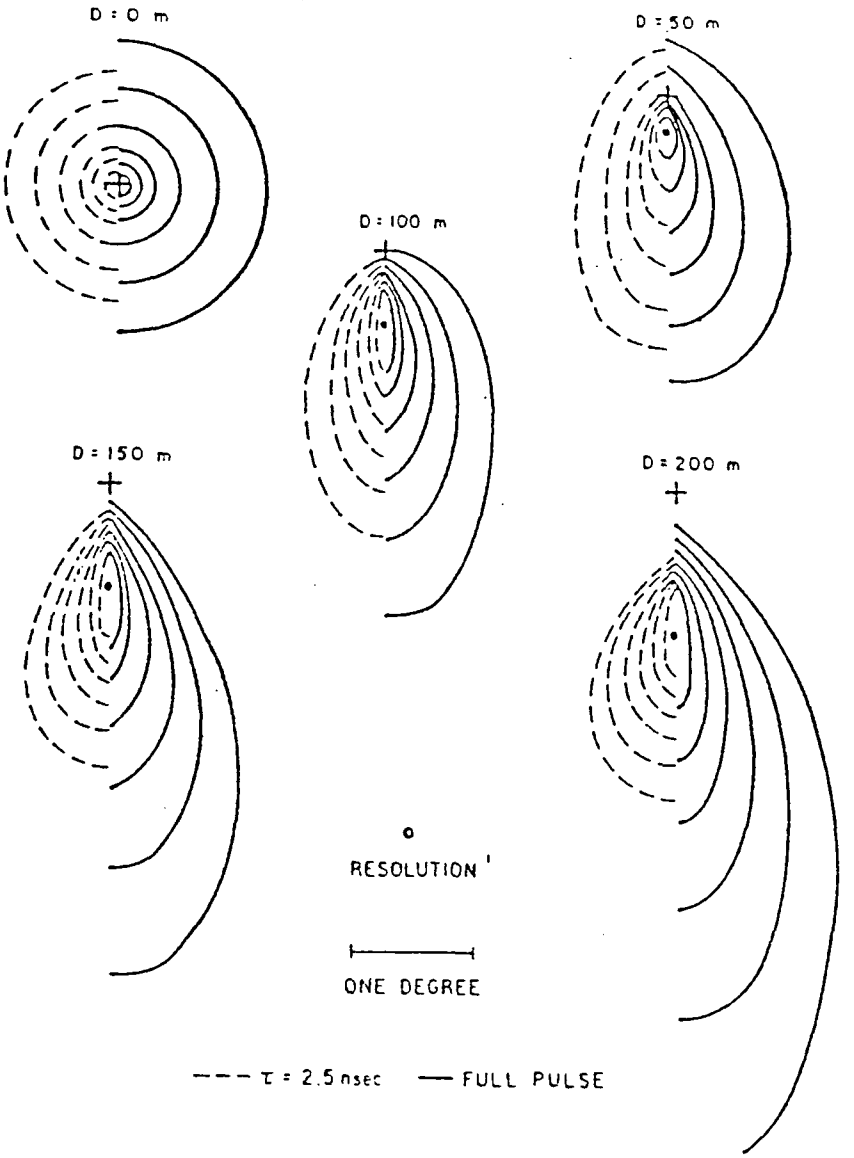

Figure 2.4 : Angular distribution of Cerenkov photons as a function of impact parameter D. Each isophote corresponds to a reduction in intensity by a factor of √10. The incident particle is a 0.1 TeV photon.

(from Rieke, 1969)

2.3.5.2. On/Off Tracking

Clearly, any TeV gamma ray telescope may be used in the drift scan mode to search for d.c. excesses from a source position. An alternative technique is to repeatedly change the field of view between the object region and an off-source test region and hence look for a d.c signal from the source. There are two ways of approaching this task. One is to simply alter the pointing of the detector's field of view for a given time interval and alternate on- and off-source observations. The Whipple group use 28-minute scans in this mode (Cawley et al., 1989). A disadvantage of this method is that the important on-source time is diluted. The second method avoids this problem by using an extra detector in the focal plane with a preset angular offset. The on- and off-source positions are then continually viewed by one detector or the other. This well-established technique of "chopping" on a timescale of 2-5 minutes has been frequently used by the Durham and Haleakala groups (see Chapter 3).

2.3.5.3. Continuous Tracking

The tracking mode requires the source to be continually monitored by sidereal steering of the detector over the course of an observation. For economy and ease of construction, most Cerenkov telescopes use computer controlled alt-azimuth mountings rather than the equatorial type. The benefit of the tracking mode is its provision of maximum uninterrupted on-source time, which is particularly useful for later pulsar timing analyses.

2.3.6. Fast Timing of the Cerenkov Radiation Wavefront

Monte Carlo simulations may be used to predict not only the lateral and angular structure of a Cerenkov shower wavefront, but also its temporal characteristics. The Cerenkov light produced during the development of a shower emanates from different heights in the atmosphere, but the change in refractive index with altitude means that the time delay between the front and back of the wavefront is virtually cancelled. The Coulomb scattering of electrons and scattering of the emitted light means that on reaching the ground, the visible photons have been formed into an almost plane wavefront.

Direct measurements may be made using a widely separated array of detectors to sample across the full extent of the shower. These have shown that a more accurate 3-D representation of the wavefront is that of a flattened cone with the central shower axis at the vertex (Orford and Turver, 1976). There are two aspects of the temporal profile of the shower which may be exploited experimentally.

By use of an array of detectors of total dimensions comparable with that of the Cerenkov light pool, fast timing on the scale of ≈1 ns can be employed to measure the arrival time of the light front at each element. Reconstruction of the time sequence of arrival at each detector may then be used to accurately reveal the location of the shower source on the celestial sphere. This is a technique more commonly employed in PeV particle detector arrays, e.g. the GREX array at Haverah Park (Lambert et al., 1987), than Cerenkov telescope systems since the centre of an extensive air shower is far better defined than that of a Cerenkov light pool.

However it has also been successfully used at TeV energies by the University of Durham telescopes at Dugway (see Chapter 3) and by the University of Potchefstroom group (de Jager et al., 1986). Two more advanced detector systems based on this technique have recently been deployed at Themis in the French Pyrenees - ASGAT (Goret, 1991) and THEMISTOCLE (Baillon et al., 1991).

The most recent applications of fast-timing information have been based on a different technique. A proton-induced Cerenkov shower contains a significant component of penetrating muons which radiate Cerenkov light much nearer ground level (≈100's of metres) than the electron component (Grindlay, 1971). This results in the shower front being much more chaotic in its temporal structure than that of a gamma ray induced shower, which arises solely from relatively well-behaved electron cascades, the light from which is scattered and the profile 'smoothed' by the time of reaching the ground. Fast

timing studies of the time-profile of a Cerenkov flash can therefore be used to attempt to discriminate the smooth, brief gamma ray induced pulse from the noisier, longer proton induced pulse.

This technique was investigated by Tumer et al.(1990) and yielded tentative positive results for a d.c. flux from the Crab Nebula based on human selection of gamma ray candidates from a library of video records of many Cerenkov pulses. More recently, the Adelaide group have used an *a priori* automated selection procedure to successfully apply the technique of rise time measurement to observations of Hercules X-1 (Roberts et al., 1993). A pulse shape measuring facility has also been included as part of the University of Durham Mk.5 Cerenkov telescope (see Chapter 3).

2.3.7. Field of View Reduction : The Guard Ring Technique

As discussed briefly in Section 2.3.2.2, the field of view of a Cerenkov telescope should correspond as closely as possible to the angular extent of a Cerenkov flash in order to reduce background light whilst deriving maximum information on the gamma ray shower. Having an optimal field of view centred on the source direction ensures that the maximum benefit is derived from the excess of Cerenkov showers expected to be induced by a gamma ray flux from the source. This is due to the background of cosmic ray proton-induced showers showing an isotropic distribution and hence no preference for an origin at any position on the celestial sphere. Even if the d.c. excess from the source position is then insufficient to yield a statistically significant detection, the prospect of the identification of a weak periodic signal in the direction of a pulsating source makes this a worthwhile method.

A refinement to the method described above is to investigate the fact that proton-induced showers have a substantial muon content which reveals itself by production of Cerenkov light much nearer ground level than the electron cascade, due to the greater penetration depth of the muon flux. The effects of this are most prominent 1-2° from the shower axis due to the change in Cerenkov angle and production height for optical emission from this more

penetrating component. Therefore, even for a shower originating from the on-source direction, the detection of a substantial amount of light at this angle from the main shower axis indicates a greater likelihood of the shower being due to a proton primary. In addition, the detection of a faint Cerenkov flash from the source direction may be due to a large flash originating just outside the field of view, which is unlikely to be due to a gamma ray from the source.

Both of the factors outlined above may be exploited by the deployment of a number of secondary photomultiplier tubes with an angular offset of 1-2° from the tube viewing the source itself. The term "guard-ring" for this configuration was originally coined by Grindlay, Helmken and Weekes (1976), who used a set of 6 off-source photomultipliers to provide an anti-coincidence system for Cerenkov flashes with greater angular extent than expected for a TeV gamma ray from the source direction. In fact this early work was primarily aimed at providing a crude image of the Cerenkov shower with a view to rejecting the more extended images typical of hadronic showers (see Section 2.3.3.4). The Durham group's use of this guard-ring configuration has been aimed purely at artificially reducing the field of view of the on-source detector by rejecting Cerenkov events which produce a significant amount of off-source light. This approach has proved to be highly successful and is discussed in more detail in Chapter 3.

2.3.8. Development of the Imaging Technique

The technique of directly imaging Cerenkov flashes has become a subject of great interest in recent years. The measured shape and photon density of a Cerenkov shower are related to the primary energy, the angle of incidence, the intrinsic shower light distribution, the variation of Cerenkov angle with height,the impact parameter with respect to the detector, among other factors. Simulations indicate that showers arriving on and parallel to the optic axis of a detector display a circular image, with intensity decreasing concentrically (e.g. Rieke, 1969), the shape becoming more elongated in the

focal plane as the impact parameter and angle of incidence increase.

With this elongation comes an important factor vital to the imaging technique. Even from the early days when an image intensifier was used to view large showers by Hill and Porter (1961), it was realised that the orientation of an ellipsoidal Cerenkov flash could contain information on its projected source location. However, given the uncertainties in the precise angular distributions of light produced in Cerenkov showers (see Figure 2.5, and references therein), the effort and sophistication required to study a large number visual images, and the high energy threshold characteristic of the image intensifiers ($\geq 10^{15}$ eV), no detailed imaging could be carried out.

The key to the practical use of imaging techniques lies in the fact that whilst proton-induced showers, being isotropic in origin, will give rise to elongated flashes aligned completely randomly in the field of view, gamma ray showers from a discrete source at the centre of the field of view should show a clear orientation towards the source position. This is aided by the expectation that the hadronic content of proton-induced showers causes the shape of the images to be much more irregular and extended than images of a gamma ray induced shower. Monte Carlo simulations by Plyasheshnikov and Bignami (1985) demonstrated that for TeV gamma ray showers, a quasi-uniform distribution of orientations is expected out to an off-axis distance of $\approx$50 m, partly due to their near circular shape and partly due to large fluctuations in the light received near the centre of the shower. However, beyond this distance the fluctuations decrease to a level where the distribution is dominated by showers aimed towards the centre of the field i.e. the on-source position. It was suggested that showers near the centre of the field of view could be rejected, as well as those beyond about 150 m, the distance where the fluctuations were minimised. Given a high resolution detector and good optics, gamma ray selection was proposed to be feasible (Hillas, 1985). The techniques used have recently been successfully applied and are discussed in Chapter 10.

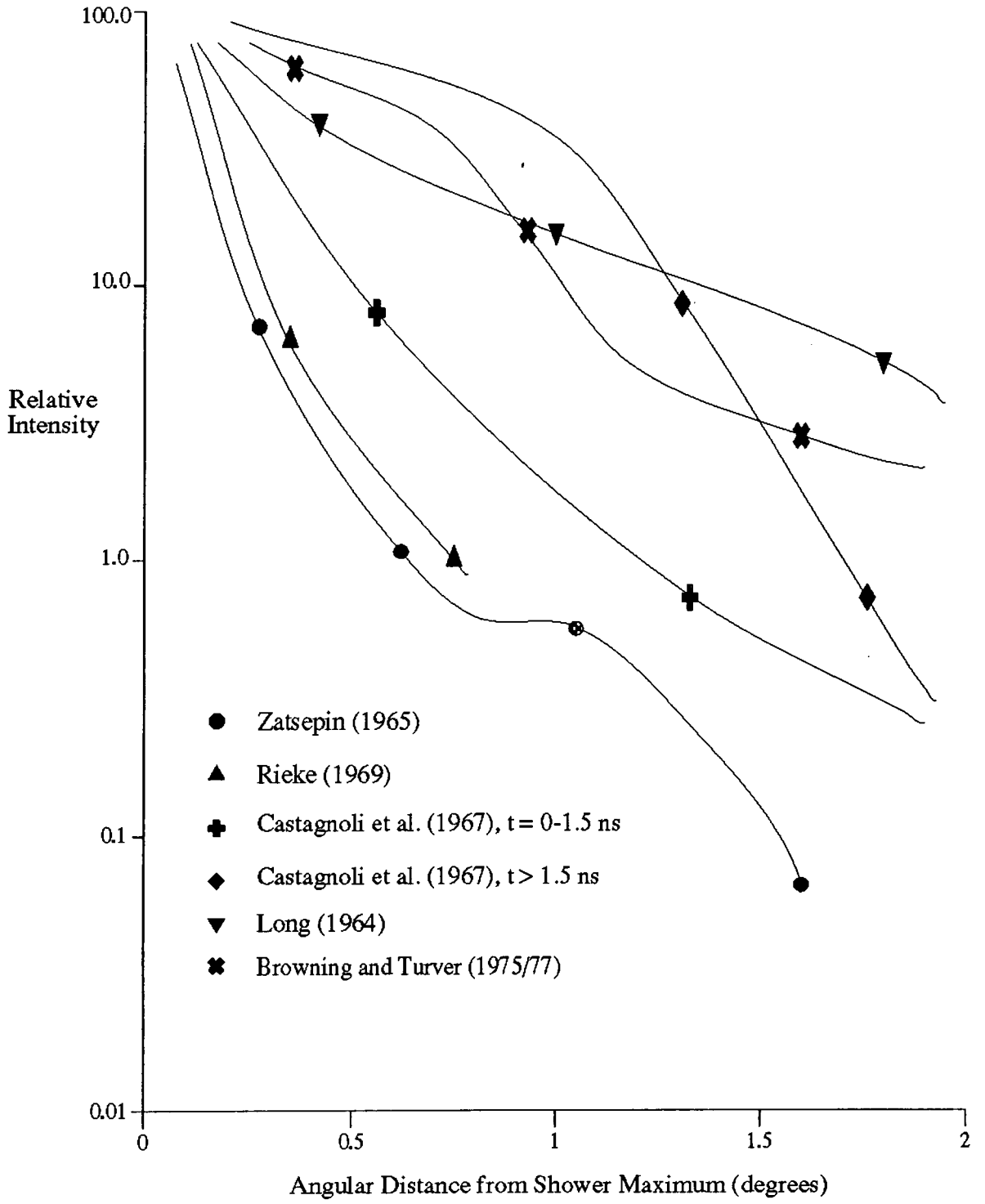

Figure 2.5 : Simulations of angular distribution of Cerenkov light for primary particle energies of around 1 TeV.

(after Fegan, 1992)

CHAPTER 3 - THE DURHAM GAMMA RAY TELESCOPES

3.1. Philosophy and Development

3.1.1. Design Philosophy

The design of the University of Durham group's ground-based gamma ray telescopes has been based on a number of basic principles, and has been steadily reviewed and improved as a result of experimental experience. This chapter provides a brief summary of the development of gamma ray detection techniques by the Durham group, and includes a detailed report of the properties of the Mark 3 telescope, used in the observations analysed in later chapters.

One common element of all the telescopes designed by the Durham group has been the operation of a multiple-coincidence system for the identification of genuine Cerenkov showers. This ensures that the lowest possible threshold energy is reached by overcoming the problem of accidental events being induced by rapid variations in the background night sky illumination, noise in the photomultiplier tubes, and spurious events generated by the passage of muons through the glass of the tubes. By assuming a constant acceptable accidental coincidence rate of 3 hr^{-1}, calculations have been performed to find which number of dishes n operated in n-fold coincidence give most efficiency for a specified total reflector area (Brazier et al., 1989). The calculations were carried out for a coincidence gate time of 5 ns and experimentally-determined values of the noise rate and photomultiplier gain. The results are shown in Figure 3.1. It can be seen that the overall count rate for a constant accidental rate increases with n, but soon reaches a plateau. By consideration of the sophistication and cost of a system with a given number of reflectors, a 3-fold coincidence was selected as most efficient and cost effective, coming within 15% of the theoretical maximum detector efficiency.

The greatest problem in Cerenkov gamma ray astronomy is the rejection of

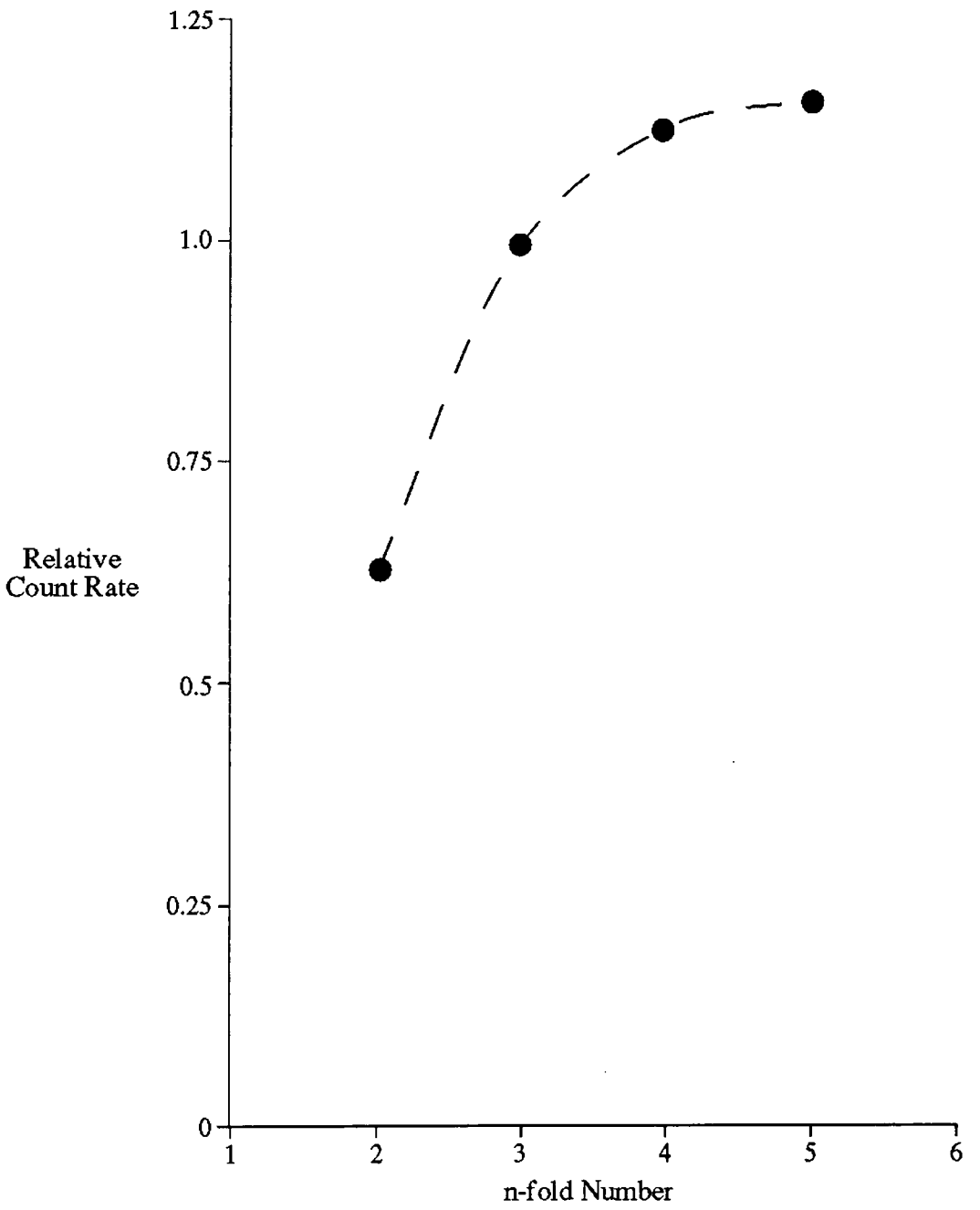

Figure 3.1 : Variation of cosmic ray count rate with n-fold coincidence for a fixed total reflector area and accidental coincidence count rate.

(after Brazier et al., 1989)

the isotropic charged particle cosmic ray background, largely consisting of protons, in order to improve the signal to noise ratio for the detection of TeV gamma rays. The consistent approach of the Durham group to overcoming this problem has been to specify an optimal field of view around the observed source which restricts the angular acceptance for incident particles and thus increases the detected ratio of gamma ray to proton primaries. This arises from the fact that showers initiated by gamma rays from a point source should show a significant clustering around the source position. Simulations and observations of Cerenkov light showers have suggested a field of view of about 1° as best for this technique (Dowthwaite, 1984; Macrae, 1985). The background of proton-induced showers with random arrival directions and angles should be scattered across the field of view, and the larger angular extent of these off-axis showers suggests a further rejection technique (see section 3.2.6).

3.1.2. Development of the Durham Telescopes

The early University of Durham telescopes at Dugway reduced the field of view by combining a narrow angular acceptance with localisation of the arrival direction within the aperture by the use of fast timing of the arrival of a Cerenkov shower wavefront across a small array of identical telescopes (the Mark 1 telescope). Experience with an updated telescope (the Mark 2) suggested that, given the available resources, the concentration of effort into the production of a single, highly sensitive narrow aperture telescope would be a more productive path to the improvement of background rejection. Two similar telescopes of differing sizes (the Marks 3 and 4), were built and deployed at different sites. The later use of the two in tandem at the same site provided valuable experience of the response of a system of two large telescopes to Cerenkov showers. Effort has recently been directed into adapting and constructing a pair of large telescopes of similar capabilities to achieve extra sensitivity in Cerenkov shower detection. The promising results gained by the Whipple group using the high resolution imaging technique have

demonstrated the successful use of this method. A low energy threshold and a unique stereoscopic imaging capability are the aims of the Durham group's pair of similar telescopes. It is expected that they will deliver significant advances in revealing the TeV gamma ray sky. These prospects are discussed further in Chapter 10.

3.1.3. The Dugway Experiments

The first gamma ray telescopes designed and built by the University of Durham group were sited at the Dugway Proving Grounds in Utah, U.S.A. (40° N, 113° W, 1450 m above sea level) and operated from 1981 to 1984. The facility consisted of four independent telescopes (the Mark 1 telescope) arranged with one at each corner of a 125 m equilateral triangle and the other at the centre (Dowthwaite, 1987). Each telescope consisted of three paraxial 1·5 m searchlight mirrors in a Cassegrain optical system which increased the effective focal length from 0·6 m to 1·5 m. A 125 mm photomultiplier tube was placed 8 cm behind the Cassegrain focus of each reflector, and baffles were used to shield the tubes from direct night sky illumination and to define a geometrical aperture of 1·75°. Computer controlled alt-azimuth mounts were used to give a steering accuracy of 0·1°.

When a three-fold coincidence was detected in at least one of the telescopes, data were recorded on the time of the event, the photomultiplier responses, and the relative arrival times (accurate to <1 ns) of any signals seen in the other telescopes. Multiple telescope responses enabled fast-timing analyses to further reduce the effective angular aperture around a source. The energy threshold was estimated to be ≈1000 GeV. The aggregate count rate was about 50 minute^{-1} at the zenith, whilst each telescope counted at a maximum rate of 15 minute^{-1}.

In 1983, one of the four telescopes of the array was substantially upgraded to become the Mark 2 telescope. Its searchlight mirrors were replaced by 21 purpose-built solid aluminium mirrors of 0·6 m diameter and 55% reflectivity. These were arranged in three hexagonal groups of seven mirrors,

each forming a paraboloidal reflecting dish of focal length 1·9 m. A 46 mm RCA 8575 photomultiplier tube was placed at the prime focus of each dish to give a field of view of 1·25°. This telescope counted at a rate of ≈ 11 minute^{-1}, with an energy threshold of ≈800 GeV and was of sufficient quality to allow some significant analyses to be made on data from this detector alone. A later version, the Mark 2a, was constructed using lightweight high reflectivity mirrors manufactured by the same technique employed in the flux collectors of the Mark 3 telescope (see section 3.2.2.2).

3.2. The Narrabri Experiments

3.2.1. Choice of Site

Before the mid-1980's, the southern skies had been given little attention in TeV gamma ray astronomy, despite containing such potentially interesting objects as the Vela pulsar, the galactic central regions and Centaurus A. Therefore, a Southern Hemisphere location was desired for the deployment of a new, more sensitive telescope. A site was chosen in the Pilliga State Forest near Narrabri in N.S.W., Australia, which was previously occupied by the University of Sydney's giant cosmic ray air shower array, SUGAR. The position of the site is 149° 49' E, 30° 29' S and 260 m above sea level. The telescopes which have been deployed there are shown in Figure 3.2 and a schematic plan of the current layout is given in Figure 3.3.

Australia's eastern inland areas are a popular choice for optical astronomy due to the high proportion of clear nights (≈50% as measured at the Anglo Australian Telescope, 100 km south of Narrabri), the moderate and infrequent rainfall, and the darkness and clarity of the rural skies, coupled with the good logistical facilities of the region. A disadvantage of the climate is the frequent occurrence of convectional electrical storms in the hot summer months. The threat of lightning strikes from local storms on the equipment used in the Durham Cerenkov telescopes means that precautions must often be taken to isolate the sensitive electronic systems. Problems also

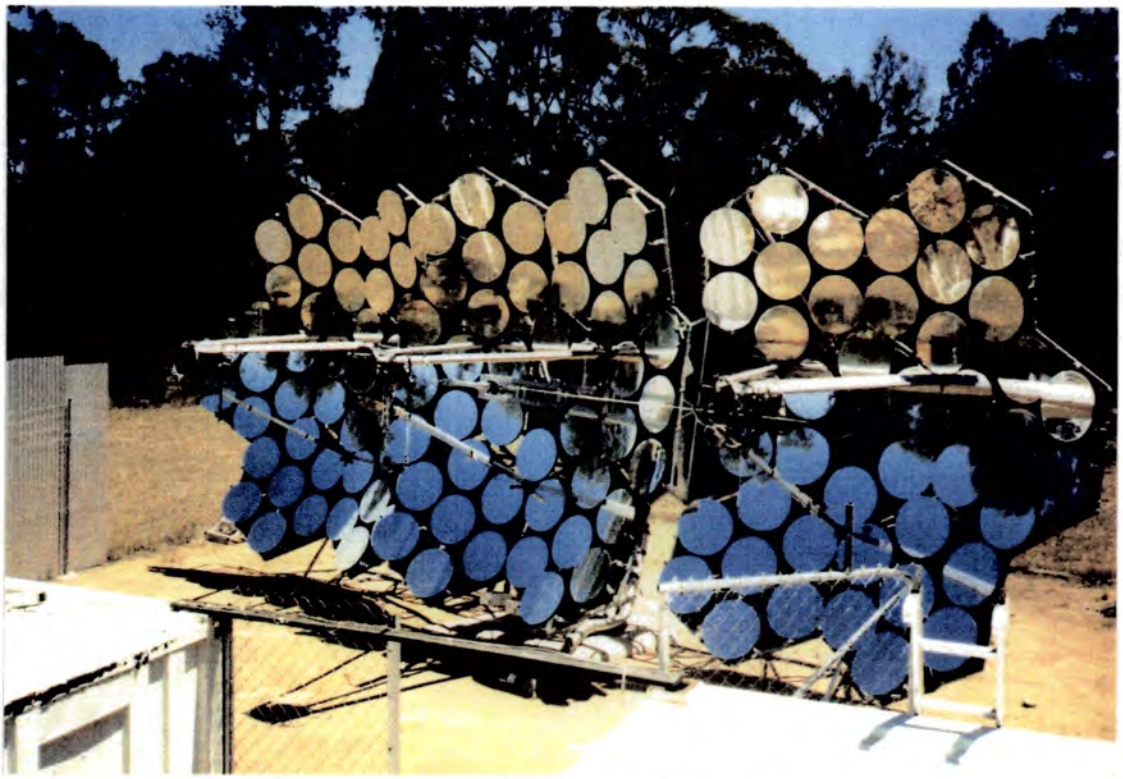

The Mark 3 Telescope

The Mark 4 Telescope

Figure 3.2 : The Durham atmospheric Cerenkov telescopes at Narrabri

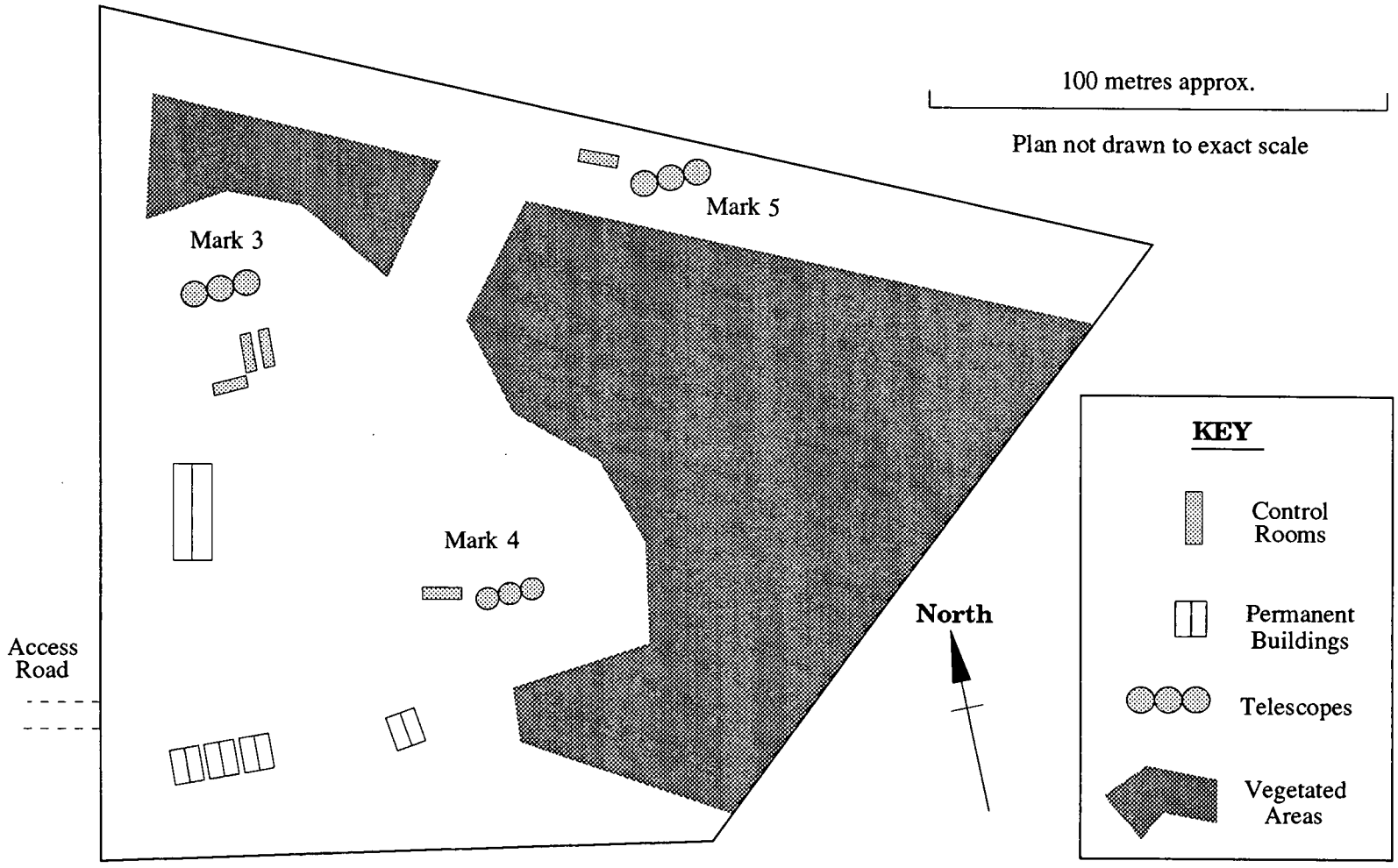

Figure 3.3 : A schematic diagram of the site of the Durham telescopes at Narrabri, N.S.W..

arise from distant night-time storms which may damage the fragile photomultiplier tubes by overillumination, or at a more subtle level may give rise to spurious coincidences in the recorded data. The former problem is countered by suspending an observation if lightning becomes too intrusive, and the latter by careful data checking techniques.

3.2.2. The Mark 3 Telescope

3.2.2.1. Telescope Mounting and Steering

The Mark 3 telescope was installed at Narrabri in 1986 September. A summary of its properties is given here, and further details may be found in reports by Chadwick (1987) and Brazier et al. (1989).The central support for this telescope is a modified military surplus alt-azimuth gun mounting. This central pillar supports the aluminium box-section structure which forms the holders of the three flux collectors (see section 3.2.2.2), and is set in a 9 m^2 concrete base.

The alt-azimuth steering is provided by d.c. servo motors, with angles being sensed by 12-bit digital shaft encoders with a resolution of 5 arc minutes. Every 100 ms the position is compared with the target directions for the source being viewed and any errors are passed via digital-to-analogue converters to the motors for suitable correction. The maximum slew rate of the steering assembly is $1^{o}\ s^{-1}$, and velocity feedback is used to damp the motion thus avoiding overshoot and damage to the telescope structure.

Any slight non-verticality of the azimuth axis is measured and compensated for in the steering software. Direct and continuous confirmation of the telescope's pointing is available by the use of a CCTV camera paraxially mounted beneath the central dish, with the centre of the telescope field of view marked on a television screen against the background star field.

3.2.2.2. Flux Collectors

The optical system of the Mark 3 telescope is based on three paraxial flux collectors, each of effective area 11 m^2 and focal length 2·45 m. The

overall surface of each is approximately paraboloidal and formed from a hexagonally based arrangement of small circular reflectors. The centre collector is made up of 44 reflectors, while the outer collectors each have 43. Each small reflector has a spherical surface of 0·6 m diameter. The design requirements for these mirrors were that they be of sufficient optical quality for Cerenkov astronomy, lightweight in construction for easy mounting on a supporting structure, of low cost, and relatively easy to manufacture in large numbers.

The method of mirror manufacture followed that used in the construction for the U.K. James Clerk Maxwell Telescope by the Rutherford Appleton Laboratory. The core material is a 25 mm thick aluminium honeycomb of cell size 8 mm and foil thickness 0·4 mm. A former of the required spherical curvature was machined from steel and polished to the required tolerance. Circular sections of the honeycomb were cut and pressed against this former before their back surfaces were bonded to a flat 1·4 mm thick dural plate and their edges to a rolled dural ring for extra rigidity. The same former was used to curve the front reflecting surface, made from 0·5 mm thick Alanod 410G Special aluminium sheet, anodised in manufacture to give a nominal 84% reflectivity. This was then bonded to the honeycomb/dural backing and the edges trimmed. A cross-section of a completed segment is shown in Figure 3.4. For a rapid production rate, the sections were cured at 150°C for two hours. Each completed mirror facet weighed about 3·5 kg.

The structure used to merge these facets into a large paraboloidal dish was constructed from welded box-section aluminium . Each mirror was mounted on this structure at three points on its backplate to allow easy adjustment for the final optical alignment.

Since some of the sections placed near the outer portions of each dish were required to produce an image in the focal plane some distance from their optic axis, they were constructed with a longer focal length (2·60 m) to give an image size comparable with that produced by the more central sections

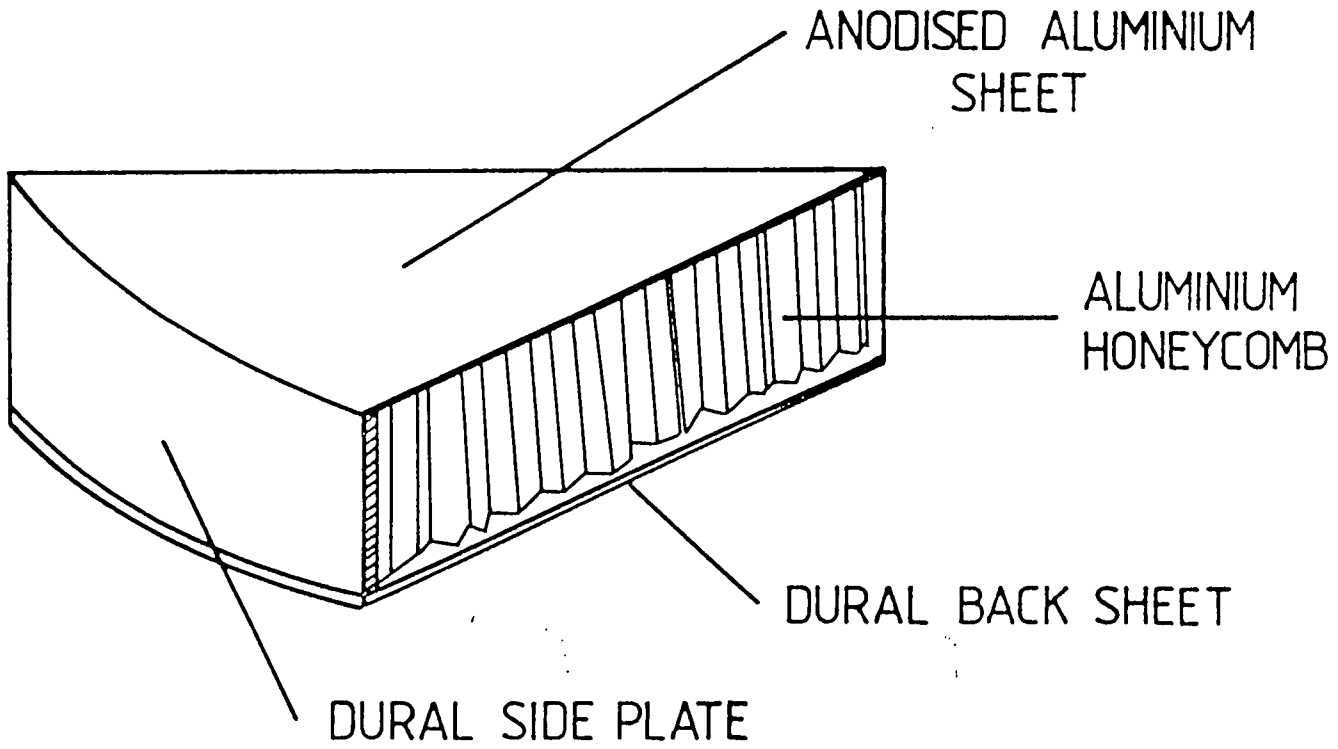

Figure 3.4 : An illustration of the construction of the mirror facets employed in the atmospheric Cerenkov telescopes operated by the Durham group at Narrabri.

(focal length 2·45 m). Tests showed that the spread of focal lengths of the mirror segments varied by only ±0·02 m from the desired values. Field tests on a stellar image in the focal plane showed a linear size of <10 mm giving an angular spot size <0·2°. The reflectivity was shown to be over 75% in the wavelength range 300-500 nm, and no noticeable loss in performance has been observed in almost a decade of operation since their installation.

A common problem during observations is that of condensation, since the mirror surfaces have a temperature at least 3-5° below ambient due to their becoming radiation coupled with the cold night sky. During the coolest winter nights, or after heavy summer rain, the temperature of the mirrors often falls below the dewpoint,and condensation can occur, which adversely affects the reflectivity and hence threshold energy and count rate. Various remedies for this problem were tested; an excellent solution was found to be the spraying of the mirrors at dusk with a high quality wetting agent. This has been successful in preventing droplet formation for up to 12 hours, and gives mirror performance equal to that on dew-free nights. A further problem on the coldest nights is that of hoar frost forming on the mirror surfaces when their temperatures fall to several °C below freezing. Although this frost may be temporarily removed by methanol spraying, the icing soon becomes too great and the poor reflectivity brings observations to an end.

3.2.2.3. Light Detector Packages

The most suitable form of detector for Cerenkov astronomy is determined by the spectrum of the radiation, which peaks at blue/UV wavelengths, and the very short duration of the light pulse. Photomultiplier tubes are very well suited to recording such a phenomenon, but further demands are also placed on them by the requirements for a low noise rate despite the high anode currents resulting from illumination from the background night sky, and stable behaviour of gain with changing illumination. After tests on a number of tubes both in the laboratory and in the field, the 46 mm diameter RCA 8575 was

selected as an acceptable compromise of good stability and reasonable noise rate, combined with a photocathode material of high quantum efficiency which showed no effects of ageing even after extended use in the Mk.2 telescope (Chadwick, 1987).

The 21 photomultiplier tubes used in the Mark 3 telescope are arranged in three groups of 7 tubes contained in cylindrical plastic holders at the focus of each parabolic reflector. Each group is hexagonally packed so that the centre tube is surrounded by a ring of 6 others, as shown in Figure 3.5. The individual tubes are held in watertight modules which are shielded both magnetically and electrostatically.

The tubes in corresponding positions in each of the three detector packages are operated in three-fold fast coincidence, with each set of three being defined as a separate recording channel. A light pulse detected above a preset threshold within a gate time of 5 ns in each of the three tubes making up a channel triggers the recording of a Cerenkov "event". The arrangement of tubes is such that the source being observed in the centre channel is surrounded by 6 off-axis channels which record information on the extent of the light pool and/or the background noise rate.

Given a focal length of 2·45 m, the tube diameter of 46 mm corresponds to 1·1° FWHM in the focal plane. However, this was directly measured by noting the anode current variation as a star transited the field of view, and found to be 0·9° FWHM. The off-axis channels were originally offset by 2° from the centre, but this was reduced to 1·5° in 1991 March after simulations indicated that this smaller spacing would increase the efficiency of the background rejection technique (see section 3.2.2.8).

3.2.2.4. Automatic Gain Control

For a fast response to the risetime of a Cerenkov pulse (≈1 ns), a photomultiplier tube must be maintained at a high voltage per stage and thus to avoid exceeding the anode current limit the signal is taken from the 11th dynode in the chain. In clear conditions, a discrimination level set at 50 mV

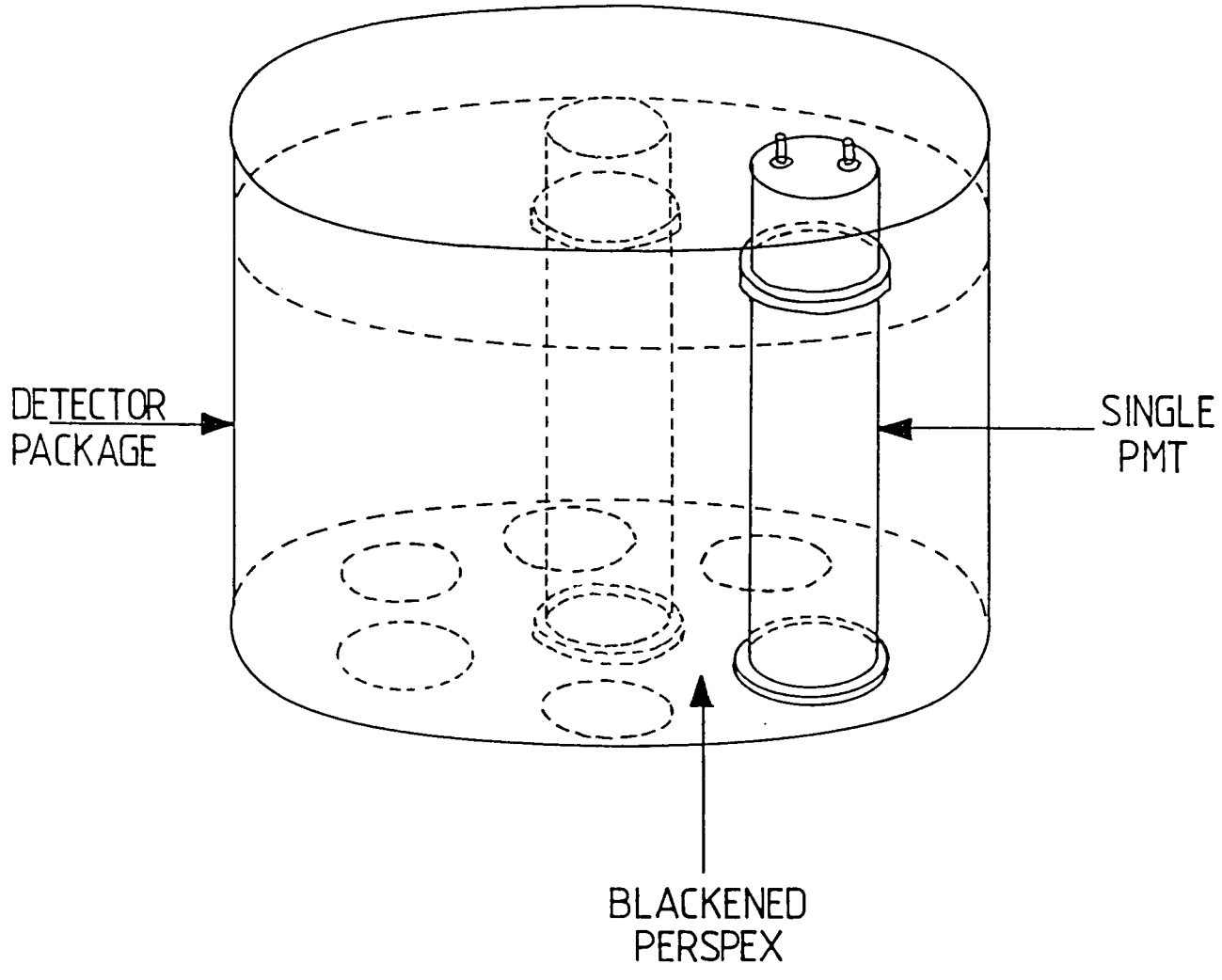

Figure 3.5 : A diagram showing the design of the detector packages placed at the focus of each flux collector of the Mk.3 telescope. The centre tube is surrounded by 6 others in order to gain the benefits of the guard-ring technique.

results in a noise rate of ≈30 kHz in each tube and a typical anode current of 25 μA. Combined with the gate time of 5 ns, this noise rate results in a three-fold "accidental" rate due to noise of only ≈3 hr^{-1}.

The entry of a star into the field of view, or some other external cause of an increase in the cathode illumination, significantly increases both anode current and noise rate. Other factors which may have a similar effect, albeit on a longer timescale, include variations in the temperature of the dynode chain, in the magnetic field present around the tubes, and in the voltage supplied to each. However, these may be countered by a careful choice of dynode chain design, photomultiplier tube housing, and voltage supply. An increase in the cathode illumination may occur over seconds rather than hours, and this may cause the gain to vary rapidly by up to 5-10%. For a cosmic ray integral spectral index of -1·6, this causes a change in count rate of a few %, similar to the excess signal expected from a gamma ray source.

The tubes' anode currents are maintained against such short-term variations by employing an LED in a feedback loop to illuminate the face of the tube. This added brightness keeps the anode current constant to within the limits whereby the detection of a gamma ray signal of 2-3% of the total count rate would not be affected. For the RCA 8575, this requires an anode current held constant to within ≈1%, i.e. about 1 μA. A drawback of this brightness control mechanism is that the noise rates in each tube are marginally increased, but this is not a problem since the three-fold coincidence in each channel eliminates virtually all but Cerenkov light flashes.

3.2.2.5. Data Recording Electronics

The electronics systems in the Mk.3 telescope were described in some detail by Chadwick (1987). The d.c. component of the anode current in each photomultiplier tube is recorded, whilst the a.c. component is magnified (x10) by a LeCroy 612A amplifier. The output signals are encoded by a charge-to-time converter, which digitises the charges recorded within a 30 ns gate, and a

discriminator unit, which identifies any pulses exceeding a 50 mV threshold value. A pulse above threshold is passed to the relevant three-fold coincidence unit, one allocated to each of the 7 recording channel, and tested for a coincidence within ≤10 ns. If such an event is seen, the channels responding are passed to a register unit which stores the "fire pattern", and the charge-to-time converter is accessed to give details on the individual tube responses.

The system for recording data is built around a Motorola 68000 based microcomputer designed by the University of Durham Microprocessor Centre, which is coupled with a CAMAC system to give a data logger characterised by great speed and versatility and a low dead-time (≈350 μs). Data recording is assigned 1 Mb of RAM and with each event occupying 64 bytes, up to 16000 may be stored in a buffer before transfer to magnetic tape. This enables bursts of events at a rate in excess of the transfer rate to tape to be held in memory. The format of each record includes details of the responses in each channel and other relevant information (see Chapter 4, section 4.1.1). System and environmental information are broadcast at 2 s intervals and recorded on tape once a minute as a "housekeeping block".

A local area network of 8 microcomputers give the user access to all of the necessary areas, in particular the central control and data recording system and the telescope steering. Dedicated displays show the current status of the anode currents and noise rates in each photomultiplier tube, the three-fold coincidence rates in each channel and the time history of these coincidence rates. Details of the weather are also displayed and an alarm screen is used to provide audiovisual warnings of any unusual or dangerous changes in the telescope environment, e.g. high wind, no events being recorded in a minimum preset interval, or an error in steering.

3.2.2.6. Timekeeping

For an experiment where the periodic analysis of pulsar signals is of high priority, accurate timekeeping is essential. Since some pulsars have

periods as short as ≈1 ms, and a series of observations may be made over an interval of several months, it is desirable to have a clock with a drift rate known to better than ≈1 ms month^{-1}. An Efratom FRK-L rubidium crystal oscillator is used in the Mark 3 telescope for this purpose and provides a 10 MHz output. This time base is scaled, and the scalers are latched on the recording of an event to provide a time resolution of 1 μs. The housing of the clock is magnetically shielded for protection against the possible presence of high field gradients in the control room which could alter the crystal's resonant frequency. A battery backup is maintained which is sufficient for 10 days' operation in the event of a power cut.

The Rb clock was initially synchronised against an off-air radio signal in 1987 January, and then compared daily during observing sequences against an Australian timing standard radio signal. Uncertainties in the precise transit time from the radio transmitter used (see below), largely due to variations in the height of the ionospheric reflecting medium, set a limit to the precision with which the relative timing accuracy could be known. The measured drift rate was 0·027±0·007 s day^{-1}. Following a restart of the Rb clock in 1990 July, a drift rate of 0·05354 ms day^{-1} has been measured.

In 1992 April a receiver for the Global Positioning Satellite system (GPS) was installed at the Narrabri site, and this is now used to provide accurate reference time signals. Measurement of time at each of the telescopes on the site is now carried out by comparing the output of the Rb clock (maintained against the GPS standard timing signal) with that from the internal clocks of the relevant CAMAC logging systems.

The availability of absolute time is particularly useful when attempting absolute phase analysis from a given pulsar ephemeris. This was initially measured against the standard signal broadcast by the Australian radio service VNG, whose transmitter was originally situated at Lyndhurst, Victoria and later moved to Llandilo, New South Wales. The transit times from these sites

to the Anglo Australian Observatory, 100 km from the Narrabri site, were precisely known by use of a portable Cs clock. The time difference between the clocks at each site were such that the uncertainties in these values were greater than the extra transit time required to reach the Narrabri site.

In 1991 January, a Rb clock was used as a portable system for comparison with a UTC standard clock at the Australian National Radio Observatory at Parkes, N.S.W.. The offsets of the portable Rb clock relative to the Parkes standard and the fixed Rb clock at Narrabri were measured. The transit time from Llandilo to Narrabri was obtained with great accuracy (the value derived was 2·69±0·03 ms). The reception of a GPS standard UTC timing signal means that absolute timing information is now available on a regular basis and to an accuracy of much better than 1 μs.

3.2.2.7. Observational Modes

The techniques of drift scanning and tracking are used with the Mk.3 telescope as with many other Cerenkov telescopes (see Chapter 2). The vast majority of observations from Narrabri are made in tracking mode, primarily for analysis of periodic signals from pulsars. The most important characteristic of the Mk.3 telescope when operating in these modes is its use of the guard ring technique to suppress the cosmic proton background (see section 3.2.2.8).

The other mode used for the Mk.3 telescope's observations is on- and off-source tracking, also known as "chopping". This has the capability of long exposures on a source, coupled with the means to detect a d.c. signal. The centre channel and an off-axis channel in the same horizontal plane are used alternately to point at a source for an interval of two minutes before the telescope is slewed in azimuth (which takes ≈5 s) and the roles of the channels are switched - the channel previously viewing the source becomes the off-source channel and vice versa. By combining the two sets of on-source data a period search may be carried out, and by searching for a count-rate excess in the on-source channel, a d.c. signal may also be hunted. The use of data from

channels viewing at the same zenith angle allows the effect of the zenith angle dependence of the count rate to be eliminated.

3.2.2.8. The Guard Ring Technique for Background Rejection

The basic premise for gamma ray event selection in the Durham telescopes is the expectation that the gamma ray events originating from a point source on the telescope axis should show a strong concentration in a field of view of about 1° around the central axis. The random background of cosmic proton events are expected to be isotropic in origin, and should therefore show no preference for any position of origin on the celestial sphere.

Thus the first step in rejecting the proton background is the choice of a minimum acceptance angle whereby the gamma ray signal is not reduced. This was designed to be 1·1° FWHM for the central channel of the Mk.3 telescope, and was later measured experimentally as 0·9° FWHM. Whilst this measure cannot directly discriminate between gamma ray and proton primary particles, the use of a narrow field of view immediately rejects many of the showers which cannot be due to gamma rays originating from the direction of the source being studied.

The next step is the operation of the "guard-ring" of 6 outer channels in anti-coincidence with the central on-source channel. An on-axis gamma ray event from the source being viewed should not cause any response in the guard-ring, the channels of which are separated from the centre by an appropriate angular distance (2° before 1991 March, 1·5° from 1991 March). A background proton event originating towards the edge of the field of view of the on-source channel may also cause a three-fold coincidence in this channel, but is also likely to spread sufficient light into one or more of the guard-ring channels to cause a coincidence. This would enable it to be identified as an unwanted contaminant and rejected from the final dataset (see Figure 3.6).

This hardware-based rejection system has therefore been routinely used for data from the Mk.3 and Mk.4 telescopes to select only those events with no

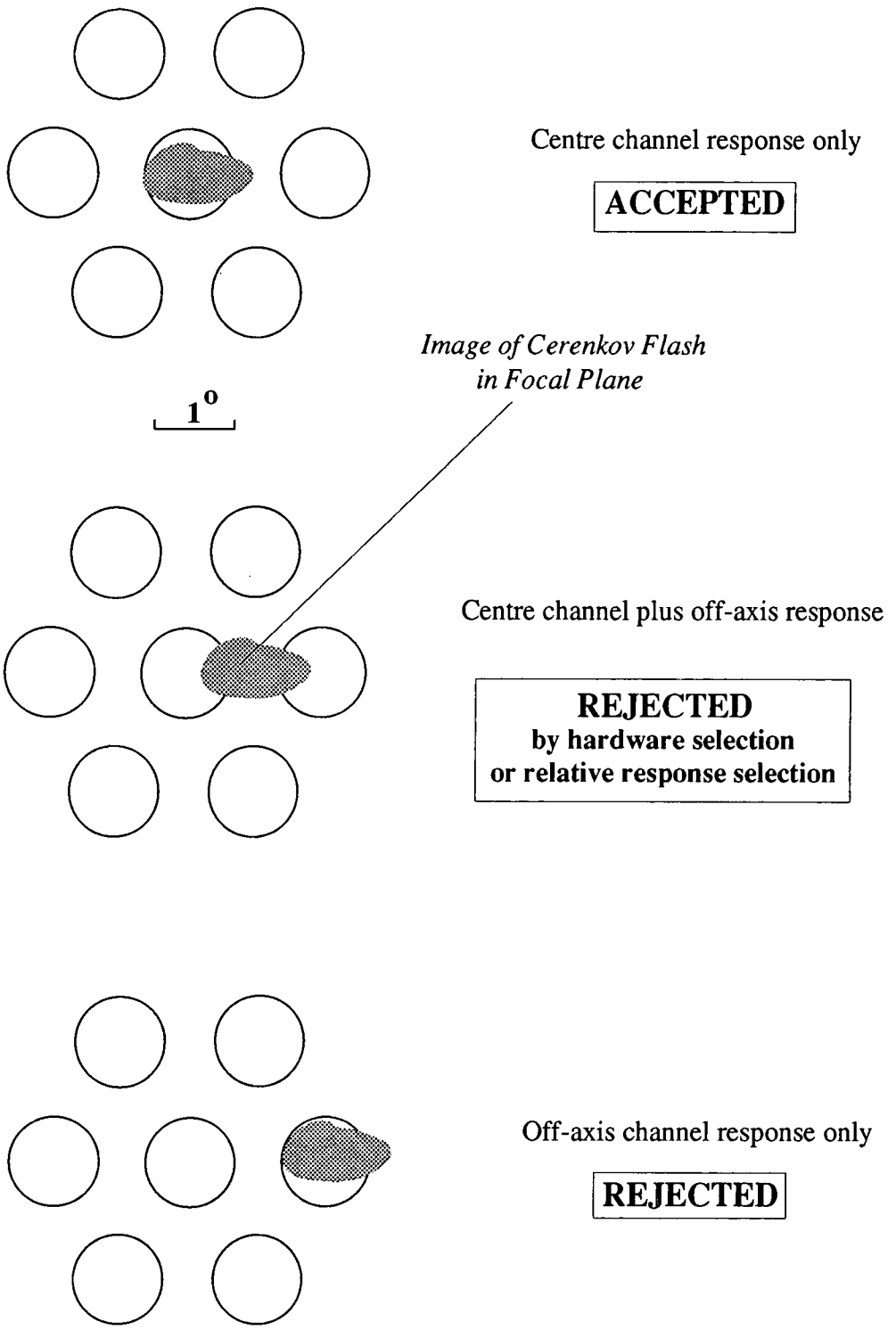

Figure 3.6 : An illustration of the principle of background rejection via the guard-ring technique.

signal above threshold in any of the guard-ring channels. With the guard-ring spacing at 2°, this rejected ≈40% of the events involving a response in the central channel, and this rejection increased to ≈60% with the introduction of the optimised closer spacing of 1·5°. In both cases, most of the gamma ray candidate events were apparently retained, resulting in an improvement by a factor of around 2 to 3 in the signal to noise ratio.

There are some disadvantages of this technique which are worth noting. Firstly, the signal to noise ratio has an absolute maximum value corresponding to the ratio of gamma rays to protons as observed even in the small field of view of the central channel. Secondly, the steeply decreasing energy spectrum of the particles being detected means that many of the Cerenkov flashes will be registered only just above the threshold of a given channel. If this is the centre channel, then even an extended shower image at the edge of the field, indicative of an off-source proton, is unlikely to cause a signal to be detected above threshold in any one of the guard-ring channels. Therefore a bias towards faint Cerenkov flashes of any origin will be introduced, though this may actually favour gamma ray selection. Thirdly, at large zenith angles, the apparent size of the Cerenkov flash decreases in size due to the greater distance of a shower's maximum development from the observer. A smaller flash from any primary particle makes it less likely to be detected across two channels, and so proton rejection is less efficient. This effect is somewhat countered by the increased scattering of the Cerenkov light during its journey through a larger atmospheric depth to the telescope (observations using the Mk.5 telescope have shown this effect to be only slight). The experimentally measured zenith angle dependence of the background rejection is shown in Figure 3.7.

3.2.2.9. A Refined Background Rejection Technique

There is a solution to the problem discussed above of the biasing of the guard-ring rejection technique towards faint flashes which do not reach the threshold discrimination level in any channel but the centre. By careful study

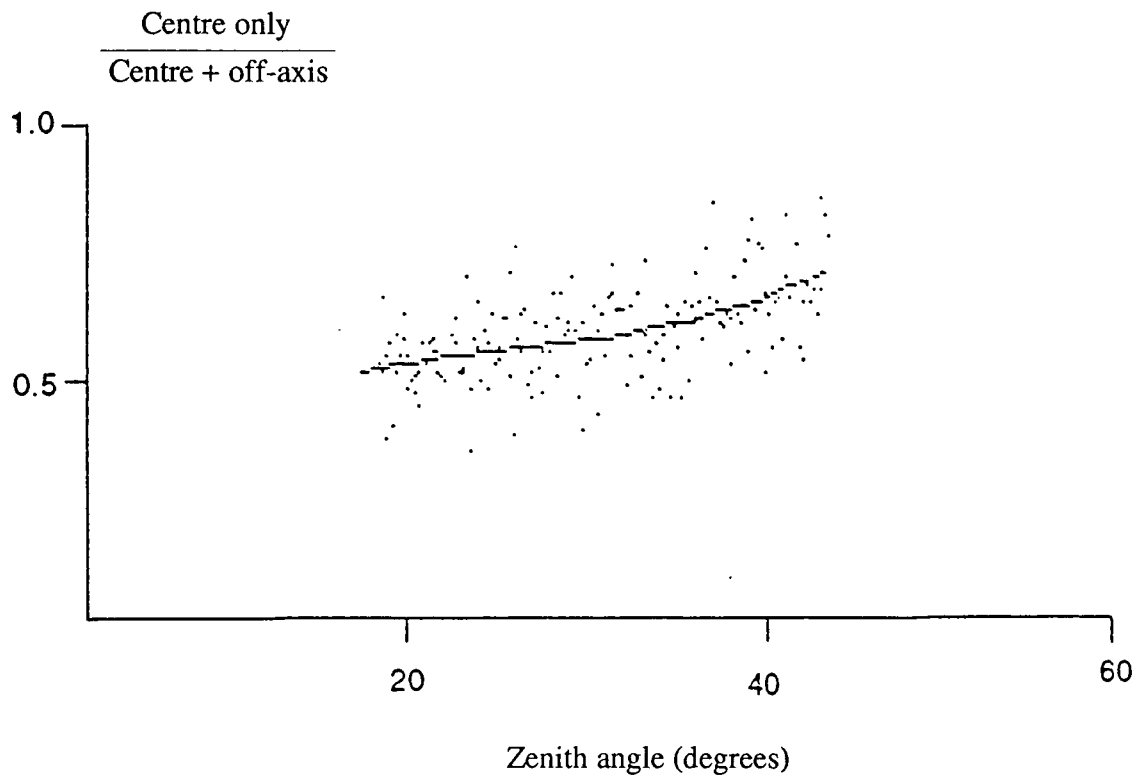

Figure 3.7 : The variation of the proportion of events accepted under the hardware selection technique with the zenith angle.

(from Brazier, 1991)

of the spectrum of pulse amplitudes (charge integrated over time) registered by each photomultiplier tube, the resultant distributions may be normalised relative to one another (see Chapter 4).The signals recorded below the threshold level in each off-axis channel may be investigated to form the basis of an a posteriori rejection technique (Brazier, 1991).

By studying the signals recorded in the guard-ring channels in an event which has caused an above-threshold response in the centre channel only, a further rejection level is possible. Bearing in mind that the aim is to remove the bias towards the selection of faint showers, the key to this technique is the measurement of the relative, rather than absolute, responses in the outer channels. The criterion used is to reject any event which has a response in any of these channels greater than a preset percentage of the response measured in the centre channel. This enables Cerenkov flashes of any intensity to be treated with equal weight in the rejection procedure. The only limitation for the very low responses is then determined by the inherent photomultiplier tube noise.

Although a minority of events will scatter light into three or more channels, the hardware selection already carried out favours events with a significant response in only one off-axis channel. About 80% of events are found to be of this nature after the hardware selection. Therefore, the least complicated procedure, that which rejects an event based on the relative amplitude of the highest guard-ring response rather than the total guard-ring response, is quite acceptable. The application of this rejection technique as part of the routine procedure of processing of data recorded using the Mk.3 telescope is described in Chapter 4.

3.2.2.10. Telescope Performance

Prior to the installation of the Mk.3 telescope a Cerenkov event count rate of about 75 minute^{-1} *per channel* was predicted. In operation, this rate was found to be in good agreement with that observed, and subsequent

improvements in the optical alignment, operation of the photomultiplier tubes, and recording electronics have enabled count rates in excess of 120 minute^{-1} *per channel* to be recorded in the zenith. The dependence of count rate C on the zenith angle Z has been found to be approximately

$$C(Z) = C(0) \cos^n Z \ , \qquad (3.1)$$

where the experimentally observed index n=2·3 ± 0·5.

The energy threshold of the early Durham telescopes at Dugway could be calculated by accurate measurement of the effective area and acceptance angle via inter-telescope coincidences. A combination of simulations with these experimental measurements allowed an 800 GeV threshold to be assigned to the Mk.2 telescope (Chadwick et al., 1985). This was scaled using the appropriate parameters to give an initial threshold of 300 GeV in the zenith for the Mk.3 telescope, increasing to about 400 GeV at a zenith angle of 50° (Brazier et al., 1989). The estimated threshold has since been reduced to around 250 GeV, in line with the increased count rates attainable. The systematic uncertainty in these threshold values is estimated to be ≥50 GeV.

3.2.3. The Mark 4 Telescope

3.2.3.1. Design and Operational History

The Mark 4 telescope was originally designed as a smaller, portable counterpart to the Mk.3 telescope. With the success of the Dugway experiments in detecting TeV gamma ray sources such as Cygnus X-3, it was felt that a more sensitive Northern Hemisphere telescope was a worthwhile investment, especially when based on experience gained from the similar Mk.3 design. This smaller telescope was first deployed in 1988 April at the Observatorio del Roque de los Muchachos on La Palma in the Canary Islands (17° 53' W, 28° 46' N, 2500 m above sea level). After two successful seasons of operation, it was transported in 1990 April to a position 100 m south of the Mk.3 telescope at the Narrabri site.

The designs of the Mk.4 flux collectors and photomultiplier packages are essentially identical to those of the Mk.3. The major difference is the number

of small 0·6 m mirrors, manufactured as for the Mk.3, which form each parabolic dish. A total of 54 are used to give each dish an effective collection area of 6 m^2. The support structure is somewhat lighter and less strongly supported than that of the much heavier Mk.3 and this gives the Mk.4 its portability.

Since the Mk.4 telescope's relocation to the Narrabri site, it has often been operated in tandem with the Mk.3 telescope (see section 3.2.3.2). When both have been used to view the same source near the zenith, the count rate of the Mk.4 has been found to be about 60% that of the larger telescope as would be predicted by scaling the relative areas of the flux collectors. Assuming a cosmic ray spectral index of -1·6 and a Mk.3 telescope threshold of 250 GeV, this suggests an energy threshold of about 450 GeV.

3.2.3.2. Simultaneous Observing with Mark 3 and Mark 4 Telescopes

When both Mk.3 and Mk.4 telescopes are viewing the same object, the proportion of Cerenkov events seen by both can measured by identifying the coincidences in event arrival times registered by each telescope. The fraction of common events has been experimentally shown to be of the order of 15-20% for a source at a zenith angle less than about 50° (e.g. the simultaneous observations of Vela X-1 discussed in Chapter 7). At greater zenith angles, this proportion increases due to the elongation of the Cerenkov light pool on the ground and the north-south alignment of the two telescopes. The high number of common events then makes the less sensitive Mk.4 telescope most useful in independently confirming variations in count rate, and short-lived bursts of events from a source under observation. The value of its presence in this respect was amply illustrated when both telescopes independently recorded a strong burst of events from the direction of AE Aquarii (Bowden et al., 1992b). The datasets recorded contemporaneously by Mk.3 and Mk.4 on the same source may be combined to produce a single enhanced dataset by identifying common events and including the Mk.3 event record only in the final dataset.

3.2.4. The Mark 5 Telescope

3.2.4.1. A New Atmospheric Cerenkov Telescope

The Mark 5 telescope was developed as a half-scale prototype to investigate the various capabilities of a large Cerenkov telescope. Its design combines a limited imaging capability with the benefits derived from a triple fast-coincidence triggering system. It was installed at the Narrabri site in 1992 April, 100 m east of the Mk.3 telescope. The design of the telescope is briefly summarised here and in Bowden et al. (1991a). Further details will be presented by Dickinson (in preparation).

3.2.4.2. Flux Collectors and Telescope Structure

The three flux collectors are each parabolic in form, each with a collecting area of 9·2 m^2. Each collector is made up of twelve identical wedge-shaped segments of area 0·83 m^2 and focal length 3·32 m, weighing 12 kg each. These were constructed using the method given in section 3.2.2 for the circular segments in the Mk.3 and 4 telescopes. Each front reflective surface was clamped to the former and shaped by vacuum suction. After bonding to an aluminium honeycomb core and backplate each segment was cold-cured to ensure the quality of the final mirror surface. The optical quality of each finished segment is sufficient to give an image of an infinite point source of $\leq 0{\cdot}2^\circ$ FWHM. The flux collectors are placed on an aluminium box-structure backing, with each segment mounted at three points to allow for ease of alignment. A new alt-azimuth mount was designed for the pointing of the telescope, which is based on a purpose-built system of d.c. servo-motors driving gears on the altitude and azimuth axes. The telescope attitude is constantly sensed by absolute 11-bit optical shaft encoders.

3.2.4.3. Light Detector Packages

The left and right flux collectors each focus light onto a detector package in the focal plane made up of 7 photomultiplier tubes with active diameters of 46 mm. The 3·32 m focal length means that each tube has an angular acceptance of $0{\cdot}7^\circ$; the axis of each is separated by $1{\cdot}0^\circ$. A Winston

cone is placed around each tube face to act as a light guide thus increasing the efficiency of light collection. The central detector package is an imaging "camera", consisting of 19 hexagonally packed 23 mm photomultiplier tubes, each used as a separate "pixel", surrounded by an outer ring of larger tubes. The centre 19 provide a coarse (0·5° per pixel) image of the Cerenkov light flash. The routines used to compensate for the varying levels of thresholds and gains across these imaging tubes will be described elsewhere (Dickinson, in preparation).

3.2.4.4. The Pulse Timing Facility

A fourth parabolic flux collector has been positioned above the central dish for use in temporal pulse-shape studies of Cerenkov events. Constructed from 12 segments, it has a smaller area of 6 m^2 but its focal length of 3·32 m is identical to the larger dishes. A single 125 mm fast photomultiplier tube is positioned centrally in the focal plane. If a three-fold coincidence is detected in the main telescope, the signal from this large tube is passed to a pulse digitiser unit which provides fast analogue-to-digital conversion for the total response plus up to 13 portions of the pulse each lasting several ns and overlapping by 1 or 2 ns. From these processed signals, the shape of the Cerenkov flash can be reconstructed, based on its risetime, duration and amplitude, and a discrimination based on the expected differences of photon and proton showers may be attempted. Results will be reported elsewhere.

3.2.4.5. Performance of the Mk.5 Telescope

In the observations made with this telescope to date, three-fold coincidence rates of $\geq$120 $minute^{-1}$ have frequently been achieved, suggesting an energy threshold very similar to that of the Mk.3, i.e. about 250 GeV. The data are initially stored on a local hard disc drive before transfer to a demountable 44 Mb hard disc for transportation to Durham. As in the Mk.3 telescope, timekeeping is maintained by an local Efratom FRK-L Rb clock, which sends 1 MHz pulses to the CAMAC system to be scaled and latched when an event

is recorded.

The anode currents and noise rates from each photomultiplier tube, the three-fold coincidence rates for each recording channel, and other system and environmental data are recorded by purpose-built electronic systems and displayed on monitor screens. The addition of the Mk.5 telescope to the facility at Narrabri has brought about the construction of a master control room where operational and environmental data from all of the telescopes in use are constantly monitored in real time via broadcasts from each over the local area network.

CHAPTER 4 - DATA PROCESSING AND ANALYSIS

4.1. Data Processing

4.1.1. Format of Records

A fundamental part of the operation of the University of Durham atmospheric Cerenkov telescopes is the maintenance of a continual record of systematic and environmental information which may later be cross-checked with any abnormalities in the data recorded on the detected Cerenkov light. To this end, three separate computer files are formed containing the essential information pertaining to each observation.

At the beginning of each night of operation in Australia, a run-start file is recorded. This contains a brief description of the relevant weather details, the names of the observers, the appropriate civil and Julian date, and information on the status of the telescope. This will normally be the only run-start file recorded for that date.

Since the telescope is generally used to observe two or three objects in the course of a full night, a source-start file is also produced at the initialisation of each independent observation. This consists of the name of the source and its coordinates on the celestial sphere, the start time of the observation, steering information, and any comments made by the observers.

The central data file consists of the records of the Cerenkov light events detected by the telescope. Each event record has a size of 128 bytes (or 64 bytes if recorded during the dead time of the system) and holds temporal, directional and amplitude information for each Cerenkov flash, as follows :

(a) the Universal Time of each recorded to an accuracy of 1 μs,

(b) the photomultiplier channels with responses exceeding the preset 50 mV threshold, as well as an indication of the channel which was viewing the on-source position,

(c) the digitised responses recorded by each photomultiplier tube within

the 30 ns gate time, as scaled by analogue-to-digital converters with 11-bit resolution,

(d) the target and actual steering positions of the telescope.

In addition to this information, details of the instantaneous rate of the single-fold responses and anode currents in each photomultiplier tube are recorded at intervals of one minute.

The data files from the Mk.3 telescope are recorded on magnetic tapes with a storage capacity of 67 Mb. Data from the Mk.4 and Mk.5 telescopes are recorded on local hard discs for later transfer and storage on portable discs.

On return to Durham, the run-start, source-start and prime data files are transferred to a central hard disc for routine pre-analysis processing. The three relevant files for each source observation are processed in such a way as to form two complementary files. The first contains information from the background monitoring of the anode currents and single-fold responses for each photomultiplier tube in addition to details of the weather and the performance of the telescope steering throughout the observation. This 'housekeeping' file is archived for later reference.

The second processed file is the larger and more important, and contains the key information extracted from each Cerenkov event record. This ASCII format prime data file includes the arrival time of the event, a list of channels triggered by a signal above the 50 mV threshold, the on-source channel, a marker representing the telescope with which data was being recorded, and the pulse height integrals from each photomultiplier tube expressed in decimal form. An example of the format of an actual event record is shown in Figure 4.1.

4.1.2. Correction of Event Times

4.1.2.1. Adjustment for Motion within the Solar System

Once processed to the required format, each event in the prime data file contains an arrival time of the event measured with respect to the reference

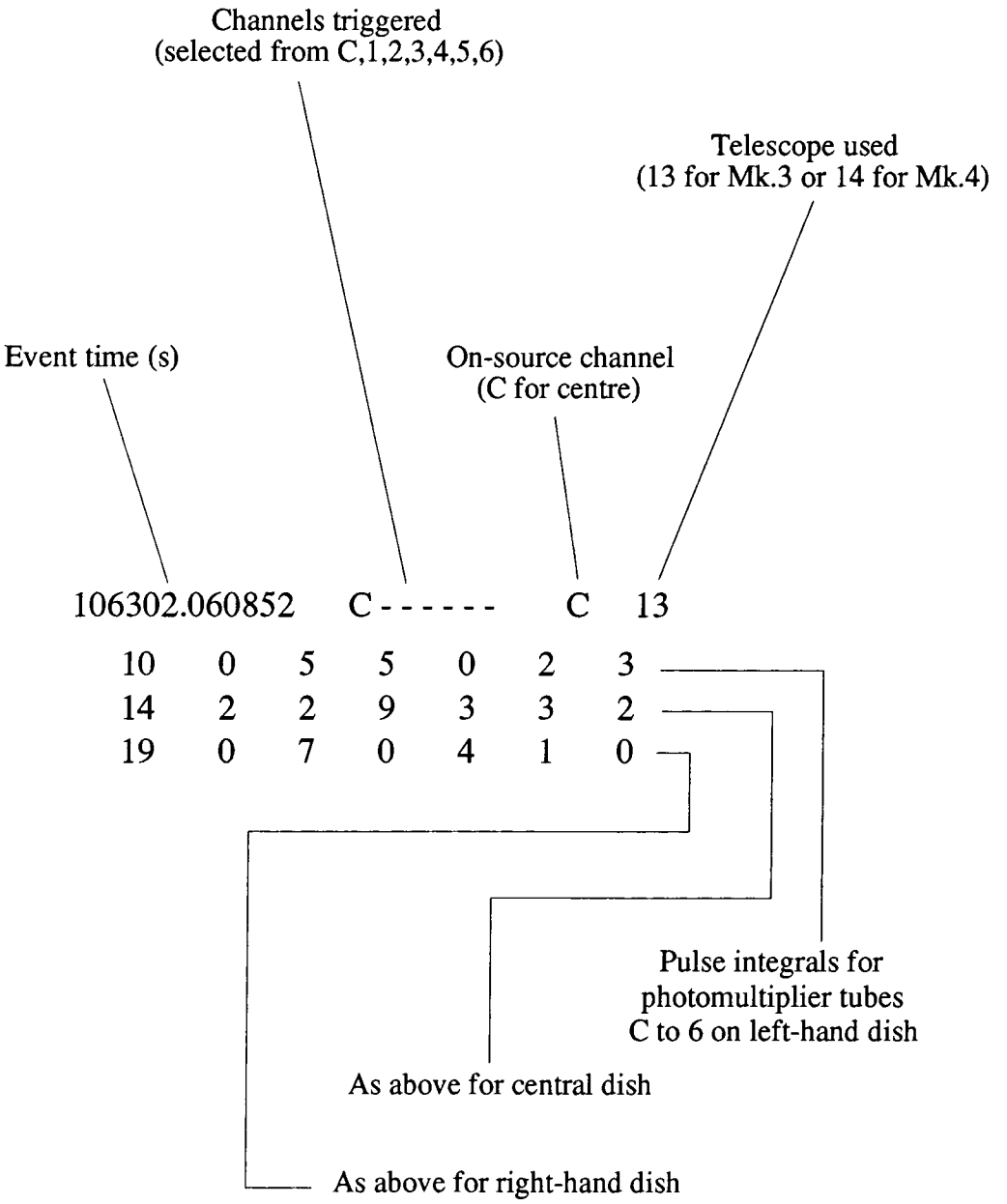

Figure 4.1 : An example of the format of an actual event record from a datafile generated by a Mark 3 telescope observation.

frame of the telescope. However, this frame is not stationary with respect to that of the source being observed, which is presumably the origin of the gamma ray photons which are being sought. Therefore, a set of corrections must be made to allow for the Doppler shifting effects introduced by the relative velocity of the detector and regain the relative timing information present in the flux of celestial photons at the time of their emission.

The transformation to the barycentre of the Solar System is carried out using the JPL DE2000 Earth ephemeris (Standish, 1982). The first correction is made to compensate for the motion of the telescope around the centre of the Earth with respect to the direction of the source being observed. The component of the Earth's orbital motion with respect to the source direction is also allowed for by further correcting the detector position to the barycentre of the Solar System. The final stage involves taking account of the relativistic effects introduced by (a) the high velocity of the Earth's motion around the Sun, and (b) the difference in gravitational potential between the position of the telescope and the barycentre.

4.1.2.2. Adjustment for Motion within a Binary System

The actual site of emission of gamma ray photons may have a significant orbital velocity with respect to the stationary reference frame of a binary system. Since the components may have masses considerably greater than that of the Sun, the orbital velocities of each may be considerably greater than those found in the Solar System, making the corrections to the rest frame of the binary system of great importance.

The correction to the barycentre of the binary system requires knowledge of a set of parameters, known as the orbital ephemeris. For high mass X-ray binaries, the X-ray source is a neutron star orbiting a non-degenerate primary star of 10-20 times greater mass, and therefore the barycentre of the system will be near to the centre of the more massive primary. In low mass X-ray binaries, the compact object is often the more massive of the pair and is thus very near to the barycentre, describing only a very small orbit. The elements

essential to the barycentring procedure are :

(a) the projected semi-major axis of the orbit of the X-ray source ($a\sin i$ where i is the angle between the pole of the orbit and the line of sight),

(b) the binary orbital period, P_b, and its long-term first derivative, if known,

(c) a reference epoch T_o referring to the time of passage through a particular orbital phase (usually mid-eclipse of the X-ray source),

(d) the eccentricity, e, of the orbit (in which case the reference epoch may be taken as periastron passage, the time of closest approach of the X-ray source to its companion star).

The correction to be made is briefly discussed here for the case of a circular orbit. Note that modifications must be made for an eccentric orbit, but the greatest eccentricity for any of the high mass X-ray binaries discussed in the present work is only 0·08 (Vela X-1), so that the deviation from the treatment for a circular orbit is only small.

The motion in the line of sight to the observer of an object in a binary orbit will cause a Doppler shift to be introduced into the relative emission times of the photons. This shift may be eliminated by adjusting the site of emission of the photons to the plane perpendicular to the line of sight which contains the barycentre of the system. This may be done by simply calculating the light transit time from the source to this plane. Given the value of the orbital period and a reference epoch, the contemporary orbital phase φ, as measured with respect to a value of 0 at mid-eclipse, may be calculated. Knowledge of the value of $a\sin i$ allows the light transit time t to be expressed as :

$$t = a\sin i \,.\, \cos\varphi \,.\, c^{-1} \,, \qquad (4.1)$$

where c is the speed of light (which is unity if $a\sin i$ is expressed in the conventional notation of light seconds). The geometry of the correction is shown in Figure 4.2. This transit time is subtracted from the arrival time of

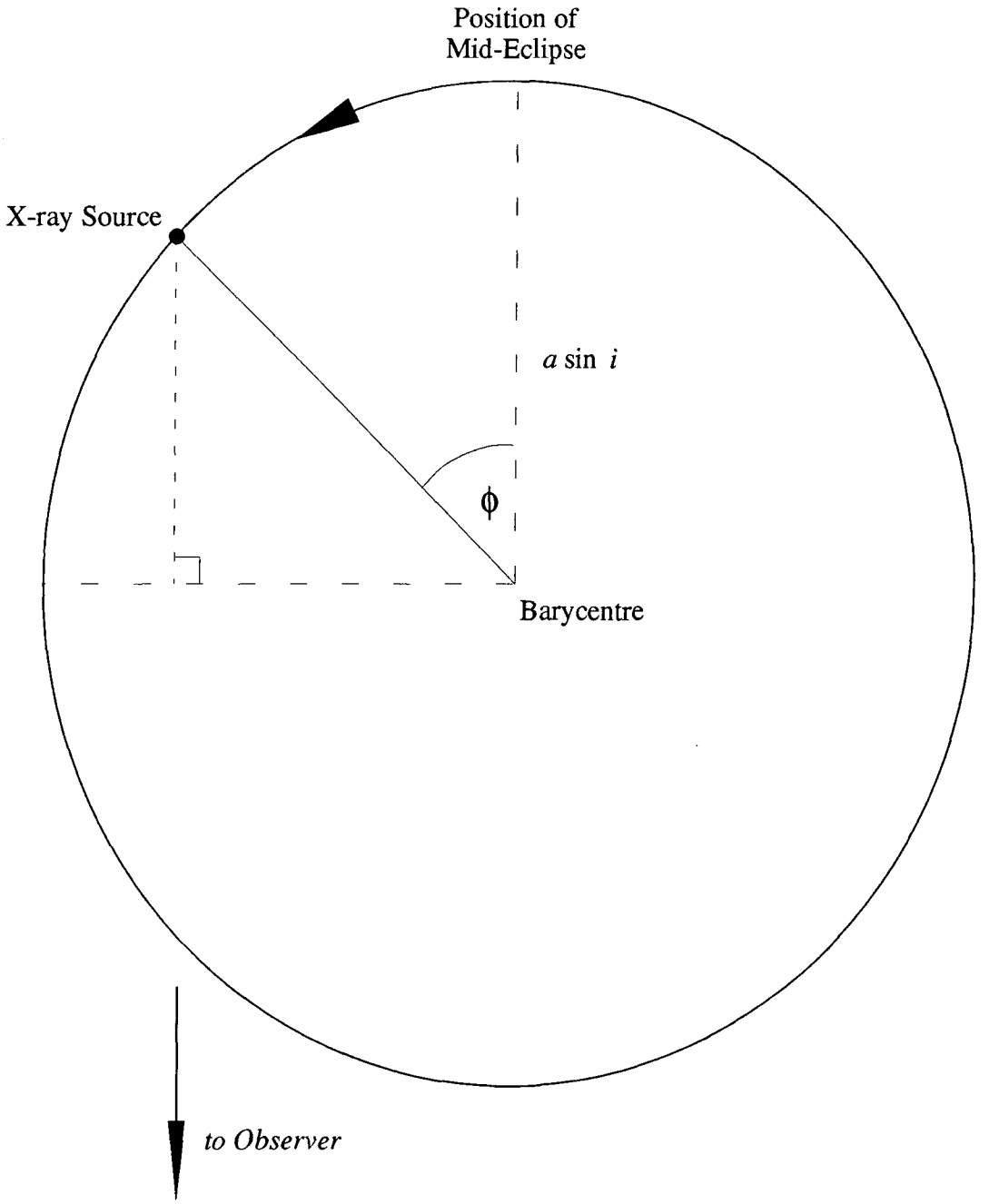

Figure 4.2 : A diagram showing the geometry for the transformation of event times to the barycentre of an X-ray binary system.

an event corresponding to the source being located at a phase φ. The full set of events may be similarly transformed to an origin at the barycentre of the orbit. A technique which extends this correction to search for any gamma ray emission site displaced from the X-ray source is described in Section 4.2.3.

4.1.3. Preparation of Processed Data for Analysis

4.1.3.1. Normalisation of Pulse Integrals

Once the data have been converted to a format suitable for analysis, and the event times have been corrected for the motions of the source and the detector, the records of the pulse integrals for each event may be used to preferentially select those most likely to originate from gamma ray progenitors. To obtain full benefit from the available information on the pulse integrals, it is necessary to normalise the spectra of these values from each photomultiplier tube to enable the consistent application of the relative response rejection technique.

By taking a large dataset of all events recorded during a single observation (typically tens of thousands) the distribution of the pulse integrals may be constructed for each individual photomultiplier tube. This spectrum is found to be smooth and single-peaked with most events having a pulse integral value below $\approx$20, caused by the coupling of the general faintness of the Cerenkov flash with the fact that not all of the recorded events will give a signal above the 50 mV threshold in every individual tube. Figure 4.3 shows typical pulse integral spectra for two of the photomultiplier tubes recording data during an observation of Vela X-1. The pulse integral values are simply the decimal forms of the 8-bit numbers registered.

Each such spectrum may be defined by a pedestal offset and a gain, characteristic of the photomultiplier tube used. Whilst some variation is seen in the gains between different tubes, the quantised nature of the digitised pulse integrals makes it difficult to correct the shape of the distribution and in any case the variation is only $\approx$15% (Brazier, 1991). More important to the normalisation of the spectra is the simpler calculation of the pedestal

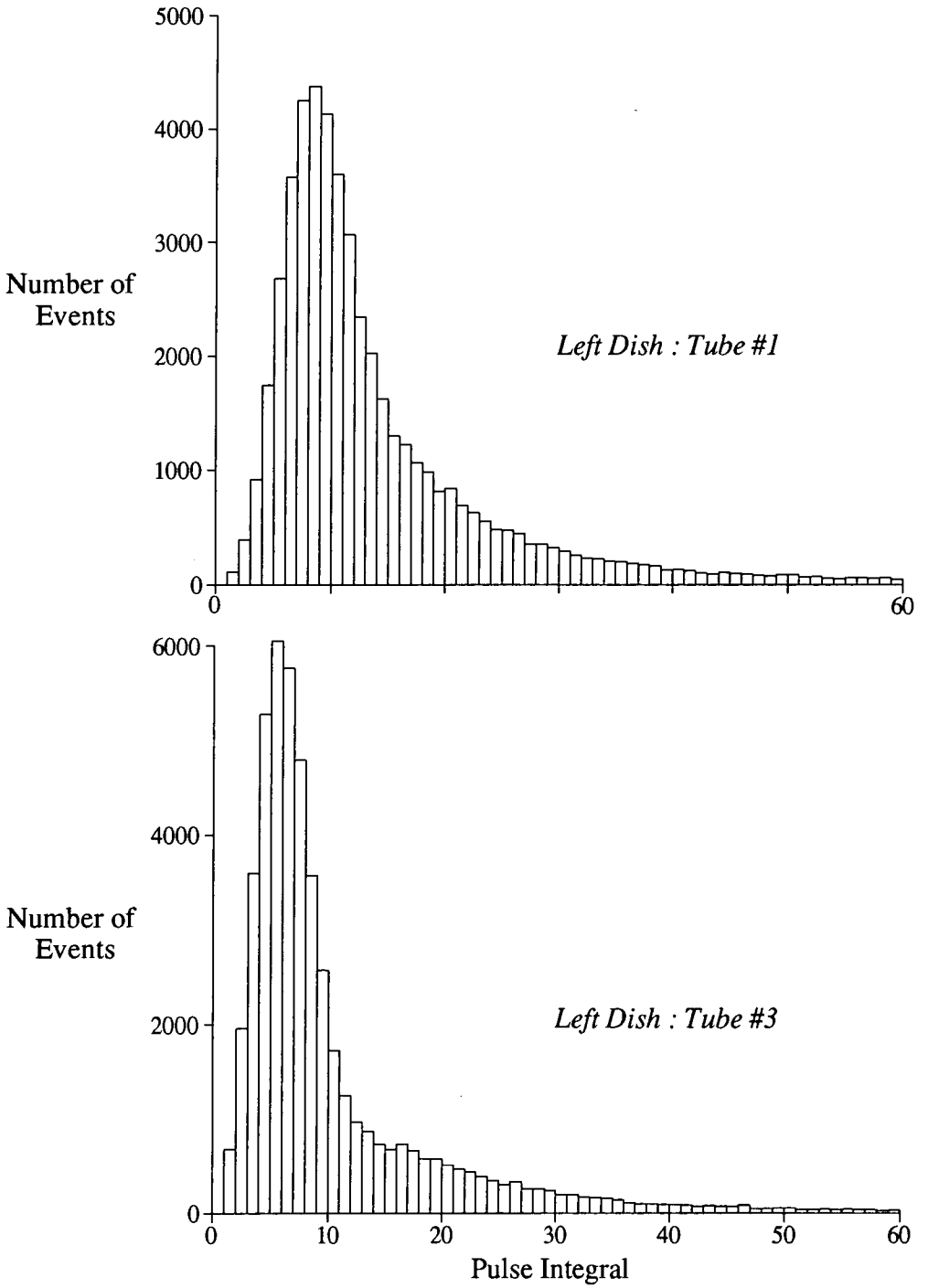

Figure 4.3 : Distribution of pulse integrals prior to normalisation for data recorded in two comparison tubes during the same observation.

offset. The peak of the distribution corresponds to the mode and this is chosen as preferable to any other estimate of the average since it is not weighted by irregularities in the distribution. Lightning-induced events may saturate the photomultiplier tubes and hence cause a spurious peak at the highest 8-bit pulse integral value of 255. Alternatively a large number of faint events may be recorded below the origin of the pulse integral scale, being registered as zero, if the mode is only several bits from this zero value. To eliminate false offsets due to these effects, the range of pulse integrals used to measure the mode extends only from 1 to 99.

Since very few events are found to have pulse integrals below a value of 3, the pedestal offset is defined as (mode - 3) for a distribution derived from a given observation. A set of pedestals is calculated for every photomultiplier tube for each observation and the appropriate values are subtracted from each of the pulse integrals in order to normalise the relative distributions. Figure 4.4 shows the same datasets as used for Figure 4.3 after the application of this technique, and it is seen that the modes of each distribution are now aligned. Typical experimentally derived pedestal values are in the range -1 to 10. Whilst the effect on the distribution may appear only slight, the use of this technique in conjunction with a relative response threshold of ≈50% or less can result in a reduction of 5-10% in the number of events accepted as compared with the same selection applied without the normalisation technique.

In the present work, the normalisation technique using pedestal values is applied for the first time to the full database on SMC X-1 and X0021-72, and also to recent observations of Centaurus X-3 and Vela X-1.

4.1.3.2. Background Discrimination and Event Selection

The dataset is optimised for analysis purposes by initially rejecting those events which have caused a response above threshold in any off-source channel. This requires the application of the hardware selection technique

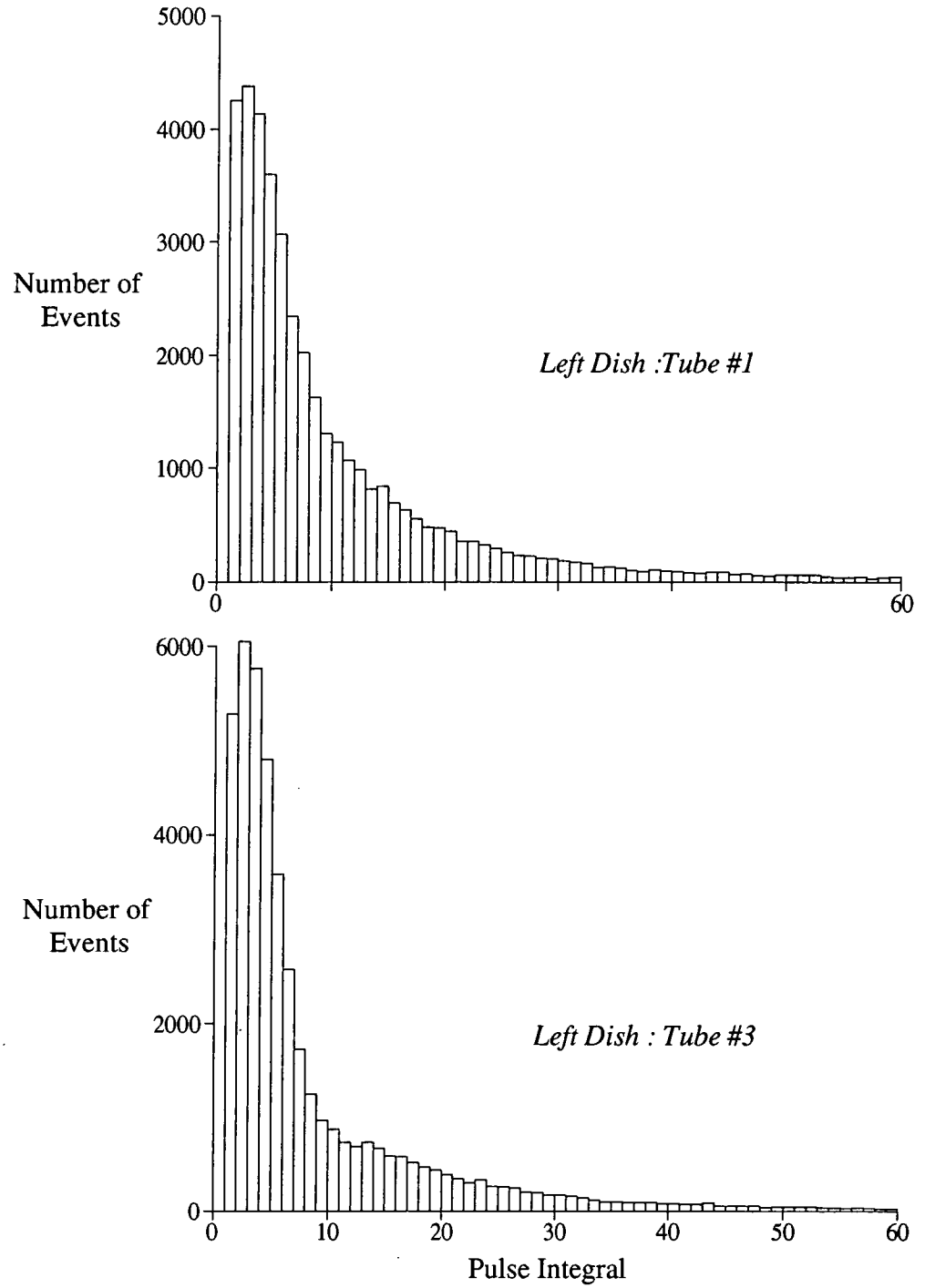

Figure 4.4 : Distribution of pulse integrals after normalisation for data recorded in two comparison tubes during the same observation.

(c.f. Figure 4.3)

discussed in Chapter 3, and is carried out in the software system by checking the portion of each event record which lists the channels which have registered a three-fold coincidence above threshold. Only events which show such a response in the on-source channel alone are accepted for inclusion in the filtered dataset. For the data recorded by the Mk.4 telescope, the hardware selection represents the final stage of data processing since the electronic systems used for measuring pulse integrals do not allow further selection.

Once the pulse integral records from each event recorded by the Mk.3 telescope have been normalised using the method described in the previous section, the data are subjected to further selection by the application of the relative response threshold technique. The algorithm used for selection based on the relative response of the guard-ring tubes is very simple :

Accept IF (On-source response) x T% ≥ (Each off-source response),

where T is the preset threshold percentage. The problem is then the setting of the threshold percentage. Setting a threshold percentage of zero would severely constrain events to those with no scattered light in any outer channel, and in practice a threshold of ≤10% rejects almost all events due to the low noise level present in each photomultiplier tube. As the size of the dataset is reduced as T decreases, an optimum T must be found where the events contributing to a genuine gamma ray signal form a maximum proportion of the total data. A spurious signal not rejected by the hardware selection would be expected to weaken under the relative response selection being part of a noise background with no gamma ray characteristics.

The decrease in the apparent size of the Cerenkov flash with increasing zenith angle has been shown to have little effect on the relative response rejection technique (Brazier, 1991) probably due to the hardware selection, which does depend slightly on zenith angle, having already been carried out. The favoured percentage thresholds for a number of sources have been estimated by applying the technique at different threshold rejection levels to datasets

found to show some evidence of periodic gamma ray emission under the hardware selection. Enhancement of the periodic signal has been consistently demonstrated, with the favoured thresholds usually in the range 30-50%.

This event selection technique is therefore routinely applied to all observations made with the Mk.3 telescope. A new object under observation, or one for which no strong periodic gamma ray signal has ever been identified, is routinely assigned a percentage rejection threshold equal to that for one of the threshold-tested sources at a similar zenith angle. Once the data from each observation have been selected in this way, a search for evidence of a TeV gamma ray signal in the dataset may be carried out using the techniques detailed in the next section. A flowchart summarising the main stages of data processing is given in Figure 4.5.

4.2. Analysis Techniques

4.2.1. Statistical Tests

4.2.1.1. Choice of Appropriate Treatment

All of the objects studied in the present work are X-ray pulsars with reasonably well-known pulse periods. These differ from the more common radio pulsars in a number of respects. Whilst isolated radio pulsars, such as the Crab pulsar, may be studied almost continually and show an extremely steady time signal, some more reliable than the best terrestrial atomic clocks, the pulse sequences from X-ray pulsars may show significant variation on timescales of hours or days, the period increasing or decreasing in an unpredictable manner (e.g. Nagase, 1989). It is therefore not possible to derive the expected period for a given observation with any great precision, due to the transient nature of X-ray satellite observations as much as to the transient behaviour of the X-ray emission. Thus it is simply not possible to gain and utilise absolute phase information on the periodic signal from these objects, which is a disadvantage in the effort to increase the statistical significance of a detection.

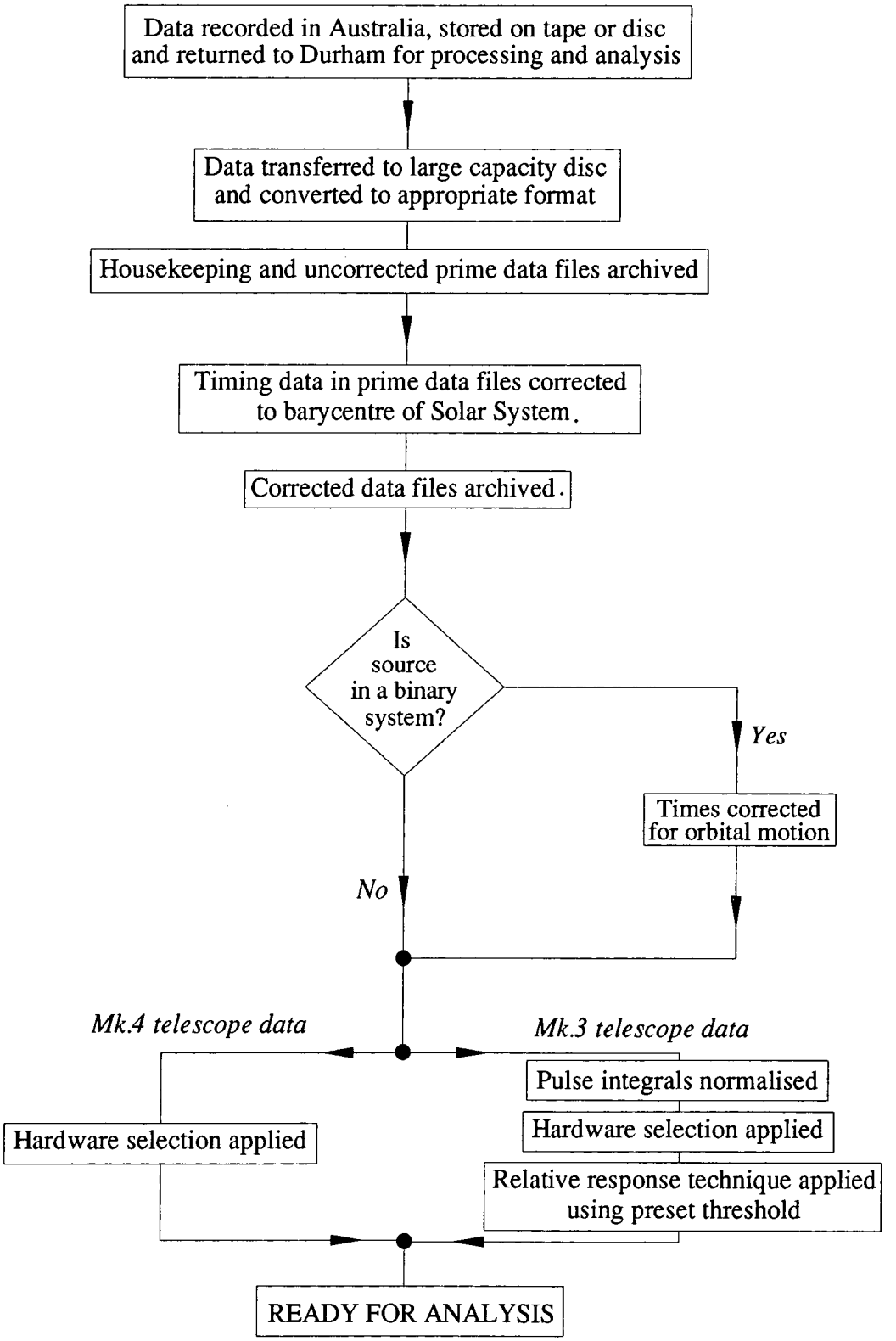

Figure 4.5 : A simplified flowchart showing the procedure of pre-analysis data processing.

Another factor to be taken into account is the generally broad nature of the peaks seen in the light curves of X-ray pulsars. Duty cycles are typically of the order of 20-60% and show considerable variation with energy, frequently switching to a multi-peaked structure. Therefore any statistical test designed to detect such an irregular periodic pulse should be the most powerful in recovering a significant signal from a time sequence within which the behaviour of the signal cannot be predicted.

The method used for testing for periodicity when a known period with a known absolute reference phase is believed to be present is simple "epoch-folding". This requires a set of "bins" representing relative phase intervals to be defined, whereupon each event in the time series may be assigned to a particular phase interval so as to produce an overall light curve. This may be tested for uniformity by the application of one of two methods. Pearson's χ^2 test may be used to evaluate the deviation of the number of counts in each from the respective expectation values (Leahy, Elaner and Weisskopf, 1983). Alternatively if the width and precise position (i.e. absolute phase) of the expected peak in the light curve are known then a very powerful binomial test may be carried out to compare the frequency of events in the preselected "preferred bin" with those in the rest of the light curve. However, in the case where the expected period is unknown, such a binning procedure can only be carried out in arbitrary fashion, possibly splitting a peak between two or more adjacent bins. With the number of bins also becoming a free parameter, the statistical significance of any signal detection must inevitably be reduced.

4.2.1.2. Circular Statistics

The preferred method of searching for an imprecisely known period in a sample of data in the field of TeV gamma ray astronomy has been to apply circular statistics. The primary assumption required is that the parent population from which a sample dataset is drawn does not contain a periodic

signal and hence the distribution of events around the perimeter of a circle corresponding to the folding of a cyclical period is random and uniform (Batschelet, 1981). A test for a periodic signal in a sample dataset may then be carried out by searching for a preferred direction in the circular distribution of event times as folded for a given pulse period, and attempting to prove that a preassigned level of significance has been exceeded. This requires the simple definition of a null hypothesis H_o, viz. that the parent population from which the sample is drawn is uniformly distributed, which may be rejected if the probability of occurrence P of the resultant test statistic is below the preassigned critical level of significance α (usually requiring a 3σ effect, i.e. a probability of $1{\cdot}348 \times 10^{-3}$ for a Gaussian distribution).

Whilst the P-values resulting from many independent tests, e.g. a series of successive observations, may not individually exceed the critical level, a combination of $P_1,\ldots,P_n$ for n independent tests may provide an improved chance of significance. Under the null hypothesis H_o, such probabilities may be combined by calculating the quantity N defined by

$$N = -2 \sum_{i=1}^{k} \ln P_i \ , \qquad (4.2)$$

which is exactly distributed as χ^2 with 2k degrees of freedom (Fisher, 1954).

4.2.1.3. The Rayleigh Test

We require then a circular statistical test which is "uniformly most powerful" in the case where the shape of the expected light curve is unknown. The statistic most commonly used is derived by the Rayleigh test, described in some detail by Mardia (1972). This test is based on the calculation of the resultant vector formed from a set of vectors each carrying equal weight but pointing to a direction in circular vector space corresponding to their time of occurrence in the phase cycle for the exact period T being tested. The vector for the i^{th} event will point in the direction θ_i as defined by

$$\theta_i = 2\pi \ . \ (1/T) \ . \ t_i \ (\mathrm{mod}\ 2\pi) \ , \qquad (4.3)$$

where t_i is the time of occurrence of the i^{th} event in the time series.

Clearly θ_i must also be adjusted if the time derivatives of the period T are known. Hence for a time series containing n events, the resultant vector R may be calculated as

$$R^2 = C^2 + S^2 \ , \tag{4.4}$$

where C and S are the resultant orthogonal components of each of the n events defined by

$$C = (1/n) \sum_{i=1}^{n} \cos \theta_i \ , \tag{4.5}$$

and

$$S = (1/n) \sum_{i=1}^{n} \sin \theta_i \ . \tag{4.6}$$

The product nR^2 is asymptotically distributed as χ^2 with 2 degrees of freedom for the approximation of the statistic at large values of n, which is $\exp(-nR^2)$. More accurately, the probability may be derived from

$$P\ (nR^2 \geq K) = \exp(-K).\ A \ , \tag{4.7}$$

where

$$A = \left[1 + \frac{(2K-K^2)}{4n} - \frac{(24K-132K^2+76K^3-9K^4)}{228n^2} \right] , \tag{4.8}$$

which reduces to $\exp(-nR^2)$ if n is large, as is invariably the case in TeV gamma ray datasets. Notice that R corresponds to the fraction of the events in the dataset which contribute to any detection of a pulsed signal.

The Rayleigh test may be understood as the convolution of a sine wave modulated at the test period with the phased event distribution, and as such is most sensitive to a broad single-peaked light curve, i.e. a unimodal distribution. In the case of a double-peaked light curve with a separation of 180°, i.e. a bimodal distribution, much of the power in the fundamental period may be lost, contributing instead to the second harmonic. A weak interpulse will allow a diluted signal to remain detectable. Therefore, when the Rayleigh test is applied to the search for a pulsar with period T, it is common practice to test for the rejection of the null hypothesis of uniformity of

phase at both T and T/2 where a double-peaked light curve is thought likely. For a broad light curve, the Rayleigh test has the great advantage that no arbitrary binning of data is required.

It is conventional when applying circular statistical methods to allow for the fact that the assumption of a uniformly distributed parent population requires that an integral number of periods be fitted into the full length of the dataset. This is not always the case in astronomical applications, e.g. a 2 hour observation of a pulsar such as Vela X-1 with a period of several hundred seconds will only cover a small number of cycles, making it highly likely that the event distribution will contain a remainder unevenly distributed through the final cycle. To avoid a spurious rejection of the null hypothesis of a uniform phase distribution, Poincare's correction is applied to truncate the length of the dataset to an integral number of cycles of the test period.

4.2.1.4. Other Tests

Whilst the Rayleigh test is that most frequently used for the type astronomical applications which are the subject of the present work, other related circular statistical tests have also been used in some cases due to having attributes more suited to a particular situation.

The Hodges-Ajne test (Hodges, 1955; Ajne, 1968) is often simpler to calculate though not as uniformly powerful as the Rayleigh statistic. It is most useful for very broad light curves, when the points on the circular distribution are divided into two bins of phase width 0.5, separated by a diameter of the circle. This diameter is rotated in order to find a position where a maximum number of points are located on one side. If this anisotropy is significant, uniformity of phase may be rejected and directedness is found in the distribution. A modified version may be used to split the circle into much smaller bins in order to test for a narrower light curve (Cressie, 1977).

Another test which has been applied is the Z_n^2 test, a modification of the Rayleigh test which searches for harmonics in the distribution (i.e. T/2,

T/4,....) to the n^{th} harmonic. The statistic is distributed as χ^2 with 2 degrees of freedom and is dependent on the duty cycle of the pulsar being studied (Buccheri et al., 1983). Protheroe's test (Protheroe, 1985) uses the T_n statistic to detect a suspected narrow light curve by searching for a grouping in the distribution of events as revealed by the separation of adjacent pairs. It is limited by being a specific test requiring prior knowledge of the shape of the light curve.

4.2.2. Periodicity Searching

4.2.2.1. Consequences of Searching for Unknown Periodicity

Whilst the discussion of Section 4.2.1 concentrated on the application of a circular statistical test to search for a single given period (or its harmonic spectrum) it was also pointed out that many X-ray pulsars do show predictable pulse behaviour, a factor which such tests cannot intrinsically allow for. Uncertainties will also exist in the calculation of the time derivative of the pulse period, and in the orbital ephemeris used in correcting the emission time for each event. To compensate for such problems, it is necessary to conduct the test for uniformity of phase over a range of test periods. However, to avoid the introduction of a large number of degrees of freedom, the sampling is restricted to a minimum set of trial periods which are calculated as follows.

For a pulsar with a estimated period T_1, the phase difference, $\Delta\varphi$ between the first and last events in a dataset spanning a time D is

$$\Delta\varphi = D/T_1 \ . \qquad (4.9)$$

If a small increment is added to T_1, the phase difference is decreased slightly. Eventually, such increments lead to a value T_2 where the relative phase of the first and last events has slipped by a full cycle. The periods T_1 and T_2 are then not coherent and are said to be independent trial periods. The difference between the two is often referred to as the Fourier interval.

For the general case where a range of periods is to be tested between T_1

and T_n, the number of independent trial periods required is given by

$$N_P = (D/T_1) - (D/T_n) \quad , \qquad (4.10)$$

and the Fourier interval between adjacent independent periods can then be shown to be

$$\Delta T = (T_1)^2/D \quad , \qquad (4.11)$$

provided T_1 and T_n do not differ too greatly (which is desirable if the number of degrees of freedom in a period search is to be minimised). In practice, a range of no more than 3 trial periods either side of the central period T_1 is tested, and each Fourier interval is oversampled 3 times to allow for a signal falling in a gap between adjacent values.

4.2.2.2. Observational Limitations

Observations carried out using the atmospheric Cerenkov technique can only be made under clear weather conditions during the hours of astronomical darkness. Coupled with the effect of atmospheric absorption at large zenith angles, the length of a typical on-source exposure is limited to only several hours. To identify a weak but persistent gamma ray signal above the intrusive background of cosmic ray particles it is usually necessary to combine a series of observations.

4.2.2.3. Searching for an Incoherent Pulsed Signal

Where the behaviour of a pulse period is poorly known over a timescale of several days, or a combination of independent datasets recorded over a span of several months or years is to be made, it is most useful to merge the observations without the use of relative pulse phase information (i.e. incoherently) and the best method of doing this is that mentioned in Section 4.2.1.2. Equation 4.2 showed that a set of n independent probabilities of uniformity of phase could be combined to produce a resultant statistic distributed as χ^2 with 2n degrees of freedom. In the relevant situation here, the set of n independent probabilities corresponds to the the set of values resulting from the application of the Rayleigh test to search for a uniform phase distribution at a given independent trial period in n independent

observations. The null hypothesis may be rejected if the resultant of n non-statistically significant phase distributions gives a significant effect at the constant trial period. Note that the effective uncertainty in the period T recovered has a contemporary value proportional to 1/D where D is the average duration of the individual datasets used.

For the implementation of an incoherent combination over a range of test periods, the set of values chosen must form a constant matrix to be applied to each dataset. The choice of a set of trial periods may be made in one of two ways. Where the approximate predicted period T_x is not expected to change by an amount greater than one Fourier interval during the full span of the dataset, the matrix is simply calculated by sampling over two to three independent trial periods either side of T_x. This is the technique most commonly used and requires no additional calculations. However, in the special case where a period has been found to wander unpredictably over a long timescale at lower energies, knowledge of its behaviour enables a matrix of trial periods to be set up with reference to an origin at the approximate contemporary period, each independent trial period having a fixed offset from this origin. This method was applied in the present work to the full dataset recorded on Centaurus X-3 (see Chapter 5).

4.2.2.4. Searching for a Coherent Pulsed Signal

Where the behaviour of a pulse period may be well predicted over a span of several days, as is certainly the case for radio pulsars but requires some assumptions for most X-ray pulsars, the observations may be combined by applying the Rayleigh test and retaining the relative pulse phase information between each event (i.e. coherently). This is a powerful technique of recovering a persistent pulsed signal and simply requires a range of independent trial periods to be defined as for a single dataset. Since the effective duration of the dataset is much longer than that of a single observation (typically 50-100 times), the Fourier interval between trial

periods is greatly reduced and a much more accurate determination of any detected period is possible. The much smaller Fourier interval necessitates the use of a known period derivative since coherence of phase is otherwise likely to be lost over the course of a dataset spanning several days.

The disadvantages of this coherent technique include the fact that if a period is not sufficiently well known, a large number of degrees of freedom are used in sampling over a range of very narrow Fourier intervals. Aliasing of the recovered period is also introduced due to several characteristic periodic cycles being present in the combined data:

(a) the duration of each observation (several hours),

(b) the typical 24-hour interval between observations,

(c) any longer gaps induced due to poor weather or equipment failure.

This causes "envelopes" to be introduced into the periodogram (see Figure 4.6) which disguise the precise periodic signal. However, the nature of the search for coherence in the gapped dataset does not produce spurious strong signals due to random phase alignment, a point discussed by Bowden et al. (1991b) in response to the objections put forward by Lewis et al. (1991). It should also be noted that this technique is routinely used as a test for phase coherence in a combined dataset, and is not simply an additional test to be carried out if evidence for an incoherent signal is not found.

4.2.3. Searching in Orbital Parameters

4.2.3.1. Calculations for Orbital Corrections

The adjustment of times to the barycentre of a binary stellar system was discussed in Section 4.1.2.2, where it was shown that for a circular orbit the correction was simple (equation 4.1). It is clear that the effect of the correction depends greatly on the orbital parameters of the system, the pulsar period, and the length of the dataset. For many compact X-ray binary systems containing a pulsar with a period of a few seconds or less, the correction is very sensitive to the assumed orbital parameters and a small shift could cause the loss of a signal.

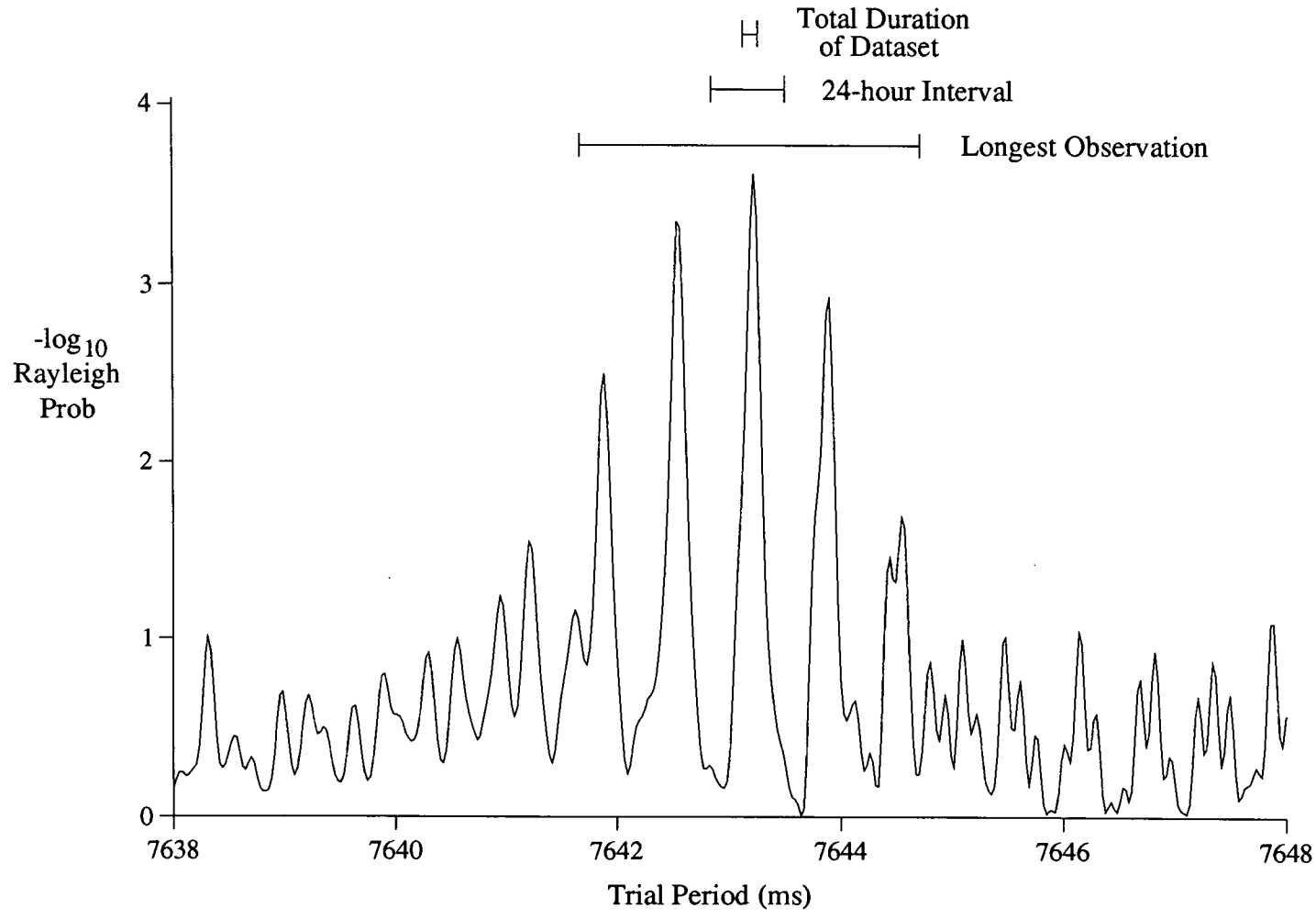

Figure 4.6 : Illustration of independent sampling intervals in trial period for a dataset merged with phase coherence retained.

However, where such a system has an accurately measured orbital ephemeris this sensitivity may be turned to the benefit of the observer as it becomes possible to gain information on the spatial position of the site of photon production. This is particularly useful in TeV gamma ray astronomy since as shown in Chapter 9, the origin of the TeV photons may be substantially displaced from the X-ray source (i.e. the neutron star). Therefore it is possible to apply a technique which is analogous to that used in X-ray astronomy, where the cyclical Doppler shifting of an approximately defined X-ray pulse period reveals the nature of the underlying orbital motion which is responsible (e.g. Rappaport and Joss, 1983). The procedure described here was developed and first applied by Mannings (1990).

The technique is based on adjusting the assumed position of the proposed TeV gamma ray pulsar by applying the Rayleigh test for uniformity of phase over a fixed matrix of values of $a\sin i$ and $\Delta\varphi$ where $\Delta\varphi$ is the offset in orbital phase from the ephemeris position of the X-ray source. The adjustment is based on equation 4.1, which may be restated in terms of $a\sin i$ and orbital phase offset as follows :

$$t = t' - a\sin i \; . \; \sin \left[\frac{\pi}{2} + \frac{2\pi t'}{P_{orb}} \right] , \qquad (4.12)$$

where t is the time of emission in the rest frame of the binary, t' is the event arrival time registered by the observer (measured with respect to a value of zero at the epoch of X-ray mid-eclipse) and P_{orb} is the orbital period. The Doppler shift correction is made to all of the event times using a fixed pair of values of $a\sin i$ and eclipse epoch. In the present procedure these pairs of values are varied in such a way as to define a matrix of spatial positions.

Now in the same way that a set of independent trial periods exist for a given observation, so there are also distinct trial values for these orbital elements. The intervals in between can be thought of as areas in the orbital

plane within which the corrections made to the event times are indistinguishable. The spacing of the trial values depend on the values of the elements themselves, the duration of the dataset, the orbital phase range of the observation, and the trial pulsar period. For all of the X-ray binaries with well known ephemerides which are analysed later, the spacing between independent intervals is greater than the errors in those parameters derived from X-ray measurements, and thus the original correction is sufficient to recover periodicity at the X-ray source position. This means that the precise position of the neutron star is well known, so that the *relative* position of a TeV gamma ray emission site may be investigated by careful choice of the trial orbital values. It can be shown (Mannings, 1990) that the independent sampling intervals in the parameters tested, i.e. $\Delta a \sin i$ and $\Delta\varphi$, may be expressed as follows :

$$\Delta a \sin i = \frac{T}{\sin \varphi_i - \sin \varphi_f} , \qquad (4.13)$$

and by solving for $\Delta\varphi$ in

$$q_1 \sin^2(\Delta\varphi) + q_2 \sin(\Delta\varphi) + q_3 = 0 , \qquad (4.14)$$

where (i) $q_1 = B^2 + C^2$, $q_2 = -2AB$, $q_3 = A^2 - C^2$,

and (ii) $A = (T/a\sin i) - \sin \varphi_f + \sin\varphi_i$,
$B = \cos \varphi_i - \cos \varphi_f$,
$C = \sin \varphi_i - \sin\varphi_f$,

and φ_i and φ_f are the initial and final orbital phases as measured with respect to the ascending node, and T is the trial pulsar period.

The magnitudes of the sampling intervals in $a\sin i$ and eclipse epoch minimise at the nodes and conjunctions of the orbit respectively. These intervals are sensitive to both the range and particular value of orbital phase sampled in the observation. Whilst the matrix of test values in the orbital parameters could be optimised for each orbital position for each binary observed, ease of calculation has dictated that a fixed matrix of values is set up appropriate to the orbital parameters of a given binary and applied to all observations, irrespective of the orbital phase. The values of

the independent spatial sampling intervals for a 5-hour observation of each of the high mass X-ray binaries analysed in this thesis are given in Tables 4.1 and 4.2.

In order to reduce the effect of the unavoidably high number of degrees of freedom introduced by searching for an origin with no prior knowledge of its position, only one Fourier interval is used in the test for uniformity of phase. Some of the TeV gamma ray observations of X-ray pulsars have suggested that the gamma ray period may be displaced from the X-ray period (e.g. Her X-1 (refs. in Weekes, 1988); Vela X-1 (North et al., 1989)). If these effects are caused by Doppler shifting due to a displacement of the emission site, this orbital searching technique will recover the original periodicity and remove the need for a wider search range.

4.2.3.2. Presentation of Results of Orbital Searching

The result of the orbital searching technique is a set of values of the chance probability of non-uniformity of phase at the trial periods as calculated at each point in the matrix of values of $a\sin i$ and $\Delta\varphi$. The favoured method of displaying these values for interpretation is to construct a contour chart on which equal levels of chance probability are joined and plotted with respect to orthogonal axes representing the values of $a\sin i$ and $\Delta\varphi$. Each contour is marked with the appropriate value of $-\log_{10}$(Rayleigh probability) for its position. In all of the diagrams of this type given in the later chapters, the interval between these contours of $-\log_{10}$(Rayleigh probability) is 0.5. The position of the X-ray source is placed near the centre of the contour plot since it represents the reference position from which the orbital offsets are measured. Obviously, if the range of orbital phases sampled is large, this technique of representing in a rectangular frame the results calculated in polar coordinates is limited in its use for spatial interpretation. The most important point to be noted is that a position to the left of the X-ray source position represents a site trailing the neutron star

TABLE 4.1

Sampling intervals in $a \sin i$ at the nodes of the orbit (calculated for a 5-hour observation)

Binary System	Pulsar Period (s)	Orbital Period (d)	$\frac{\Delta\, a \sin i}{a \sin i}$
Vela X-1	283	8.96	$\approx$ 1200%
Centaurus X-3	4.82	2.09	20%
SMC X-1	0.71	3.89	5%

TABLE 4.2

Sampling intervals in eclipse epoch at conjunction (calculated for a 5-hour observation)

Binary System	Pulsar Period (s)	Orbital Period (d)	$a \sin i$	$\frac{\Delta\varphi}{2\pi}$
Vela X-1	283	8.96	113	> 100%
Centaurus X-3	4.82	2.09	39.6	10%
SMC X-1	0.71	3.89	53.5	3%

(from Mannings, 1990)

in its orbit. It is also important to realise that the $a\sin i$: $\Delta\varphi$ plane is not the precise orbital plane but rather the plane intersecting the orbit which contains the line of sight to the observer. A circular orbit will have an elliptical projection in this plane, and for a binary system viewed near to face-on, very little information can be gained from this type of analysis. This point is discussed further in Chapter 8 with respect to 4U1626-67.

An alternative method of displaying the results of the orbital searching technique has recently been developed. This uses the results from a modified process which speeds up the calculation across the matrix of test values by testing for uniformity of phase at a single trial period and factorising the correction to be made to each event time. This is most useful for the analysis of data from millisecond pulsars in close binary systems where the amount of computing time required can otherwise be prohibitive. Whilst not necessary for datasets recorded on typical X-ray pulsars, which are less demanding due to the larger sampling intervals, this can be used in a purely illustrative way to demonstrate the variations in chance probabilities and sampling intervals across the full orbit.

4.2.4. Calculation of Flux Limits and Source Luminosities

The application of the Rayleigh test to data from TeV gamma ray astronomy gives one of two results :

(i) the null hypothesis H_o, that the sample is drawn from a parent population with a uniform phase distribution, cannot be rejected,

(ii) the null hypothesis H_o may be rejected and the probability that the non-uniform phase distribution occurred by chance is P.

The consequence of case (i) is that only an upper limit may be placed on the pulsed gamma ray flux from the source, defined by the parameters of the dataset. The consequence of case (ii) is that an approximate pulsed flux of gamma ray photons from the source may be calculated, of sufficient magnitude to produce the observed signal detection. In each case knowledge of the source distance and cosmic ray spectral index allows an estimate of the source

luminosity to be made.

It is conventional to express gamma ray fluxes in units of photons cm^{-2} s^{-1}. Since the cosmic ray background spectrum is known, and the Rayleigh test yields an estimate of the fractional strength of a detected signal, the measurement of the threshold energy of the telescope enables the gamma ray flux to be calculated. The known background spectrum is expressed in terms of $cm^{-2}s^{-1}sr^{-1}$ and hence by measuring the rate of three-fold coincidences recorded by the Cerenkov telescopes used in the present work (see Chapter 3), and making estimations of the effective collecting area and the detector's field of view, a value for the threshold energy can be calculated. Such measurements have enabled the threshold energy of the Mk.3 telescope to be estimated as 250 GeV, a value which has decreased as improvements have been made to the telescope's performance. Above this threshold energy, the cosmic ray counting rate is $\approx 6.6 \times 10^{-9}$ $cm^{-2}s^{-1}$, assuming an integral spectral index of -1.6 (Craig, 1984). The Mk.4 telescope has been estimated by similar means to have an energy threshold of 400 GeV, and a cosmic ray count rate of $\approx 3.0 \times 10^{-9}$ $cm^{-2}s^{-1}$.

It is then simple to convert a significant detection of a pulsed gamma ray signal into a photon flux, by merely multiplying the pulsed fraction by the overall cosmic ray counting rate. For example, a 1% pulsed signal corresponds to a flux of 6.6×10^{-11} photons cm^{-2} s^{-1} above an energy of 250 GeV in the Mk.3 telescope. Where a significant detection is not achieved, it is standard procedure to quote a 3σ upper limit as the signal strength which would have produced a chance probability of 1.348×10^{-3} for uniformity of phase in the dataset. Using the Rayleigh test to derive a resultant signal strength R from a set of N event arrival times, we have

$$P(\text{uniform phase distribution}) = \exp(-NR^2) , \qquad (4.15)$$

and setting $P = 1.348 \times 10^{-3}$ and rearranging for the 3σ limit, we derive

$$R^2 = (1/N) \cdot \ln(1.348 \times 10^{-3}) . \qquad (4.16)$$

In this way R can easily be calculated for any dataset containing N event times combined with phase coherence. The value of P should first be adjusted to allow for the degrees of freedom used in the analysis.

Knowing a value or upper limit for the photon flux F, in $cm^{-2}s^{-1}$, it is possible to calculate the source luminosity L, assuming isotropic emission, by

$$L = 4\pi X^2 \,.\, F \,.\, E_A \quad , \tag{4.17}$$

where X is the source distance (cm), and E_A the average photon energy. If the differential photon spectrum is of the form

$$S(E) = B \,.\, E^{-z} \quad , \tag{4.18}$$

then for a mean photon energy of E_o, the luminosity is

$$L = 4\pi X^2 \,.\, F \,.\, E_o \,.\, \frac{1-Z}{2-Z} \,. \tag{4.19}$$

The uncertainty in the derived luminosity arises from a number of factors. The source distance itself is unlikely to be known to better than ±10%, whilst the estimation of the flux of pulsed gamma ray photons is based on the Rayleigh test which is a poor indicator of the signal strength (Mardia, 1972). The energy threshold E_o of the telescope can only be estimated to a precision of ≈50 GeV.

CHAPTER 5 - X-RAY BINARY SYSTEMS

5.1. Introduction

The aim of this chapter is to provide a very brief overview of the development of observational and theoretical work on X-ray sources in binary stellar systems. This is followed by an account of how gamma rays may be produced and absorbed in such objects, and finally some of the candidate sources from which TeV gamma ray emission has been detected are reviewed.

This wide field has been excellently reviewed by Nagase (1989), and by a number of authors in the works edited by Lewin and van den Heuvel (1983) and by Ogelman and van den Heuvel (1989). In the following three chapters, more detailed reviews are presented of the X-ray observations relating to the X-ray binaries under investigation at TeV photon energies.

5.2. Observational Characteristics

5.2.1. Discovery of Celestial X-ray Sources

The first discovery of a celestial X-ray source outside the solar system was that of Scorpius X-1 in 1962. Several other sources were discovered in the same decade, all having X-ray luminosities in the region of 10^{37} erg s^{-1} (10^4 times the total power output of the sun) assuming an origin within our galaxy. Shklovskii (1967) was the first to propose that a possible explanation for this emission was that of an accreting compact object in a mass-exchanging binary system (inspired by the explanation of dwarf novae outbursts put forward by Crawford and Kraft, 1956), with energy released from the infall of material into the deep gravitational potential well.

5.2.2. High Mass X-ray Binaries

The hypothesis of accretion as the energy source could not be confirmed until Cygnus X-1 was found to be a compact object in a binary orbit around an early-type supergiant, and Centaurus X-3 was found to display X-ray pulsations and accompanying evidence of Doppler shifting due to orbital motion (see

Chapter 6). The high X-ray luminosities of these objects could then be attributed to the release of energy from the accreting material in a small volume at the surface of the degenerate star, where temperatures of over 10^6 K could easily be reached. The X-ray luminosity L_{37} in units of 10^{37} erg s^{-1} is given by

$$L_{37} = 1.33\ M_{17}\ M_*\ R_6^{-1}\ \text{erg s}^{-1}\ , \qquad (5.1)$$

where M_{17} is the rate of accretion of matter (in units of 10^{17} g s^{-1}), M_* the mass of the compact object in solar masses, and R_6 the radius of the compact object in units of 10^6 cm (Rappaport and Joss, 1983).

Around 30 of these X-ray sources have been associated with high mass ($\geq$10 $M_\odot$) blue supergiant primaries. Due to the large size of the supergiant compared with orbital radius of the compact object, regular eclipses of the X-ray flux are often seen enabling further information to be gained on the orbital motion of the system. A subgroup of the high mass X-ray binaries has been identified where the primary star is a main sequence Be star, i.e. spectral type B with emission lines indicative of a strong stellar wind, more compact than the evolved supergiants in the typical high mass systems. These sources have long orbital periods (10s of days or more) and show only transient X-ray emission.

Figure 5.1 shows the distribution of the high mass X-ray binaries on the celestial sphere in galactic coordinates. This reveals a marked concentration towards the galactic plane indicative of a Population I origin. The young neutron stars in these systems are believed to have high magnetic fields of $\geq 10^{12}$ G. The pulsating behaviour is therefore easily explained on the basis of a high rate of mass transfer ($\approx 10^{17}$ g s^{-1}) channelled by the strong magnetic field onto a small region at the magnetic poles, which are displaced from the axis of rotation. Typical characteristics of a sample of the systems containing X-ray pulsars are given in Table 5.1.

5.2.3. Low Mass X-ray Binaries

Another class of X-ray source was discovered which displayed slightly

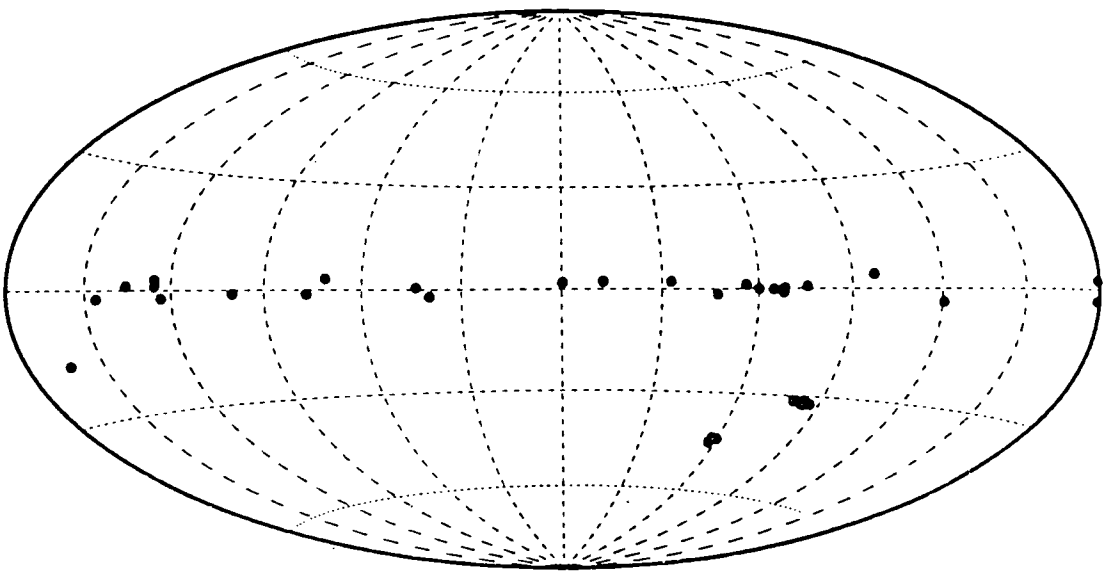

Figure 5.1 : A sky map in galactic coordinates showing the distribution of the high mass X-ray binary systems on the celestial sphere. All of the objects included here have been identified with optical counterparts. Several sources shown at the lower right of the picture are located in the Magellanic Clouds. The marked concentration of the remainder toward the galactic equator is indicative of a Population I origin.

(from van Paradijs, 1989)

TABLE 5.1 - A sample list of 16 of the binary X-ray pulsars for which the physical parameters are reasonably well measured (based on Nagase, 1989). The selection is intended to show the variations between such objects and is arranged in order of decreasing pulse period.

Key to abbreviations : XRB=X-ray binary
HM=High Mass system
LM=Low Mass system
Be=System with primary star of spectral class Be

Object	Pulse Period (seconds)	Orbital Period (days)	Distance (kpc)	Lx (erg s^{-1})	Type of XRB
A0535-66	0.069	16.66	50	1×10^{39}	Be
SMC X-1	0.710	3.892	65	5×10^{38}	HM
Her X-1	1.24	1.700	5	2×10^{37}	LM
4U0115+63	3.61	24.31	3.5	1×10^{37}	Be
Cen X-3	4.82	2.087	8	1×10^{38}	HM
1E2259+58	6.98	< 0.08	3.6	5×10^{35}	LM
4U1626-67	7.66	0.0288	6-10	1×10^{37}	LM
LMC X-4	13.5	1.408	50	6×10^{38}	HM
EXO2030+37	41.8	46 ?	5	1×10^{38}	Be
A0535+26	104	111	2.4	2×10^{37}	Be
GX1+4	114	304 ?	9	1×10^{38}	LM
GX304-1	272	133	2.4	1×10^{36}	Be
Vela X-1	283	8.96	1.9	5×10^{36}	HM
4U1907+09	438	8.38	7	4×10^{37}	HM
4U1538-22	529	3.73	7	4×10^{36}	HM
GX301-2	696	41.5	1.8	3×10^{36}	HM

lower X-ray luminosities, no evidence of pulsations or eclipses, and only intrinsically very faint optical counterparts. The evidence for the binary nature of these systems is therefore less certain. The optical spectra are bluish, showing no evidence of the absorption lines seen in stellar spectra (Lewin and Joss, 1983). In a very few sources this spectrum has been seen to fade at times, to reveal an underlying stellar spectrum typical of a cool main-sequence dwarf (e.g. Aql X-1, Cen X-4). Whilst this is the only direct evidence for the accepted model of a neutron star accreting from a dwarf companion, the observations of most of these systems are explained well if the dwarf is of mass 0.1-1 $M_\odot$ and fills its critical Roche potential lobe. The material donated to the neutron star is believed to form a an accretion disc which provides most of the optical emission from the system. A visual comparison of the models of high and low mass X-ray binaries is given in Figure 5.2.

The distribution of these sources in galactic coordinates is shown in Figure 5.3. Most are scattered around the galactic plane, particularly towards the central bulge, and a substantial fraction are found to be located in globular clusters. This indicates that these systems are of Population II, and that both components are advanced in their evolution, the ageing neutron star having a magnetic field which has decayed to $\approx 10^8$ G. Many of these low mass X-ray binaries are found to show X-ray burst behaviour, with recurrence timescales of the order of months or years, believed to be due to thermonuclear detonation of material on the neutron star surface. Such bursts are not seen from X-ray pulsars due to the stronger magnetic fields in these objects which funnels the accretion flow into a smaller area at the magnetic poles. This gives greater efficiency of energy transport, and thus greater protection against the build-up of instabilities at the surface.

5.2.4. Cataclysmic Variables

A third class of stellar X-ray sources was discovered in the late 1970's

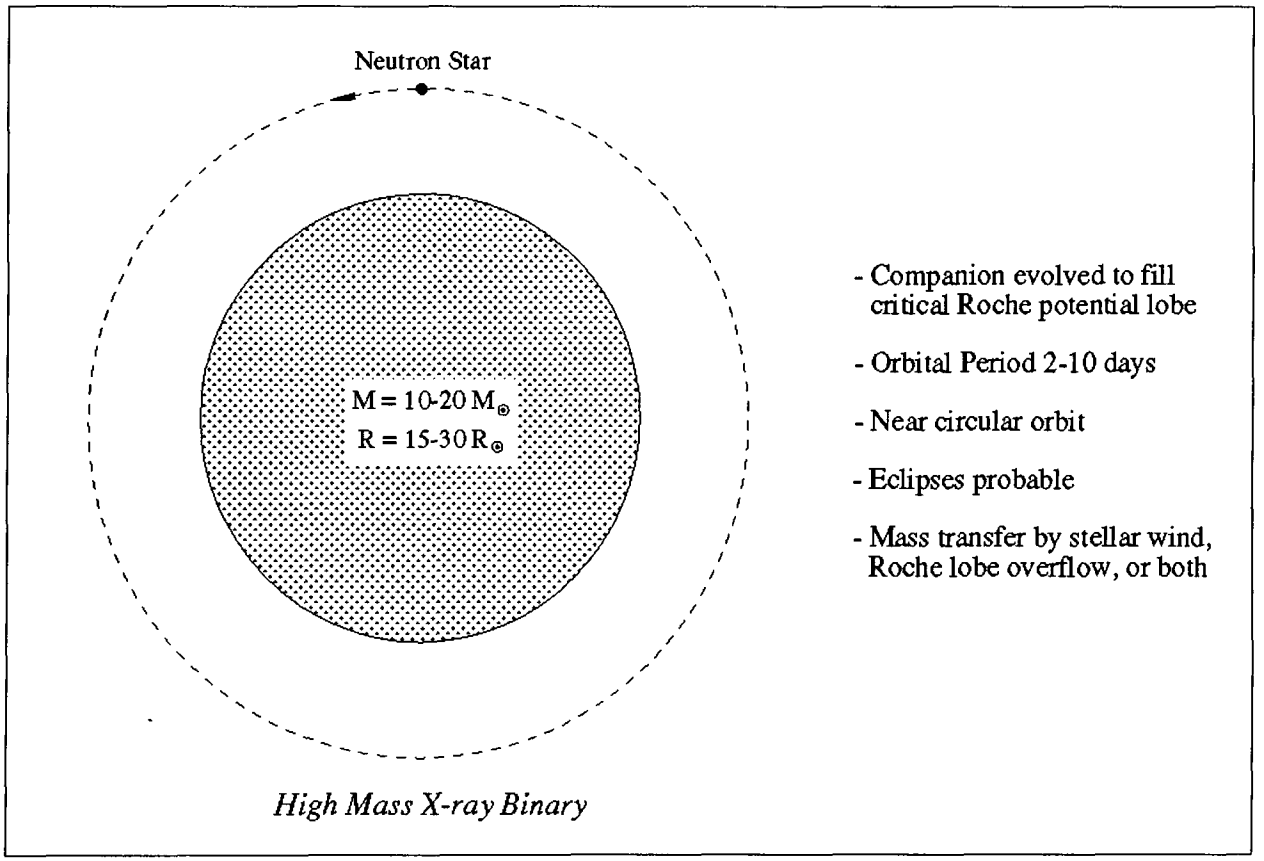

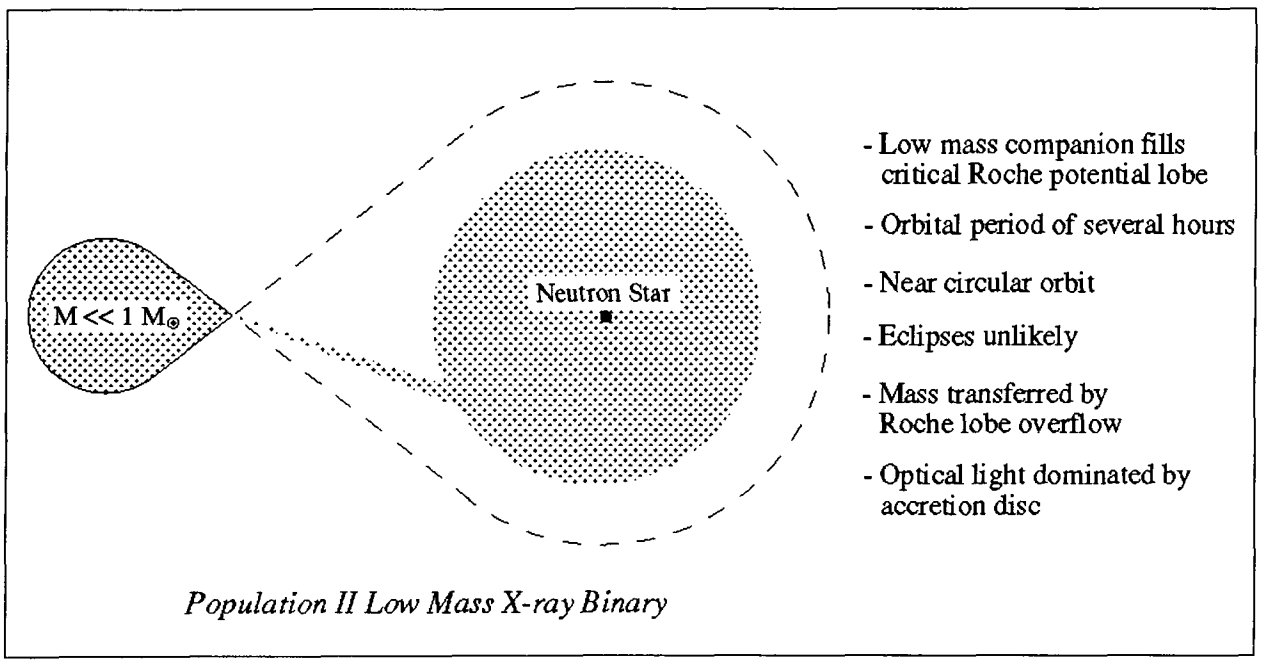

Figure 5.2 : Schematic diagrams of the two major types of X-ray binary systems. The relative scales are not equal.

(after van den Heuvel, 1983)

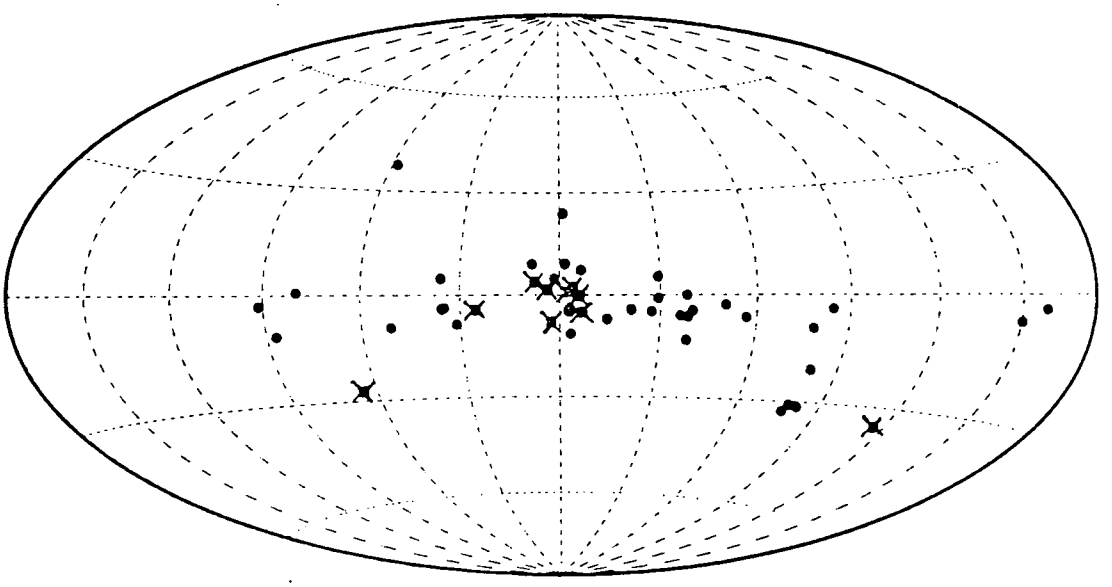

Figure 5.3 : A sky map in galactic coordinates showing the distribution of the low mass X-ray binary systems on the celestial sphere. All of the objects included here have been identified with optical counterparts. The sources marked by crosses are those located in globular clusters. The remainder show a scatter in galactic latitude and a concentration toward the central galactic bulge, indicative of a Population II origin.

(from van Paradijs, 1989)

which showed evidence of a much lower X-ray luminosity of $\approx 10^{30}$-10^{32} erg s^{-1} and substantial emission at soft X-ray energies. These were identified with the cataclysmic variables (CVs), which had long been studied for their outbursts at optical energies (e.g. Liebert, 1980). Cataclysmic variables are believed to contain a degenerate helium star (a white dwarf) accreting material from a main sequence dwarf companion, with most of the optical emission arising from an accretion disc (Cordova and Mason, 1983; Pringle and Wade, 1985). The outbursts seen in these systems are believed to be due to a temporary enhancement in the accretion rate propagating through the disc and onto the white dwarf (King and Shaviv, 1984). A number of these systems are found to show optical pulsations with a period of 10s of seconds, which are ascribed to the rotation of a strongly magnetised white dwarf with a surface field of $\approx 10^{7}$ G.

5.2.5. Accretion in X-ray Binary Systems

5.2.5.1. Stellar Wind Transfer and Roche Lobe Overflow

The concept of equipotential surfaces defined by gravitational and rotational forces on a test particle is a valuable tool when considering mass transfer between the components of a binary system (Savonije, 1983). That surface of equal potential energy which contains the inner Lagrangian balance point L_1 defines the Roche lobe of each object, within which the gravitational potential field is dominated by the relevant component. For a binary system consisting of the masses M_1 (non-degenerate star) and M_2 (compact object) separated by a distance a then we have

$$R_c/a \approx 0.38 + 0.2 \log_{10}(M_1/M_2) \quad \text{for } 0.3 \leq (M_1/M_2) \leq 20 , \qquad (5.2)$$

$$R_c/a \approx 0.462 \, (M_1/M_2)^{1/3} \quad \text{for } (M_1/M_2) \leq 0.8 , \qquad (5.3)$$

where R_c is the radius of a spherical volume equal to the volume of the Roche lobe (Paczynski, 1971).

Most high mass binary systems will be born with the non-degenerate star contained well within its Roche lobe so that material can only be accreted onto the compact object from the stellar wind of the evolving primary (c.f. Be

binary systems). However, if the star expands to an extent whereby its atmosphere begins to overflow its Roche lobe, a large increase in the rate of mass transfer results as the gas pressure at L_1 drives material into the Roche lobe of the compact object. Roche lobe overflow is expected to be the dominant mass transfer process in low mass X-ray binaries as a consequence of the much smaller separation of the components and the lack of a substantial stellar wind from the surface of a main sequence dwarf star (though some "self-excited" wind mechanism may occur as material is driven off by X-ray reprocessing).

These two regimes of mass transfer may be distinguished in high mass binaries if knowledge of the physical parameters of the system can be used to predict the X-ray luminosity (from equation 5.1) on the basis of the expected rate of mass accretion from a stellar wind or from Roche lobe overflow (Savonije, 1983; Henrichs, 1983). The radii of many of the supergiant stars in typical high mass X-ray binaries are reasonably well known from eclipse measurements. By comparing these radii with the estimated critical Roche lobe sizes, a good agreement with theoretical estimates of the consequent X-ray luminosities is found.

5.2.5.2. Formation of an Accretion Disc

An accretion disc may form provided that the infalling gas has a sufficiently high angular momentum to avoid direct infall on the compact object (Petterson, 1983). If this is so, the accreting material may enter a Keplerian orbit within which interaction with other particles can cause the slow drift of gas towards the accreting object (viscous spreading). In addition to this requirement, the specific gravitational potential energy of the material in the gas stream must be at least twice the specific kinetic energy ($0.5\ v_{rel}^2$ where v_{rel} is the velocity relative to the compact object). Disc formation is dependent on the relative masses and separation of the binary components and is generally expected in the case of Roche lobe

overflow. In the case of accretion from a stellar wind, a temporary disc may form given a change in the velocity and density of the stellar wind. Many detailed disc models have been developed and the interaction of the inner disc with the magnetosphere of the compact object was considered in a series of papers by Ghosh and Lamb (1978, 1979a,b) and later by other authors (e.g. Wang, 1987; Anzer and Borner, 1983). These considerations are discussed where relevant in Chapters 6-9.

5.2.5.3. Accretion Torques Acting on a Compact Object

The formation of an accretion disc rotation rotating in the same sense as the accreting object means that a reservoir of angular momentum is available. In a simple picture, this extra angular momentum may be transferred to the stellar surface by steady accretion leading to a gradual reduction in the rotation period of the X-ray pulsar (i.e. a spin-up). However, more complex torques can act due to the interaction of the accretion flow with the magnetosphere of the neutron star (e.g. Ghosh and Lamb, 1978; Henrichs, 1983). The interaction of the magnetic field originating at the surface of the compact object with the rotating accreting material will significantly affect the rotation rate of the star. The precise value of spin-up then depends on the position of the corotation radius, where the Keplerian orbital angular velocity of the accreting material is equal to the angular velocity of the pulsar. The net torque may even act to slow down the compact object's rotation under certain conditions.

Observations of pulsars accreting primarily from a stellar wind (e.g. Vela X-1, GX301-2) have revealed a much more random behaviour of the spin period. Varying rates of spin-up or spin-down are found to affect the pulsar period on unpredictable timescales reflecting the variations in the magnitude and direction of the accretion torque due to the spherically infalling material. A picture of the expected distribution of material in a binary accreting from a stellar wind is given in Figure 5.4.

Since the response of a compact object to a given angular momentum

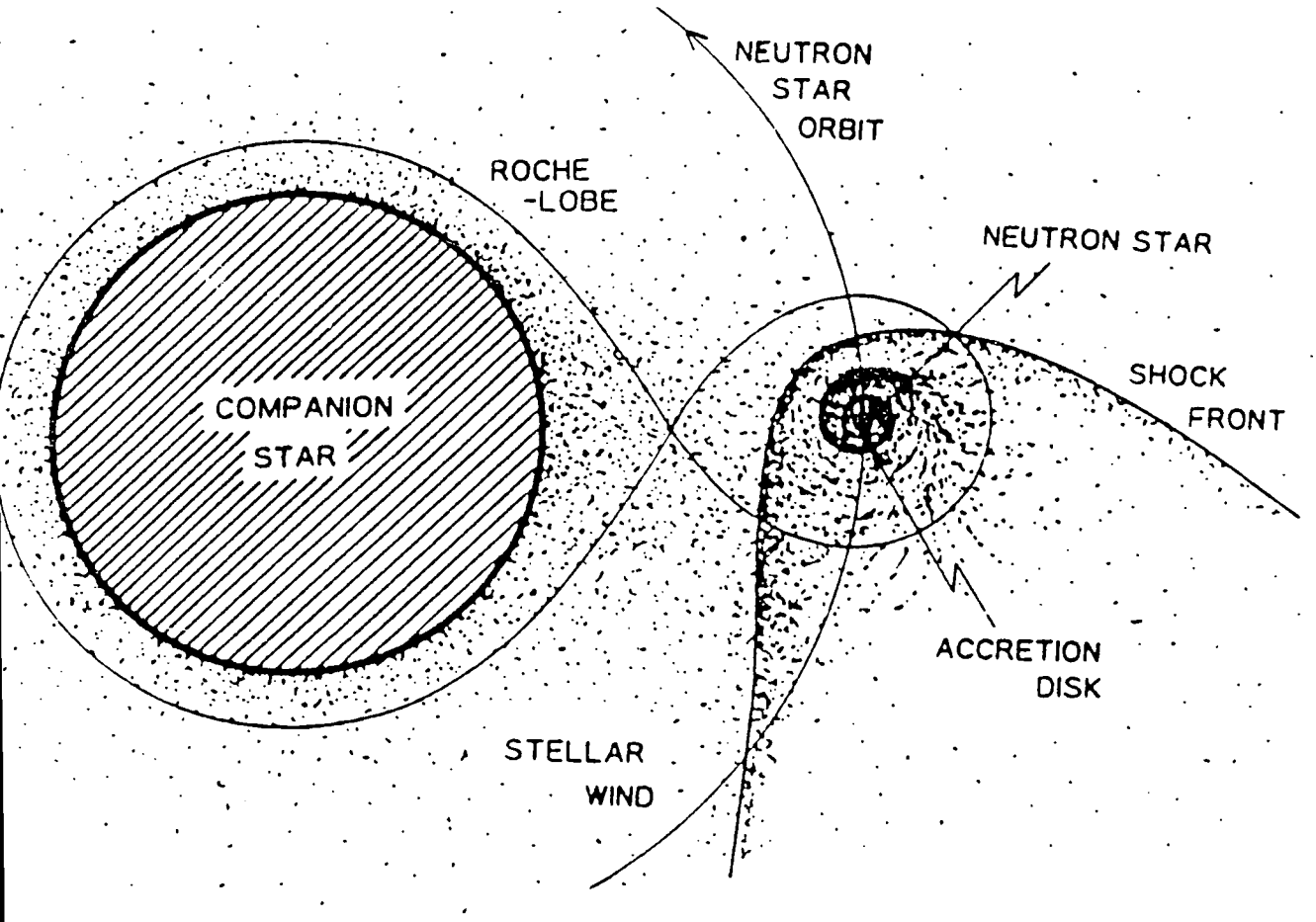

Figure 5.4 : A schematic diagram showing the possible mass flow in a high mass binary system where the primary does not fill its Roche lobe and the neutron star accretes spherically from the stellar wind. An accretion wake will be caused by the motion of the neutron star through the material entering its Roche lobe. The formation of an accretion disc is less straightforward, and will probably be only temporary.

(from Nagase, 1989)

transfer will differ depending on whether it is a neutron star or a white dwarf, it is instructive to compare the maximum predicted spin-up rate for a source with a given X-ray luminosity. Since equation 5.1 relates the mass accretion rate to the luminosity, the rate of period change can be determined from

$$\dot{P}/P = 7.1 \times 10^{-5}\ I_{45}^{-1}\ \mu_{30}^{2/7}\ M_*^{-3/7}\ (R_6.L_{37})^{6/7}\ P\ yr^{-1}, \quad (5.4)$$

where $\dot{P}$ is the period derivative (in s yr^{-1}), I_{45} is the moment of inertia in 10^{45} g cm^2 and μ_{30} the magnetic moment in 10^{30} G cm^3. This relationship was used by Rappaport and Joss (1977) to demonstrate that the binary X-ray pulsars are almost certainly neutron stars. Figure 5.5 shows the result of the standard technique of plotting $\dot{P}/P$ against $P.L^{6/7}$ with the best fit lines shown for the predicted physical parameters of neutron stars and white dwarfs.

5.3. TeV Gamma Ray Production in X-Ray Binaries

5.3.1. Interaction of Particles with Target Material

Gamma ray photons with energy of $\approx$ 1 TeV can be produced in X-ray binary systems either by decay of a neutral pion or as a result of one of the electromagnetic energy loss processes acting on energetic electrons (pair annihilation, inverse Compton or curvature radiation) as discussed in Chapter 1.

Neutral pion decay is the favoured explanation for the fluxes of TeV gamma rays observed from such objects. This process will be initiated by the interaction of a proton or neutron of energy $\approx 10^{13}$ eV or more with target nuclei present in the system via a reaction such as

$$p + N \longrightarrow \pi^0 + \pi^{+/-} + \text{other hadrons}$$
$$\pi^0 \rightarrow 2\gamma \qquad \pi^{+/-} \rightarrow \mu^{+/-} + \nu \qquad \pi^{+/-} \rightarrow e^{+/-} + \nu + \bar{\nu}$$

(Gorham and Learned, 1986). Due to the large number of secondary particles produced in addition to the pair of gamma rays, these photons will carry only $\leq$ 10% of the energy of the primary nucleon. Note that the lifetime of the

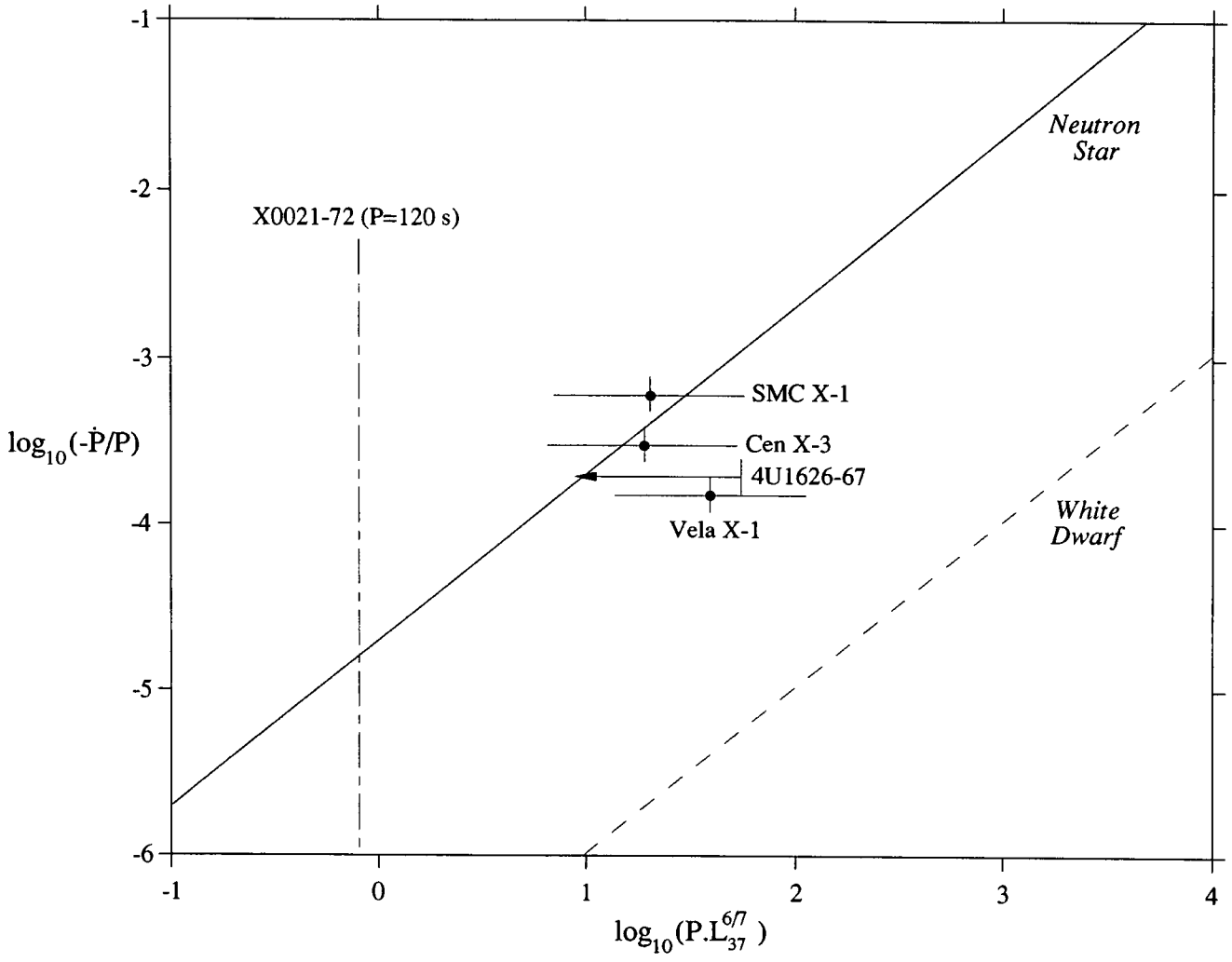

Figure 5.5 : Relation between fractional pulse period change ($\dot{P}/P$) and $P.L_{37}^{6/7}$ illustrating the method of determining the type of compact object in an X-ray binary by use of these parameters. The fit lines show the values expected for a one solar mass object. $\dot{P}/P$ is measured in s yr^{-1} and L_{37} in units of 10^{37} erg s^{-1}.

(after Rappaport and Joss, 1983)

neutral pion is so short that it has essentially no chance of interaction before decaying to produce the gamma ray pair.

The processes by which particles may be accelerated to such high energies are discussed in Chapter 9. Assuming a beam of protons or neutrons can be produced, the requirement for the subsequent emission of a detectable flux of TeV gamma rays is the presence of target material in the system with sufficient column density to give a high probability of interaction for the incident particles. In conjunction with this requirement is the necessity that the resultant gamma rays are not completely absorbed before they can escape.

This problem was investigated by Stenger (1984) who considered the energy loss from a proton beam interacting with material and losing particles via both interaction and decay. The quantitative results were dependent on four parameters - (i) the intensity of the proton beam at 1 TeV, (ii) the proton spectral index, (iii) the matter density, and (iv) the integrated path length. Using a differential spectral index of -2.3, the optimal value for gamma ray production was found to be $\approx$ 50 g cm^{-2}, as shown in Figure 5.6. The decline in the flux of gamma rays at higher column densities results from energy losses due to the electromagnetic interaction of photons with the material traversed after their production. For these denser targets, further photon production will result from pair annihilation in the resultant cascade and if the energy of the original proton is sufficiently high, TeV gamma rays could still escape via this secondary mechanism. The high Lorentz factor of the primary particle means that the directional spread of the secondary photons and other particles will be small, typically $\approx 10^{-3}$ radians. Thus whilst a target with low column density will favour the escape of the gamma rays immediately resulting from pion decay, a spectrum of less energetic photons can result from a thicker target.

5.3.2. Energy Loss Processes

In Chapter 9 it is shown that acceleration of particles to very high

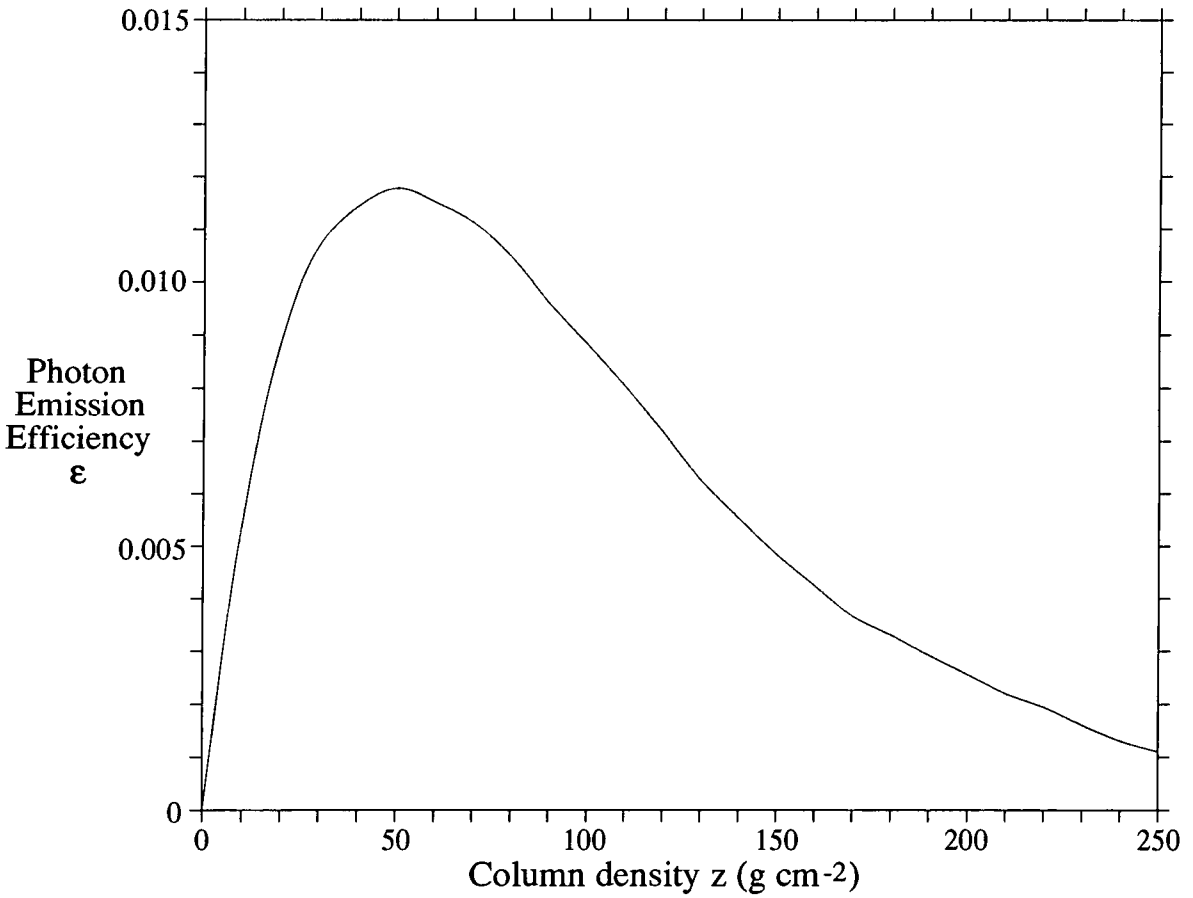

Figure 5.6 : Gamma ray production efficiency ε as a function of the integrated path length, or column density z, in a given medium.

Proton differential spectral index α is assumed to be -2.3.

Energy of the incident photon is assumed to be 1 TeV.

Photon production efficiency ε is defined as the ratio of the rate of production of photons via neutral pion decay in a given energy band to the rate of incidence of the incoming protons, i.e.

$$\varepsilon = \frac{N_\gamma (E,z)}{N_p(E)}$$

(after Stenger, 1984)

energies via accretion-driven processes in X-ray binaries is most efficient when the maximum amount of accretion power may be directed into the particles. This is possible when the acceleration occurs very close to the surface of the neutron star, but as has already been mentioned there are two problems with such a scenario.

The first is the limitation set by the Alfven radius of the magnetosphere where the infall of accreting material is halted due to the pressure exerted by the neutron star magnetic field. This region is where particle acceleration by disc dynamo action or plasma instabilities may be initiated. For a neutron star with a typical field of 10^{12} G the Alfven radius is too large for a sufficient amount of the accretion luminosity to be released to account for the high energy particle acceleration. The second problem is the absorption of gamma ray photons in the very strong magnetic field near the pulsar surface. Sturrock (1971) showed that gamma rays of energy E_g (in eV) may produce an electron/positron pair in the presence of a magnetic field with a perpendicular component B_p (in Gauss) where

$$B_p . E_g > 10^{18.6} \quad . \tag{5.5}$$

Since neutron stars have a dipolar magnetic field, it is more useful to consider another expression (Hardee, 1977) giving the maximum value of B_{pmax} which will be encountered by a photon emitted at a radius r_g and a polar angle θ_o with respect to the polar coordinate system of the magnetic field :

$$B_{pmax} \approx 0.08 \, . B_s . (R_s/r_g)^3 . \theta_o \quad , \tag{5.6}$$

where $\theta_o << 1$, and B_s and R_s are the surface magnetic field and radius of the neutron star respectively. The equations 5.5 and 5.6 may be combined to produce a value of r_g for which the optical depth for $e^{+/-}$ pair production by the photon in the magnetic field has a value of unity (Mastichiadis, 1987):

$$r_{max} = 2.7 \times 10^3 \, . (E_g . B_{12} . \theta_o)^{1/3} . R_6 \text{ cm} \quad . \tag{5.7}$$

For example a gamma ray of energy 1 TeV which is emitted at a polar angle of $\approx 5^o$ must be produced at least 12 neutron star radii from the pulsar surface in order to pass through an optical depth of unity before escaping the

magnetosphere given a 10^{12} G surface field and a stellar radius of 10^{6} cm.

Other absorption processes also operate on particles and photons due to the intense X-ray flux near the accreting poles of the neutron star. At the TeV energies considered here, the primary energy loss mechanism for gamma rays in a softer photon field is $e^{+/-}$ pair production. This can occur if the energy available from the photon collision in the centre of mass frame exceeds $2m_ec^2$. For gamma rays with energy $>10^{15}$ eV interacting with an X-ray photon field, double pair production will dominate. The cross section for single pair production is a function of the quantity so given by

$$so = E_g.E_x.(1-\cos\alpha) \ , \qquad (5.8)$$

where E_g and E_x are the energies of the gamma ray and X-ray photon respectively expressed in units of m_ec^2 and α is the angle between their trajectories before collision (π for a head-on collision). The gamma rays may be absorbed in the X-ray photon flux from the neutron star itself, which will be strongest above the poles where the accreting column cannot act as a shield (Leung, Cheng and Fung, 1993), or from the inner regions of the accretion disc. Less severe attenuation will occur in the softer photon fluxes from the remainder of the accreting material and the companion star. The resultant $e^{+/-}$ pairs may also annihilate to produce further gamma rays which later produce further $e^{+/-}$ pairs and an electromagnetic cascade will develop .

The protons accelerated in the vicinity of the neutron star can also lose energy by interaction with the X-ray photon flux, predominantly by photopion production (Mastichiadis, 1987). The majority of the pions produced will be neutral, which decay to produce gamma ray photons, if the proton energy E_p satisfies the condition

$$E_p > 1.5 \times 10^{14} E_{kev}^{-1} (1-\cos\alpha)^{-1} \ , \qquad (5.9)$$

where E_{kev} is the X-ray photon energy in keV. This is therefore most important at proton energies in excess of 10^{15} eV. Photopion production may continue until the energy of the proton falls below the threshold E_p or the

mean free path λ_p exceeds the size of the system. Many of the gamma rays produced by the pion decay in these regions of high X-ray flux will give rise to $e^{+/-}$ pairs as described above.

5.4. X-ray Binaries as TeV Gamma Ray Sources

5.4.1. Introduction

This section summarises TeV gamma ray observations of three of the X-ray binaries regarded as providing the most convincing evidence for emission at these energies. The prospects for TeV gamma ray production in such systems are discussed in Chapter 9. Chapters 6,7 and 8 deal specifically with TeV gamma ray observations of Centaurus X-3, Vela X-1, SMC X-1, 4U1626-67 and XO021-72 where an appropriate review of the properties of each system is given.

5.4.2. Cygnus X-3

Cygnus X-3 has long been regarded as one of the most unusual objects in the galaxy showing great variability in its emission from radio to UHE energies (full reviews are given in Weekes, (1988) and Bonnet-Bidaud and Chardin (1988)), though frustratingly no optical counterpart has been identified. Recent observations by the Compton Observatory's EGRET instrument have detected weak emission from the direction of Cyg X-3 at energies ≥100 MeV (Mattox et al., 1993). One common facet over the numerous positive detections is its 4·8 hr periodicity, which is generally accepted to be due to orbital motion in a low mass X-ray binary system. This was first detected at TeV energies by the Crimean group (Vladimirsky, Stepanian and Fomin, 1973; later observations by this group have been reviewed by Weekes (1985)). Several groups have since successfully identified this periodicity, with a peak at orbital phase 0·2 or 0·6 and a gamma ray flux variable around 10^{-10} $cm^{-2}s^{-1}$.

Possibly the most important TeV measurements of this system came from the Durham telescopes at Dugway. In a seven minute burst of emission at orbital phase 0·625, evidence was found for periodicity at 12·59 ms (Chadwick et al., 1985). This prompted reanalysis of other data, which led to the discovery of

another periodic outburst at precisely the same window in the 4·8 hr cycle. Subsequent evidence for this fast pulsar activity came from observations made by the Durham group from La Palma in 1988 (Brazier et al., 1990a). Although other groups have reported detection of a similar periodicity with marginal significance, the 12·59 ms pulsar awaits substantiation. The best independent confirmation came from observations made at 100 TeV energies by the Adelaide group (Gregory et al., 1990). These revealed evidence for 12.59 ms periodicity in a 600 s phase window centred 1000 s earlier than that predicted by the earlier Durham reports. The Durham group were routinely observing Cyg X-3 from La Palma in 1989 and some of the data were recorded very near to the times of the Adelaide observations. In a search for 12.59 ms periodicity in the phase window defined by the near-simultaneous Southern Hemisphere observations, two datasets were found to show significant evidence for the existence of the predicted pulsed emission (Bowden et al. 1992c).

5.4.3. Hercules X-1

Hercules X-1 is a low mass X-ray binary containing a 1·24 s pulsar. As well as a 1.7 d orbital period, a 35 day modulation of intensity has also been noted. TeV gamma ray emission was first noted from this system in the form of a three minute outburst seen by the Durham group at Dugway (Dowthwaite, 1984a). Periodic analysis of this burst revealed a signal at the well-defined X-ray period, and the peak flux was $1{\cdot}2 \times 10^{-9}$ cm^{-2}s^{-1} above 1 TeV. This was seen as the 35 day intensity cycle was switching to an "on" state. No further outbursts were seen in this experiment, but later observations from La Palma by the same group revealed a burst at a similar phase in both the orbit and the 35 day cycle (Brazier et al., 1990b).

The Whipple group also observed a number of outbursts generally lasting ≥28 minutes (i.e. the duration of an on-source scan) and with a flux strength of $2\text{-}3 \times 10^{-10}$ cm^{-2}s^{-1} above 250 GeV (e.g. Gorham et al., 1986). One of these, on 1984 April 4, was found to be simultaneous with an observation by the Durham group at Dugway and the 28 minute extracted datasets from each both

showed evidence for weak periodicity at 1.24 s (Chadwick et al., 1987). Another significant result from the Whipple observations was the observation of an outburst on 1985 June 16 when the neutron star was eclipsed. This directly suggested that the emission site was not co-located with the neutron star. A number of outbursts showed a periodicity significantly shorter than the precise X-ray period and this was also the case for an outburst of periodic TeV gamma ray emission lasting about 15 minutes observed by the Haleakala group (Austin et al., 1990). No explanation could be found for this effect.

5.4.4. 4U0115+63

4U0115+63 is a high mass X-ray binary containing a 3.6 s pulsar in a wide 24 d orbit. Its X-ray emission is sporadic, suggesting that mass transfer in the system is unstable (Rappaport et al., 1978). The Durham group were the first to detect TeV gamma ray emission from 4U0115+63. Observations spanning 7 days made at Dugway in 1984 revealed a steady 3.6 s periodicity with a chance probability of 10^{-5} after allowing for all degrees of freedom (Chadwick et al., 1985). This gamma ray signal constituted 2% of the cosmic ray background, corresponding to a flux above 1 TeV of 7×10^{-11} cm^{-2}s^{-1}. A recent reappraisal of the event selection used for this dataset resulted in a slightly more significant result. Further evidence for this emission came from later data recorded by the Durham group using the Mk.4 telescope on La Palma where a steady flux of 4×10^{-10} cm^{-2}s^{-1} was measured above 400 GeV over several days (Brazier et al., 1990b).

An earlier detection of TeV emission from this object may have been achieved by the Crimean air-shower group (Stepanian, Vladimirsky and Fomin, 1972), who detected a localised $3{\cdot}9\sigma$ excess over several nights of drift-scan measurements intended to search for emission from the galactic plane. This excess was found to originate at a position less than 1° from 4U0115+63 in the constellation of Cassiopeia, but the association was not made at the time and

the source was labelled Cas γ-1. The signal was variable, but indicated a flux of about 3×10^{-10} $cm^{-2}s^{-1}$ above 2 TeV. The Durham group's detection of TeV gamma rays from 4U0115+63 led Lamb and Weekes (1986) to propose that this was the same source as seen previously by the Crimean group. Subsequently, Neshpor and Zyskin (1986) demonstrated the existence of 24 d periodicity in the 1972 Crimean database and attributed this to orbital modulation at the source. No definite independent confirmation of a steady TeV gamma ray flux from 4U0115 has been found, but brief episodes of emission pulsed at the X-ray period were reported by the Whipple and Haleakala groups (Lamb et al., 1987; Resvanis et al., 1987).

CHAPTER 6 - TeV GAMMA RAY OBSERVATIONS OF CENTAURUS X-3

6.1. The Centaurus X-3 Binary System

6.1.1. Discovery of a Pulsating Celestial X-ray Source

The celestial X-ray source known as Centaurus X-3 was discovered as a result of rocket borne observations made in 1967 (Chodil et al., 1967a). A significant flux of $\approx 3 \times 10^{-8}$ erg $cm^{-2}s^{-1}$ from the object was recorded in the energy range 2.1-9.5 keV. The major subsequent breakthrough came in 1971 as a result of data taken by the UHURU satellite. The emission from Cen X-3 was found to be 70% pulsed between 1-20 keV at a period of ≈4.8 s as shown in Figure 6.1 (Giacconi et al., 1971). This was the first observation of a regularly pulsating X-ray object. In addition, distinct high and low intensity levels were noted, with an order of magnitude decrease occurring in less than an hour. A significant change in the 4.8 s period in data taken 3 months apart could only be explained by Doppler shifting as a result of the source moving in a binary system of unknown dimensions.

The binary nature of the object was confirmed and made quantitative from further observations by UHURU (Schreier et al., 1972a) and OSO-7 (Baity et al.,1974). A 2.1 d periodicity was seen in both the intensity variations and in the sinusoidal Doppler shifting of the pulse period. In the higher intensity levels, the emission was found to be 80-90% pulsed, but this dropped to ≤20% in the lower states, leading to the suggestion that an eclipsing binary X-ray source was responsible. A compact object rotating every 4.8 s was postulated to be eclipsed every 2 days by the passage behind a large companion star. Preliminary estimates of the radius and mass of the companion based on the gradual onset of the eclipse (≈1 hour) and its duration (≈20% of the orbit) pointed to a early-type supergiant.

6.1.2. Determination of the Nature of the System

A well-defined X-ray position enabled a search to be made for the optical counterpart and this was duly found to be an O7 supergiant, V779 Cen, now

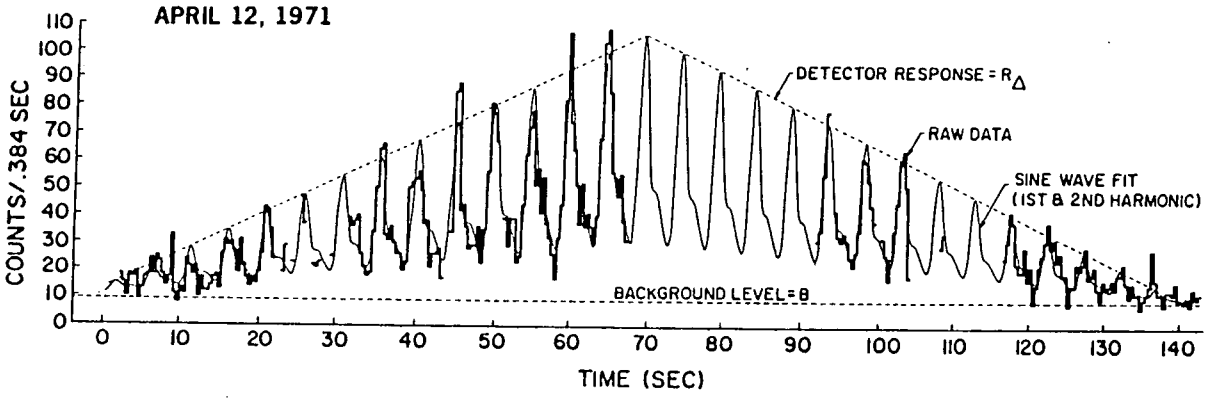

Figure 6.1 : The discovery of 4.8 s pulsations from Cen X-3 in data recorded by the UHURU satellite in 1971 April (energy range 2.0-6.0 keV). The time resolution is 0.384 s.

(from Giacconi et al., 1971)

better known as Krzeminski's star after its discoverer (Krzeminski, 1974). The interstellar reddening of this star suggests it to be at a distance of 8 kpc. The identification also enabled the masses of the components and further orbital parameters to be measured (e.g. Avni and Bahcall, 1974; Fabbiano and Schreier, 1977; Kelley et al., 1983). The orbit was found to be nearly circular (e=0.0004) with a projected semi-major axis of 39.7 ls.

Monte Carlo simulations based on the measured orbital parameters have enabled limits to be placed on the masses of the components (Rappaport and Joss, 1983). The neutron star mass is 0.5-1.7 M_o, whilst the primary has a mass of 17-25 M_o and a radius of 10-15 R_o (95% confidence). The inclination angle is estimated to be >63°. The large catalogue of X-ray observations of this source has enabled continual refinement of the accuracy of the orbital ephemeris (e.g. Kelley et al., 1983; Nagase et al., 1992).

The X-ray light curve of the 4.8 s pulsation has usually shown a single asymmetric peak throughout the observed energy range (e.g. Ulmer, 1976). However, a double pulse structure has occasionally been observed at lower X-ray energies (≤10 keV), the two peaks separated by 0.5 in phase, with the interpulse becoming the dominant peak (Tuohy, 1976; Schreier et al.,1976; Nagase et al, 1992). No optical pulsations have been detected (Lasker, 1974).

6.1.3. X-ray Observations of Distinct Intensity States

As well as the variation in intensity arising from the eclipsing nature of the system, unpredictable longer term fluctuations are also observed. These have been seen as gradual increases or decreases in the average flux level during observations lasting several orbital cycles (e.g. Baity et al., 1974) or as a series of successive "high" and "low" states in longer sets of observations. A study of UHURU data recorded between 1970 December and 1973 June established the basic characteristics of each intensity state (Schreier et al., 1976). A typical high state was defined by a count rate of 150 s^{-1} (E = 2-6 keV) and lasted from one to four months. A typical low state showed a

count rate below 20 s^{-1}, similar to the level in mid-eclipse, and lasted for a shorter time than most high states, two weeks to two months. In a high state, the luminosity in X-rays, L_x is observed to be about 5 x 10^{37} erg s^{-1}, for a source distance of 8 kpc (e.g. Nagase et al., 1992).

Of additional interest were the intervals of transition between the two states, which lasted 3 to 5 orbital cycles. A typical transition from low to high initially saw a "spike" in intensity appear near orbital phase 0.5. This gradually heightened until saturating near the usual high-state intensity, extending from orbital phase 0.12 to 0.88. A typical transition from high to low was more rapid but showed much less structure; simply a gradual reduction in intensity over the course of 3 to 4 orbital cycles.

6.1.4. Measurements of the Pulsar Period

The observed spin-up of the pulsar period since its initial measurement has provided compelling evidence for the presence of an accretion disc in the system. Since the discovery of the 4.8 s pulsations, the period has been observed to show intervals of spin-up with substantially differing rates, from -1 x 10^{-12} ss^{-1} to -1 x 10^{-10} ss^{-1}, occasionally larger on a time scale of a few days. Short intervals of spin-down lasting for several weeks have also been observed (e.g. Fabbiano and Schreier, 1977). The pulse period history is given in Figure 6.2.

A large number of X-ray observations were made in the 1970's so that the pulse period was well-defined and the rate of change closely monitored by a number of satellites (UHURU (e.g.Schreier et al., 1972a), Copernicus (Tuohy and Cruise, 1975), ARIEL-V (Pounds et al., 1975), SAS-3 (Kelley et al.,1983), OSO-7 (Baity et al., 1974), COS-B (van der Klis, Bonnet-Bidaud and Robba, 1980) and HEAO-I (Howe et al., 1983)). Fewer X-ray satellites were deployed in the 1980's and consequently observations have been more sparse (e.g. Hakucho (Murukami et al., 1983), GINGA (Nagase, 1989), Roentgen-KVANT (Gilfanov et al., 1989)). Hence less information on the detailed variation of the pulse period has been available. The implementation of the Compton Observatory, in

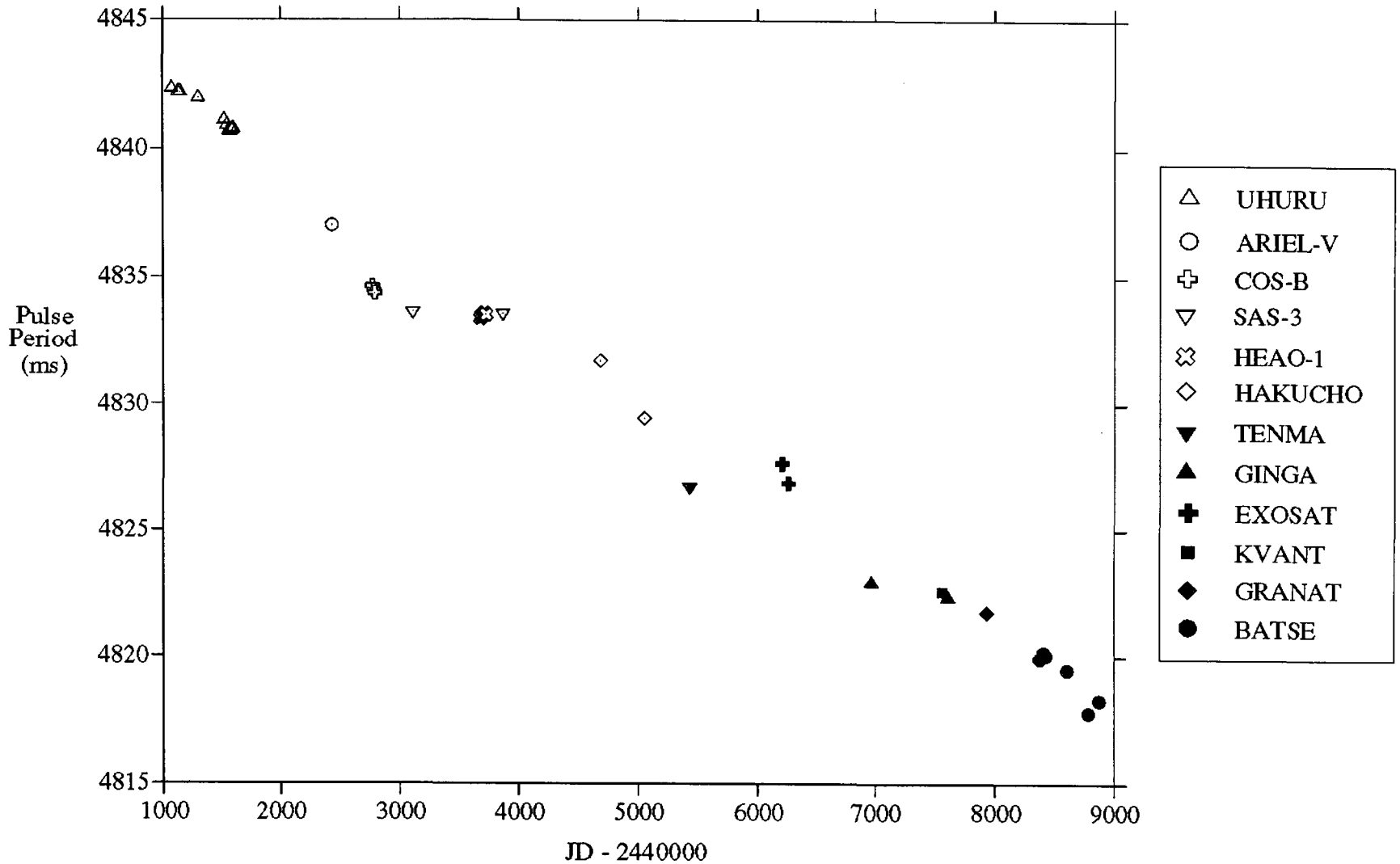

Figure 6.2 : The period history of the X-ray pulsar in Cen X-3. The later BATSE results are shown here as spot points which are derived from the data given later in Figure 6.3.
(refs. in Nagase, 1989; Gilfanov et al., 1989; Finger et al., 1992; Finger et al., 1993)

particular the BATSE instrument, has enabled long-term study of the unpredictable variations in the pulse period to be viable once more (Finger et al., 1992, 1993).

6.1.5. Correlation of Changes in Intensity and Pulse Period

Whilst the observed spin-up of the pulse period suggests an accretion disc is imparting angular momentum to the neutron star, the rates observed are less than would be expected on the basis of the simple disc model of Pringle and Rees (1972) - only about 10% of the torque available from accretion on this model appears to contribute to spinning up the pulsar (Gursky and Schreier, 1975). This strongly suggests that additional braking torques must be present in the system, and this would also explain the intervals of spin-down which have been observed (Fabbiano and Schreier, 1977).

A model of an accretion disc accounting for the additional effects of the magnetic field coupling with the accretion flow near the neutron star (Ghosh and Lamb, 1978) has produced good correlation with the effects observed in Cen X-3. As first detailed by Fabbiano and Schreier (1977), the long term period change may be understood by a natural equilibrium between the Alfven radius r_a and the corotation radius r_{co}. The neutron star would therefore be expected to spin-up most rapidly when the accretion rate is high. A higher accretion rate would cause greater absorption of X-rays near the pulsar, thus an interval of rapid spin-up would be expected to correlate with a low intensity state, particularly in the transition to a low state. Some observations have suggested that this does indeed appear to be the case in Cen X-3 (e.g. van der Klis, Bonnet-Bidaud and Robba, 1980; Howe et al., 1983). More recent BATSE results show a complex variation of the pulse period with an intriguing relation to the most significant changes in the X-ray luminosity as shown in Figure 6.3 (Finger et al., 1993).

6.1.6. Models of Accretion in the System

The actual mode of accretion has been the cause of some conjecture.

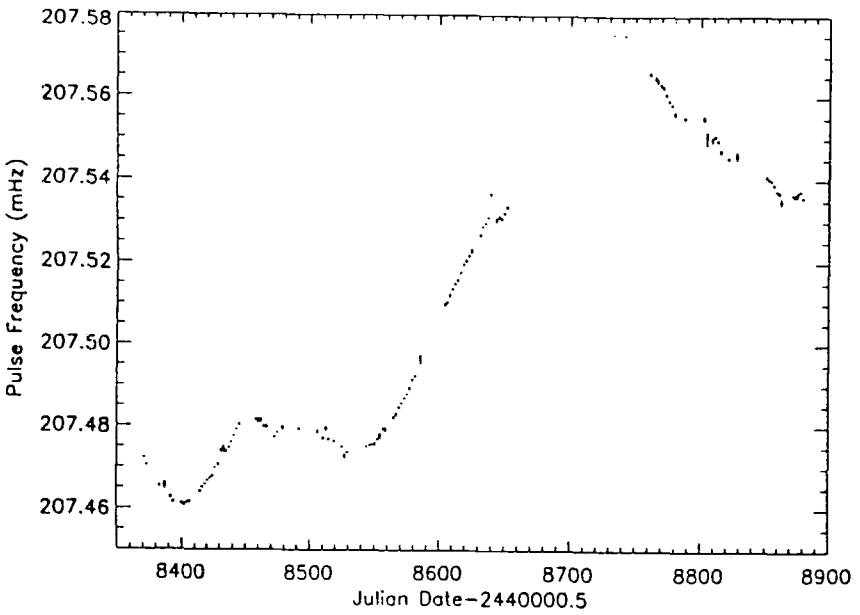

Figure 6.3a : BATSE measurements of the pulse frequency of Cen X-3 in the energy range 20-60 keV determined over each binary orbit.

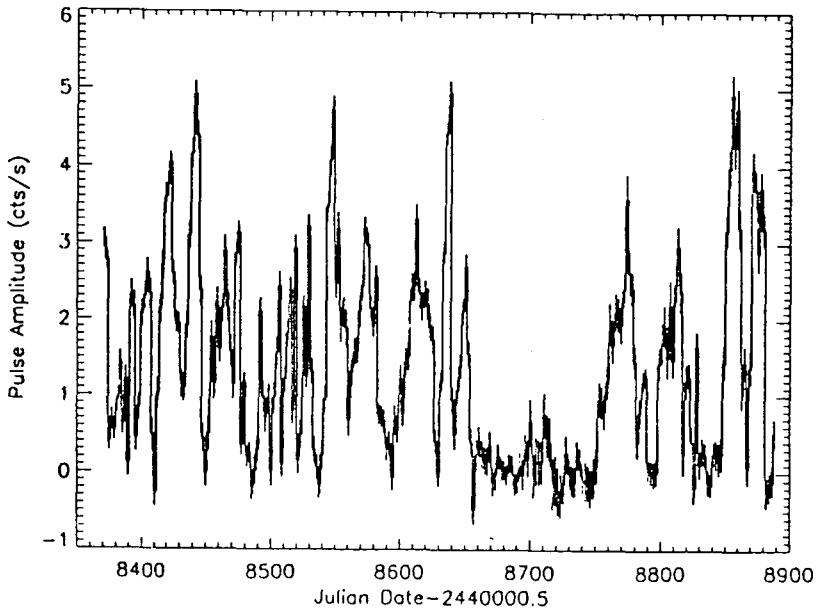

Figure 6.3b : BATSE measurements of the pulsed flux from Cen X-3 in the energy range 20-60 keV correlated with the timing data given in Figure 6.3a.

(from Finger et al., 1993)

Observations of the stellar wind driven off by Krzeminski's star have shown that accretion of this wind would be unable to account for more than 10% of the observed L_x (Lamers, van den Heuvel and Petterson, 1976). The alternative is Roche lobe overflow, with a gas stream transferring matter into an accretion disc. Analysis of published optical light curves has suggested that (a) the primary star is close to filling its Roche lobe and is tidally distorted, (b) an additional light-source is present in the system (Tjemkes, Zuiderwijk and van Paradijs, 1986). However, a simulation of the system which reproduced the general shape and spectral variation of the light curve by including a realistic accretion disc model, with a radius of ≈10 ls, produced too much light from the disc. Nagase et al. (1992) have demonstrated that their observations of the time variation in the strength of the 6.4 keV Fe emission line from Cen X-3 suggest an origin in a reprocessing site ≤1 ls from the neutron star. Later work has shown that this line is pulsed at the 4.8 s period of the neutron star and most likely arises in a shell of material at the Alfven radius rather than over a substantial area of the inner disc (Day et al., 1993) .

For the formation of such an accretion disc via Roche-lobe overflow, the accreting matter must be captured in the gravitational field of the neutron star. Material with too little specific angular momentum may fall directly onto the neutron star, while material with too much kinetic energy may either escape through the outer Lagrangian point or return to the companion (Petterson, 1983). A neutron star provides a small target for the accreting material so that much of the gas flowing through the inner Lagrangian point will overshoot leaving only a fraction of the material to contribute to disc formation (Petterson, 1978). Disc formation is much more likely if the non-degenerate companion is in virtual corotation, as is the case in Cen X-3. The uncaptured gas-stream can form a fan-like structure flowing out of the neutron star's Roche lobe the presence of which could be revealed by strong absorption of the X-ray source between orbital phases 0.5 and 0.8.

6.1.7. Observations of Brief Intensity Dips

The presence of dips in the X-ray intensity during the orbital phase cycle has frequently been observed. These were apparent in UHURU observations of the high intensity state, occurring between orbital phases 0.65 and 0.80 (Schreier et al.,1976). A lesser dip was also noted between 0.4 and 0.5. Data from OSO-7 also suggested the presence of dips at similar orbital phases (Baity et al., 1974). Copernicus observations reported a 70% decrease in intensity at phase 0.51, followed by an increase in flux from 0.53-0.83, interrupted by several declines, lasting for 1-2 hours (Tuohy and Cruise, 1975). Sets of three dips were seen at similar phases in observations taken 3 months apart. ARIEL-V data further confirmed the presence of these reductions in the flux (Pounds et al., 1975) which were again observed in the range 0.5-0.8. The intensity was reduced to 20% of the maximum as compared with the residual 5-10% level detected during eclipse. In all cases the dips were only seen during high intensity states (see Figure 6.4).

6.1.8. Absorption Origin of Intensity Dips

Explanations of these dips initially concentrated on the likelihood of an accretion wake forming behind the neutron star (Jackson, 1975; Fabbiano and Schreier, 1977). The rapid onset of the dip was attributed to absorption in the dense shock front of the accretion wake. The subsequent dips and secondary maximum were attributed to absorption in further structure parallel to the shock front.

These observations could also be linked with the onset of a change between intensity states. The sharp absorption seen at phase 0.51 in the Copernicus data (Tuohy and Cruise, 1975) was followed by a markedly slower egress from the eclipse state, indicating an increased stellar wind density, and hence a denser shock front. Fabbiano and Schreier (1977) postulated that a low intensity state was associated with a high stellar wind density heavily absorbing the neutron star's emission. An ionisation zone around the neutron

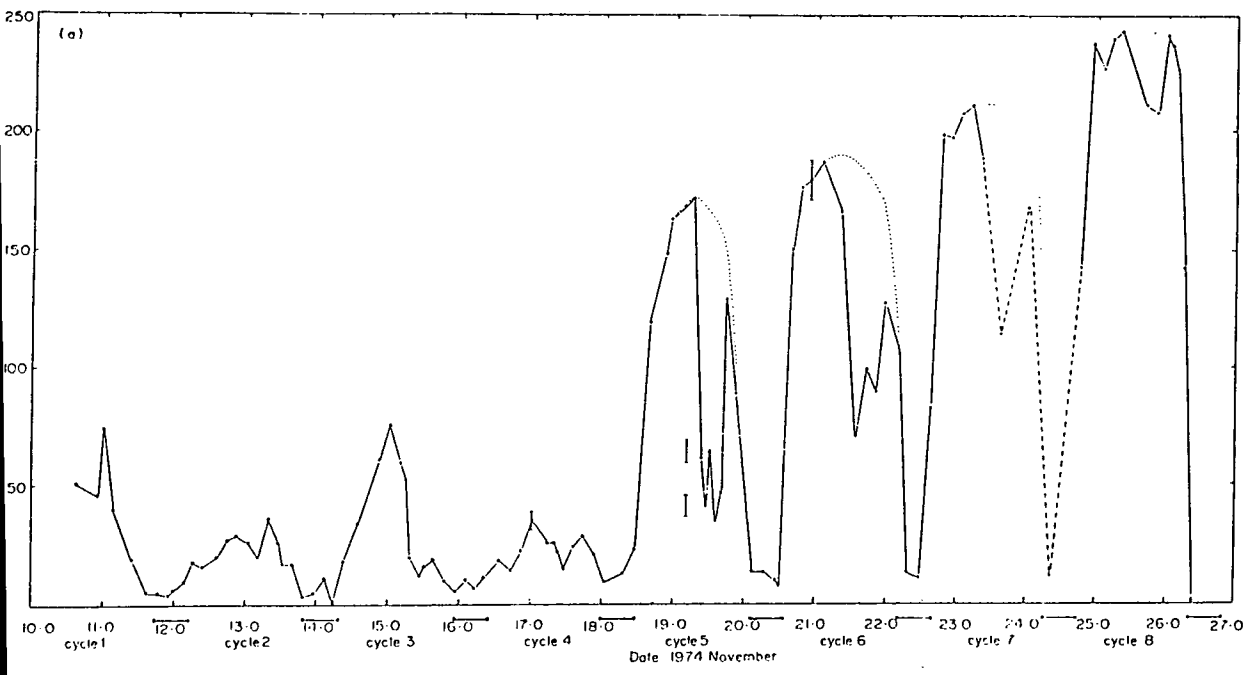

Figure 6.4 : ARIEL-V measurements of intensity dips in the emission from Cen X-3 at 2.4-19.8 keV in 1974 November. The greatest reduction occurred at phases 0.6-0.8, and immediately after the onset of a high intensity state. The eclipses of the X-ray source are also clearly visible.

(from Pounds et al., 1975)

star was considered to expand once the wind density reduced and form a narrow "cone" through which X-ray emission could become visible first at phase 0.5. As the wind density continued to decrease so the range of orbital phases for which emission would be seen would also increase until the process was reversed by an increased stellar wind.

The basic idea of absorption causing the dips in emission has been supported by X-ray spectral data showing a larger value for the low-energy cut-off during dips and low intensity states (e.g. Fabbiano and Schreier, 1977; Nagase at al ,1992). It has already been noted that the spin-up rate of the neutron star increases during low intensity states indicating increased accretion and correlated absorption. However, Petterson (1978) has pointed out that due to the high speed and low density of the stellar wind, the model described in the previous paragraph cannot fully account for either the observed amplitude of the absorption dips or their extension beyond phase 0.75. It appears likely that the state of material in this system is complex, with gas streams from the primary forming a fan-like structure around a stable accretion disc. At least 90% of the accretion-induced X-ray luminosity must arise directly from Roche lobe overflow from Krzeminski's star (Lamers, van den Heuvel and Petterson, 1976).

6.1.9. Information Gained from Orbital Period Changes

The fact that Cen X-3 displays strong evidence for an accretion disc implies that the companion star is close to corotation (Petterson, 1978). This suggests that angular momentum must have been transferred between the orbit and the rotation of Krzeminski's star (Sparks, 1975), a conclusion supported by the circularisation of the orbit (Murukami et al., 1983). The result of this would be a long-term decrease in the binary orbital period. Early observations did not provide conclusive evidence for this hypothesis (e.g. Fabbiano and Schreier, 1977). A measurable rate of orbital period decay was first reported by Kelley et al. (1983). The temporal baseline used by Kelley et al. was doubled in length by Nagase et al. (1992), who included eclipse

measurements from the Hakucho, Tenma and Ginga spacecraft. This enabled the orbital period derivative to be precisely determined as $-(1.738 \pm 0.004) \times 10^{-6}$ yr^{-1}. Cen X-3 was the first X-ray binary for which a finite rate of orbital period decay was measured, and recent observations have shown that Hercules X-1 (Deeter et al., 1991) and SMC X-1 (Levine et al, 1993) show a similar phenomenon.

6.2. Previous TeV Gamma Ray Observations

6.2.1. Observations by the Durham Group

Given its southerly declination of -60°, Centaurus X-3 has only recently become subject to long-term observation with the expansion of southern hemisphere TeV gamma ray facilities. The first detection of Cen X-3 at TeV energies was reported by the Durham group (Carraminana et al., 1989a; Brazier et al., 1990c) based on data recorded using the Mk.3 telescope at Narrabri (as described in Chapter 3). The total dataset comprised 58 observations, recorded between 1987 January and 1989 June. After applying a standard data selection, the datasets were tested for periodicity over a fixed range of trial periods, centred on the X-ray period appropriate to the midpoint of the dataset, and combined incoherently. No significant periodic effect was noted. The data were then split into 10 subgroups divided by orbital phase. Of the 10, only that corresponding to 12 observations in the phase range 0.75-0.85 was found to show evidence for emission at the X-ray period. The chance probability of this effect was estimated as 6×10^{-6}. The strongest emission at the expected X-ray period appeared to come from 8 observations made in the phase range 0.77-0.82. The peak flux at energies >300 GeV was 6×10^{-10} cm^{-2}s^{-1}.

6.2.2. Observations by the Potchefstroom Group

The Potchefstroom group have reported results which may confirm the existence of TeV emission. Their initial analysis of 35 observations recorded between 1986 May and 1989 April (North et al., 1990), concentrated on dividing the observations by orbital phase. Only the interval 0.7 to 0.8, containing 3

observations, was found to show significant evidence for emission, with a chance probability of 3×10^{-3}. This corresponded to a photon flux of $\approx 1 \times 10^{-10}$ cm^{-2}s^{-1} above 1.9 TeV. A factor weighing against this claim of emission was the period identified for TeV emission of 4.175 ± 0.010 s. This was almost 5 independent sampling intervals (0.005 s) below the contemporary X-ray periods subsequently identified (Nagase, 1989; Nagase et al., 1992) and the implied period derivative was much larger than any ever seen at X-ray energies.

A later study by the Potchefstroom group took a different approach (North et al., 1991a). The database was extended to include data from 1990, resulting in a total of 41 observations being used. Ignoring the previous division of data into 10 segments, the hypothesis tested was that TeV gamma ray emission only occurred when an accretion wake of the type observed with ARIEL-V (Pounds et al., 1975; Jackson et al., 1975) passed through the line of sight.

In practical terms, this meant defining the "wake" passage as orbital phase 0.52-0.76 and forming two datasets, one "in-wake" and one "out-of-wake". 9 of the 41 observations were recorded in the specified phase range. Both datasets were tested for periodicity on a night-by-night basis, using the appropriate X-ray periods, and the results combined incoherently. Only the in-wake dataset showed evidence for a periodic signal; the significance was estimated as 2×10^{-2}. 8 of the 9 observations in the wake were found to contribute to this signal, but 3 observations recorded just above phase 0.76, just beyond the defined accretion wake position, were also found to contain a periodic signal. The periodograms and phase relation of the emission are shown in Figure 6.5. The flux from the in-wake dataset was calculated to be 3.9×10^{-11} cm^{-2}s^{-1}.

6.2.3. Results of Other TeV Gamma Ray Observations

The earliest observations of Cen X-3 at TeV energies were made in 1972 April (Grindlay et al., 1975). A 3 hour dataset was recorded at energies ≥ 0.6

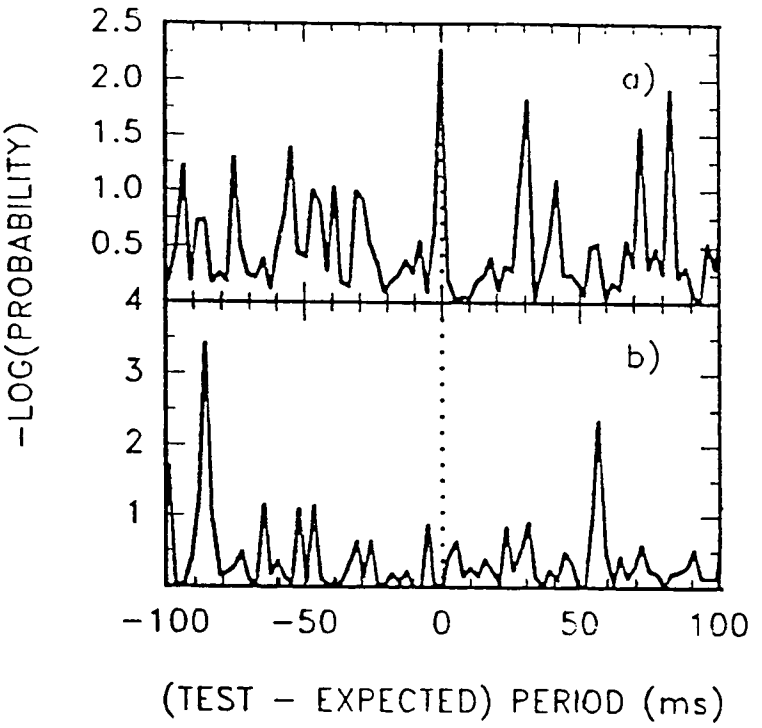

Figure 6.5a : Rayleigh probability versus trial period for an incoherent combination of 41 observations of Cen X-3 by the Potchefstroom group. The upper periodogram shows the result for the data recorded in the orbital phase range 0.52-0.76; the lower shows the result for all remainder. The dotted line indicates the X-ray period.

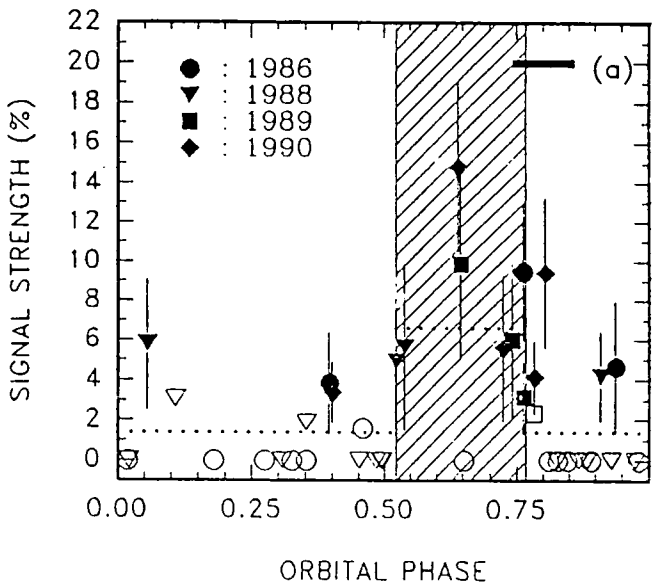

Figure 6.5b : Pulsed signal strength as a function of orbital phase for each of the Potchefstroom observations of Cen X-3. The hatched area corresponds to the region of the accretion wake.

(from North et al., 1991a)

TeV, resulting in an upper flux limit of 4.3×10^{-11} photons $cm^{-2}s^{-1}$. Further analysis yielded no evidence for a pulsed signal or any enhancement associated with the orbital phase.

The Adelaide group have reported their results from data recorded in 1991 February-April at energies ≥0.6 TeV (Thornton et al., 1991). 11 observations were made between orbital phases 0.77 and 0.83. The observations were analysed for periodicity at the X-ray period and the results combined incoherently. No significant signal was seen, nor was any improvement gained by subdividing into smaller segments. However, given the sensitivity of the telescope used, it was concluded that a decrease in luminosity of only 50% from earlier positive results would explain this null result.

The JANZOS collaboration have reported the results of 5 observations of Cen X-3 made in 1988, 2 of which were near the ascending node of the orbital cycle (Allen et al., 1993). No periodic signal or d.c. excess was found at energies ≥1 TeV and an upper flux limit of 4×10^{-11} $cm^{-2}s^{-1}$ was derived. Again, this was consistent with all of the detections and upper flux limits previously reported.

6.3. The Durham Cen X-3 Database

6.3.1. Observations and Data Reduction

This study is concerned with the analysis of the large dataset collected using the University of Durham Mk.3 telescope at Narrabri, N.S.W., where observations of Centaurus X-3 have been made in every year since its installation. The telescope has been used to observe atmospheric Cerenkov flashes from the direction of Cen X-3 on over 100 separate nights, spread over 19 dark moon intervals, from 1987 January to 1992 May. Most of the observations were made with the telescope in tracking mode but 17 were recorded whilst the telescope was in chopping mode to search for a d.c. excess in the signal.

For this analysis, the event times recorded were reduced to the solar

system barycentre and also corrected for the orbital motion in the binary system using the orbital elements given in Table 6.1. The detection of pulsed TeV emission from Cen X-3 would require the appropriate 4.8 s periodicity to be established within the data, and thus the database first had to be reduced to contain only those nights of fine weather. No significant interruptions due to cloud passing through the field of view were allowed since the could introduce spurious periodicities into the counting rate. On checking weather records and the count-rate histories for each observation, a number were deemed too poor to be used at all, and a further 7 had short spells of bad weather at the beginning or end of the run extracted and discarded. The dates and details of the 109 observations passed as suitable for analysis are given in Table 6.2.

6.3.2. Selection of Data for Analysis

The data accepted for analysis purposes was subjected to the standard event rejection procedures. Only events which produced a response in the on-source channel unaccompanied by any of the off-source channels were accepted for inclusion in the final dataset. In addition, the records from the guard-ring of photomultiplier tubes were studied in order to apply the relative response technique. A previous analysis has determined the effect of the relative response threshold selection in the case of Cen X-3 (Brazier, 1991). The greatest enhancement of a possible gamma-ray signal was achieved when the off-source channels were restricted to a response of no more than 30% of the central on-source channel.

This selection was therefore used on all of the tracked data used in this work with the exceptions of (a) the data recorded in 1992, which for technical reasons were restricted to the basic selection of a centre channel response only, and (b) the data recorded with the telescope in chopping mode. The latter category of data could not be selected using the relative response technique as the source was viewed alternately by the on-source tube, fully surrounded by the guard-ring, and an outer off-source tube, with only a

TABLE 6.1 - Orbital ephemeris for Centaurus X-3

Epoch of mid-eclipse [a]	:	JD 2448562.156702 ± 0.000071
$a \sin i$ [b]	:	39.636 ± 0.003 ls
Orbital Period P_{orb} [a]	:	2.08706533 ± 0.00000049 d
$\dot{P}_{orb}$ [c]	:	$(-0.993 \pm 0.002) \times 10^{-8}$
$\dot{P}_{orb}/P_{orb}$ [c]	:	$(-1.738 \pm 0.004) \times 10^{-6}$ yr^{-1}

[a - Finger et al., 1993 ; b - Kelley et al., 1983; c - Nagase et al., 1992]

TABLE 6.2 - Catalogue of Mk.3 telescope observations of Cen X-3

Observation Date	Duration (hours)	Events Selected	Orbital Phase at Midpoint	Notes
28 01 87	2.5	2339	0.28	
29 01 87	2.3	2745	0.76	
30 01 87	1.7	1284	0.23	
31 01 87	2.5	2113	0.72	
01 02 87	2.5	1964	0.20	
02 02 87	2.5	2636	0.69	
03 02 87	2.6	2790	0.16	
04 02 87	2.5	2884	0.63	
06 02 87	2.5	2279	0.59	
07 02 87	2.0	3241	0.08	
29 04 87	3.0	2674	0.80	
03 05 87	3.0	2344	0.72	
19 05 87	2.0	1773	0.33	
20 05 87	3.5	2995	0.83	
21 05 87	3.0	1468	0.32	
22 05 87	4.0	4672	0.78	
23 05 87	3.3	4086	0.25	
24 05 87	3.5	3088	0.74	
25 05 87	3.5	4932	0.21	
26 05 87	3.5	2571	0.69	
27 05 87	3.5	4253	0.17	
28 05 87	4.0	3841	0.66	
29 05 87	3.5	4268	0.13	
30 05 87	3.7	3454	0.62	
31 05 87	3.3	3418	0.09	
17 01 88	2.0	2684	0.89	Chopped
18 01 88	3.3	5411	0.36	Chopped
19 01 88	3.0	6043	0.84	Chopped
20 01 88	3.5	6501	0.32	Chopped
21 01 88	2.7	5159	0.80	Chopped
22 01 88	2.7	5221	0.28	Chopped
24 01 88	2.7	5637	0.24	Chopped
25 01 88	3.6	5698	0.69	Chopped
15 02 88	3.5	7425	0.77	Chopped
17 02 88	4.2	8715	0.73	Chopped
19 02 88	4.3	8379	0.69	Chopped
24 02 88	5.4	6345	0.08	Chopped
25 02 88	4.5	6304	0.57	Chopped
26 02 88	3.4	5273	0.05	Chopped
28 02 88	1.6	1665	0.03	Chopped
11 05 88	3.5	2526	0.86	
13 05 88	3.5	7770	0.82	Chopped
15 05 88	4.0	1162	0.80	
19 05 88	3.0	788	0.77	

TABLE 6.2 (continued)

Observation Date	Duration (hours)	Events Selected	Orbital Phase at Midpoint	Notes
05 06 88	3.3	2059	0.85	
07 06 88	3.1	6261	0.82	Chopped
06 01 89	3.0	2011	0.98	
09 01 89	2.0	2329	0.43	
14 01 89	4.0	5174	0.80	
16 01 89	3.0	3444	0.78	
01 03 89	3.7	3240	0.77	
27 04 89	3.0	2951	0.06	
28 04 89	4.2	5060	0.55	
29 04 89	4.0	4012	0.06	
30 04 89	2.0	3133	0.52	
01 05 89	2.0	2701	0.01	
02 05 89	4.0	3036	0.49	
03 05 89	3.0	3495	0.96	
04 05 89	3.0	3481	0.44	
28 05 89	5.0	5186	0.92	
29 05 89	4.7	3681	0.40	
01 06 89	3.0	1779	0.85	
07 06 89	1.7	2306	0.71	
29 01 90	2.0	1305	0.91	
30 01 90	4.0	3553	0.36	
31 01 90	4.5	2737	0.84	
22 02 90	4.6	1994	0.37	
23 02 90	2.0	1753	0.84	
24 02 90	1.7	2517	0.31	
25 02 90	1.7	2877	0.78	
26 02 90	1.7	2882	0.27	
01 03 90	3.0	2073	0.70	
04 03 90	2.5	2517	0.16	
14 05 90	1.0	412	0.08	
15 05 90	2.7	690	0.56	
21 05 90	2.5	354	0.43	
10 01 91	1.5	186	0.63	
11 01 91	2.0	380	0.13	
14 01 91	4.7	2073	0.58	
15 01 91	3.0	960	0.07	
17 01 91	2.5	1286	0.03	
18 01 91	3.0	2184	0.51	
19 01 91	3.4	2159	0.99	

TABLE 6.2 (continued)

Observation Date	Duration (hours)	Events Selected	Orbital Phase at Midpoint	Notes
08 02 91	3.0	758	0.50	
10 02 91	1.7	629	0.52	
11 02 91	2.5	1402	0.01	
19 02 91	4.5	2617	0.79	
21 02 91	3.0	1333	0.80	
11 03 91	1.5	252	0.40	
12 03 91	5.2	1379	0.87	
13 03 91	5.3	1375	0.30	
14 03 91	4.3	964	0.79	
16 03 91	5.2	1049	0.74	
17 03 91	8.6	2102	0.25	
18 03 91	8.4	1787	0.73	
19 03 91	4.1	839	0.19	
20 03 91	8.3	1409	0.70	
21 03 91	4.3	974	0.15	
22 03 91	3.5	933	0.65	
23 03 91	1.0	214	0.14	
28 02 92	1.6	1228	0.97	
02 03 92	1.3	1374	0.42	
07 03 92	3.9	3583	0.79	
09 03 92	2.0	2204	0.79	
10 03 92	1.7	1523	0.27	
26 05 92	2.7	2868	0.11	
28 05 92	5.3	5193	0.07	
29 05 92	4.3	4223	0.54	
31 05 92	5.2	5772	0.50	
TOTALS :	356.3	321033		

partial guard-ring. The lower rejection resulting from the incomplete guard-ring would result in too great a difference in count-rates between the two tubes. Events recorded in this mode were selected provided that they triggered a response in the on-source channel alone.

The final total of 109 observations used in this analysis consisted of 356 hours of on-source time, producing 321000 events which were selected by the above procedures.

6.4. Testing for Uniformity of Phase in Individual Observations

6.4.1. Selection of Period Search Range

The data from each individual night were tested for uniformity of phase by employing the Rayleigh test. The 4.8 s pulsar is known to be spinning up although occasional intervals are known to occur in which the rate of spin-up significantly decreases or even changes to spin-down. These intervals occur unpredictably and therefore a unique secular period derivative cannot be used to precisely link observations made over the course of a year or more. Fortunately, several X-ray measurements of the pulsar period were made between 1987 and 1992 (see Figure 6.2) and therefore the expected period could be reasonably estimated to an accuracy of ±0.5 ms for any date in the range of this study.

For a typical observation lasting ≈3 hours, the independent sampling interval when searching for a 4.8 s period is ≈2 ms so that the expected periodicity may be recovered within a single trial period interval. However, unless a gamma-ray signal is present with a strength of at least several per cent of the remaining proton background, it is unlikely that a single observation would be sufficient for any emission to be detectable.

6.4.2. Identification of Datasets Showing Evidence of Emission

Of the 109 observations used here, 3 showed evidence for non-uniformity of phase at the correct contemporary period with an uncorrected probability $\leq 10^{-3}$ that the signal occurred by chance. These were 1987 May 22, 1988 January

21 and 1991 March 13 (see Table 6.3). The corrected probabilities are also given for the observations listed in Table 6.3, i.e. after allowing for 3 degrees of freedom used in oversampling the trial period interval and 109 for the number of observations analysed. None of the three are sufficient on their own to provide evidence for a 3σ signal detection.

The observation producing the most significant result, that of 1988 January 21, was made with the telescope in chopping mode. The corresponding off-source data recorded on the same channels whilst pointing 2° from the source direction have been analysed and show no evidence for any similar periodicity. The atmospheric clarity on this date was not stable enough on a timescale of a few minutes to allow a direct comparison of the on- and off-source count rates to be made.

6.4.3. Search for "Bursts" of Periodic Emission

Each of the three datasets identified in the previous section was also studied to determine whether the weak periodic signal was in the form of continuous steady emission, or characterised by one or more bursts of activity. The data from each were split into segments 2400 seconds long, consecutive bins beginning 800 s after that immediately before, i.e. stepping one-third of a bin at a time. The period search was taken over the same range as for the whole dataset, though the independent sampling interval was wider due to the shorter timespan. No evidence was found for any significant short-lived enhancement in the periodic signal during any of the observations.

6.4.4. A Search for Orbital Phase Dependence

The relationship of the observed chance probability of TeV gamma ray emission to the orbital phase of the relevant observation was also studied. The chance probability of uniformity of phase within 1 ms of the calculated X-ray period for each night was found for each dataset and the results plotted against the orbital phase of the observation in question (Figure 6.6). It is clear that the most significant results coincided with the passage of the

TABLE 6.3 - Observations showing strongest evidence for non-uniformity of phase at the X-ray period			
Observation Date	Chance Probability [raw (corrected)]	Signal Strength	P* (ms)
1987 May 22	5.4×10^{-5} (1.7×10^{-2})	4.6 %	4823 ± 1
1988 Jan 21	1.9×10^{-5} (6.2×10^{-3})	4.6 %	4823 ± 1
1991 Mar 13	6.7×10^{-4} (2.2×10^{-1})	7.3 %	4820 ± 1

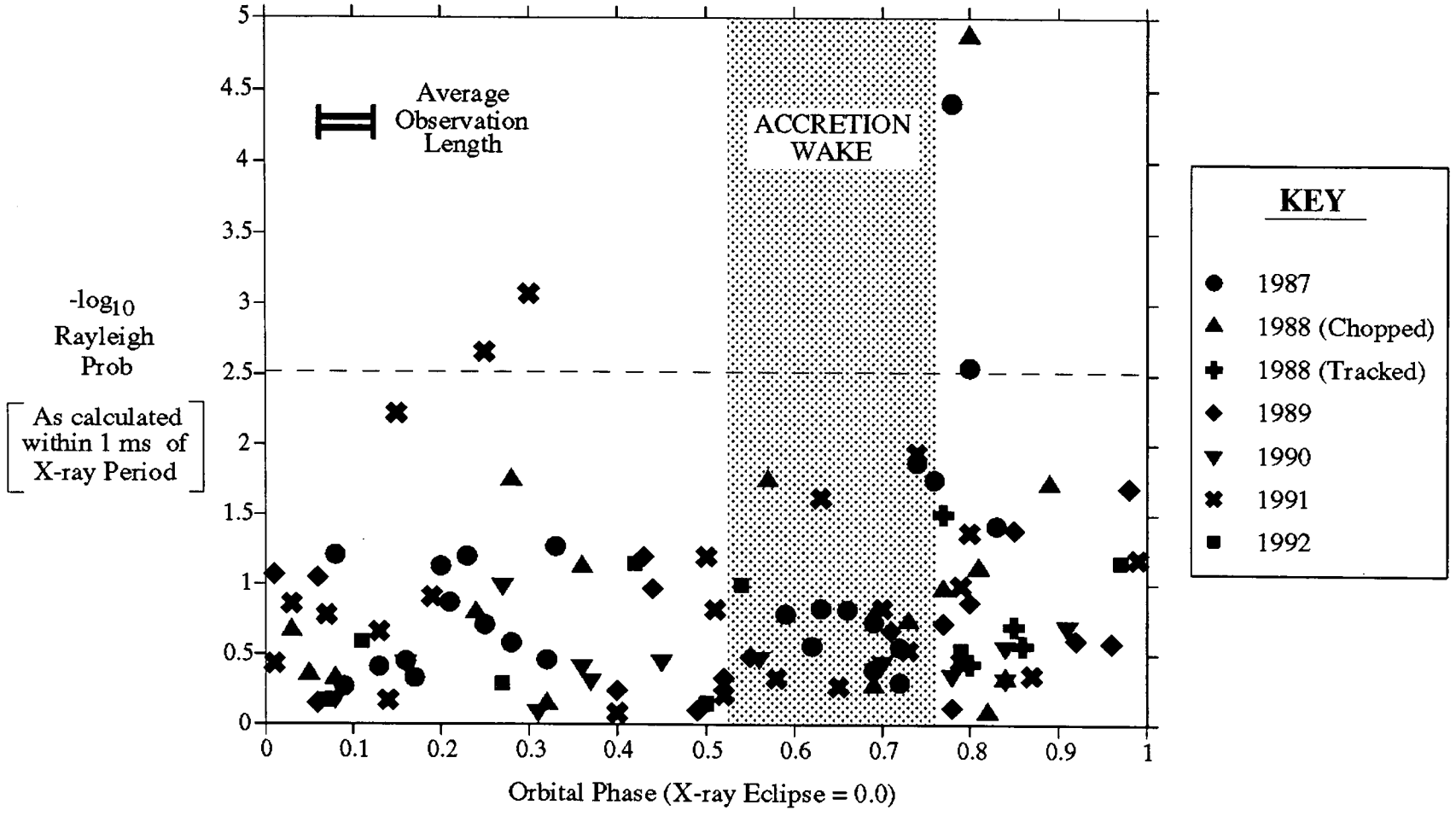

Figure 6.6 : Rayleigh probability of uniformity of phase at the X-ray period for all Mk.3 telescope observations of Cen X-3. The orbital phase is taken to be that at the midpoint of each observation. The horizontal dotted line shows a chance probability of unity after allowing for 327 degrees of freedom (3x109). The position of the accretion wake is based on the work of Pounds et al. (1975) for comparison with the Potchefstroom results shown in Figure 6.5.

neutron star through the nodes of its orbit, although this is partly explained by the fact that more observations were taken near the nodes after encouraging results from early analyses.

As described in section 6.2.2, the Potchefstroom group have reported the results of their 41 observations of Cen X-3 in which they tested the hypothesis that TeV emission only occurred between the phases 0.52-0.76. Their conclusion was that this was the case, though only at a significance of 2.4σ. The position of the accretion wake which they assumed to be the most likely source of TeV gamma ray emission is marked by the grey area in Figure 6.6. It can be seen that the lowest levels of chance probability in the present observations coincide with the trailing edge of the accretion wake being in the line of sight to the observer, which was not in fact well defined by the Ariel-V X-ray measurements. Given an average observation length corresponding to ≈ 0.06 in orbital phase, the results reported here would be consistent with a TeV gamma ray production site within the proposed accretion wake. However, as outlined in section 6.1.8 it appears more likely that the absorption near these phases is caused by streams of gas much narrower than the proposed accretion wake. Such material would make a far more intermittent and localised target for TeV gamma ray production and would account for the nature of the orbital modulation suggested here.

6.5. Periodic Analysis of Combined Observations

6.5.1. Combination of Entire Dataset

A combination of the complete set of observations of Cen X-3 was made in order to search for unambiguous evidence of a gamma-ray signal with the same periodicity as that seen at X-ray energies. Since the dataset consists of 109 observations from six years of observing, the effect of the gradually changing X-ray pulsar period had to be taken into account and suitable corrections included. This was done by studying the history of the pulsar period and hence assigning to each night a discrete value for the expected periodicity which

was assumed to be correct to within 0.5 ms of the genuine contemporary period.

Since the pulsar period has never been observed to change by more than 0.5 ms within a timescale of a month, the data from each dark moon interval, which normally spanned about 2 weeks, were assigned a single candidate period, as listed in Table 6.4. The test for uniformity of phase was then applied over a constant matrix of candidate periods defined at 0.5 ms intervals either side of the contemporary period P_x. All 109 results at each period value were combined using the formulation given in equation 4.2 to produce a χ^2 statistic with 2x109 degrees of freedom.

The resultant periodogram (Figure 6.7) showed a minimum chance probability of 1×10^{-3} at a trial period 0.5 ms longer than the contemporary period, within the bounds of the error introduced by the uncertainty in the periods used. Given the lack of data manipulation or orbital phase selection involved, and the adherence to as close a period to the X-ray measurements as possible, this result is modified by the 3 degrees of freedom which were used in oversampling the trial period range, and the probability of chance occurrence therefore increases to 3×10^{-3}. This is marginally below the level required for a 3σ detection of a pulsed signal but represents the clearest evidence to date for a persistent 4.8 s periodicity in the Durham database. Given the uncorrected chance probability of 4.5×10^{-4} which would have produced a 3σ detection, and the total of 321000 events used in this analysis, the upper limit on the pulsed signal strength may be set at 2.1%. This corresponds to a time-averaged pulsed flux above 300 GeV of 1.0×10^{-10} ss^{-1}. After scaling to allow for the energy threshold of the Mk.3 telescope, this limit is below the values reported by the Potchefstroom and JANZOS groups, which were a claimed detection and upper limit respectively.

6.5.2. Combination of Data from Single Dark Moon Intervals

6.5.2.1. Incoherent Combinations of the Data

Since the effective duration of an incoherently merged dataset is similar to that of a single night, the independent sampling interval remained at ≈2

TABLE 6.4 - Contemporary Cen X-3 pulse periods	
Month of Observation	Period (ms)
1987 January, February, April, May	4823.0
1988 January, February, May, June	4822.5
1989 January, March	
1989 April, May, June	4822.0
1990 January, February	
1990 May	4821.5
1991 January	4820.5
1991 February, March	4820.0
1992 February, March, May	4818.0

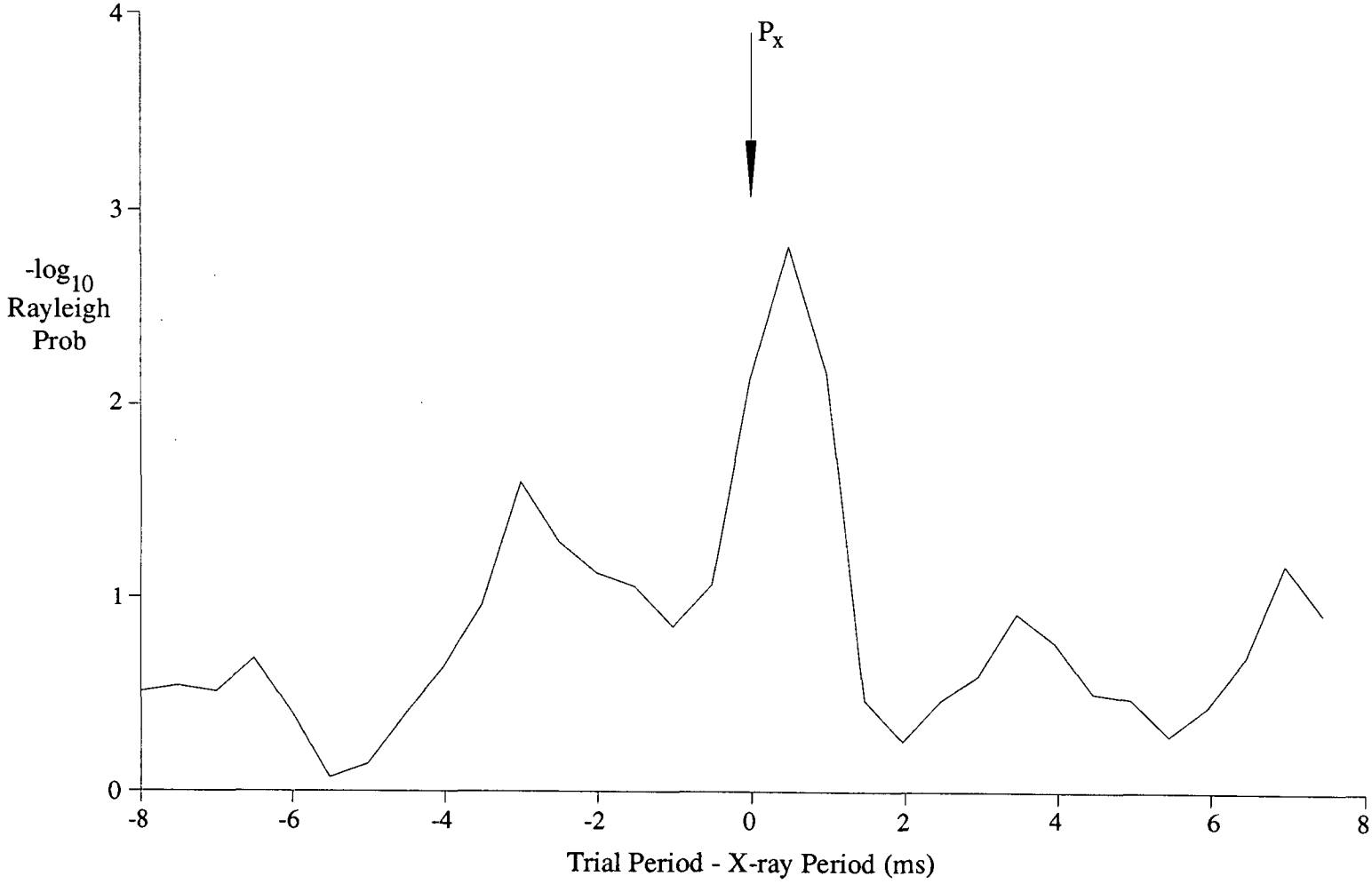

Figure 6.7 : Rayleigh probability versus trial period for an incoherent combination of all 109 Mk.3 telescope observations of Cen X-3 used in the present work. The fixed matrix of trial periods used is defined with respect to contemporary X-ray measurements.

ms, and thus the same sampling range in period could be used as that for a single night. The use of a short-term period derivative was not required. All of the 16 dark moon intervals consisting of 3 or more nights were merged in this way. Only two datasets, the 8 nights recorded in 1988 January and the 13 nights of data from 1991 March, showed evidence for a pulsed gamma ray signal at the expected period, with raw chance probabilities of 7×10^{-4} and 4×10^{-3} respectively. These figures increased to 3×10^{-2} and 2×10^{-1} after allowing for degrees of freedom used (3 for oversampling and 16 for the number of intervals tested).

Since the 1988 January data were recorded in the chopping mode, the off-source data were also tested for uniformity of phase. No evidence for a signal at the pulsar period was found. The on-source channel recorded 0.6% more events than the off-source channel though the significance of this excess was only 1.3σ (42624 events on-source compared with 42359 off-source).

6.5.2.2. Coherent Combinations

For a coherent combination of a number of observations, the length of the independent sampling interval in period becomes much shorter than that for a single observation (see Chapter 4). A strong periodic signal will be revealed with minimal aliasing due to the 24-hour periodicity in the data. All of the coherently merged datasets were therefore analysed over a preset period range 1 ms either side of the contemporary X-ray pulse period.

The pulsar period derivative must be used to correct for the accumulated pulse phase difference induced when merging times recorded over a timespan of $\approx$10 days. Up to 1990, the period derivative used was the lower value of -8×10^{-12} ss^{-1}, but as prescribed by contemporary satellite observations the more rapid rate of -4×10^{-11} ss^{-1} was used for 1990 and 1991 data. By 1992, the BATSE instrument was producing a near continuous contemporary record of the pulsar period history and appropriate values of the period derivative were used; -2×10^{-10} ss^{-1} for 1992 February and $+7 \times 10^{-11}$ ss^{-1} for 1992 May

(Finger et al., 1992).

The data from two dark moon intervals were found to show some evidence for a pulsed signal at the expected pulsar period; 1987 May and 1991 March as shown in Table 6.5 and Figures 6.8a,b. Both datasets included one of the strong observations listed in Table 6.3 which will obviously reinforce any weaker persistent signal. After correction for the degrees of freedom used in the Rayleigh test (5 for oversampling in trial period and 16 for the number of datasets tested) neither month gave a result significant at the 3σ level. The dataset of 1987 May enabled the placing of an upper limit on the photon flux of 7.5×10^{-10} $cm^{-2}s^{-1}$ above 300 GeV. For the smaller dataset of 1991 March the upper limit was 1.4×10^{-10} $cm^{-2}s^{-1}$ at photon energies above 300 GeV.

One point to note about the result for 1991 March is that when the initial analysis was made, in mid-1991, the signal discovered was at a period too short (4820.8 ms) to be consistent with the X-ray satellite measurements then being used to define the expected pulsar period. However, contemporary 20-60 keV observations later reported by the Compton Observatory BATSE group (Finger et al, 1992) revealed the pulsar to be spinning up rapidly once more. The pulsar period was shown to be variable about a value of 4820.0 ms in mid-1991. Despite the low significance of the TeV gamma ray result reported here, this could be viewed as independent confirmation of the pulsar's behaviour. Although this was the best evidence for emission from any of the datasets, it did not appear to coincide with the renewed spin-up of the pulsar, which began in late 1989. The observations made in 1990, 1991 pre-March and 1992 show no significant periodic emission.

6.5.3. Combination of Data Grouped by Orbital Phase

6.5.3.1. Division into 10 Phase Intervals

The 109 observations of Cen X-3 were spread randomly throughout the 2.1 day binary cycle. Virtually 100% orbital phase coverage was achieved since a typical observation lasting ≈3 hours covered a range of ≈0.06 in phase. With a database of this nature it was possible to search for orbital phase

TABLE 6.5 - Coherent combinations of data showing evidence for non-uniformity of phase			
Observation Month	Chance Probability [raw (corrected)]	Signal Strength	P* (ms)
1987 May	9.9×10^{-4} (7.9×10^{-2})	1.2 %	4822.7 ± 0.3
1991 March	1.6×10^{-4} (1.3×10^{-2})	2.6 %	4820.8 ± 0.3

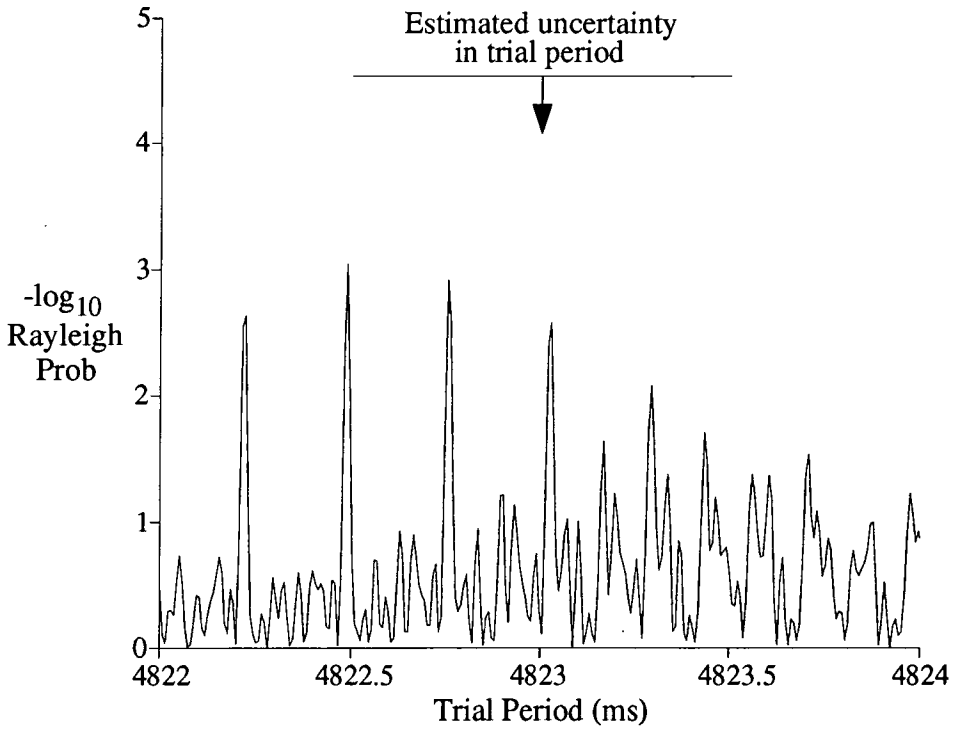

Figure 6.8a : Rayleigh probability versus trial period for a coherent combination of the 13 Mk.3 telescope observations of Cen X-3 recorded during 1987 May.

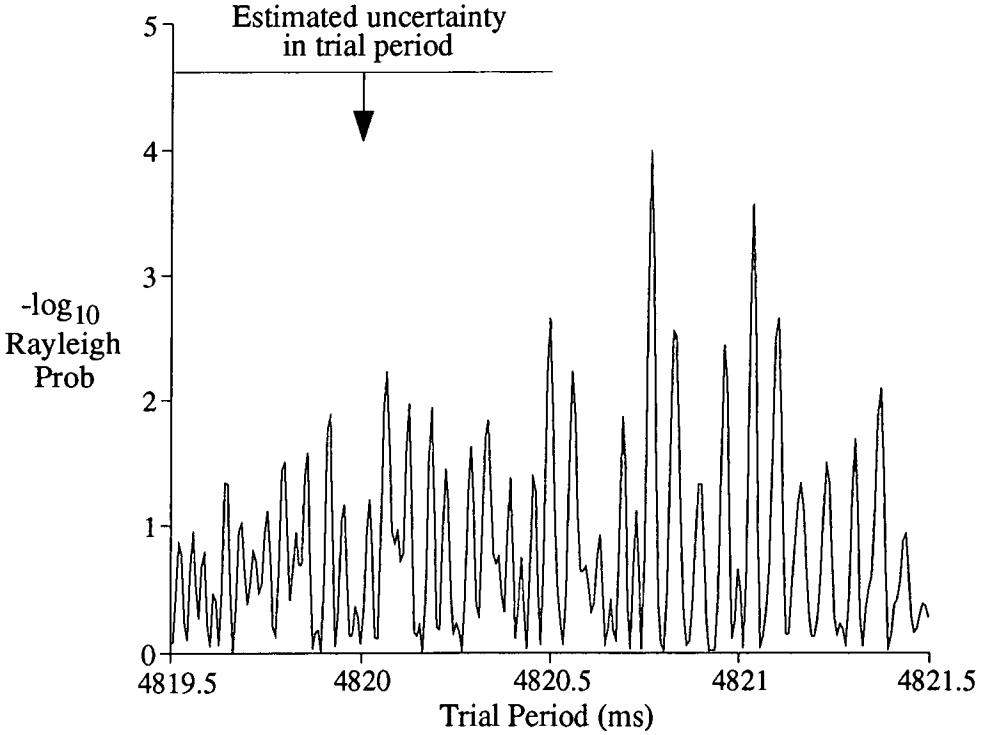

Figure 6.8b : Rayleigh probability versus trial period for a coherent combination of the 12 Mk.3 telescope observations of Cen X-3 recorded during 1991 March.

dependence, as is often seen at X-ray energies, in any gamma-ray emission.

The data were divided into sections corresponding to 10% of the orbit, i.e. beginning with phases 0.05 to 0.14, 0.15 to 0.24, and so on, ending with 0.95 to 0.04 (with respect to phase 0.00 at the time of mid-eclipse of the X-ray source). Each observation was assigned an orbital phase corresponding to the midpoint time of the observation, as given in Table 6.2. The number of datasets in a given phase bin varied between 7 and 22. This was partly due to some targetting of nights when the pulsar was near the ascending node of its orbit, after the night of 1987 May 22 (at orbital phase 0.78) was originally found to show some evidence of TeV emission.

Since the data in any given phase bin were spread over several years, the change in pulsar period during this interval had to be allowed for. As before, this was done by determining the appropriate contemporary period P_x for each observation to within 0.5 ms. The combined probabilities were calculated over a constant matrix of periods at 0.5 ms intervals with P_x taken as the origin. All 10 segments were analysed in this way, and one was found to show evidence for a strong periodic signal - 0.75 to 0.84, as shown in Table 6.6a and Figure 6.9. Two of the three observations previously identified in Table 6.3 were contained in this phase bin; 1987 May 22 at phase 0.78 and 1988 January 21 at phase 0.81. After correction for the degrees of freedom used in the search, 3 for oversampling and 10 for the number of segments tested, the probability of this effect occurring by chance was 1.6×10^{-3}, i.e. marginally less significant than a 3σ detection. The resultant 3σ upper limit which can be placed on the long term photon flux in this phase interval is 1.2×10^{-10} $cm^{-2}s^{-1}$ above 300 GeV.

6.5.3.2. Further Study of Optimum Emission Phase

To test for further localisation in the optimal phase of the emission, subdivisions of width 0.05 and stepped by 0.01 were selected from the phase bin 0.75-0.84. Two of these subdivisions were found to show stronger signals

TABLE 6.6a - Tests for uniformity of phase in the data grouped by orbital phase				
Range of Phases	Chance Probability [raw (corrected)]		Number of Observations	Events Recorded
0.05-0.14	4.2×10^{-1}	(1.0)	12	34 342
0.15-0.24	2.7×10^{-2}	(8.1×10^{-1})	9	25 190
0.25-0.34	3.6×10^{-2}	(1.0)	11	31 787
0.35-0.44	1.9×10^{-1}	(1.0)	8	22 075
0.45-0.54	3.2×10^{-1}	(1.0)	8	20 089
0.55-0.64	3.4×10^{-2}	(1.0)	8	22 930
0.65-0.74	2.6×10^{-1}	(1.0)	15	48 942
0.75-0.84	5.3×10^{-5}	(1.6×10^{-3})	22	77 620
0.85-0.94	2.4×10^{-1}	(1.0)	7	16 918
0.95-0.04	1.2×10^{-1}	(1.0)	9	21 140

TABLE 6.6b - Subdivision of data at ascending node		
Orbital Phase Range	Chance Probability [raw (corrected)]	Number of Observations
0.76-0.80	1.3×10^{-3} (2.0×10^{-1})	15
0.77-0.81	4.1×10^{-6} (6.3×10^{-4})	15
0.78-0.82	1.8×10^{-5} (2.7×10^{-3})	15
0.79-0.83	5.3×10^{-4} (8.0×10^{-2})	12
0.80-0.84	1.6×10^{-4} (2.4×10^{-2})	11

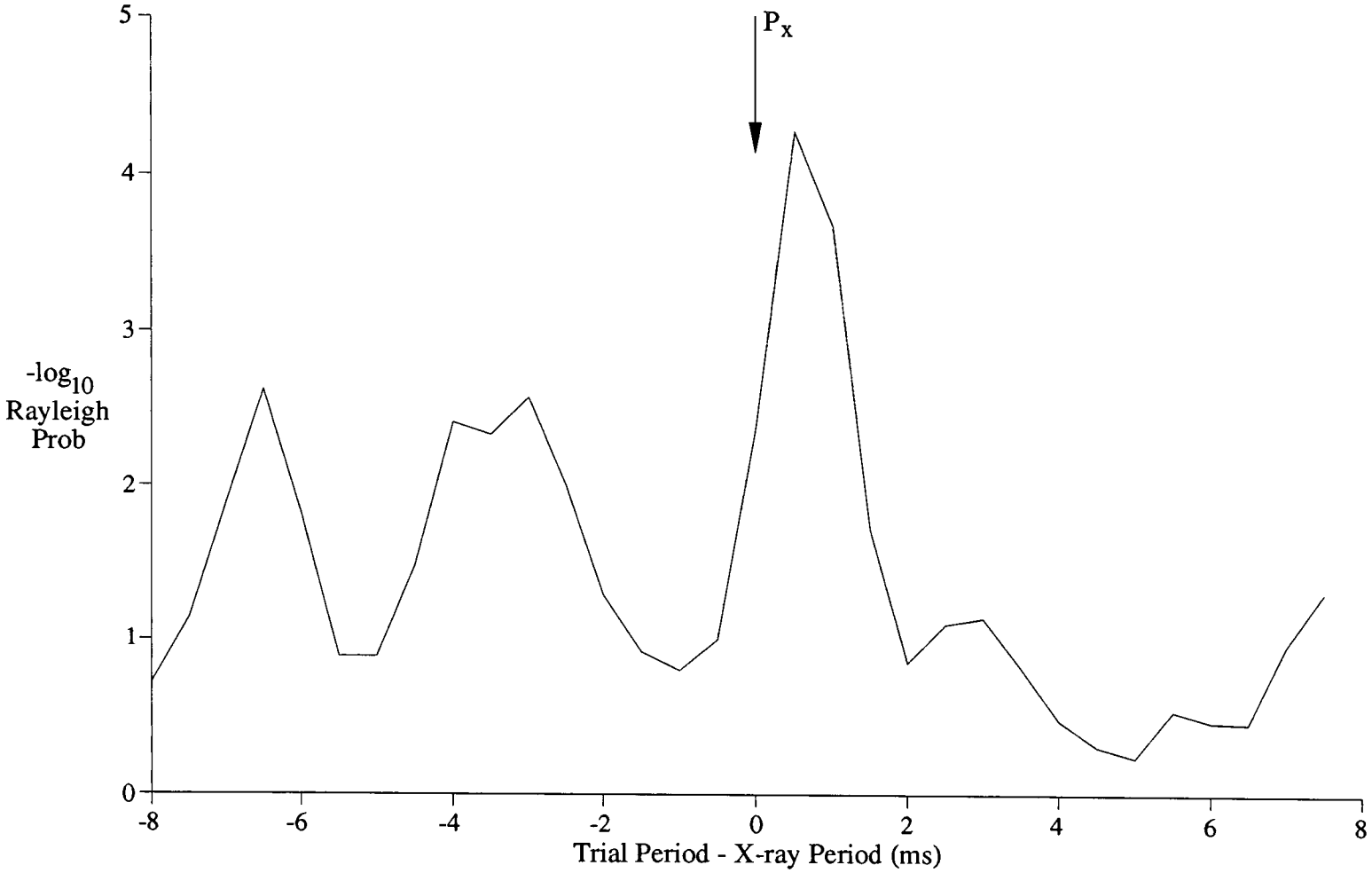

Figure 6.9 : Rayleigh probability versus trial period for an incoherent combination of the 22 Mk.3 telescope observations of Cen X-3 made in the orbital phase interval 0.75-0.84.

than any other (see Table 6.6b) and the presence of single observations showing evidence for a strong signal in these smaller bins was checked.

The strongest phase intervals were 0.77-0.81 and 0.78-0.82, which both contained two of the strong observations from Table 6.3, 1987 May 22 and 1988 January 21. Each segment contained 15 nights in total, so the loss of one strong observation from the selections had a limited effect, and several other selections also showed a lesser periodic signal. The phase bin 0.77-0.81 showed a pulsed signal at the expected period with a chance probability of 6.3×10^{-4} after correction for all degrees of freedom (3 for oversampling in trial period, 10 for identifying the optimal phase segment and 5 for the subdivision within this interval) as shown in Figure 6.10. This corresponds to a pulsed signal strength of 2.9% within this interval, and a photon flux above 300 GeV of 1.4×10^{-10} $cm^{-2}s^{-1}$. At a distance of 8 kpc, the gamma ray flux from Cen X-3 is 4.1×10^{35} erg s^{-1} in this optimum phase region. This result, using data selected from the complete updated catalogue of observations from 1987-1992, confirms the optimum phase interval identified at an earlier stage in the Durham observations of Cen X-3 reported by Carraminana et al., (1989a). This result is compared with those from other observations at TeV energies in the spectrum of Cen X-3 given in Figure 6.11.

6.6. Testing for Displacement of a TeV Gamma Ray Production Site

6.6.1. Determination of Sampling Intervals

Pulsed TeV gamma-ray emission from a high mass X-ray binary would be expected to show the same periodicity as the X-ray emission, in that both would be produced by processes associated with the rapidly rotating compact object. However, both need not necessarily arise from identical points in the system (as discussed in Chapter 9) and if the physical origins of each are sufficiently separated then correcting for orbital motion using the X-ray ephemeris may be erroneous when searching for pulsed gamma-ray emission. The application of the orbital searching technique described in Chapter 4 is

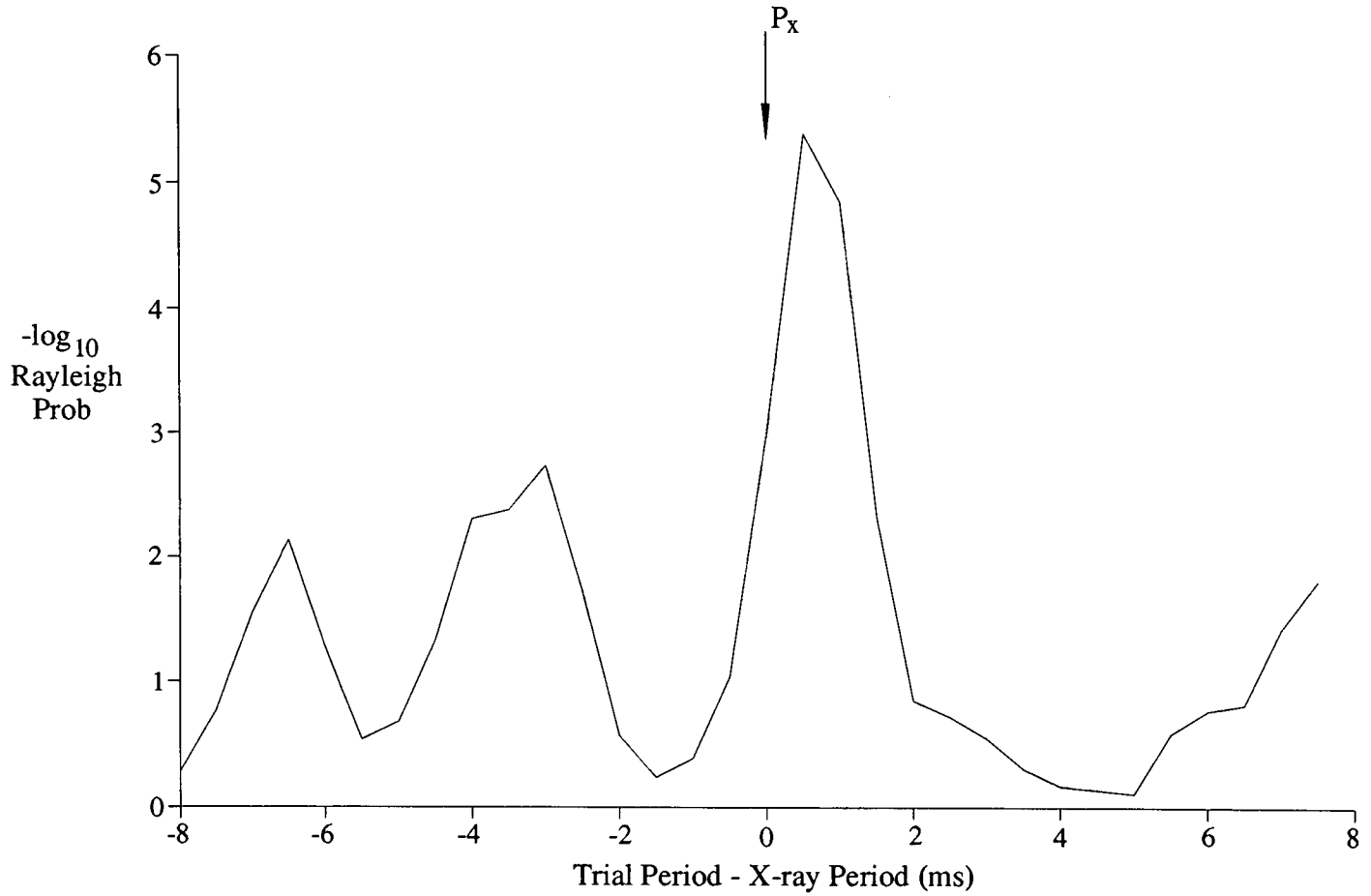

Figure 6.10 : Rayleigh probability versus trial period for an incoherent combination of the 15 Mk.3 telescope observations of Cen X-3 made in the phase interval 0.77-0.81.

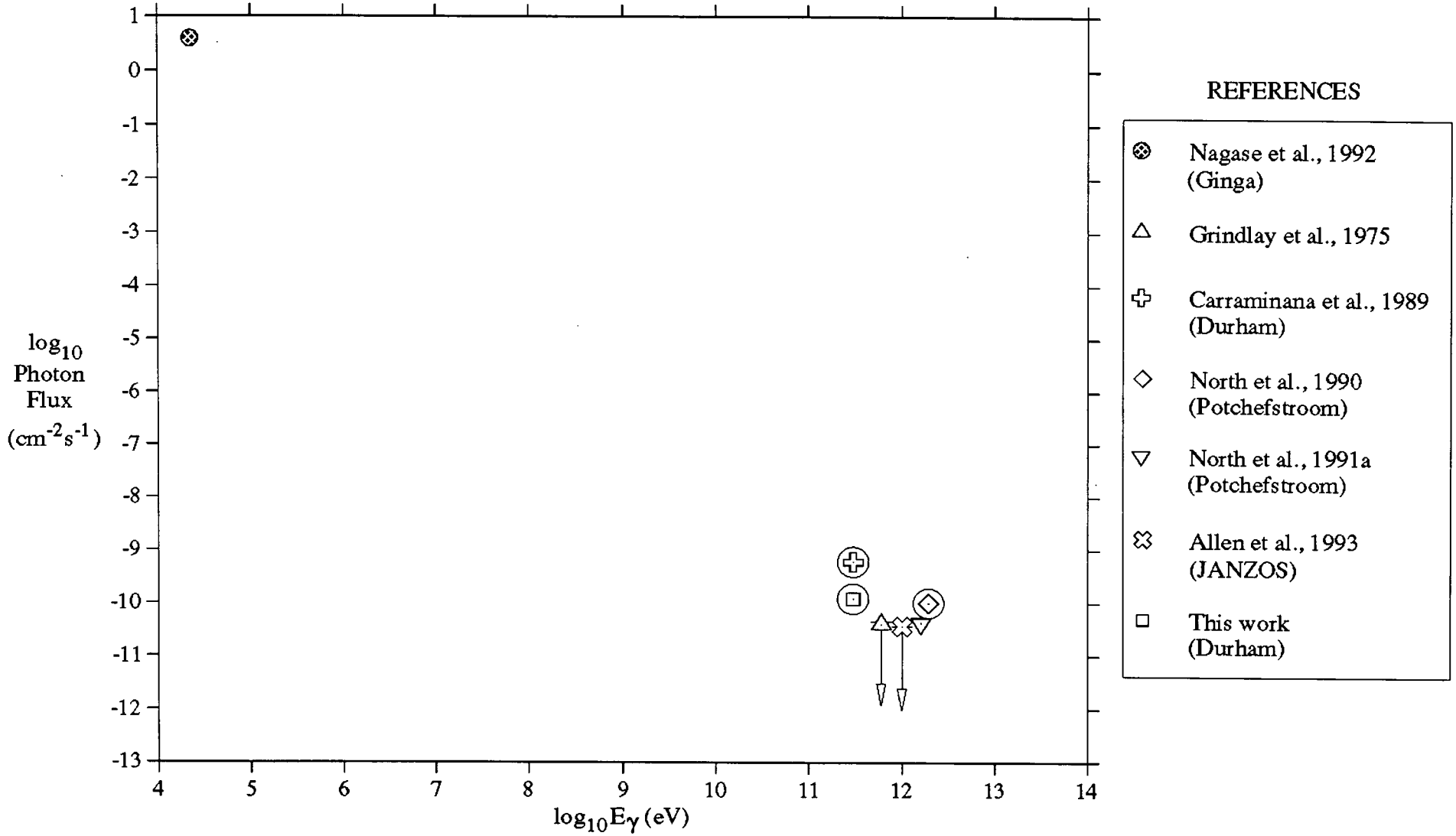

Figure 6.11 : The TeV gamma ray spectrum of Cen X-3. Detections made at the ascending node only are indicated by the circled points. Upper limits are indicated by the downward arrows. The flux in the energy range 1-37 keV based on measurements with the Ginga satellite is shown for comparison.

required. The independent sampling intervals in the two orbital parameters used, $a\sin i$ and eclipse epoch, vary with orbital phase for any given system (Mannings, 1990). In the case of a 5-hour observation of Cen X-3, these intervals minimise at ≈20% for $a\sin i$ at the nodes, and ≈3% for epoch shift at conjunction. Both of these values represent a distance of ≈8 ls, similar to the size of the Roche lobe of the neutron star. Such a search is therefore of marginal importance for the analysis of data from a single observation. For datasets merged so as to retain phase information, these intervals are reduced and the orbital parameter search is a valuable and necessary tool.

6.6.2. Analysis of Individual Observations

For individual observations, the sampling intervals in the orbital parameters are large and the simplest technique is the method of factorising the time corrections when using a single well-known trial period. This routine was developed for carrying out detailed searches for favoured emission sites in close binaries containing a millisecond pulsar, but is also a useful illustrative tool for a larger, slower binary such as Cen X-3.

Therefore, this technique was applied to each of the observations listed in Table 6.3 which showed evidence for periodicity. All 3 were at one or other of the nodes of the orbit so that the sensitivity in $a\sin i$ was much greater than that for any epoch shift. The results are shown in Figure 6.12, and demonstrate that for each dataset, the neutron star position is superimposed on a band of low values of the probability of uniformity of phase at the trial period. Most interestingly, in each case the lowest chance probabilities are seen to occur in a short range of epoch shifts, corresponding to a single sampling interval, at a position trailing the neutron star in its orbit. This suggests that emission is most likely to occur when the accretion wake is aligned in the line of sight to the observer. In section 6.4.4 a similar conclusion was reached, although the spatially resolved data given here lend much firmer support, and clarify the physical situation.

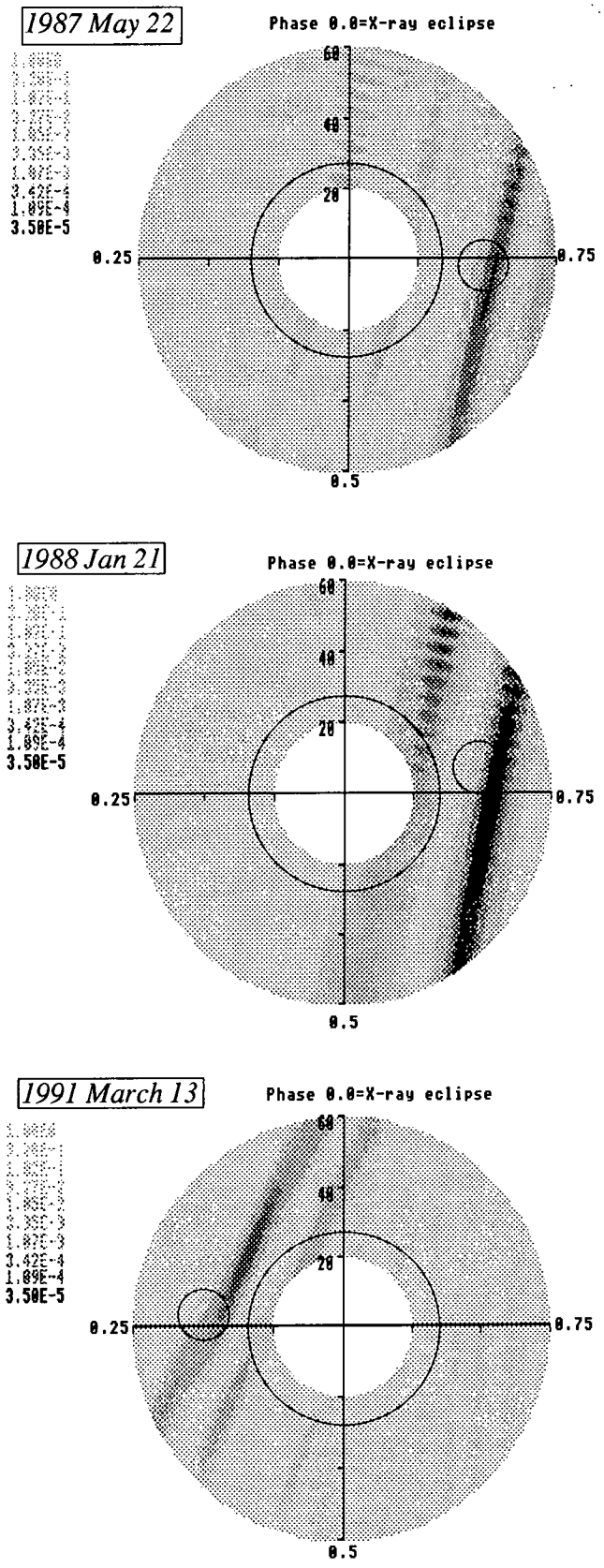

Figure 6.12 : Orbital searching applied to the Cen X-3 data from the three observations showing strongest evidence for a pulsed signal (Table 6.3). The grey scale on the left shows the threshold chance probability in each interval. The crosshair axes show the values of $a\sin i$ in light seconds.

The size of the primary star is indicated by the black circle at the centre of each diagram, and the neutron star's Roche lobe by the smaller black circle placed at the appropriate orbital phase.

6.6.3. Analysis of Combined Datasets

6.6.3.1. Individual Dark Moon Intervals

The data from observations in each single dark moon interval were combined coherently, retaining relative pulse phase information, and analysed for periodicity over a fixed range of the two orbital parameters used. The range in $a\sin i$ was from 30 to 50 light seconds, with a step size of 2 ls, and the epoch of mid-eclipse was varied by 25% of the orbital period, stepped by 5%, either side of the ephemeris value. For simplicity, these ranges and step sizes were used for each of the datasets, regardless of the exact phase of the observations. The range of periods used for testing for periodicity was either 0.5 or 1.0 ms either side of the approximate contemporary X-ray value for each month, depending on the effective duration of the dataset. For 1987 January, the range was 4822-4824 ms, and this decreased to 4817-4819 ms by 1992 February. The pulsar period derivatives used were as for the tests detailed in section 6.5.2.2..

The results were plotted as contours joining levels of equal chance probability of uniformity of phase at the trial period. The months showing the most significant periodic signals (defined as having a raw chance probability $\leq 10^{-4}$) are given in Table 6.7a, along with the approximate orbital position at which the relevant minimum occurred (N.B. the X-ray ephemeris position of the neutron star corresponds to $a\sin i$ = 39.6 ls and epoch shift = 0.0%). The contour plots are shown in Figures 6.13a-d. The degrees of freedom used were 5 for oversampling in trial period, 16 for the number of datasets tested and $\approx$50 in orbital sampling. As a result, none of the datasets analysed here provided evidence for periodic emission at the 3σ level.

On the basis of this small sample of datasets, conclusions drawn about any offset in the sources of the X-ray and gamma ray emission can only be tentative. The less sensitive parameter was $a\sin i$ and no preferential values were found. However, the favouring of an epoch shift of between -10% and -20% suggested a genuine effect and implied that the site of gamma-ray production

TABLE 6.7a - Application of orbital searching to the coherent combinations of data from within individual dark moon intervals				
Observing Month	Raw Chance Probability	$a \sin i$ (ls)	Epoch Shift	No. of Nights
1987 January	$10^{-4} > p > 10^{-4.5}$	≈44	≈-20%	10
1988 January	$10^{-5} > p > 10^{-6.5}$	≈37-48	≈-10%	8
1989 April	$10^{-4} > p > 10^{-4.5}$	≈38	≈-15%	8
1991 March	$10^{-4.5} > p > 10^{-5}$	≈46	≈-15%	12

TABLE 6.7b - Division of data from individual dark moon intervals					
Observing Month	Raw Chance Probability	$a \sin i$ (ls)	Epoch Shift	No. of Nights	Orbital Phase
1987 May	$\leq 10^{-4}$	39-42	≈0%	6/13 [a]	0.62-0.83
1988 January	$\leq 10^{-5}$	38-50	≈-10%	4/8 [a]	0.69-0.89
1989 April	$\leq 10^{-4}$	41-43	≈-15%	4/8 [a]	0.96-0.06
1991 March	$\leq 10^{-5}$	31-39	≈0%	6/12 [a]	0.14-0.40
	$\leq 10^{-4.5}$	38-46	≈-15%	" [a]	"

[[a] - Number of nights is given as number selected/total number]

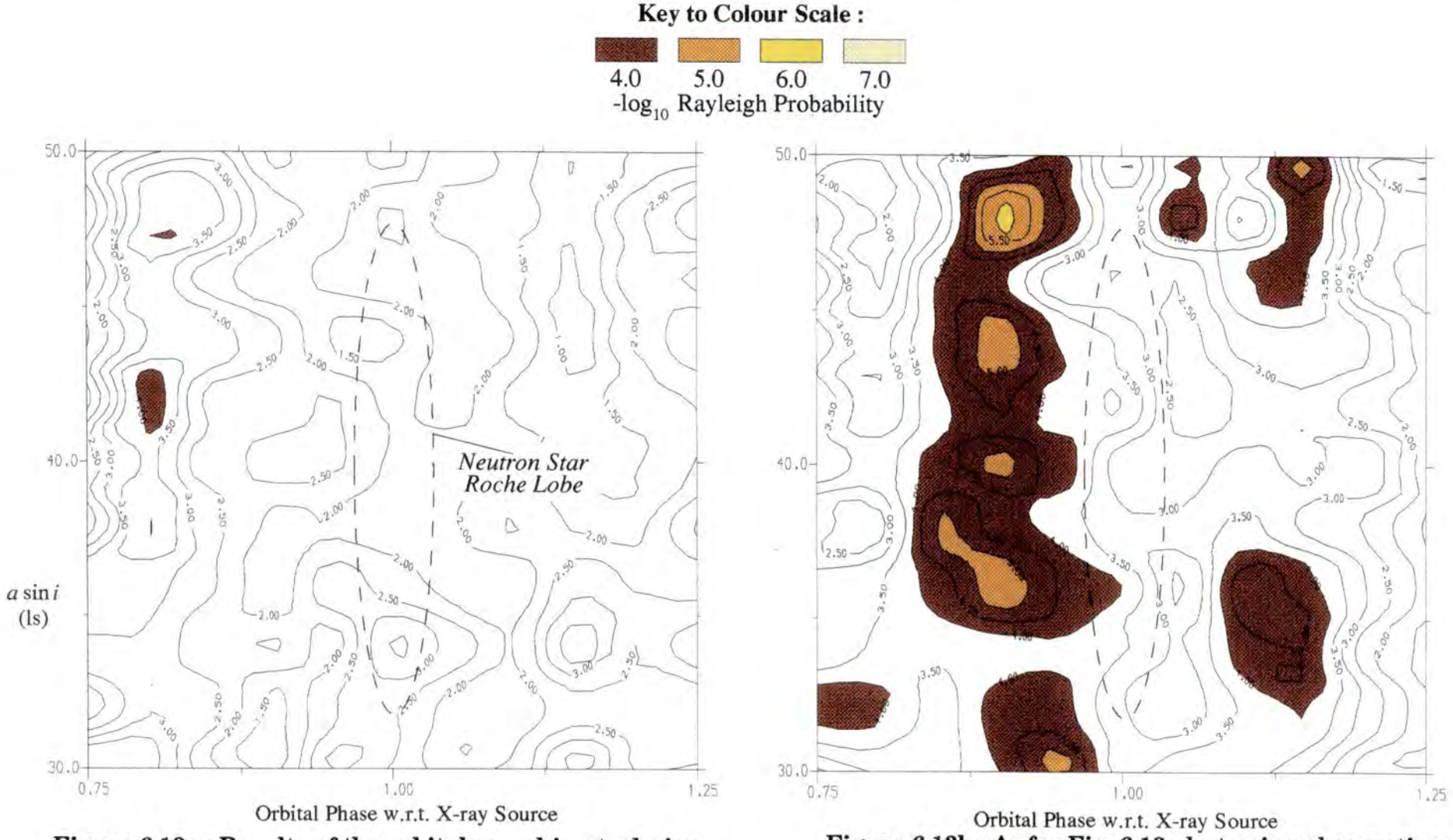

Figure 6.13a : Results of the orbital searching technique applied to Mk.3 telescope observations of Cen X-3 in 1987 January. The data were merged coherently and the Rayleigh test applied over the period range 4822-4824 ms.

Figure 6.13b : As for Fig. 6.13a but using observations made in 1988 January.

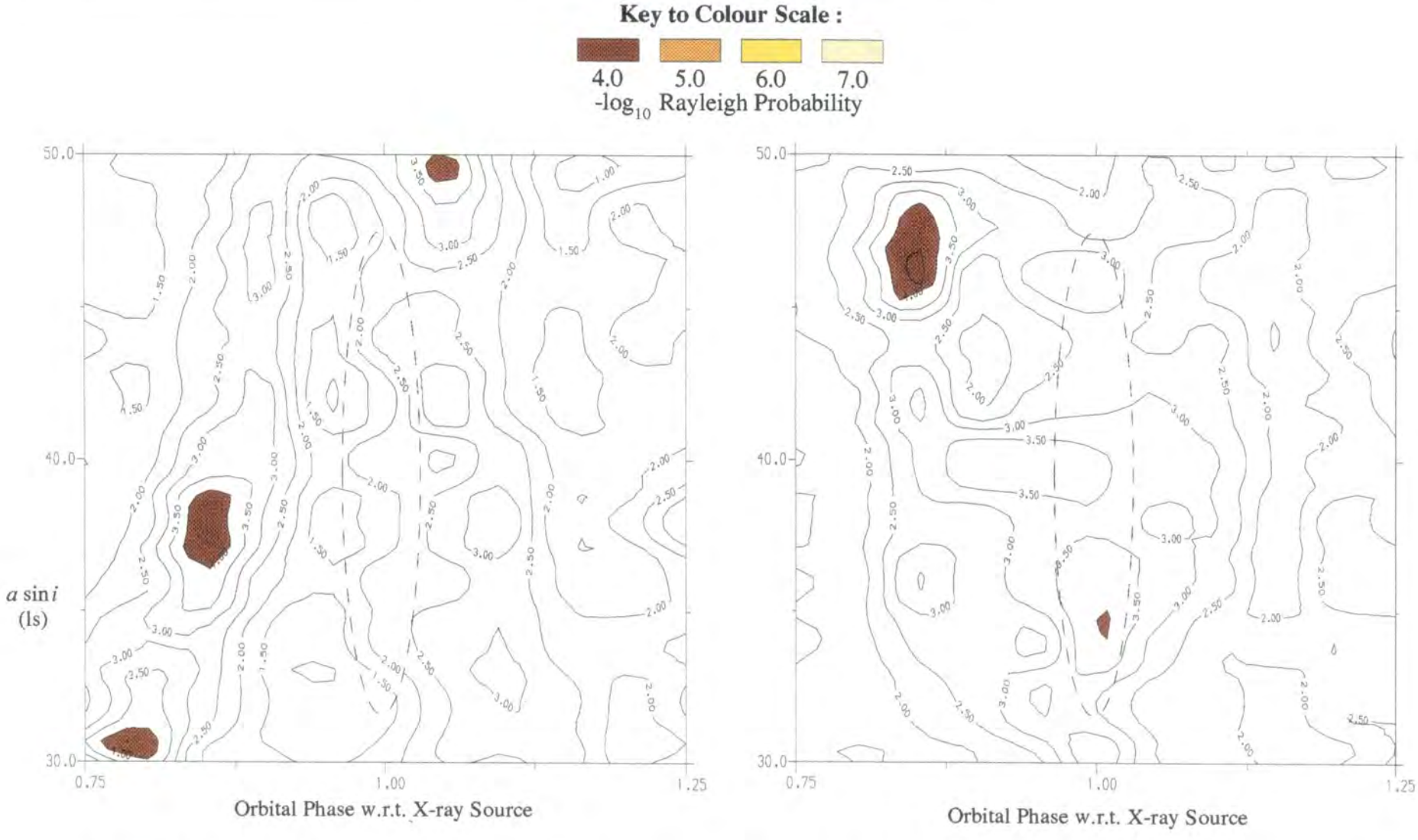

Figure 6.13c : As for Fig. 6.13a but using observations made in 1989 April.

Figure 6.13d : As for Fig. 6.13a but using observations made in 1991 March and a period range 4819.5-4821 ms.

trails the neutron star in its orbit, consistent with an origin in an accretion wake.

6.6.3.2. Dark Moon Intervals Divided by Orbital Phase

Since the orbital period of Cen X-3 is 2.09 days, each dark moon interval, spanning ≈10 days on average, sampled opposing sides of the orbit. By selecting alternate nights only (if an observation was made) two datasets each covering an orbital phase range of ≈0.2 were formed for each dark moon interval. If the strength of the signal was related to the orbital phase, as has been suggested already, then one of each pair of datasets might have been expected to display more significant periodicity than its counterpart. In this orbital searching analysis, two opposing sides of the orbit may be directly compared because the independent sampling intervals in the parameters will be identical for both.

The subsets of each dark moon interval were combined with phase coherence and analysed using the orbital searching technique described previously. Although most of the datasets displayed some asymmetry in the results from either side of the orbit, only four showed weak evidence for a periodic signal in one or the other (see Table 6.7b and Figures 6.14a-d). The periodic signal in the data from 1987 May, one of the dark moon intervals identified in the analysis made without orbital searching, was demonstrated to show clear orbital phase dependence. The data recorded in 1991 March displayed weak evidence for periodicity at two distinct positions, separated by only one sampling interval in both phase and $a\sin i$.

In the similar analysis of data from the complete dark moon intervals, it was noted that an epoch shift of ≈-20% was preferred. It might therefore have been expected that dividing the months according to orbital phase would reduce any "interference" between the opposing sides of the orbit and confirm more clearly the shift already identified. In fact, despite the preference for a single region of the orbit, the results from both 1987 May and the lower of

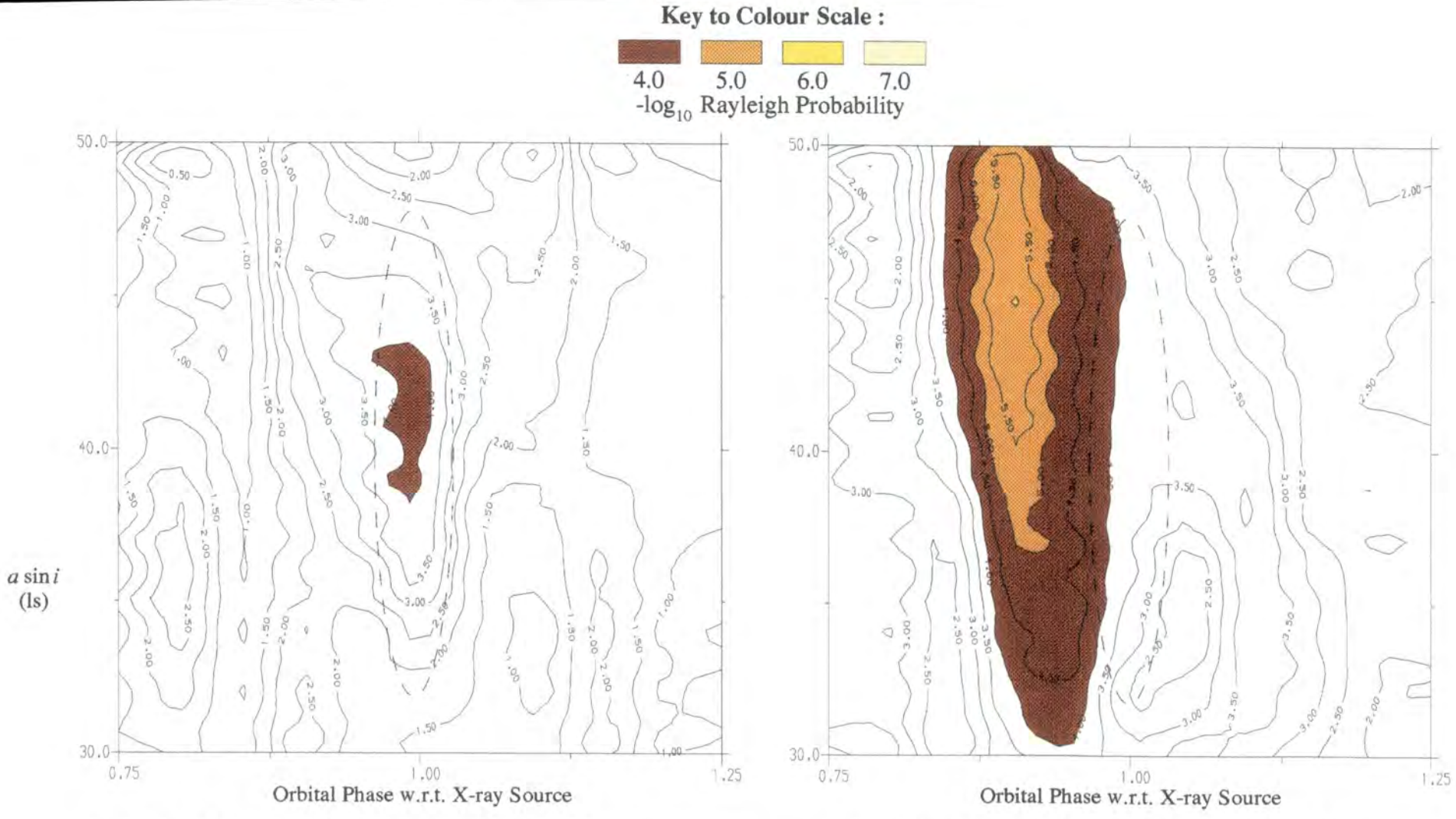

Figure 6.14a : Results of the orbital searching technique applied to Mk.3 telescope observations of Cen X-3 in 1987 May (orbital phases range 0.58-0.83). The data were combined coherently and the Rayleigh test applied over the period range 4822.5-4823.5 ms.

Figure 6.14b : As for Fig. 6.14a but using observations made in 1988 January (orbital phase 0.68-0.89).

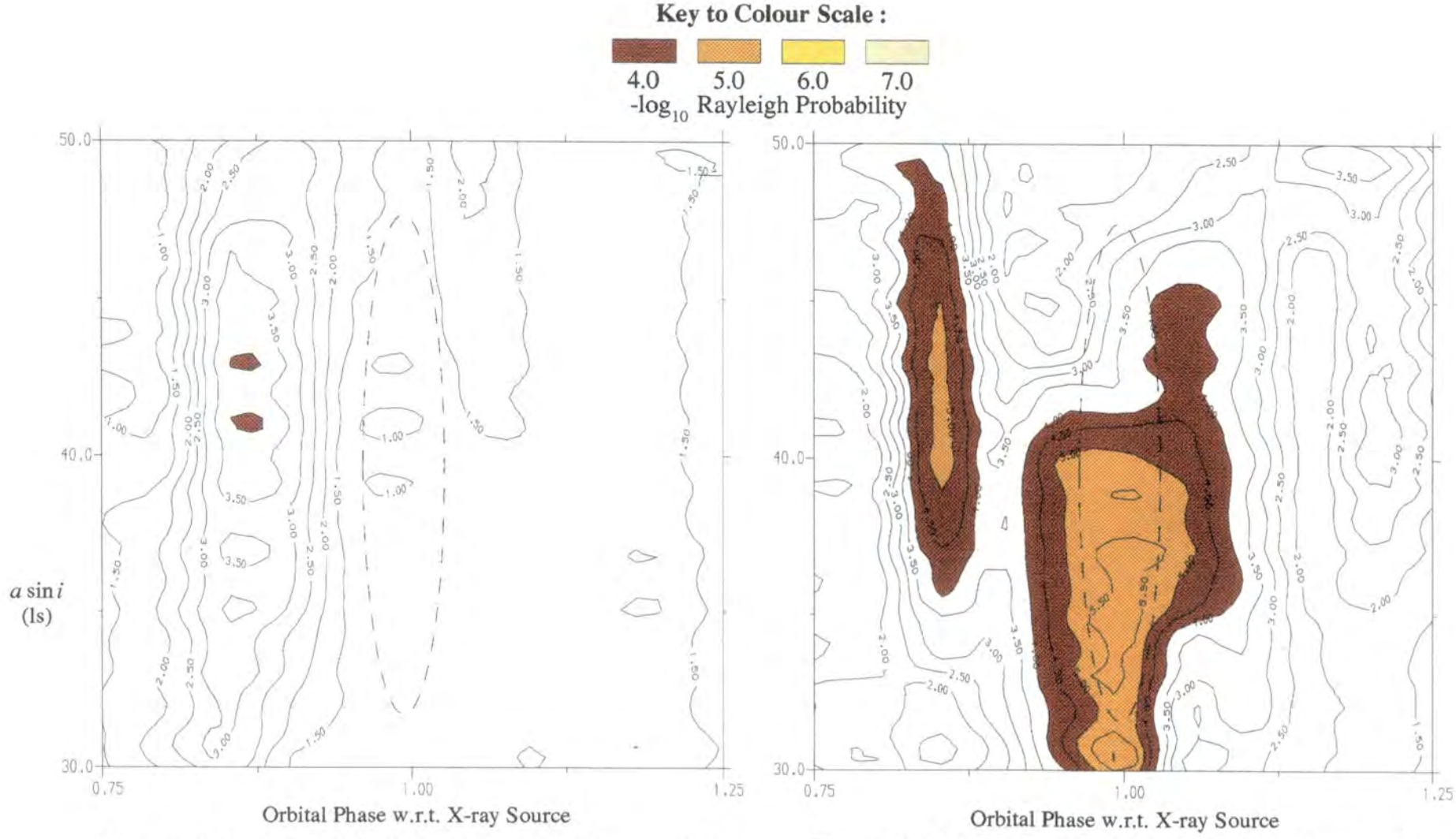

Figure 6.14c : As for Fig. 6.14a but using observations made in 1989 April (orbital phase 0.93-0.06).

Figure 6.14d : As for Fig. 6.14a but using observations made in 1991 March (orbital phase 0.11-0.40) and the period range 4819.5-4821 ms.

probability minima from 1991 March were consistent with no epoch shift being required to recover a periodic signal. The other results, including the weaker of the two minima seen in 1991 March, lent support to the origin at a position trailing the neutron star in its orbit, but none were more than one sampling interval from a zero shift. The negative epoch shift (and hence possible accretion wake origin) could not therefore be confirmed, although it was notable that no anomalous positive shift was seen in any of the results.

As for the displacements in $a\sin i$, it was possible to directly determine the independent sampling interval in this parameter from the probability contour plots. This was found to be ≈5 ls for the observations at the nodes of the orbit and even larger for the 1989 April observations made near eclipse. Hence, as is clear from Table 6.7b, all of the weak signals found here were just consistent with an origin at the radius of the orbit of the X-ray source, where $a\sin i$ is 39.6 ls.

The actual size of the accretion disc is believed to be less than 10 ls (see section 6.1.6) but the presence of streams of gas in the system is inferred from the observations of intensity dips. The actual dimensions of these streams are very uncertain but they would trail the neutron star in its orbit and could certainly explain the spatially resolved results reported here.

6.6.4. Orbital Searching in the Optimum Phase Interval

The phase interval 0.77-0.81 has been shown in section 6.5.3.2 and in the previous Durham analyses to be the region of the orbit where the pulsed TeV gamma ray emission is most significant. Here for the first time the orbital searching technique has been applied in a search for a displacement of the emission site from the X-ray source. The 15 observations were combined incoherently by applying the Rayleigh test at a single trial period only, i.e. the contemporary X-ray period (from Table 6.4), and over the range of 25-55 ls in $a\sin i$ and -20% to +15% in epoch shift. The test at only the X-ray period allows greatest sensitivity of the orbital searching technique to any period

shift induced by a physically displaced gamma ray emission region. Since the data were recorded at the ascending node and the average length of each dataset was 3.3 hours, the sampling interval in $a\sin i$ was ≈10 ls and that in epoch shift ≈10%. These estimates suggest that 3 trial intervals were sampled in each parameter.

The resultant set of probability contours is shown in Figure 6.15, with the approximate extent of the accretion disc superimposed. The strongest evidence for pulsed emission is seen to correspond to a position at the edge of the accretion disc trailing the neutron star, i.e. where the gas stream from the primary would be expected to flow into the disc. The minimum uncorrected chance probability is 5.6×10^{-6}, which is increased to 2.5×10^{-3} after allowance for all degrees of freedom (50 for identifying the phase interval, and 9 for the number of spatial sampling intervals). The degrees of freedom introduced by the orbital sampling therefore reduce the significance of the displacement of the TeV gamma ray emission site to below the 3σ level. Although the apparent location of the gamma ray source is within the sampling interval of the X-ray ephemeris position, the strength of the signal suggests that this may be a genuine displacement.

6.6.5. Combination of Data Recorded in a Single Year

Having selected groups of observations taken over several years on the basis of orbital phase, data from each calendar year was also combined incoherently. The change in period within each year (actually 5-6 months owing to the duty cycle of the observations) was obviously much less than that accumulated over several years. The change was still large enough to make combination as a single dataset meaningless without more precise knowledge of the contemporary pulsar period derivative. Merging without the use of relative pulse phase information meant that the independent sampling interval in period was large enough to envelop the full period shift which would occur in 5-6 months.

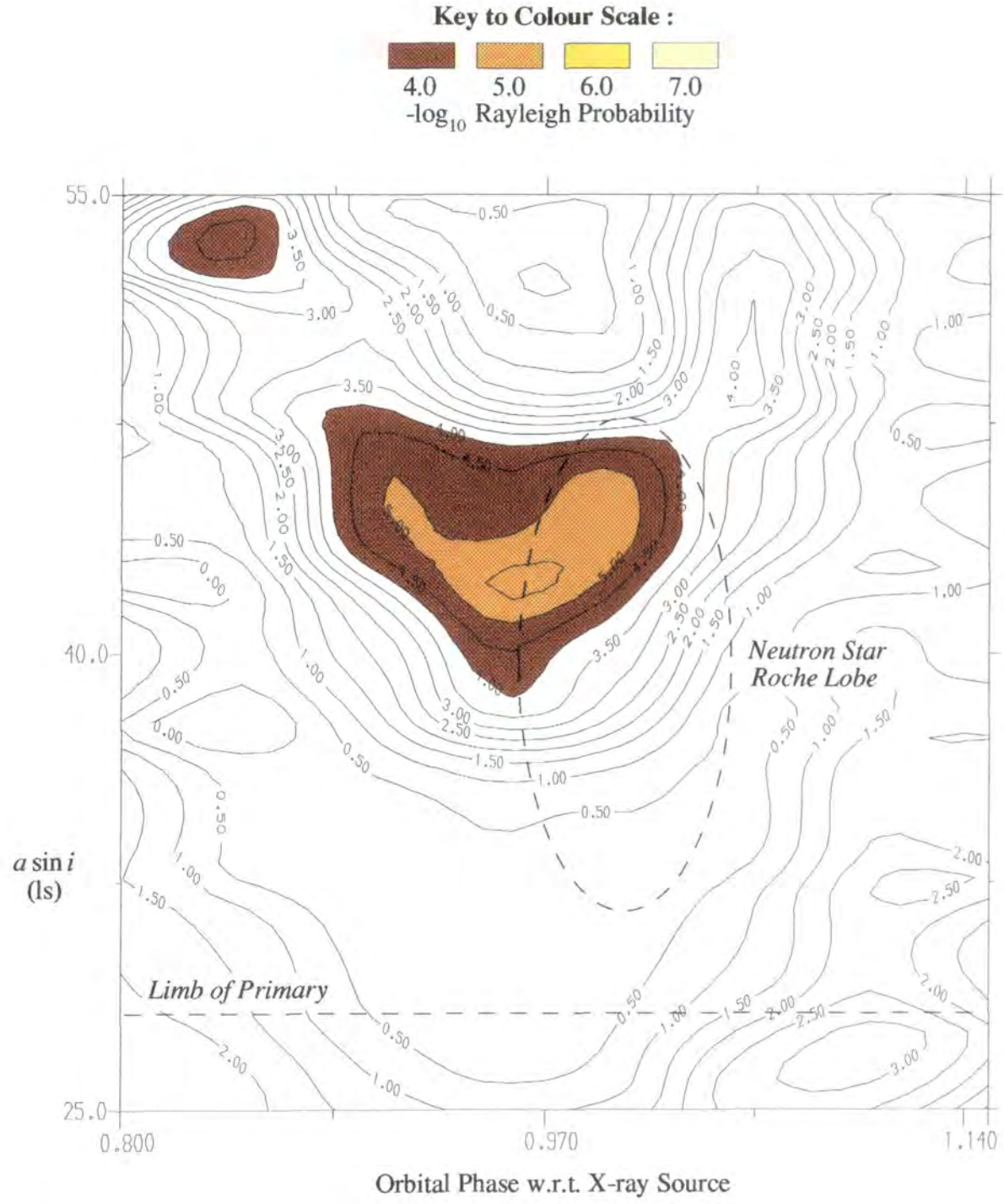

Figure 6.15 : Results of the orbital searching technique as applied to an incoherent combination of all 15 Mk.3 telescope observations of Cen X-3 made between orbital phases 0.77-0.81. The Rayleigh test was applied at the estimated contemporary X-ray period only. The positions of the limb of the primary and the accretion disc/Roche lobe are both shown.

The data recorded in each year were tested for uniformity of phase over the trial period range 4815-4825 ms and the ranges of orbital parameters used were as for the datasets grouped by orbital phase, i.e. 20-60 ls in $a\sin i$ and ±50% in epoch shift.

The best result came from the 1987 data, which showed an uncorrected chance probability minimum of $\approx 10^{-4}$ at $a\sin i \approx 48$ ls and an epoch shift of ≈-5%, as shown in Figure 6.16. The large number of degrees of freedom used does not provide evidence for a signal below the 3σ level. Since half of the 1987 observations were made in May of that year, which has already been noted as being one of two datasets showing weak evidence for pulsed emission without the use of orbital searching, the data from 1987 was also split into two; the group recorded in 1987 May and all other data recorded in that year. An uncorrected probability minimum of $\approx 10^{-4}$ was found in the 1987 May data at the same position as that for the whole year. No peak was found at the same position in the remainder of the year's data, which suggested that emission from this object was not persistent on a timescale of more than a month in 1987.

6.7. Recent Observations

TeV gamma ray observations of Cen X-3 from Narrabri have continued in 1993. The aim of the observing programme was to concentrate on recording data at the nodes of the orbit, as these orbital phases have provided the best evidence for pulsed TeV gamma ray emission in the past. In 1993 March, the Mk.3 telescope was used to make 5 observations of Cen X-3 under conditions suitable for periodic analysis. Four of the observations were made near the ascending node and the other at the descending node. The selection used for the Mk.3 telescope data was the requirement of a centre-channel response only, which left 15700 events for analysis. The appropriate period for study was judged from an extrapolation of the recent pulse period history to be 4817.5 ms. No periodic signal was identified, and the 3σ flux limit was 1.1 x

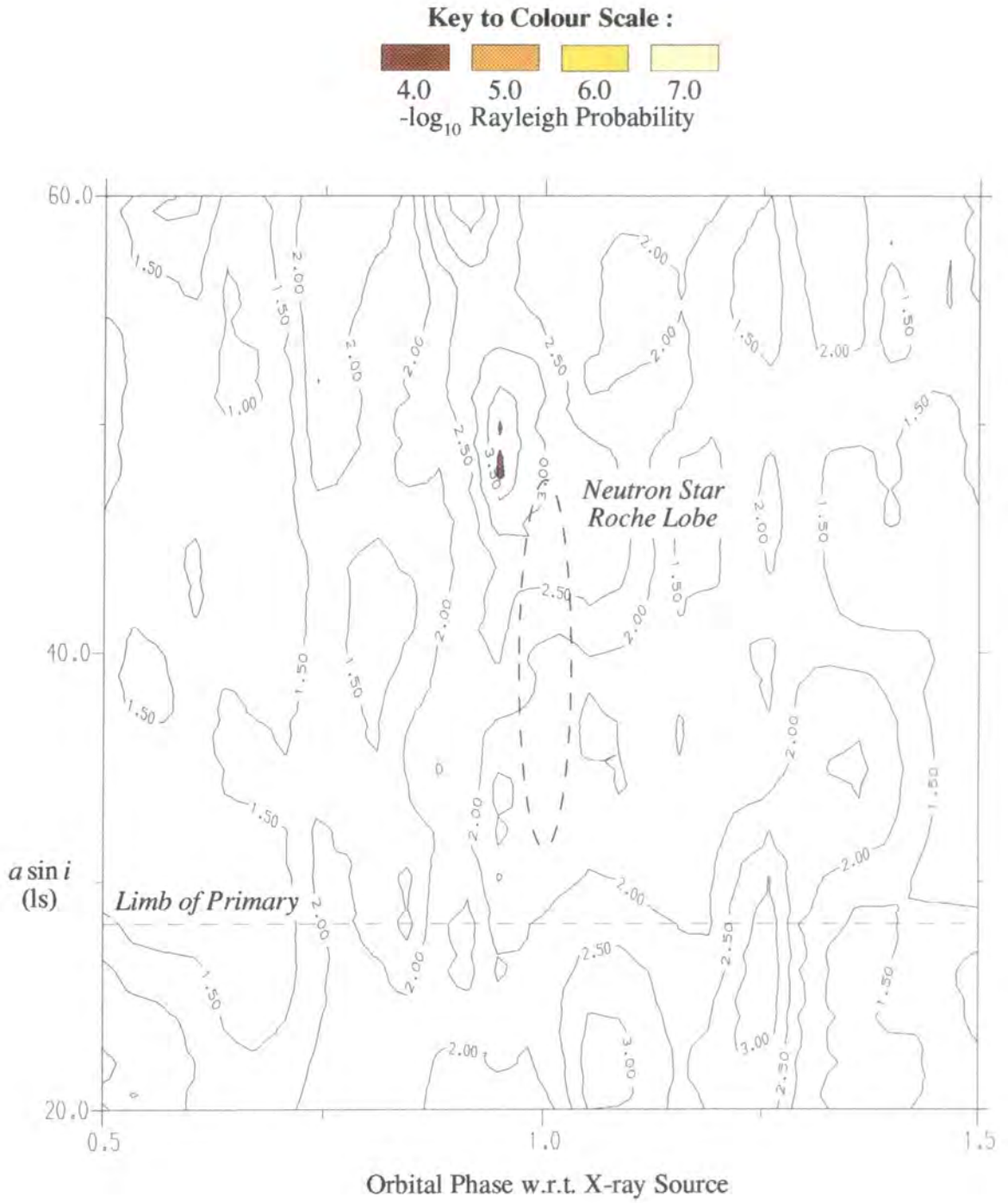

Figure 6.16 : Results of the orbital searching technique as applied to an incoherent combination of all 25 Mk.3 telescope observations of Cen X-3 made in 1987. The Rayleigh test was applied over the period range 4815-4825 ms.

10^{-10} $cm^{-2}s^{-1}$ above 300 GeV.

Data were also recorded in 1993 March using the Mk.5 telescope and the imaging capability of this instrument may provide valuable results on Cen X-3 in the future. The results of these observations will be presented elsewhere.

6.8. Conclusions

The aims of this study were to establish the emission of TeV gamma rays from Centaurus X-3, and in particular whether any emission was confined to a particular phase of the orbit, or spatial position in the binary system. The clearest result came from the combination of the entire dataset with use of knowledge of the contemporary X-ray period. The study of the full dataset yielded evidence for a periodic signal marginally below the level of a genuine 3σ detection. Division of the data confirmed that the strongest evidence for gamma ray emission pulsed at the X-ray period arose from the subset of data recorded in the phase interval 0.77-0.81.

Of the individual observations, only three were found to display weak evidence of a signal at the correct period and each was made at one or other of the nodes of the orbit. The 1992 and 1993 data, analysed here for the first time, showed no evidence for a periodic signal. In the analysis of data from a dark moon interval combined without the use of phase information, 1987 May and 1991 March were found to give the best evidence for periodic emission and on closer examination, the majority of the signal was found to arise from a number of nights recorded near one of the nodes of the orbit.

The investigation to search for a displacement between the spatial positions of the origins of X- and gamma-ray emission gave interesting results. Whilst the data from the individual dark moon intervals showed a preference for a TeV emission site trailing the X-ray emission by some 20% in phase, indicative of an origin in the region of X-ray absorption, the most significant result from the phase interval 0.77-0.81 suggested a site at the very edge of the accretion disc.

A number of the results given here have been only slightly less significant than the level required for a genuine 3σ signal detection. This suggests that an improved detector system with either a lower threshold energy and/or a better background rejection technique could produce a significant detection of pulsed emission. By simply extrapolating the cosmic ray background integral spectral index of -1.6, the Durham Mk.6 telescope with a threshold of $\approx$100 GeV will produce a 600% increase in count rate over the 300 GeV threshold Mk.3 telescope (for Cen X-3 observations) with limited background rejection (see Chapter 9). Additionally, the proportion of photons recorded should increase at the lower threshold energy (Weekes and Turver, 1977). The 2.1% upper limit on the persistent flux given here could be lowered and perhaps a positive signal detection achieved within a single dark moon interval producing a full dataset of several x 10^5 events. Alternatively, a similar improvement could be gained by increasing the gamma ray to proton ratio in the dataset using effective rejection techniques. This should be achievable with the Mk.3a and Mk.5a telescopes operating as a stereo pair and the Mk.6 in imaging mode (see Chapter 10).

Allowing for the sampling intervals used in the spatially resolved analysis, the results are consistent with an origin in the material causing the X-ray absorption dips. This is strongly supported by the evidence that the ascending node is the most region for gamma ray emission. The models of TeV gamma ray production in an X-ray binary are discussed in Chapter 9. A beam of charged particles produced near the neutron star could collide with the gas streams in the system to form neutral pions which decay to give a flux of TeV gamma rays. A balance must then be found between the material in the stream being sufficiently dense to account for the gamma ray production, but also tenuous enough to allow the photons to escape without terminal absorption. This also leaves the question of a means of acceleration of the particles in the vicinity of the neutron star.

7.1. Vela X-1 - A Stellar Wind Accreting X-ray Binary

7.1.1. The Vela X-1 Binary System

The celestial X-ray source known as Vela X-1 (or 4U0900-40) was discovered as a result of a rocket-borne experiment in 1966 (Chodil et al., 1967b). During a survey of the galactic plane in the energy range 4-25 keV, a weak flux of ≈0.2 photons cm^{-2} s^{-1} was detected from this object. Little further information was gained until the valuable measurement of a 9 day periodicity in the variable X-ray flux recorded by the OSO-7 satellite (Ulmer et al., 1972) which was ascribed to orbital motion of the X-ray source. Further measurements by UHURU gave a more precise value for the orbital period of 8.95 d (Forman et al., 1973), and showed that in addition to the regular eclipses by a companion star, the flux was also variable by a factor of ≈30 on timescales of a few hours. An accurate positional determination allowed an optical counterpart to be identified - the B0.5 Ib supergiant HD77581. Radial velocity measurements for this star confirmed that the 8.95 d periodicity was due to orbital motion (Vidal et al., 1973). The next important step in revealing the nature of this system was the discovery of X-ray pulsations with a period of 283 s in observations made by the SAS-3 satellite (McClintock et al., 1976).

The X-ray light curve of this slow pulsar has a double-peaked structure, each peak of similar magnitude and separated by 0.5 in phase. It remains similar in observations made up to hard X-ray energies of around 80 keV (see Figure 7.1). At energies below ≈20 keV, the two main peaks each decompose into a pair of sharp, asymmetric peaks (e.g. Raubenheimer, 1990). The splitting of each of these main peaks has been attributed to a cyclotron resonance in a strong magnetic field of 2-5 x 10^{12} G (Harding et al., 1984). To detect X-ray emission from both poles of the pulsar, the angle between the spin axis of the neutron star and the line of sight must be ≥85°, and for the emission to be so

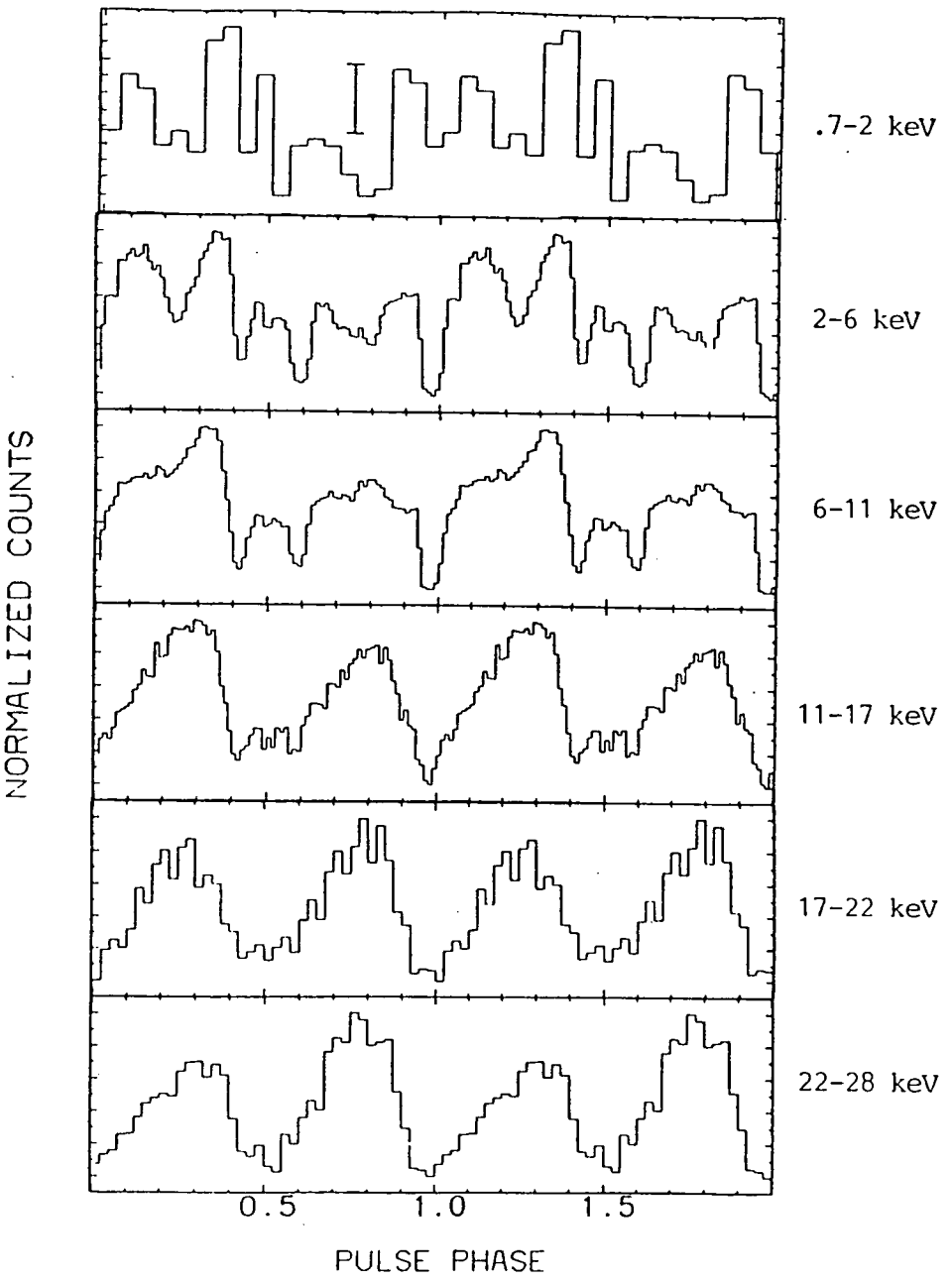

Figure 7.1 : Pulsed light curves for Vela X-1 in 6 photon energy ranges as derived from EXOSAT measurements on 1985 May 5. The increasing complexity of the pulse structure toward lower energies is evident.

(from Raubenheimer, 1990)

strongly modulated, a pulsed fraction of 45-65% being reported by Staubert et al.(1980), the viewing angle must be near the magnetic axis (Riffert and Meszaros, 1988). The angle between the rotation and magnetic axes of the neutron star is believed to be $\geq 65^{o}$.

The knowledge gained from observations of the optical counterpart allowed the derivation of many of the physical parameters of the system. The typical X-ray luminosity of the source is of the order of 10^{36} erg s^{-1}, rather low for an X-ray binary suggesting a low rate of accretion of material onto the compact object. The primary is estimated to have a mass of 20-25 M_{o} and a radius of ≈ 30 R_{o} (Rappaport and Joss, 1983). The X-ray source is almost certainly a neutron star, its mass of 1.9 M_{o} placing it among the more massive objects of its type.

During eclipses of the X-ray source, the X-ray flux reduces to below 10% of the normal amount and the pulsed fraction decreases to zero (Becker et al.,1978). The spectrum of the residual emission during an eclipse is the same as that of the uneclipsed source, implying that the X-rays seen at this phase are scattered by the extended atmosphere and stellar wind of the primary, causing their periodic modulation to be lost.

7.1.2. Pulsar Period Measurements

Most accreting pulsars in X-ray binary systems display a long-term decrease in their pulse period due to the addition of angular momentum by accreting material (see Chapter 5). Although the exact rate of spin-up is often variable, the general sense is retained. Vela X-1 is unusual in that whilst for 5 years after the discovery of the pulsar its 283 s period gradually reduced, from 1979 onwards a steady and almost uninterrupted increase has been seen. This spin-down continues to the present day, with the pulsar now rotating more slowly than at any time since its discovery (Lapshov et al., 1992).

The long-term history of the pulsar period is shown in Figure 7.2. The

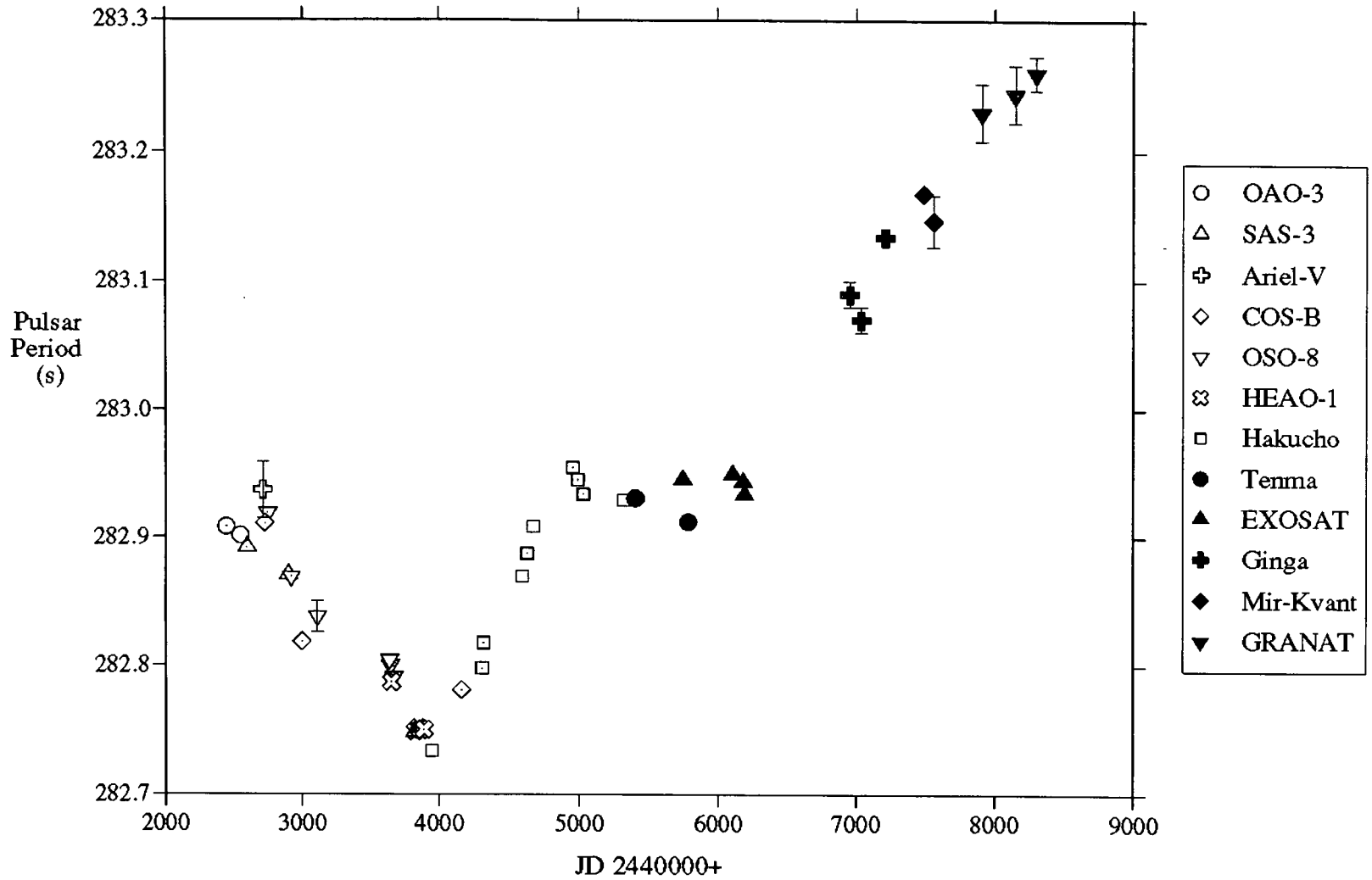

Figure 7.2 : The period history of the X-ray pulsar in Vela X-1.
(refs. in Nagase, 1989; Gilfanov et al., 1989; Raubenheimer and Ogelman, 1989; Lapshov et al., 1992)

first instance of a spin down interval was short-lived (Ogelman et al., 1977), at a rate of 2.4 x 10^{-9} ss^{-1}. The current trend for a spin-down was first observed in Hakucho measurements made in 1980 (Nagase et al., 1981). Further observations using this satellite revealed an interval lasting for ≈1 year where the pulse period remained nearly constant (Nagase et al., 1984a), before the spin-down resumed with an average value of 1-2 x 10^{-9} ss^{-1}.

Of equal interest are the unpredictable rapid variations in the spin period, where the sign of the period derivative has been observed to reverse on timescales of only a few hours (e.g. Nagase et al., 1984a; Boynton et al., 1986). The maximum short-term period change has been as great as ≈5 x 10^{-7} ss^{-1} (Van der Klis and Bonnet-Bidaud, 1984). Such variations have been interpreted as random walk behaviour (Boynton et al., 1986) where a succession of unresolved perturbations form a power spectrum of fluctuations concentrated at low frequencies (i.e. "red noise"). Taking such fluctuations into account, Deeter et al. (1987) produced an accurate X-ray ephemeris which is used in the present work.

7.1.3. Intensity Dips and Spectral Measurements

Vela X-1 shares with many other binaries the characteristic of dips in intensity apparent in the orbital phase light curve. Like the observations of varying spin-up and spin-down, these provide valuable evidence on the nature of accretion in the system. Results from Ariel-V (Eadie et al., 1975), Copernicus (Charles et al., 1978) and OSO-8 (Becker et al., 1978) showed that these dips occurred predominantly between phases 0.6 and 0.8 and wandered in phase between successive cycles. The Copernicus observations also demonstrated the hardening of the X-ray spectrum in these dips, suggestive of photoelectric absorption.

The material causing these dips is believed to be part of a gas stream which trails the neutron star after flowing through the inner Lagrangian point (e.g. Molteni et al., 1982). This was confirmed by Tenma observations where absorption was found to be an order of magnitude greater (5 x 10^{23} H cm^{-2}) at

the phase interval 0.6-0.8 than at the phase interval 0.2-0.4 (Nagase et al., 1984a). A correlation was found between the secular period change and the phase dependence of the X-ray spectrum as first noted by Hayakawa and Nagase (1982).

A detailed study of EXOSAT spectral measurements of Vela X-1 showed that the underlying neutral absorption increased by a factor of 10 from phase 0.2 to 0.85 with a base level of 3×10^{22} H cm^{-2} (Haberl, 1989). A highly variable component was also found which repeatedly lasted 10s of minutes with $N_H \approx 5 \times 10^{23}$ cm^{-2}. Intervals of greatest absorption were found to last for several hours and were not accompanied by an increase in the scattered low energy component, suggesting an origin in temporarily stable material near the neutron star. These were held to represent times where the flow of accreting material temporarily settled into a disc-like pattern, where maximum spin-up/down would be expected. Later observations using GRANAT (Lapshov et al., 1992) revealed a 10 hour interval where the flux dropped to only ≈5% of the normal non-eclipsed value for about 10 hours. Rather than invoking a large absorber, with the column density required to be $\approx 10^{24}$ H cm^{-2}, this dip was attributed to a temporary decline in the accretion rate associated with a change in the velocity and density of the stellar wind.

7.1.4. Accretion in Vela X-1

The long orbital period and wide separation of the components in Vela X-1 make it a strong candidate for a system where the dominant accretion of material is from the stellar wind rather than Roche lobe overflow. However, the details of the accretion process are uncertain in view of the varying intervals of spin-down and spin-up of the pulsar.

The velocity of material leaving the surface of the primary may be as low as 10 km s^{-1}, based on Ginga results reported by Lewis et al. (1992), and implies, given the orbital velocity of ≈275 km s^{-1}, that the radius containing the densest parts of the atmosphere must be well within the Roche lobe.

Although the primary does not fill its Roche lobe, significant mass flow may still occur though the inner Lagrangian point, and hence account for the gas streams trailing the neutron star observed as intensity dips (Petterson , 1978). The accretion rate inferred from the average X-ray luminosity of a few x 10^{35} erg s^{-1} is $\approx 4 \times 10^{-10}$ $M_\odot$ yr^{-1} indicating that only a small fraction of the total mass outflow is captured by the neutron star. A stable accretion disc is unlikely to form but strong accretion torques must act on the neutron star to produce the rapid period changes discussed in section 7.1.2.

Matsuda, Inone and Sawada (1987) have successfully modelled the random walk behaviour of the pulsar period changes by postulating a "flip-flop" wind accretion flow onto the compact object. In this picture, a conical accretion shock or a retrograde rotating disc may form for a short time depending on the sound speed and composition of material at the surface of the primary. Given the lack of a correlation of spin change and X-ray luminosity, a change in the sense of direction of the accreting material is an attractive proposition. (Nagase et al, 1984a). For an accretion surface highly inclined to the orbital plane, as predicted for Vela X-1, Wang and Frank (1981) have shown that spin-up or spin-down may occur depending on whether the orbital velocity of the neutron star exceeds its local azimuthal velocity with respect to the wind from the primary. Such changes could be induced by the frequent temporary enhancements in mass-flow rate typical of a massive early-type star.

Several observations have suggested that the pulsar magnetic field in Vela X-1 is very high ($\geq 10^{13}$ G) including the cyclotron resonance in the pulsed fraction of emission (Staubert et al., 1980) and simulations of the pulse profiles at low energies (e.g. Meszaros and Bonazzola, 1981). This implies that the interaction of the magnetosphere with the accreting material may be very important, as discussed by Borner et al. (1987). Rather than angular momentum being transferred directly to the neutron star, changes occur due to a disc formed around the closed magnetosphere near the radius of corotation. The relatively stable material situated here may cause plasma

instabilities leading to blobs of matter separating and flowing to the neutron star surface. This model was used to explain a turn-off of the X-ray source as well as an unusual flare, both seen by the Tenma satellite. The turn-off of the X-ray emission seen by GRANAT (Lapshov et al., 1992) may also be ascribed to this phenomenon.

7.2. Previous Observations of TeV Gamma Rays from Vela X-1

The first reported detection of TeV gamma rays from Vela X-1 was made by the Potchefstroom group (North et al., 1987). Based on 11 observations in 1986, the 26 hour dataset showed evidence for periodicity at 282.80 s with a chance probability of 7×10^{-4} and a signal strength of 3.1%. This corresponded to a photon flux of $(2.0 \pm 0.4) \times 10^{-11}$ $cm^{-2}s^{-1}$ above 1 TeV. No orbital modulation was observed, but a periodic burst of gamma rays was discovered in an observation made at orbital phase 0.91. This burst lasted for 4 pulsar rotations with the first peak reaching a level 5.7 standard deviations above the local background (see Figure 7.3). Further analysis of this observation revealed a 19 minute interval of emission at the pulsar period where the pulsed signal strength was $\approx$ 18% of the cosmic ray background. The period identified in all observations was significantly shorter than the contemporary X-ray period and this discrepancy was attributed to the TeV gamma ray production occurring where a charged particle beam interacted with the limb of the primary. The shift in the detected pulse period at TeV energies was suggested to arise from the lower velocity of this emission site with respect to the observer.

Later observations by this group showed evidence for the discovery of 5 bursts lasting several pulsar rotations and spread between orbital phases 0.96 and 0.29 (Raubenheimer et al., 1989). Steering of the charged particle beam mentioned above was required to account for the observation of these bursts during the X-ray eclipse of the pulsar. A later study of all of the Potchefstroom data recorded between 1986 and 1990 found a signal strength of

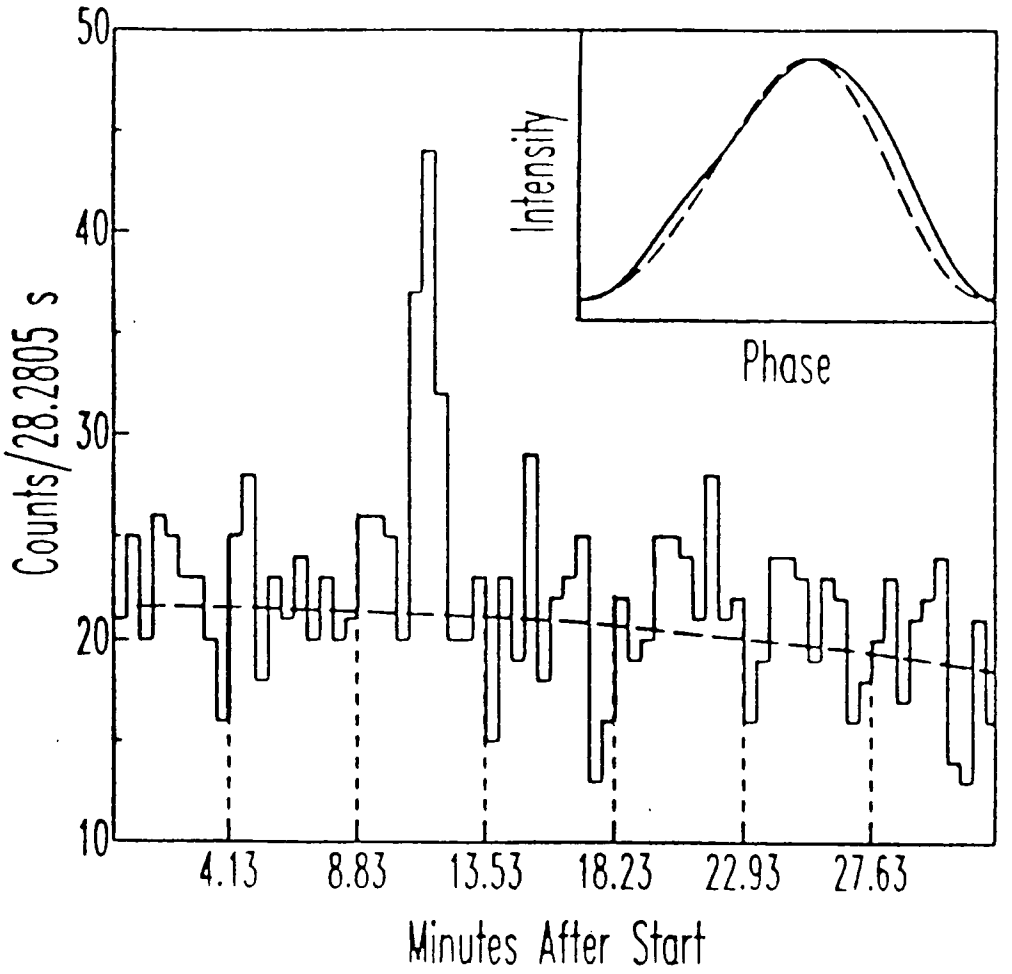

Figure 7.3 : Count rate of the TeV gamma ray observation made by the Potchefstroom group on 1986 May 4. The dashed curve represents a fit to the data excluding the outburst. The vertical dashed lines correspond to the positions of predicted gamma ray minima.

(from North et al., 1987)

(3.2 ± 0.4)% when the entire dataset was combined and tested for periodicity at the X-ray value only (North et al., 1991b). This represented a flux of 6.6×10^{-11} $cm^{-2}s^{-1}$ above 1.1 TeV. Assuming a distance of 1.9 kpc this gave a TeV gamma ray luminosity of $(1.1 \pm 0.2) \times 10^{34}$ erg s^{-1}.

The Durham group confirmed the persistent pulsed emission after analysis of three separate datasets recorded in 1986, 1987 and 1988 (Carraminana et al., 1989b). A total of 34 observations were made giving a total of 103 hours of data. A periodicity test carried out on the full dataset revealed a pulsed signal consistent with the X-ray period at a chance probability of 1.1×10^{-4}. The signal strength was (1.0 ± 0.2) % of the background giving a flux of photons above 300 GeV of $(6.6 \pm 1.4) \times 10^{-11}$ $cm^{-2}s^{-1}$ and a source luminosity of $(1.0 \pm 0.2) \times 10^{34}$ erg s^{-1}. No strong periodic effects were noted in any of the observations taken near the time of X-ray eclipse including a search for a signal at 283.1 s in overlapping segments of data lasting for 2 or 5 pulsar rotations. The 1988 March-May data was recorded in the "chopping" mode and revealed evidence for a d.c. excess of (1.2 ± 0.8) %, which was of similar magnitude to the pulsed signal strength.

No other convincing detections of Vela X-1 have been reported at TeV energies, with upper limits for persistent emission similar to the fluxes reported above being given by the JANZOS group (Allen et al., 1991) and the Adelaide group (Thornton et al., 1991). Gamma rays with energies greater than 10^{15} eV were reported to have been detected from this object using the Buckland Park air shower array (Protheroe, Clay and Gerhardy, 1984). The emission was found to be modulated with the orbital period, the most significant effect occurring in an orbital phase range 10% wide centred on phase 0.63. The time-averaged flux above 3×10^{15} eV was $\approx 10^{-14}$ $cm^{-2}s^{-1}$.

7.3. Recent TeV Gamma Ray Observations of Vela X-1

7.3.1. The 1991 February Durham Dataset

Vela X-1 was observed on 8 occasions between 1991 February 12 and 22

using the Mk.3 and Mk.4 telescopes at Narrabri. A summary of these observations is given in Table 7.1. In total, 31.7 hours of data were recorded, with weather conditions being good for all of the observations, and excellent for the four earliest.

The arrival times of the recorded events were routinely adjusted to the solar system barycentre using the Earth ephemeris of Standish (1982), and to the barycentre of the Vela X-1 binary system using the X-ray ephemeris of Deeter et al. (1987) given in Table 7.2. All 8 of the observations were made simultaneously with two telescopes, and therefore the records from each could be combined to provide a large dataset for periodic analysis. To avoid duplication of an event recorded by both telescopes (identified by simultaneous arrival times at Mk.3 and Mk.4 telescopes accurate to within several μs), the Mk.3 record only for "common" events was included in the final data together with all events seen independently in either telescope. The percentage of the total dataset due to events recorded by both telescopes was found to be 18 ± 2 %, a value which remained constant throughout.

The combined data were then subjected to the standard guard-ring selection processes. Events recorded by either telescope were accepted if a response was seen in the on-source channel alone. In addition the events recorded by the Mk.3 telescope were further selected using a preset relative response threshold of 35% in the signal from the off-source channels. This relative response threshold was also applied to the events seen by both telescopes as the Mk.3 event record was included in the complete dataset. A total of 36550 on-source events were accepted using these standard selection criteria. A dataset was also formed by using only the observations by the more sensitive Mk.3 telescope which comprised 27496 events.

7.3.2. Uniformity of Phase in the Combined Dataset

The combined dataset from the Mk.3 and Mk.4 telescopes was analysed by applying the Rayleigh test for uniformity of phase over a small range of test

TABLE 7.1 - Observations of Vela X-1 in 1991 February

Date	Duration (hrs)	EVENTS RECORDED Mk.3	Mk.4	Total	Orbital Phase
12 02 91	3.7	4239	2984	5433	0.574-0.591
13 02 91	4.2	4450	3267	5786	0.668-0.687
14 02 91	4.1	4523	3424	5968	0.763-0.782
15 02 91	4.2	2799	2657	3860	0.864-0.884
16 02 91	3.3	2521	2308	3445	0.977-0.993
18 02 91	4.1	2816	1626	3510	0.238-0.257
20 02 91	4.0	1935	2023	2847	0.476-0.495
22 02 91	4.1	4213	3092	5701	0.672-0.691
TOTALS :	31.7	27496	21381	36550	

TABLE 7.2 - Orbital ephemeris for Vela X-1

Epoch of Mid-eclipse	:	JD 2444279.0466 ± 0.0037
Orbital Period	:	8.964416 ± 0.000049 d
$a \sin i$	:	112.98 ± 0.35 lt s
Eccentricity	:	0.0885 ± 0.0025
Longitude of Periastron	:	150.6 ± 1.8°

(from Deeter et al., 1987)

periods near a contemporary X-ray pulse period measurement from GRANAT data in 1991 February of 283.260 ± 0.013 s (Lapshov et al., 1992). The hypothesis to be tested was that pulsed TeV gamma ray emission was detectable at the same period. For a pulsar with a period of this length, the simple Rayleigh test may produce spurious periodic effects if the length of the dataset is not sufficiently greater than that of the period searched for. In order to avoid this problem a modified Rayleigh test was used including a correction to eliminate end effects in the data. Without the use of relative phase information, the average length of a single observation (≈14000 s) made the independent sampling interval much larger than the uncertainty in the X-ray period given above. The lowest chance probability for uniformity of phase in the dataset, 6×10^{-2} after correction for the degrees of freedom used in oversampling the trial period interval, was found at at a pulse period of 286 ± 3 s. A similar result was found for the dataset recorded using the Mk.3 telescope alone.

The datasets were also combined retaining phase coherence and tested for uniformity of phase near the X-ray period. The contemporary pulse period derivative of 1.3×10^{-9} ss^{-1} dictated by the GRANAT results was used to maintain phase in the 10-day interval. The combined Mk.3 and Mk.4 data showed a minimum chance probability for uniformity of phase at a trial period of 283.4 ± 0.1 s. The corrected Rayleigh probability was 6×10^{-2}, after allowing for degrees of freedom, (see Figure 7.4a). Analysis of the Mk.3 dataset alone produced a similar result at a trial period of 283.4 ± 0.1 s with a corrected chance probability of 2×10^{-2} (see Figure 7.4b). Therefore no evidence was found for a significant signal pulsed at the X-ray period in the TeV gamma ray dataset.

Assuming an energy threshold for the Mk.3 telescope of 250 GeV at the zenith, a 3σ upper limit for the photon flux above this energy may be placed at 1.1×10^{-10} $cm^{-2}s^{-1}$. The Adelaide group's upper limit for their observations of Vela X-1 in 1991, including 1991 February, was 7.5×10^{-11}

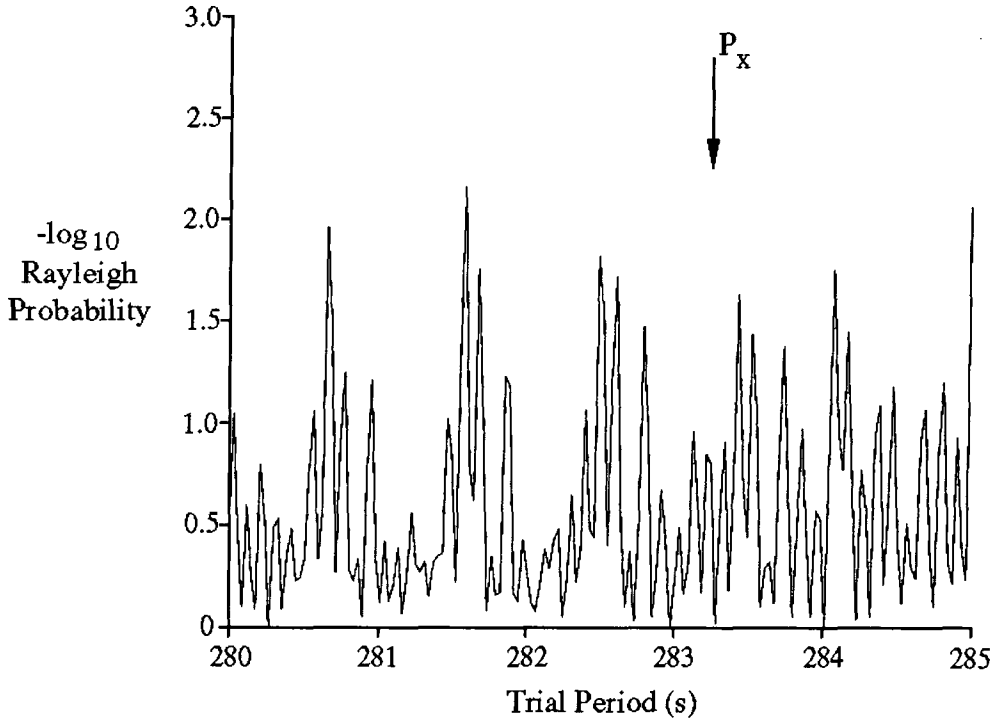

Figure 7.4a : Rayleigh probability versus trial period for the 1991 February Vela X-1 dataset recorded by the Mk.3 and Mk.4 telescopes. The data were combined coherently.

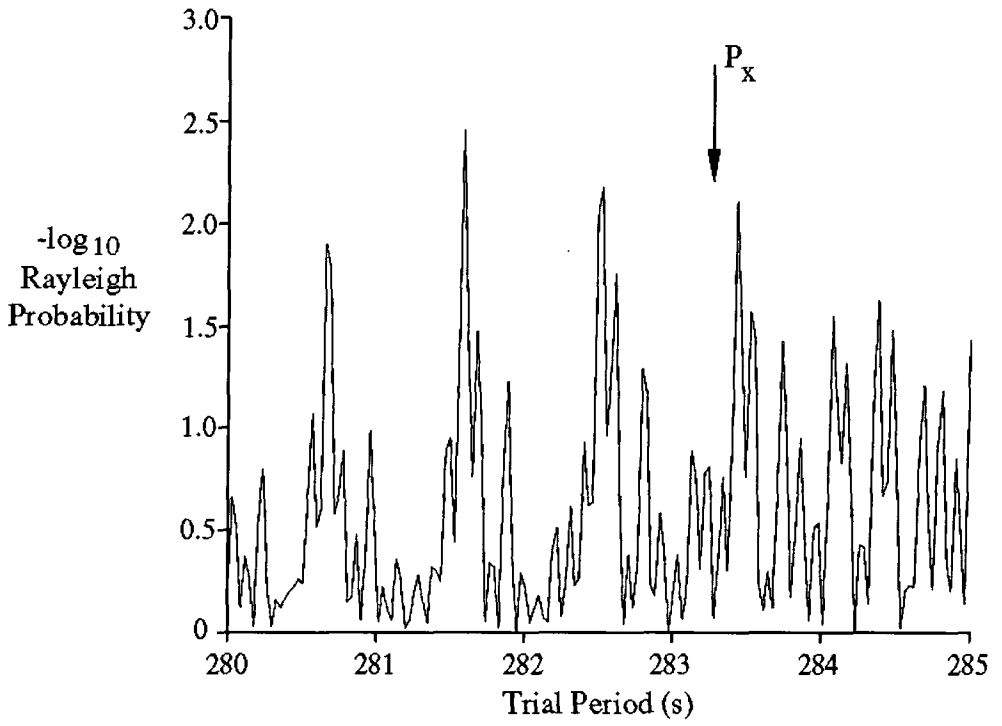

Figure 7.4b : Rayleigh probability versus trial period for the 1991 February Vela X-1 dataset recorded by the Mk.3 telescope alone. The data were combined coherently.

$cm^{-2}s^{-1}$ above 600 GeV (Thornton et al., 1991). Assuming an index of -1.6 for the integral cosmic ray energy spectrum, the upper limit reported here scales to 3×10^{-11} $cm^{-2}s^{-1}$ at energies greater than 600 GeV, and is thus entirely consistent with the Adelaide results.

7.3.3. A Search for Sensitivity to the Assumed Orbital Parameters

As discussed in Chapter 4, the orbital searching technique is most useful when analysing observations of a fast pulsar in a close binary system, for which great sensitivity to the time corrections is achieved as the independent sampling intervals in $a\sin i$ and eclipse epoch are small. Vela X-1 was shown to be very insensitive to such corrections with the sampling intervals being larger than the size of the orbit. The calculations in Chapter 4 were made for a dataset lasting only several hours.

For a test of uniformity of phase in the 1991 February dataset retaining relative phase information, the effective length of the dataset made these intervals much smaller. Whilst no evidence for a signal pulsed at the X-ray period was found in section 7.3.2, a weak periodic effect was noted at a longer period of ≈286 s. If this genuinely arose from a gamma ray signal being Doppler shifted by the motion of the emission site at the limb of the primary star, as suggested by North et al. (1989) this orbital searching technique should be able to recover the original periodicity and indicate such a displacement. The technique was therefore applied to search for any weak dependence on the assumed spatial position of the emission site. The period range used in the search was 283.1 to 283.5 s, with a spin-down rate of 1.3×10^{-9} ss^{-1}. The result is shown in Figure 7.5 and it is clear that there is little dependence on the orbital parameters and the significance of the weak periodic effect is not improved. The most favoured position in the orbit closely follows the X-ray source and is consistent with an emission site in accreted material trailing the neutron star. No evidence was found for an emission site at the limb of the companion star, where the value of $a\sin i$ is ≈

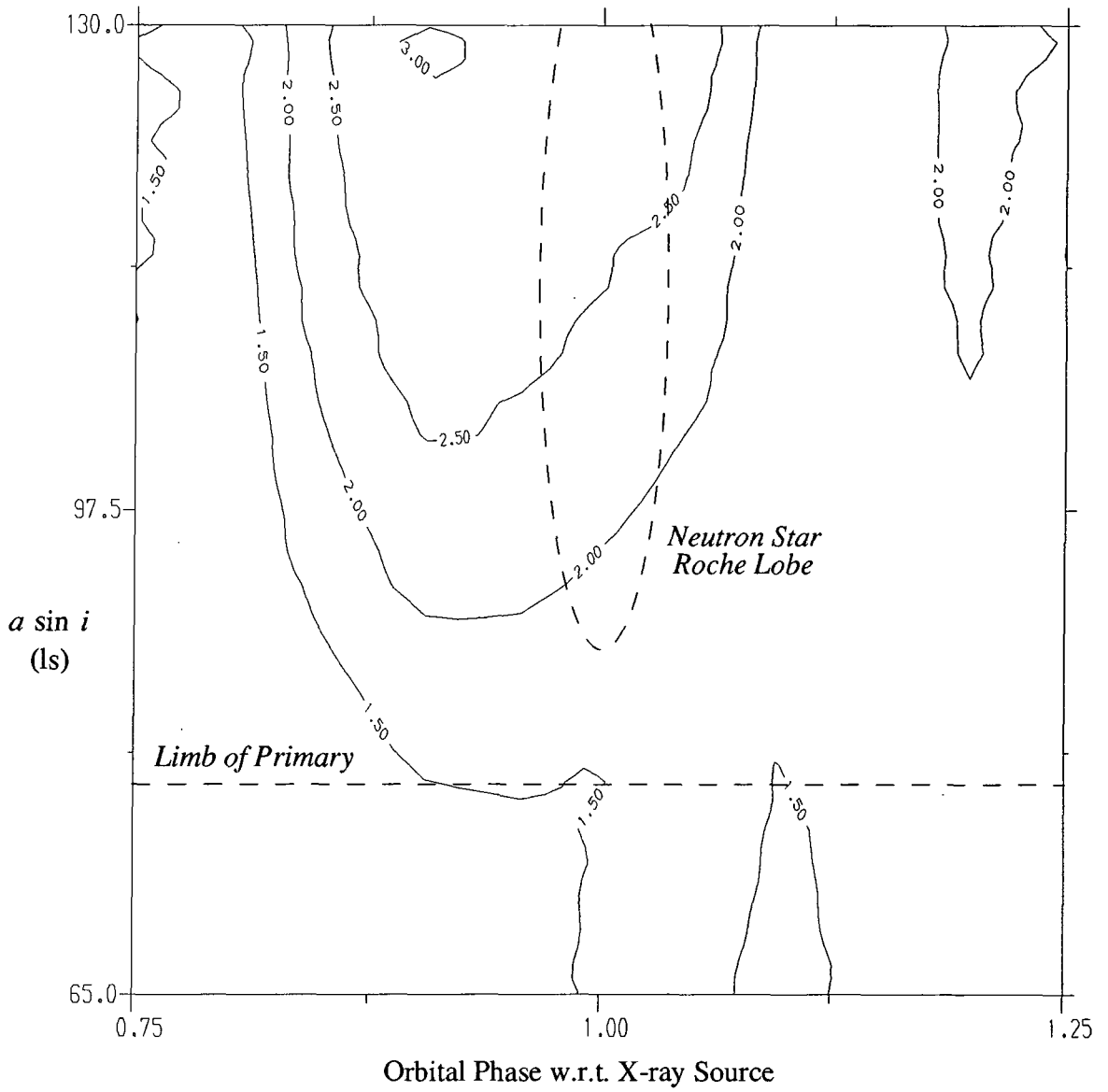

Figure 7.5 : The result of the orbital searching technique as applied to the Mk.3 telescope observations of Vela X-1 in 1991 February. The data were combined coherently and tested for uniformity of phase over the period range 283.1-283.5 s.

78 ls.

7.3.4. Analysis of Individual Observations

Whilst the evidence for periodicity gained from analysis of the combined dataset was not compelling, the results were consistent with those from the previous more extensive Durham observations and were sufficient to warrant a search for periodic emission on shorter timescales. Therefore the 8 observations were also studied individually using the data recorded by the Mk.3 telescope.

The Rayleigh test for uniformity of phase was applied over a small trial period range centred on the appropriate X-ray period of 283 s. One observation, taken on 1991 February 13, was found to show evidence for periodic emission at 284 ± 3 s with a signal strength of 3.8% of the cosmic ray background and a probability of chance occurrence of 1.8×10^{-3} (see Figure 7.6). After correcting for degrees of freedom used in discovering this emission (8 for the number of observations tested, and 3 for oversampling within the trial period range) this chance probability increased to 4.3×10^{-2}. No evidence for a similar periodic effect was found in any of the off-source control data which were recorded simultaneously. The orbital phase range corresponding to this observation was 0.672-0.691. The 3σ upper limit to the gamma ray flux which would have resulted in a significant detection on a timescale of several hours was set at 3×10^{-10} $cm^{-2}s^{-1}$ for energies ≥250 GeV.

7.3.5. Identification of Bursts of Periodic Emission

7.3.5.1. Discovery of Burst Behaviour

Following the discovery that any periodic emission was probably confined to the night of 1991 February 13, a search for further localisation of the periodic emission was carried out. The results from the Potchefstroom group suggested a timescale for enhanced emission of ≈1800 s (Raubenheimer et al., 1989) and therefore this observation was subdivided into 1800 s segments. The segments were overlapped by 300 s to optimise the sensitivity to the duration of ≈5 pulsar rotations. The Rayleigh test was used to search for uniformity of

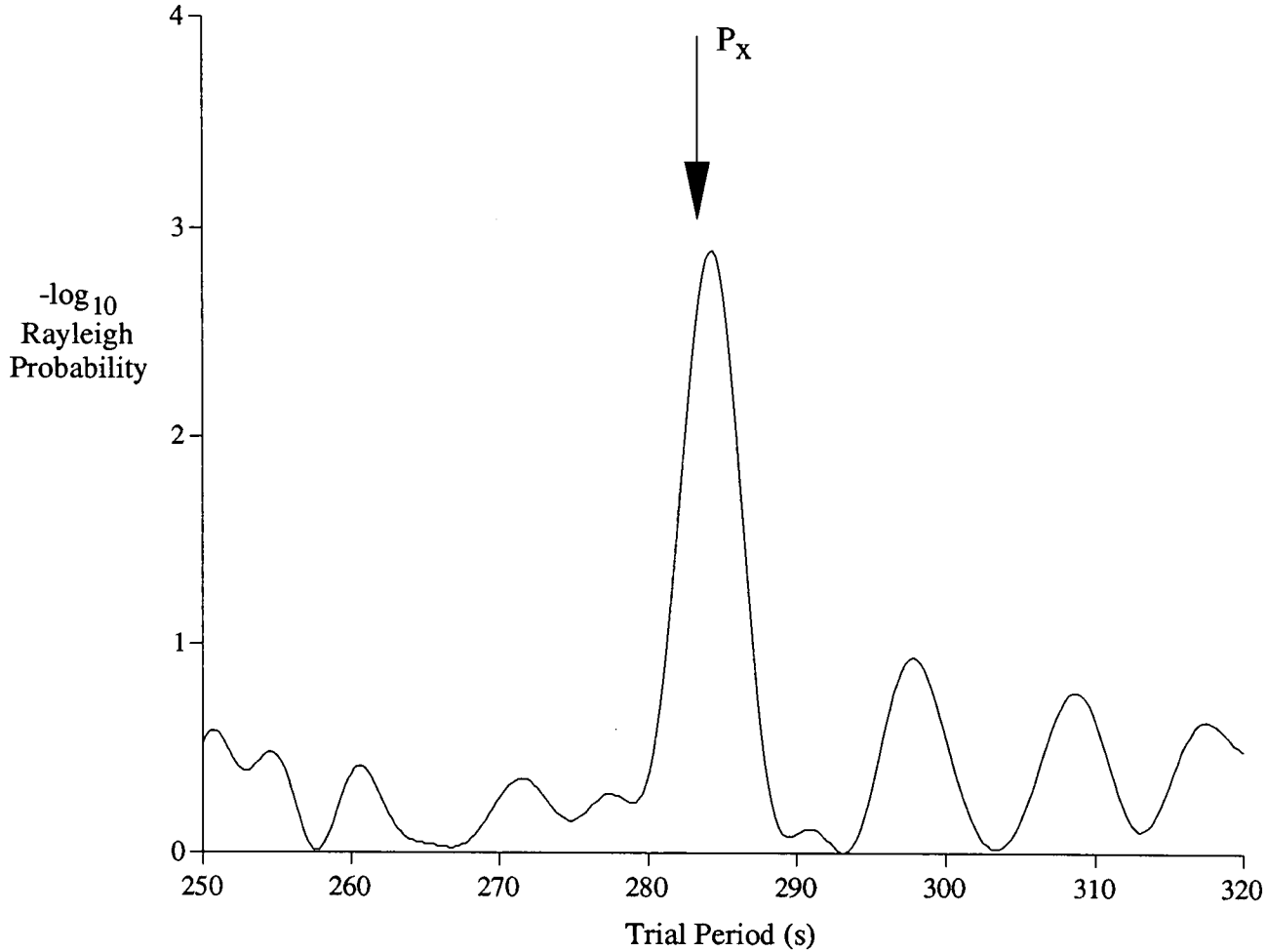

Figure 7.6 : Rayleigh probability versus trial period for the observation of Vela X-1 recorded using the Mk.3 telescope on 1991 February 13.

phase at the X-ray period in each segment.

The results showed evidence for a strong pulsed TeV gamma ray emission in an 1800 s interval near the end of the 4.2 hr observation. The periodic outburst was found to occur at UT 17:25:17 - 17:55:16 with a probability of chance occurrence of 1.5×10^{-5}. During this interval 381 Cerenkov events were registered and the pulsed signal strength was 17% of the cosmic ray background (see Figure 7.7a) corresponding to a photon flux of approximately 8×10^{-10} $cm^{-2}s^{-1}$ at energies above 300 GeV (a higher threshold due to the larger zenith angle of the burst observation). Assuming a source distance of 1.9 kpc and a cosmic ray integral spectral index of -1.6, the gamma ray luminosity reached $\approx 1.3 \times 10^{35}$ erg s^{-1} during this burst. After allowing for the 28 degrees of freedom used in identifying this interval or "burst" of TeV gamma ray emission, with an extra 3 for oversampling of the trial period range, the corrected chance probability was 1×10^{-3}.

The active interval was then removed from the total dataset for this observation and the remaining data were tested for uniformity of phase at the pulsar period. A periodic effect was found at 284 ± 3 s with a chance probability of 3×10^{-2} and a signal strength of 2.8% of the background. This provided weak evidence for the presence of a TeV gamma ray signal pulsed at the X-ray period throughout the observation.

No off-source data were found to show evidence of a similar periodic signal (see Figure 7.7b), and the authenticity of the effect is discussed in detail in section 7.5. The corresponding interval was identified in the dataset recorded by the Mk.4 telescope and a weaker signal at precisely the same period was found. Despite being consistent with a chance origin the signal strength of 9% of the background corresponded exactly to the effect seen by the Mk.3 telescope scaled to the lower energy threshold and poorer sensitivity of the Mk.4 telescope.

According to the X-ray ephemeris of Deeter et al. (1987), this outburst

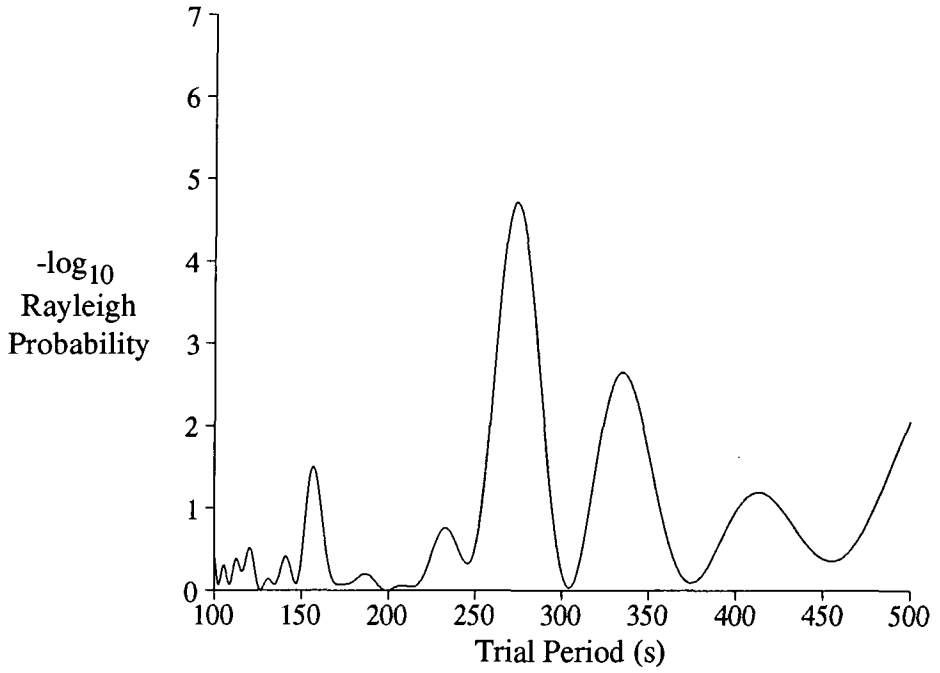

Figure 7.7a : Rayleigh probability versus trial period for the Vela X-1 "burst" dataset recorded using the Mk.3 telescope on 1991 February 13. The periodogram shown is for the data recorded in the on-source channel.

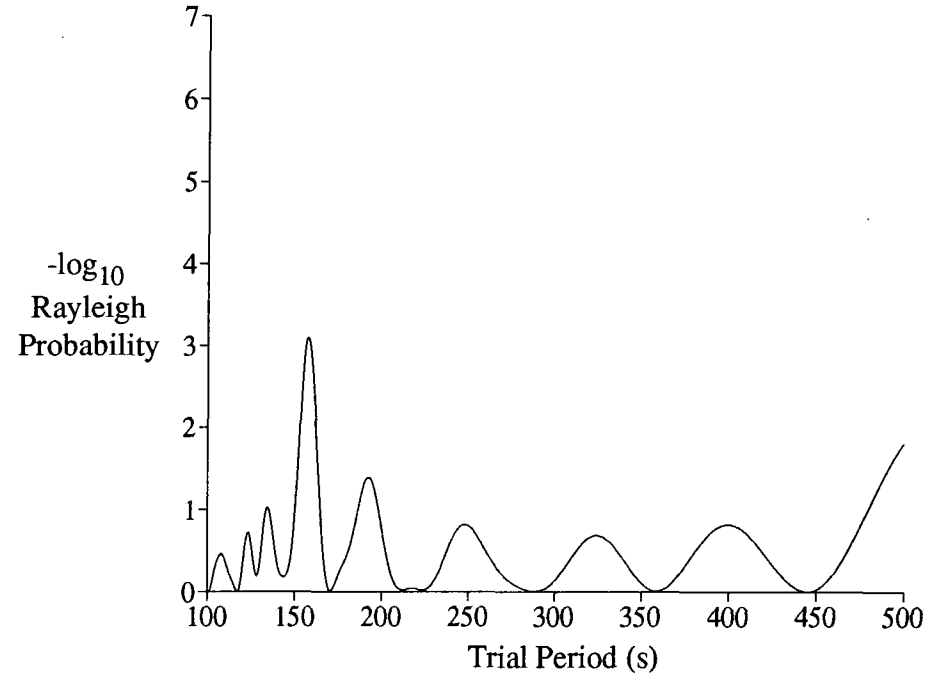

Figure 7.7b : Rayleigh probability versus trial period for the off-source dataset recorded using the Mk.3 telescope during the "burst" interval analysed in Fig. 7.7a above.

occurred between orbital phases 0.681 and 0.683 as measured with respect to mid-eclipse of the neutron star. Although none of the other 7 observations made in 1991 had been found to show evidence of persistent emission on a timescale of several hours, this candidate phase interval allowed a targeted search for a periodic signal in a specified 1800 s interval. The orbital period of the neutron star in Vela X-1 is very close to 9 days (8.9644 days). This means that an 1800 s interval at a similar orbital phase may be available in data recorded 9 days before or after 1991 February 13.

7.3.5.2. Discovery of a Second Burst

The final observation of Vela X-1 in this dark moon interval was made on 1991 February 22, 9 days after the strong periodic emission seen on 1991 February 13. Based on the exact orbital period, an 1800 s window on this date was identified where emission was expected. The appropriate segment of data was extracted based on this prediction, with event arrival times from 16:33 to 17:03 UT (± 1 minute). The Rayleigh test was applied to test for uniformity of phase at the X-ray pulsar period. This gave a null result, but as for the identification of the burst of 1991 February 13 a set of successive 1800 s segments overlapping by 300 s were also tested. These commenced 1800 s before 16:33 UT.

One 1800 s segment containing 555 events and beginning only 1600 s before the predicted interval, was found to show a periodic signal with a signal strength of 16% of the cosmic ray background (see Figure 7.8a). After correction for the degrees of freedom used in locating this active interval (12) and in oversampling the trial period range (3), the probability of this effect occurring by chance was 1.6×10^{-5}. The start and end times of this second burst were determined to be 16:06:50 and 16:36:47 UT, and it therefore overlapped the predicted active interval by about 200 s. This corresponds to a difference in orbital phase between the midpoints of the two bursts of 0.002. The orbital phase range of the burst of 1991 February 22 was 0.679-0.681.

The data recorded by the off-source channels during this outburst were

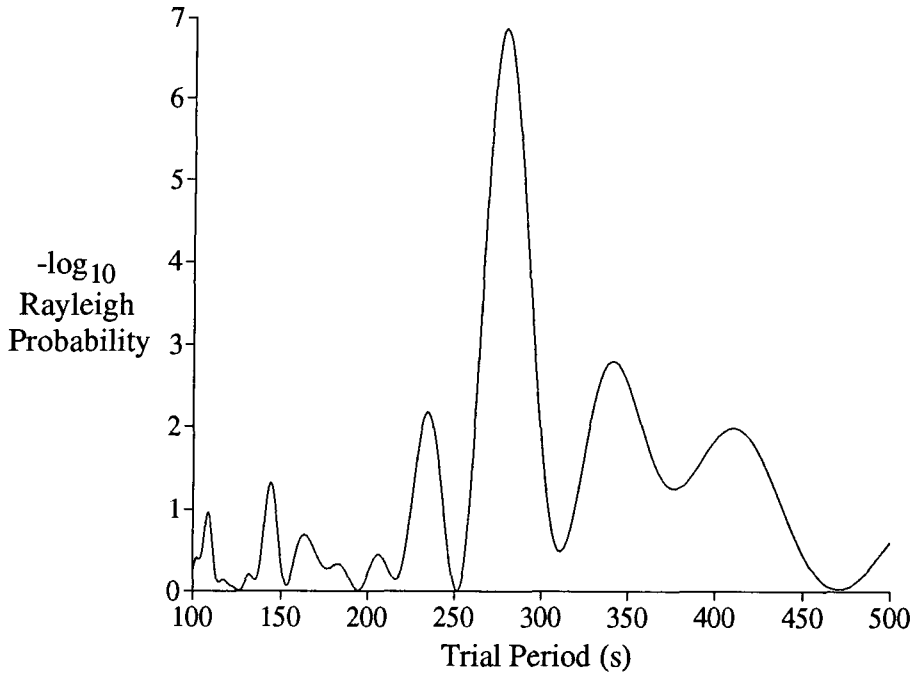

Figure 7.8a : Rayleigh probability versus trial period for the Vela X-1 "burst" dataset recorded using the Mk.3 telescope on 1991 February 22. The periodogram shown is for the data recorded in the on-source channel.

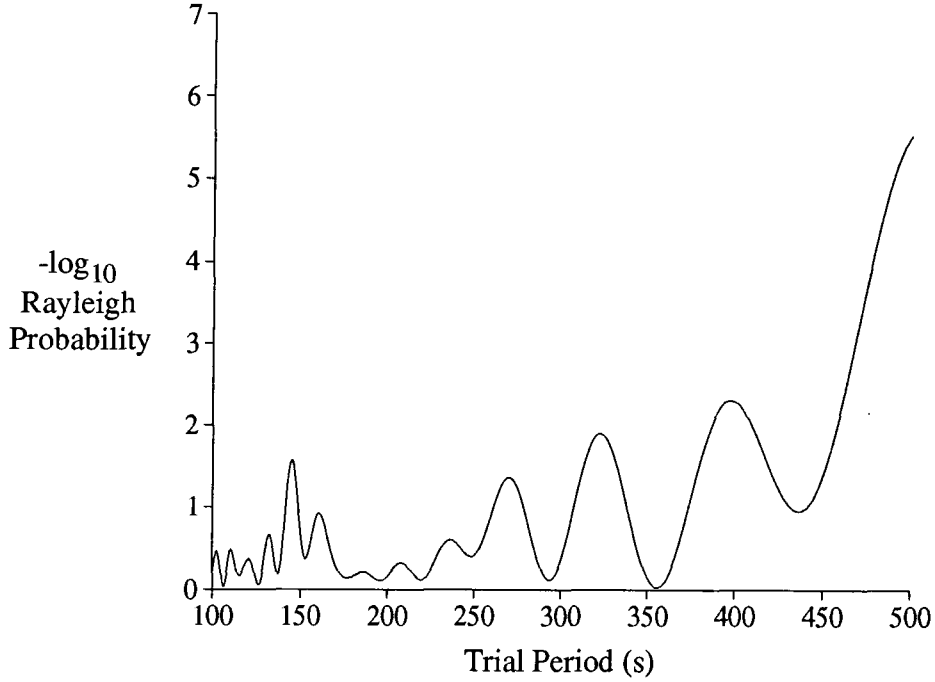

Figure 7.8b : Rayleigh probability versus trial period for the off-source dataset recorded using the Mk.3 telescope during the "burst" interval analysed in Fig. 7.8a above.

checked and no evidence for a periodic signal was found (see Figure 7.8b). It may be noted that a strong periodic signal was found in the off-source data at a period of 450-500 s. This effect is related to the 1800 s duration of the dataset and occurs with a much lower pulsed strength in some of the other segments. The data segment from the Mk.4 telescope corresponding to this burst was extracted and a weak periodic signal was found at precisely the period identified by the Mk.3 telescope; the signal strength was approximately 8% of the cosmic ray background. The TeV gamma ray emission from Vela X-1 detected by the Mk.3 telescope during these burst intervals is compared with other TeV gamma ray observations in the spectrum shown in Figure 7.9.

7.3.5.3. Relative Pulse Phase of the Burst Emission

The TeV gamma ray light curves for the two bursts are shown in Figure 7.10. In addition to the bursts, a light curve is also shown for the weak persistent periodic effect on 1991 February 13. Each is constructed using the 283.260 s period from the contemporaneous GRANAT measurements with respect to a time origin at UT 12:00 on 1991 February 12. All show the single broad peak expected as a result of the identification by the Rayleigh test.

In a preliminary analysis of the 1991 February dataset (Bowden et al., 1991c, 1992d) it was shown that the pulsed emission in both bursts did appear to show relative phase alignment with respect to the TeV gamma ray period estimated from the data recorded on 1991 February 13 excluding the burst segment. The specific hypothesis tested here is whether the gamma ray emission from both bursts were aligned in phase with respect to the more accurate contemporaneous X-ray period measurement (Lapshov et al., 1992). Absolute phase information from the GRANAT measurements is not known, and therefore the phase linkage between the bursts is based on the peak of the light curve for the 1991 February 13 data excluding the burst. Whilst the burst emission on that date does show the same absolute phase at the 283.26 s period, the burst 9 days later clearly does not.

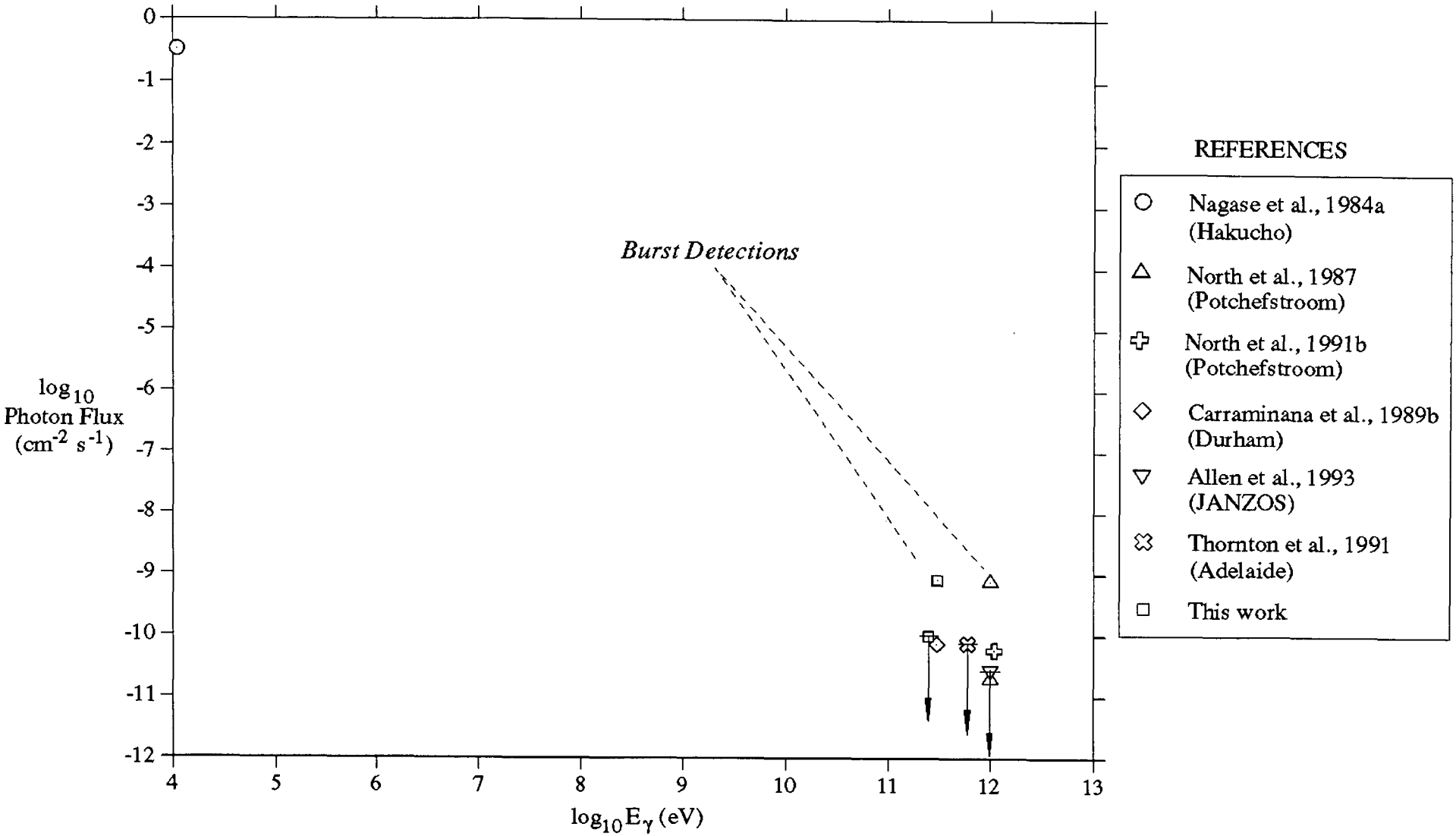

Figure 7.9 : The TeV gamma ray spectrum of Vela X-1. The arrows denote upper limits and the detections of brief bursts of emission are indicated. The X-ray flux measured by Hakucho is given for reference.

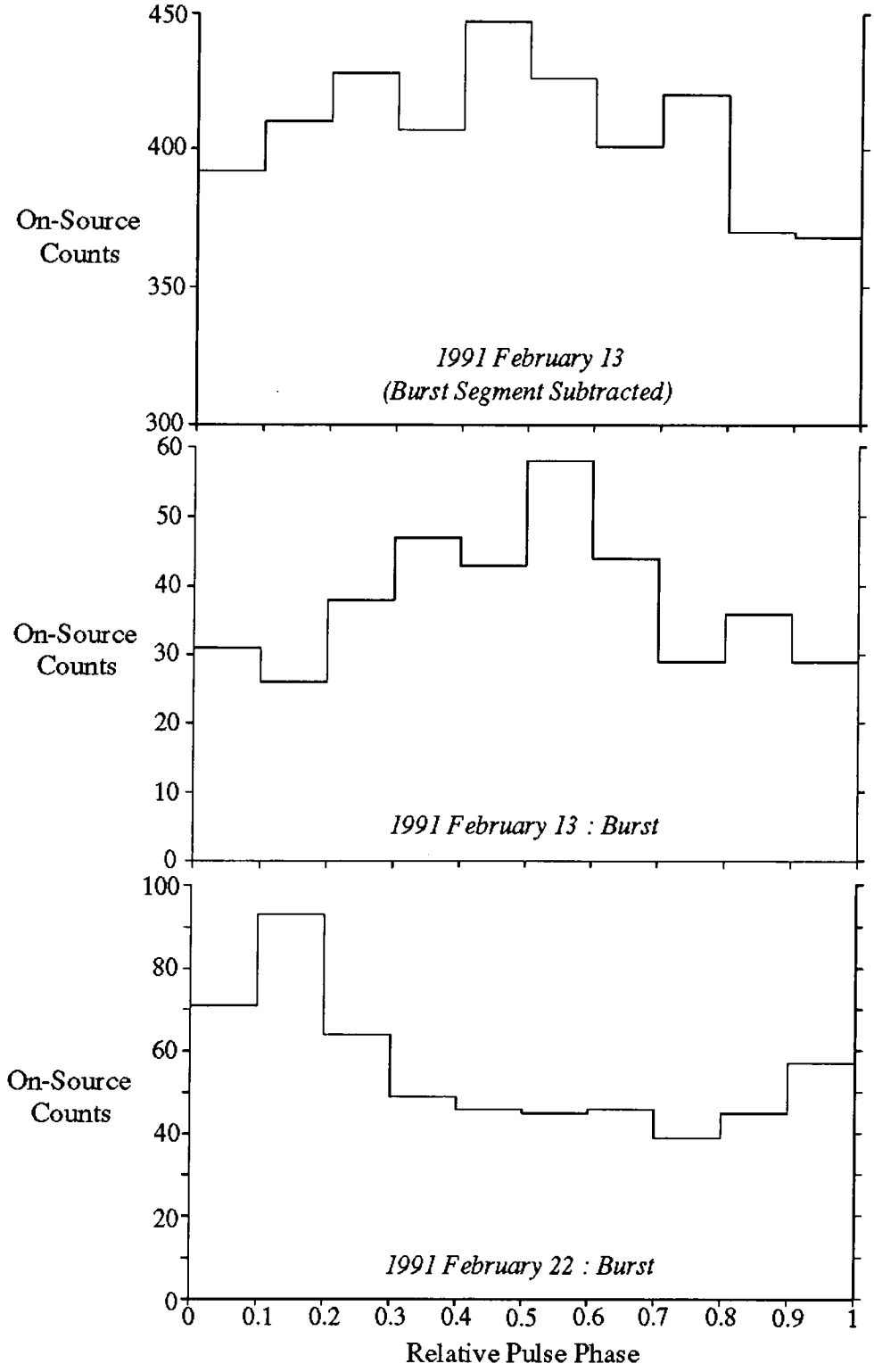

Figure 7.10 : The set of light curves resulting from folding the 283.26 s period (from GRANAT measurements) into the Vela X-1 "burst" datasets. Pulse phase is maintained relative to 12h UT on 1991 February 12. The light curve for the "non-burst" data on 1991 February 13 is also shown.

This non-alignment need not be seen as an argument against the validity of the signal detections. Timing uncertainties may induce a substantial error in the predicted position of the peak of the light curve. These may arise from the error in the X-ray period measurement (±0.013 s), the error induced by the resolution of the TeV gamma ray light curve (±5%), and the lack of knowledge of the behaviour of the pulse period derivative. The latter factor is known to be highly variable. The steady derivative was estimated as 1.3×10^{-9} ss^{-1} from the GRANAT data but on short timescales, this can increase to as much as 3×10^{-8} ss^{-1} (Nagase et al., 1984a). Combining these three factors, the error in the predicted phase of the light curve peak accumulated over 9 days may be shown to be +0.35/-0.20, i.e. similar to the shift between the peaks seen here. The lack of phase alaignment is therefore not surprising. In the previous linkage of the bursts based on the TeV gamma ray period, the large error in this period was not allowed for and would in fact increase the estimated phase error given above.

X-ray measurements of Vela X-1 using the Gamma-1 satellite showed that the major peak of the double-peaked light curve could switch between successive orbits perhaps due to a change in the accretion rates at each magnetic pole (Loznikov, Konorkina and Melioranskii, 1992). Similar random behaviour could cause a substantial change in the apparent phase of the single peak of the TeV gamma ray light curve.

7.3.6. Tests for Authenticity of the Bursts

7.3.6.1. Possible Causes of Spurious Periodicity

When analysing data obtained by use of the atmospheric Cerenkov technique in a search for a period as long as that of Vela X-1, it is always a challenge to prove that the periodicity is not due to some kind of atmospheric fluctuations which may exist on this timescale. The extensive supplementary information available at the Narrabri telescopes allows careful checking of the authenticity of the effect. As previously stated, the weather conditions and atmospheric clarity were excellent for the observation of 1991 February

13. The second burst on 1991 February 22 occurred only ≈1000 s before the passage of high cloud through the field of view. Although no cloud appears to have occluded the source position during the burst interval (a conclusion based on the records of weather and direct count rate) the possibility must be seriously considered.

Apart from this extrinsic effect, the intrinsic effect of variability induced by unstable photomultiplier tube behaviour may be discounted from the comprehensive and continual monitoring of their performance. In neither observation do the histories of photomultiplier tube anode current and noise rate show any sign of anomalous behaviour.

7.3.6.2. Count Rate Histories During Bursts

Beyond these considerations, the information required to demonstrate the authenticity of the bursts was the knowledge that the effects are confined to the source position and result from increases rather than decreases in the count rate from that direction. Using a technique similar to that described by the South African group in the report of the 1986 Potchefstroom analysis (North et al., 1987), the on-source count-rates of the 1800 second bursts of 1991 February 13 and 22 were plotted in segments of 113.2 seconds (i.e. 2/5 of the pulsar period) stepped four times in order to smooth the effects of statistical fluctuations.

The results, shown in Figures 7.11 and 7.12, directly revealed periodic enhancements of ≈ 20% in the count rates recorded during each burst observation. Also given are the combined count rates in the three off-source channels stabilised by the automatic gain control system (see Chapter 3). These were derived in precisely the same way as those for the on-source channel to look for any unusual behaviour in the count rates during each burst. No significant activity was discovered in any channel which correlated with that seen in the on-source dataset (see Figures 7.11 and 7.12). It was shown in sections 7.4.1 and 7.4.2 that no signal pulsed at the period of Vela

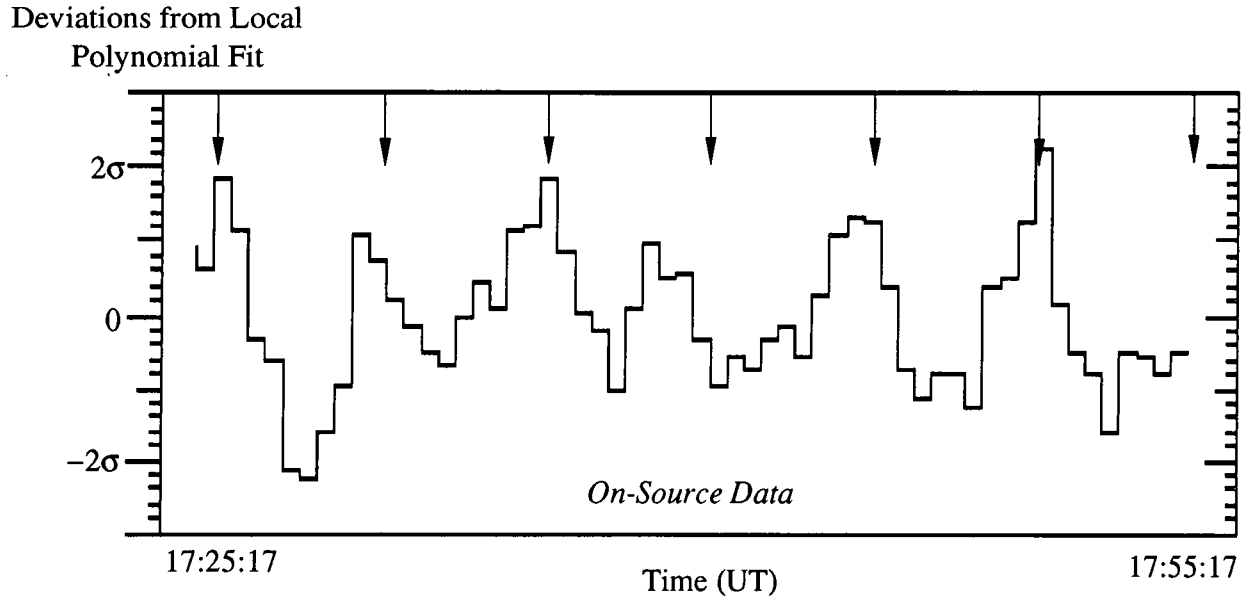

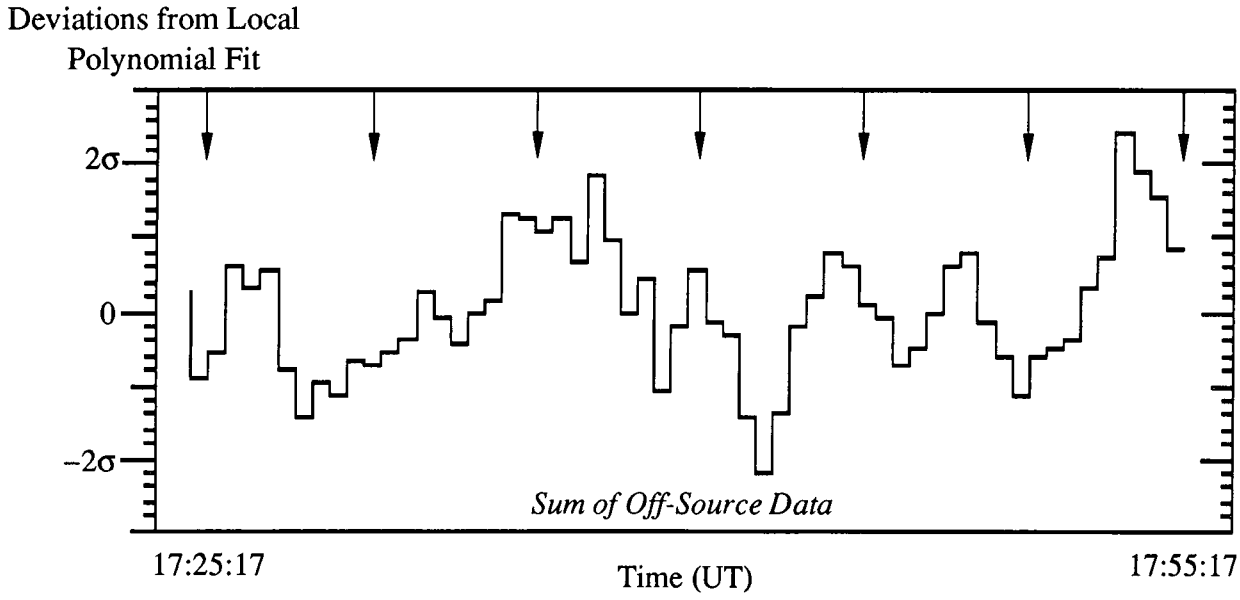

Figure 7.11 : Count-rate histories for the on- and off-source datasets recorded using the Mk.3 telescope during the burst interval on 1991 February 13. The data are divided into 113.2 s segments and stepped in 4 overlapping stages.

The arrows show the peaks predicted on the basis of the pulsed light curve obtained at a period of 283.260 s in all of the data from this date excluding the burst interval (c.f. Figure 7.10).

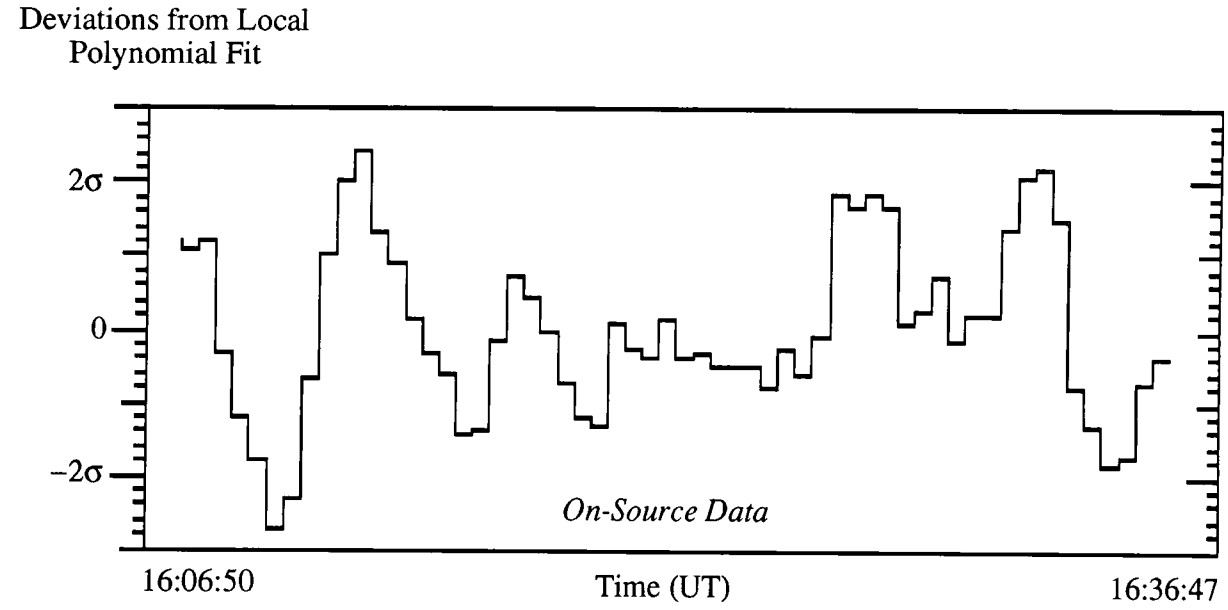

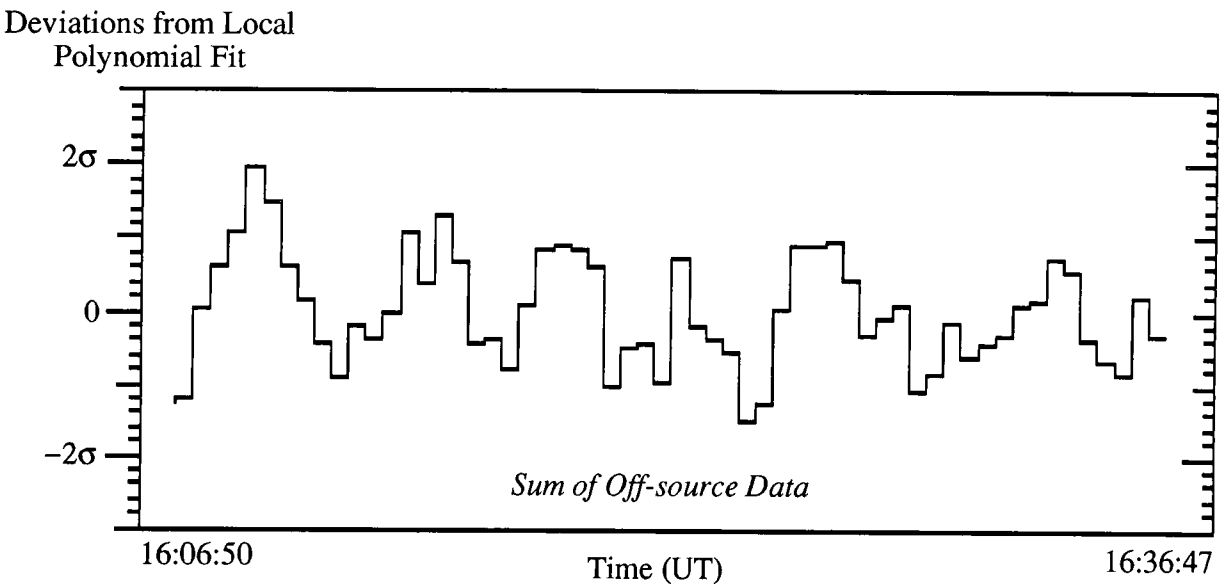

Figure 7.12 : Count rate histories for the on- and off-source datasets recorded using the Mk.3 telescope during the burst interval on 1991 February 22. The data are divided into 113.2 s segments and stepped in 4 overlapping stages.

X-1 was present in this off-source data.

By defining the phase of the peak of the gamma ray light curve for the persistent emission in the dataset of 1991 February 13 excluding the burst segment, an independent set of times were predicted where the peaks of the emission modulated at 283.26 s in the burst on this date were expected to occur. Each peak in the burst emission on this night was found to correspond well with a predicted maximum. The extrapolation of the same light curve to the burst observation 9 days later gave a poor agreement with the observed peaks, which may be explained by the points discussed in section 7.4.3.

7.3.6.3. Analysis of Events Comprising Bursts

The next step in the study of the bursts was to determine whether the events forming the peaks seen in the on-source count rate of each burst demonstrated any unusual characteristics, particularly indications of a change in the energy spectrum. First, each dataset was split into three subgroups of approximately equal size by selecting events based upon the amount of charge measured in each recording channel. The three subgroups then contained events selected on the basis of a measure of primary particle energy. Count rate plots were produced in identical fashion to those for the total datasets for each burst (see Figures 7.13 and 7.14). Whilst variations were clear between the different energy ranges, no obvious dependence emerged. Several of the individual peaks were found to be formed largely of events from one of the three divisions but no consistent preference was identified. The events from the highest energy range produced the most sharply peaked distribution, particularly for the second burst observation. The Rayleigh test for uniformity of phase was also conducted at the pulsar period in each of the energy ranges. For each burst the highest energy range gave marginally the largest signal with a pulsed strength of $\approx$20 %, compared with $\leq$16 % for the other divisions.

A method was also developed whereby a simple spectral analysis could be performed on the events in each burst. The charge registered by the

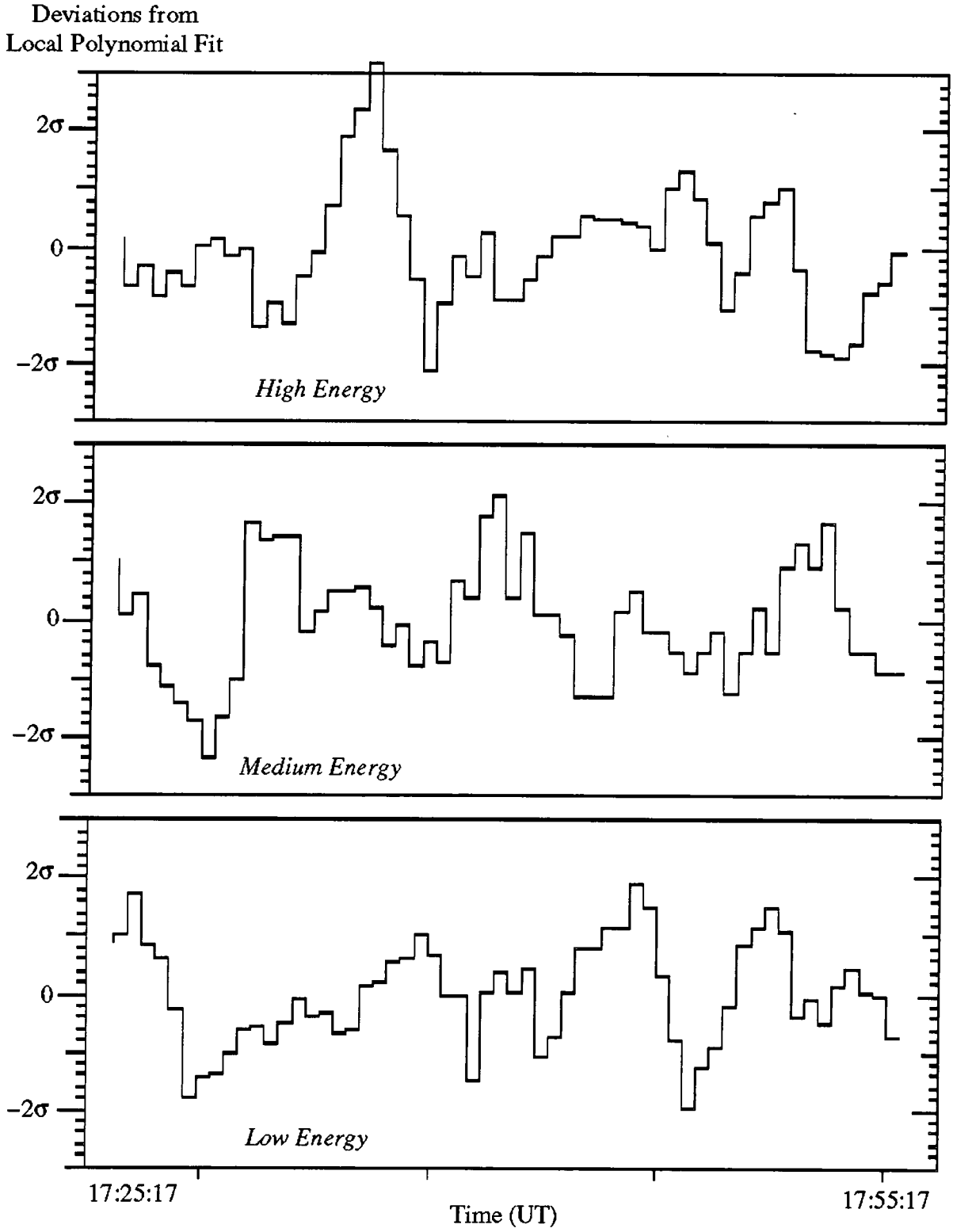

Figure 7.13 : Count rate histories for the Vela X-1 burst dataset recorded using the Mk.3 telescope on 1991 February 13. The data are split here into 3 categories based on the pulse height integral in the on-source channel for each event, in order to enable study of the events according to the relative energy of the primary particle.

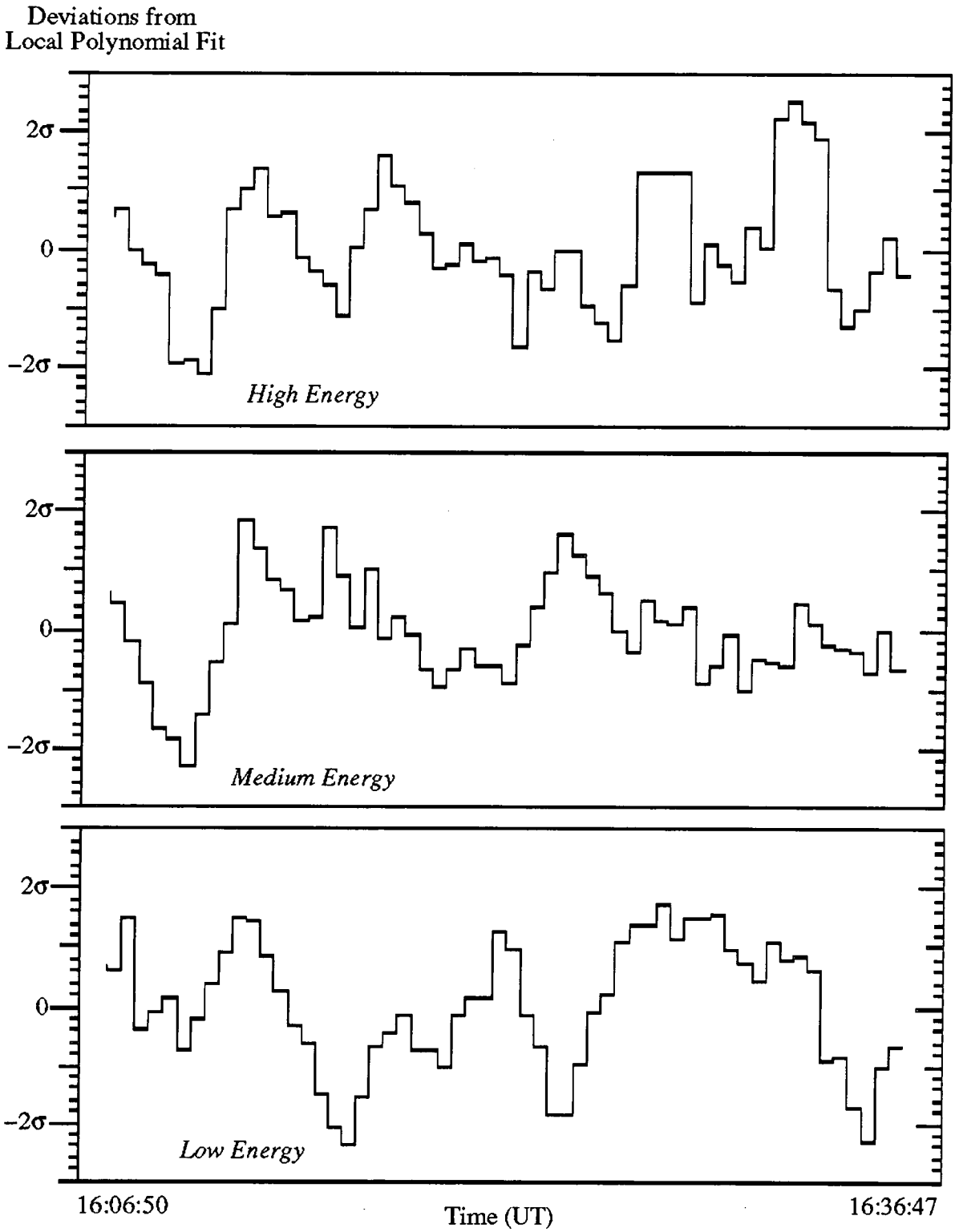

Figure 7.14 : Count rate histories for the Vela X-1 burst dataset recorded using the Mk.3 telescope on 1991 February 22. The events are divided according to the relative primary particle energy as in Figure 7.13.

photomultiplier tubes in the on-source channel (i.e. the time integral of the Cerenkov light pulse height) for each event was used to construct a spectrum, with higher registered charge corresponding to a higher energy primary as mentioned above. In addition to each burst dataset, a control group of events was extracted from the data recorded immediately before each burst, containing the same number of events as the relevant burst. The spectra produced for the datasets before and during each burst observation are shown in Figures 7.15 and 7.16. No obvious differences are apparent between the data recorded before and during either burst.

When an excess of events was detected from the direction of AE Aquarii by the Mk.3 telescope (Bowden et al., 1992b) a comparison of the "hardness" ratio of the events comprising the burst with a group sampled before and after revealed a clear shift towards higher energy primary particles in the burst interval. For the Vela X-1 bursts reported here, the spectra of the events recorded immediately before each burst were divided into two segments of approximately equal size by selecting an arbitrary pulse integral threshold. The ratio of the number of events recorded with pulse integrals below or above each threshold (corresponding to lower and higher primary particle energies) were calculated for each set of events and found to be 0.95 ± 0.10 and 0.95 ± 0.08 for 1991 February 13 and 22 respectively. The burst datasets were then analysed similarly and the ratios found to be 0.88 ± 0.09 and 1.07 ± 0.09 respectively. There was therefore no significant difference in the "hardness" of the burst events on either date.

7.3.6.4. Search for an On-source Excess in the Count Rate

A final check was carried out in order to test whether the two bursts identified by their characteristic periodicity also displayed evidence of an enhancement over the local background counting rate.

The data from 1991 February 13 and 22 were subjected to a ratiometric analysis. This involved testing for an excess of counts in the central (on-

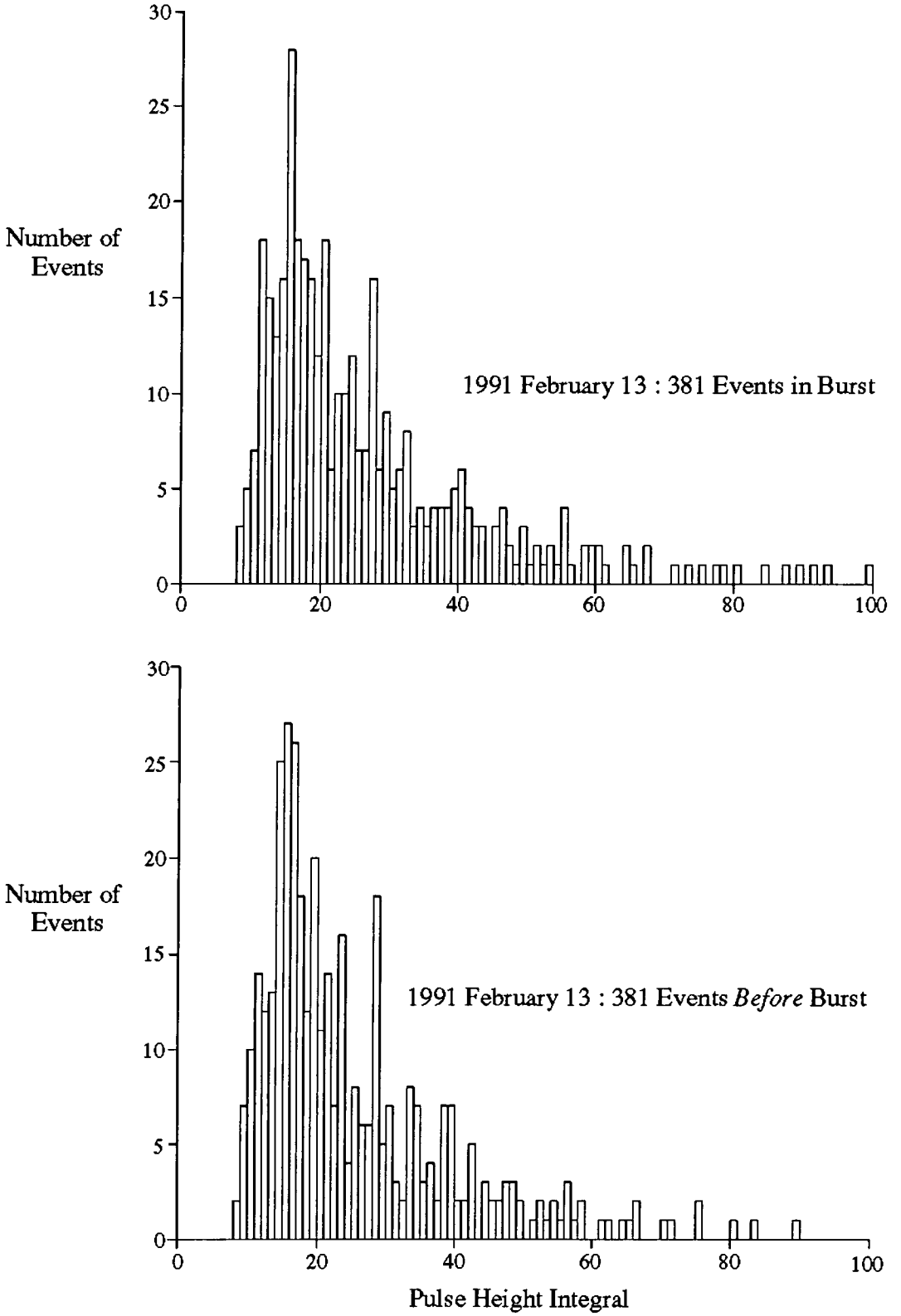

Figure 7.15 : Pulse height spectra calculated for data recorded on on Vela X-1 using the Mk.3 telescope during and immediately before the burst interval on 1991 February 13. The spectra shown are for the on-source channel only.

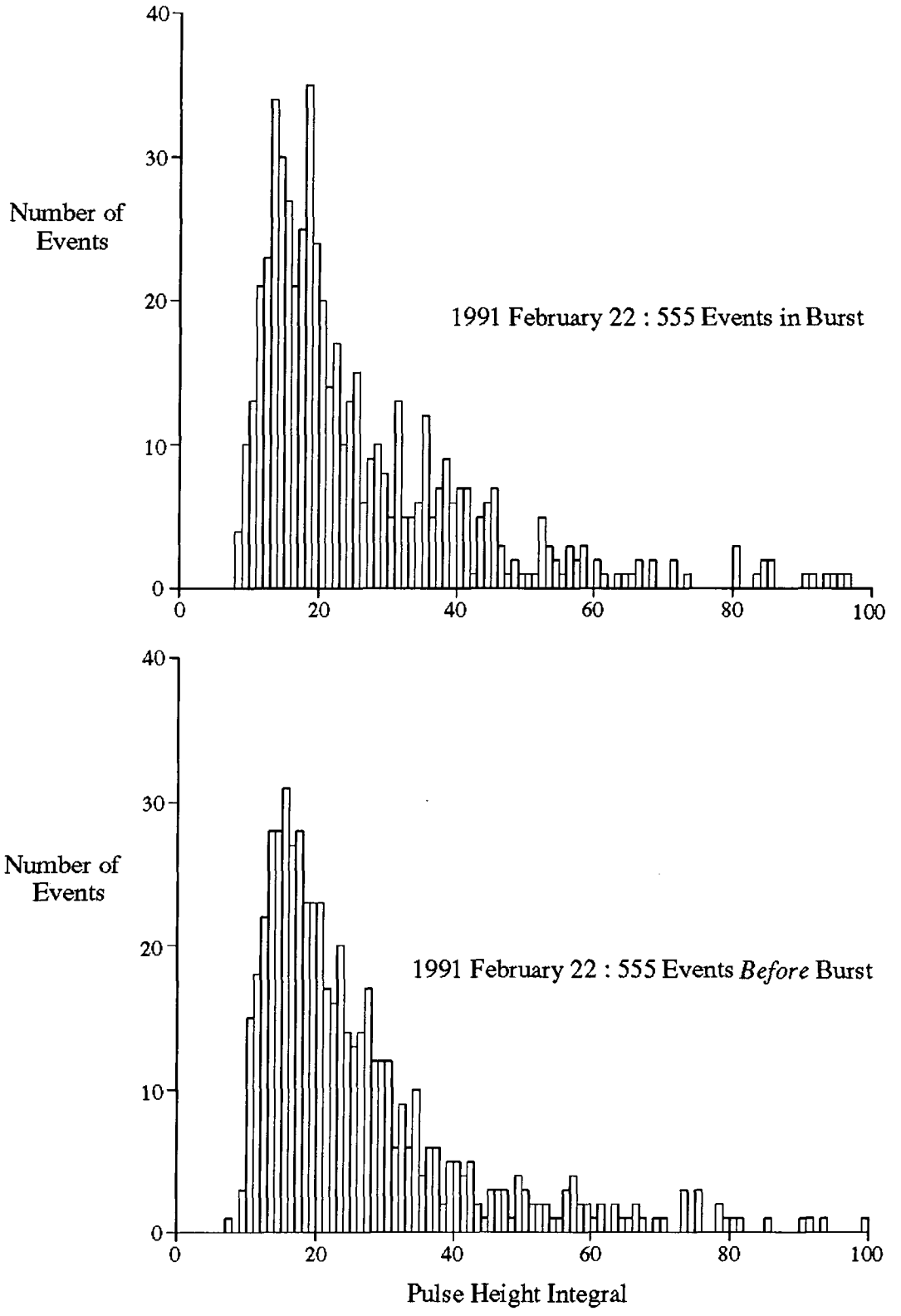

Figure 7.16: Pulse height spectra calculated for the data recorded on Vela X-1 using the Mk.3 telescope during and immediately before the burst interval of 1991 February 22. The spectra shown are for the on-source channel only.

source) channel as compared with two of the off-source channels. To gain as reliable an estimate as possible of the underlying trend in the count rate, large segments of data were selected from the events before and after the burst seen on each observation and used to define the underlying ratio of on-source/off-source count rates which would be expected during each burst with respect to each of the off-source channels selected. For 1991 February 13 this required three datasets of length 3900 s prior to the burst and one of length 1350 s immediately afterwards. Similarly, for 1991 February 22 two 3500 s datasets were used prior to the burst. On this date the passage of cloud shortly after the burst meant that two datasets of unequal lengths, 1200 s and 2700 s, and separated by a gap of 1800s to reject the cloud obscuration, were selected.

In each independent segment the number of counts in the on-source channel and each of the two off-source channels were individually recorded and the appropriate ratios calculated. Linear fits to the variation in the ratio of the counts in the on-source channel to the counts in each of the two off-source channels were then made with regard to the time elapsed.

Having determined the background on-/off-source ratios expected during each burst, the experimental ratios were found by analysing segments of data 112 s long and slid in four 28 s steps. This technique was derived from the way in which the count rates in each channel were previously calculated for the burst intervals (see Section 7.5.2). A total of 65 data segments were used to find the values of the counts in each channel over the 1800 s of each burst, with every fourth value being independent. The ratios were then determined and their variations over the course of each burst are shown in Figures 7.17 and 7.18.

The results demonstrated that the periodic effects in the on-source count-rate in each burst were accompanied by clear excesses in the ratio of this count-rate to those of both off-source channels, as compared with the ratios predicted by the independent analysis of the data surrounding each

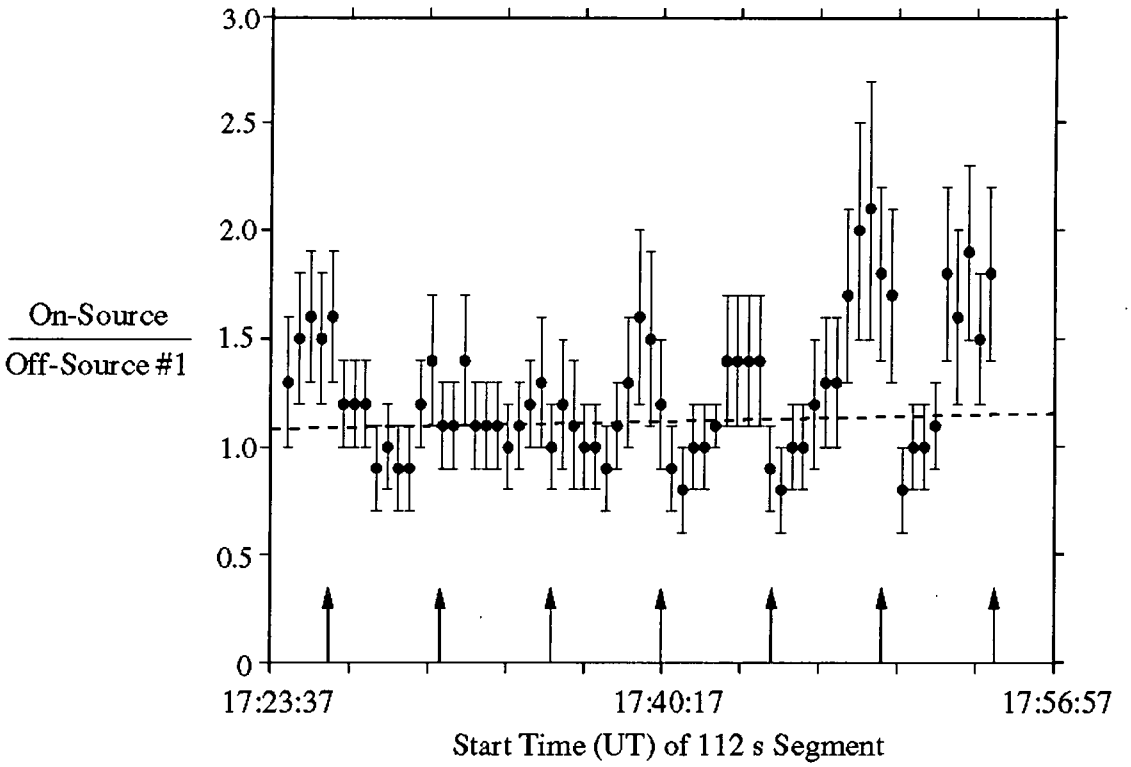

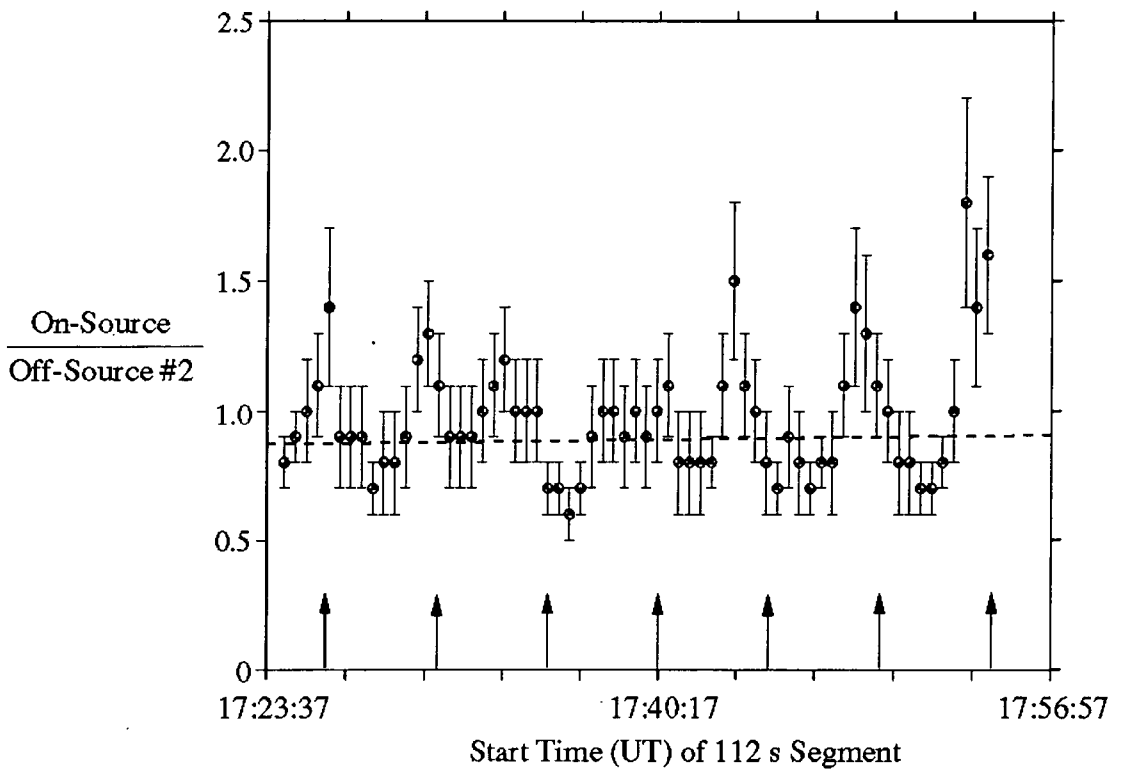

Figure 7.17 : The ratio of the on- and off-source count rates calculated for the Vela X-1 burst dataset recorded using the Mk.3 telescope on 1991 February 13. The ratios are based on 112 s segments of data slid in 4 steps. The arrows define the predicted peaks of the emission as in Figure 7.11. The dashed line shows the underlying ratio of the count rates based on the data from the rest of the observation.

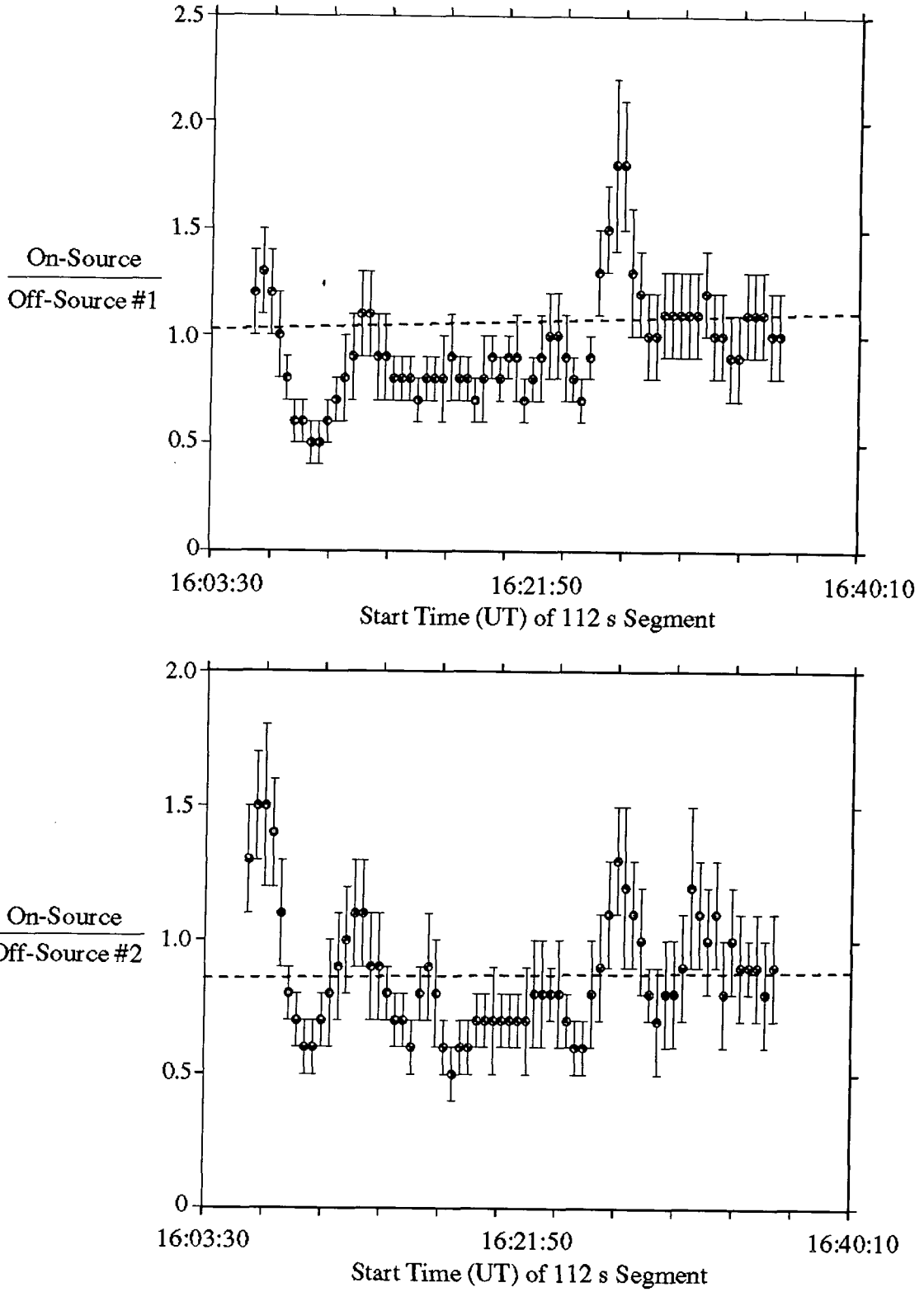

Figure 7.18 : The ratio of the on- and off-source count rates calculated for the Vela X-1 burst dataset recorded using the Mk.3 telescope on 1991 February 22. The ratios are based on 112 s segments of data slid in 4 steps. The dashed line shows the underlying ratio of the count rates based on the data from the rest of the observation.

interval. The comparison of the on-source count rate with those of the off-source channels indicated a stronger excess with respect to one (#1 in Figures 7.17 and 7.18) than the other. This was simply due to the lower absolute count rate of that channel. Two conclusions could be drawn about the authenticity of each burst :

(i) that the periodic effect was only present in the on-source channel, which had already been established,

(ii) that the observed periodicity was almost entirely due to a periodic *excess* in the on-source count rate recurring at intervals of ≈300 s. It is not due to a series of periodic deficits.

7.4. Discussion

In summary, the present work has demonstrated weak evidence for persistent emission but strong evidence for the presence of outbursts of TeV gamma ray emission from Vela X-1 lasting several pulsar rotations and apparently related to the position of the neutron star in its orbit. This adds to the results of the previous more extensive Durham observations which found evidence for a persistent signal but no evidence for outbursts of the type seen here and also reported by the South African group. This demonstrates that the detection of the weak persistent pulsed emission requires a very large dataset. The relatively small size of the dataset analysed here has a much lower sensitivity to a persistent signal than the more extensive earlier work. Nevertheless, there appears to be a strong possibility that periodic bursts of emission may be detected from the region of the orbit around the ascending node and the X-ray eclipse.

The observation of two bursts persisting over several pulsar rotations at similar values of orbital phase resembles the reports of bursts detected by the Potchefstroom group. The major difference is the differing orbital phase of burst behaviour. The bursts identified by the Potchefstroom group occurred in observations made near to eclipse ingress and egress of the X-ray source

and were thus interpreted as requiring a target at the limb of the primary star. Despite the low angular velocity of the pulsar in Vela X-1, its high magnetic field of perhaps $\geq 10^{13}$ G makes it possible that a dynamo mechanism may be capable of producing a highly energetic particle beam in the magnetosphere of the neutron star.

The bursts reported here were detected at an orbital phase of 0.68, well removed from the position of X-ray eclipse. If it is assumed that the operative gamma ray production process involves magnetic steering of the particle beam from the pulsar onto intervening matter in the system, then an alternative target to the atmosphere of the primary is required. As was discussed in Section 7.1, absorption dips are frequently observed in the X-ray emission between orbital phase 0.5 and the eclipse, suggesting the presence of significant amounts of material flowing from the primary to the compact object in addition to the spherical stellar wind. It is also believed that conditions may sometimes be favourable for an accretion disc to form. Either one or both of these could provide a suitable target for TeV gamma ray production, and the variable matter densities estimated from X-ray measurements could explain the sporadic nature of detections at TeV energies. In this context it is particularly interesting to note that the observation by GRANAT of a prolonged dip in the X-ray intensity (see section 7.1.3) was made over the orbital phase range 0.68-0.80 only 5 orbital cycles before the first of the TeV gamma ray bursts reported here.

The weaker long-term emission may be attributed to interaction of the particle beam with the more tenuous but ever-present stellar wind. These considerations are investigated further with relevance to the Vela X-1 system in Chapter 9.

Whilst the X-ray emission shows a double-peaked structure at high energies, due to the favourable alignment of the rotation and magnetic axes allowing both polar regions to be visible, the TeV gamma ray emission shows

only a single peak. No power has been observed in the second harmonic in any of the detections reported. An interesting comparison may be made with regard to the observation of a large but brief X-ray flare by the Tenma satellite (Tanaka, 1984). This outburst occurred at orbital phase 0.19 and lasted for about 4 pulsar rotations during which time the intensity of the first peak increased by a factor of 5 whilst the other remained near its normal quiescent level. Borner et al. (1987) ascribed this behaviour to an azimuthal instability in the closed magnetosphere trapping a large amount of accreting matter over one magnetic pole and prohibiting its transport to the other. The resulting enhanced emission then showed a single peak structure and a similar mechanism could explain the nature of at least the short-term TeV gamma ray emission.

The archival Durham data recorded on Vela X-1 has previously been checked for signs of burst behaviour near to the time of X-ray eclipse and no evidence for this was found (Carraminana et al., 1989b). The discovery reported here of bursts at orbital phase 0.68 suggested another search for emission at this preferred region of the orbit would be justified. Four observations were made at a similar phase in 1987 and 1988 but unfortunately none were made under the clear sky conditions which would allow a test for periodicity.

An ongoing investigation of phase-related emission is made difficult by the long orbital period of the system and the limits imposed on TeV gamma ray observations by the lunar cycle. Nevertheless, the encouraging results gained in 1991 February suggest that such a search may well be worthwhile.

8.1. TeV Gamma Ray Observations of SMC X-1

8.1.1. SMC X-1 : A High Mass X-ray Binary

8.1.1.1. Early X-ray Results

The X-ray source SMC X-1 was discovered by Price et al. (1971) and its binary nature revealed by UHURU observations (Schreier et al., 1972b) in which an orbital period of 3.89 days was detected. The optical counterpart was identified as Sanduleak 160, a BOIb supergiant in the Small Magellanic Cloud (Webster et al., 1972). Optical and X-ray studies show this star to have a mass of $\approx$17 M_o and a radius $\approx$16 R_o, and to be underluminous for its spectral type (Rappaport and Joss, 1983). Like Krzeminski's star in Centaurus X-3 this feature is believed to be a direct result of mass transfer from the primary star in an accreting binary.

The duration of the X-ray eclipse was found to be a stable 0.6 days (e.g. Davison, 1977) corresponding to an eclipse lasting from orbital phase 0.93-0.07. SMC X-1 is one of the brightest stellar X-ray sources known, with an average luminosity in the range 1-35 keV of $\approx 6 \times 10^{38}$ erg s^{-1} for an assumed distance of 65 kpc (Lucke et al., 1976). However, the short-term luminosity may vary between 10^{37} and 10^{39} erg s^{-1}. This large flux of X-rays is incompatible with a model powered by stellar wind accretion, and the high required rate of mass accretion onto the neutron star may only be explained by Roche lobe overflow.

8.1.1.2. Pulsar Identification and Spin-up Measurements

The important discovery of the pulsar in SMC X-1 resulted from a pair of X-ray observations carried out in 1973 and 1975 (Lucke et al., 1976). Fourier analysis of data recorded in the energy range 0.18-10 keV revealed significant pulsed power at 0.72 and 0.36 s. These were found to be the fundamental and first harmonic of a 0.717 s period, the light curve showing two distinct broad peaks with the interpulse strengthening towards higher energies. The total

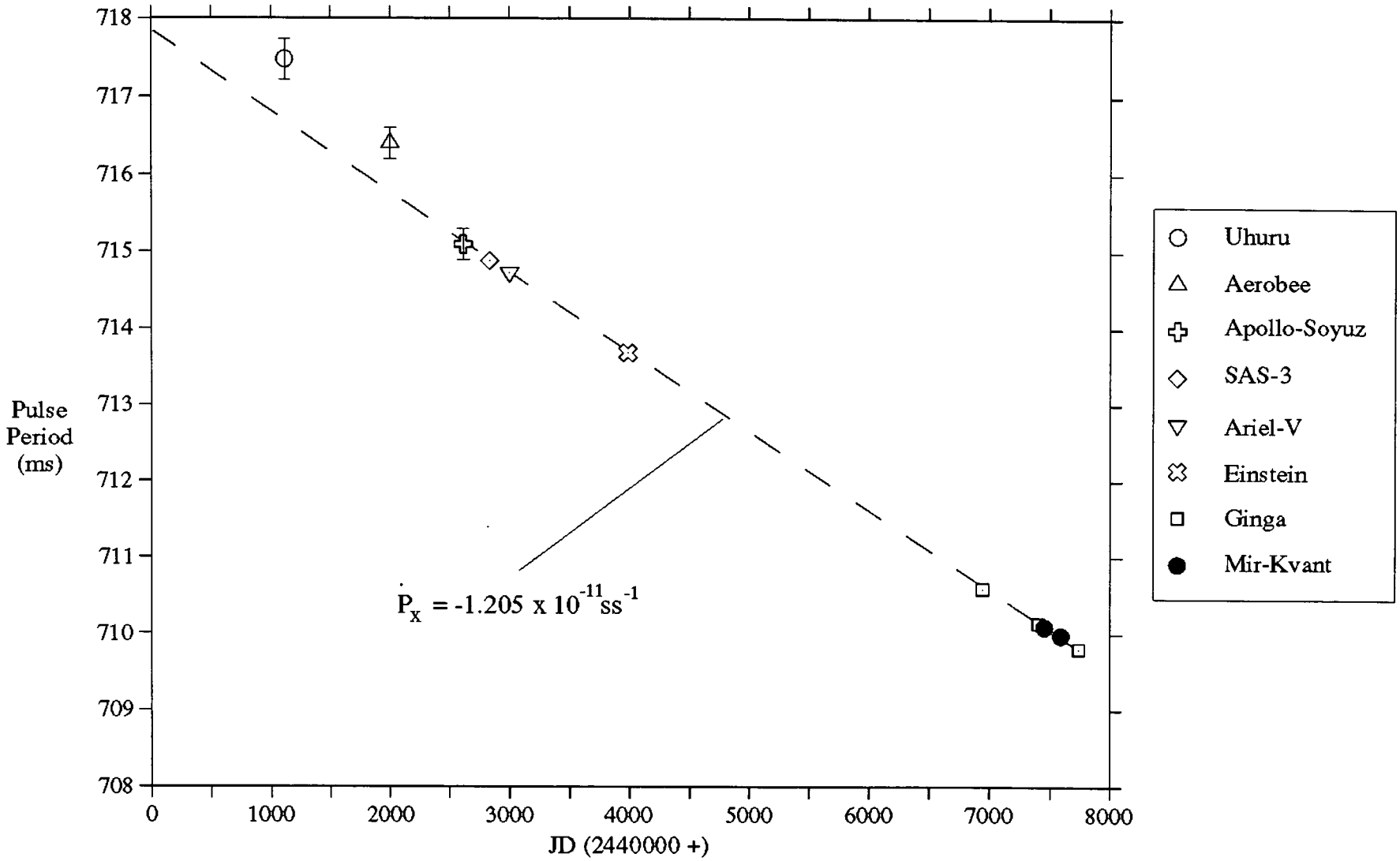

Figure 8.1 : The period history of the X-ray pulsar in SMC X-1. (Refs. in Nagase, 1989; Gilfanov et al., 1989; Levine et al.,1993)

pulsed fraction was found to vary between 30% and 40% (e.g. Davison, 1977; Henry and Schreier, 1977).

The secular spin-up rate of the 0.71 s pulsar has been remarkably uniform since its discovery, as shown in Figure 8.1. Whilst some scatter is seen in the early measurements with larger errors, by only using the set of values since the period determination by SAS-3 (Primini, Rappaport and Joss, 1977) a well-behaved period derivative may be calculated. Further accurate measurements by the GINGA satellite have recently been reported which allow a yet more precise determination to be made (Levine et al., 1993). The lack of any observed spin-down intervals suggests an almost complete absence of braking torque on the neutron star and that a random accretion process from an early-type stellar wind cannot be operating.

8.1.1.3. Flux Variability

Like Hercules X-1 and Centaurus X-3, the X-ray flux from SMC X-1 is frequently found to vary over timescales of hours or days. Extended low states lasting several orbital cycles have been noted by a number of observers (e.g. Tuohy and Rapley, 1975; Bonnet-Bidaud and van der Klis, 1981). The evidence for the presence of absorbing material during these intervals is provided by the much slower transitions to and from the eclipse state. Varying absorbing column densities were noted by Davison (1977) typical of the behaviour of massive X-ray binaries. In addition to these low states, brief X-ray flares have also been observed. EXOSAT observations reported by Angelini (1989) demonstrated the existence of a series of quasi-periodic oscillations at a typical frequency of $\approx$0.01 Hz, most strongly manifested in the form of a 100% increase in emission lasting only 80 seconds. No evidence was found in the EXOSAT data for any periodic long-term variability on timescales of 16-60 days of the type tentatively identified by Gruber and Rothschild (1984).

8.1.1.4. Modes of Accretion in SMC X-1

The presence of an accretion disc in SMC X-1 has been inferred from a

number of observations. The steady spin-up rate and very high luminosity both suggest that a large reservoir of steadily accreting material must be available. The orbital separation, component masses and primary stellar radius are all compatible with the dominant mode of accretion being Roche lobe overflow. As outlined by Bonnet-Bidaud and van der Klis (1981) the most likely picture of SMC X-1 is one where the majority of the mass transfer and X-ray absorption is due to this mode of accretion. Some of the secondary phase-dependent absorption probably arises from the stellar wind from Sk 160 whose outer layers may only just extend beyond the Roche lobe (Levine et al., 1993).

Direct evidence has also been provided by a number of optical observations and light-curve models. Van Paradijs and Zuiderwijk (1977) showed that the optical minimum at X-ray eclipse was much deeper than expected implying the existence of a large, bright light source surrounding the neutron star. A strong dip was also seen at orbital phase 0.6 possibly arising from the accretion stream. The appearance of the maximum near 0.75 was found to be noticeably irregular due to increased absorption by accreting material trailing the neutron star. Later modelling by Tjemkes, Zuiderwijk and van Paradijs (1986) supported these conclusions, producing a light curve in good agreement with the observations and based on an accretion disc of radius $\approx$12 ls and temperature 3 x 10^4 K.

Until recently, Cen X-3 was the only high-mass X-ray binary known to show a decay in its orbital period (see Chapter 6). Early observations gave weak evidence for a similar effect in SMC X-1 (Davison, 1977), but this was not confirmed until recent work by Levine et al. (1993). This phenomemenon was interpreted as arising from tidal interactions in the system with the evolutionary expansion of Sk 160 maintaining the asynchronism between its rotation rate and the orbital period. In addition to increasing its moment of inertia and thus decreasing its rotation rate, this expansion also drives the overflow from Sk 160 through the inner Lagrangian point as the Roche lobe descends into its atmosphere.

8.1.2. Previous TeV Observations

8.1.2.1. Early Work by the Durham Group

The Durham group's observations of SMC X-1 at TeV energies were first reported by Brazier et al. (1990d). This analysis was based on data recorded with the Mk.3 telescope between 1986 and 1988 and concentrated initially on the 1987 July dataset, for which a contemporaneous X-ray period was available (Takeshima, 1987). After a weak signal was found at the correct period when the full dataset was combined incoherently. An orbital shift of 2 ls and 0.02 in phase was found sufficient to give a corrected chance probability of 3 x 10^{-5} for the detection of a signal at the correct period. A similar effect was also found when the dataset was combined maintaining relative phase information, giving a signal strength of 2.2% of the cosmic ray background. This signal was found to be most significant at the nodes of the orbit (phases 0.25 and 0.75). The same optimised orbital parameters were found to give significant evidence for periodic emission in two datasets from other dark moon intervals. Combining the results from all 8 datasets gave an overall Rayleigh probability of 10^{-4} for the signal at the X-ray period occurring by chance after all degrees of freedom were allowed for.

8.1.2.2. Orbital Searching in the Durham Database

A more detailed assessment of the 1986-1989 Durham database was presented by Mannings (1990). The work on SMC X-1 was based upon 94 observing nights using the Mk.3 telescope from 1986 October to 1989 December totalling 315.6 hrs of observation. The selection procedure employed to improve the ratio of events arising from gamma-rays to those caused by cosmic protons was a restriction to those triggering the centre channel only plus the application of a relative response threshold (see Chapter 3). Based on these criteria, a total of almost 330 000 events were accepted.

The method for sampling over a range of values of semi-major axis and epoch of mid-eclipse in testing for periodicity, as described in Chapter 4,

was originally developed specifically for the study of SMC X-1. All of the 1986-1989 data were subjected to a detailed uniform analysis.

The results showed that only two of the eleven sequences, 1987 July and 1989 September-October, showed evidence of pulsed emission, with raw chance probabilities being 5.0×10^{-6} and 5.4×10^{-5} respectively. In each case, the minimum probability occurred near to the assumed position of the neutron star. No such signals were detected in the off-source channels for those months. After allowing for the fact that 11 sequences had been analysed and as a result of a series of simulations, the probability of chance occurrence increased to ≈10%. Similarly, a corrected chance probability of ≈5% was derived for the 1989 September-October data.

All of the 20 individual observations comprising these two datasets were tested independently to search for gamma ray emission on shorter timescales. Three were found to show significant evidence for a periodic signal; 1987 July 23, 1987 July 29, and 1989 October 2. Their midpoint phases were 0.72, 0.25 and 0.71 respectively, i.e. all near the ascending or descending node. Tests were carried out to discover whether the apparent emission was produced in bursts on timescales of 5-10 minutes, as seen at TeV energies from the X-ray binaries Cygnus X-3, Vela X-1 and Hercules X-1. The results showed that the signal in each observation was uniform in strength.

However, after allowing for the many degrees of freedom used in sampling over trial periods and orbital parameters, the significance of the detected signals were reduced to the level of a chance origin (≈5-10% probability of chance occurrence). Therefore, this rigorous study could only yield an upper limit on the time-averaged flux of TeV gamma-rays from SMC X-1 of 1.5×10^{37} ergs s^{-1} above 400 GeV, somewhat larger than the limits quoted for similar galactic sources due to its much greater distance. Nevertheless it was still felt that tentative evidence had been gained for TeV gamma ray emission from this binary.

8.1.3. Further Studies

8.1.3.1. A Search for Orbital Phase Dependence

The most promising result of the work outlined in Section 8.1.2 was the possibility that emission was confined to the region of the ascending and descending nodes. If confirmed, this could allow a targeted observing programme to rapidly improve the significance of a pulsed signal detection. Therefore, the main thrust of the present work was to search for orbital phase dependence in any TeV gamma ray emission detected from SMC X-1. As part of this study, the results of the observations made in 1990, 1991 and 1992 are included here for the first time. The analysis was basically similar to the previous work, and is described in detail later, but some modifications in the data selection were implemented.

8.1.3.2. Selection of Data

The weather records and count-rate histories for each observation were examined in order to choose a database of consistent quality. In those cases where the run was interrupted due to cloud or demisting of the telescope, an extracted dataset was used. Of the 1986-1989 database, one dataset used in the previous work was rejected, whilst several others which had not been used before, although of acceptable quality, were added. The final total was 132 observations, with an average duration of 3.2 hours. A catalogue of these observations is given in Table 8.1.

The event selection used in the present analysis differed from that used in the previous work in two ways. As before, only events triggering the on-source channel alone were selected. However, recent analyses of data recorded on several objects have suggested that the favoured relative response threshold level for an object viewed 45-50° from the zenith at Narrabri is 45% (Brazier, 1991). This was the level chosen for use here, though some investigation of the effect of different levels of the relative response threshold was also carried out. In addition improvements in the technique of applying pedestal corrections to each recording channel prior to the data

TABLE 8.1 - Catalogue of observations of SMC X-1

(Mk.3 telescope used unless otherwise stated)

Observation Date	Duration (hours)	Events Selected	Orbital Phase at Midpoint	Notes
24 10 86	2.0	2969	0.79	
25 10 86	2.8	3407	0.04	
26 10 86	3.4	4073	0.29	
27 10 86	3.9	3281	0.55	
28 10 86	1.6	2300	0.81	
30 10 86	2.1	2685	0.33	
01 11 86	3.5	8544	0.83	
02 11 86	1.7	6205	0.08	
03 11 86	3.3	7573	0.34	
04 11 86	2.4	4636	0.61	
21 07 87	2.9	1664	0.21	
22 07 87	3.5	1485	0.46	
23 07 87	4.3	4490	0.72	
24 07 87	4.1	4022	0.97	
25 07 87	3.3	1004	0.22	
26 07 87	1.5	1340	0.49	
28 07 87	2.8	2386	0.00	
29 07 87	4.3	1503	0.25	
31 07 87	4.9	4405	0.77	
20 08 87	2.9	2252	0.89	
21 08 87	2.8	2805	0.15	
22 08 87	2.9	2881	0.41	
23 08 87	2.7	3138	0.66	
24 08 87	3.2	2629	0.92	
25 08 87	3.2	3329	0.18	
26 08 87	3.3	3648	0.43	
28 08 87	3.3	2721	0.95	
14 09 87	2.3	1750	0.30	
15 09 87	3.3	3657	0.55	
16 09 87	3.3	3072	0.81	
17 09 87	2.2	1183	0.07	
18 09 87	3.7	3639	0.32	
19 09 87	3.8	2652	0.58	
20 09 87	3.7	1147	0.84	
21 09 87	3.8	2747	0.09	
22 09 87	3.8	2883	0.35	
23 09 87	2.8	2073	0.61	
24 09 87	3.3	1386	0.87	
25 09 87	3.2	2131	0.12	
26 09 87	2.0	1346	0.40	
27 09 87	4.3	2545	0.63	

TABLE 8.1 (continued)

Observation Date	Duration (hours)	Events Selected	Orbital Phase at Midpoint	Notes
10 10 87	1.7	1303	0.94	
11 10 87	2.9	1607	0.21	
12 10 87	4.0	1884	0.47	
14 10 87	4.3	3017	0.98	
16 10 87	5.2	3749	0.53	
17 10 87	4.0	3602	0.76	
18 10 87	4.0	3460	0.01	
19 10 87	4.3	2329	0.29	
20 10 87	5.7	6865	0.54	
22 10 87	2.9	3516	0.03	
23 10 87	3.9	3381	0.30	
24 10 87	3.8	2009	0.56	
25 10 87	2.1	2874	0.81	
13 11 87	1.9	1626	0.69	
17 11 87	3.1	1354	0.72	
18 11 87	3.1	3079	0.98	
19 11 87	3.1	3375	0.23	
20 11 87	2.2	1770	0.50	
14 07 88	3.3	4809	0.44	
16 07 88	3.4	4413	0.96	
17 07 88	3.4	5083	0.21	
18 07 88	3.4	5379	0.46	
20 07 88	3.3	1119	0.98	
04 09 88	3.8	1140	0.78	
07 09 88	4.0	4062	0.53	
09 09 88	4.5	4756	0.04	
10 09 88	6.4	7797	0.31	
12 09 88	6.0	5616	0.83	
13 09 88	5.2	11918	0.07	
14 09 88	4.8	8044	0.33	
16 09 88	5.2	5748	0.86	
01 10 88	2.6	2928	0.68	
02 10 88	2.7	4170	0.96	
22 09 89	5.3	6811	0.15	
23 09 89	3.8	4018	0.41	
24 09 89	2.4	3114	0.66	
26 09 89	2.6	2705	0.17	
28 09 89	4.2	6339	0.69	
29 09 89	4.0	6423	0.95	
30 09 89	5.1	2117	0.20	
01 10 89	4.7	6943	0.46	
02 10 89	5.6	7907	0.71	
03 10 89	4.3	5320	0.97	
04 10 89	2.3	2783	0.24	

TABLE 8.1 (continued)

Observation Date	Duration (hours)	Events Selected	Orbital Phase at Midpoint	Notes
20 10 89	1.0	1404	0.35	
22 10 89	5.8	2870	0.85	
23 10 89	2.3	1754	0.09	
25 10 89	3.8	3939	0.61	
29 10 89	2.8	2923	0.66	
30 10 89	2.8	2273	0.92	
02 11 89	1.7	1163	0.68	
18 11 89	3.3	3963	0.78	
19 11 89	4.1	5476	0.04	
23 11 89	3.3	3772	0.06	
25 11 89	3.4	2771	0.58	
29 11 89	3.0	3003	0.61	
01 12 89	1.8	2267	0.12	
14 09 90	3.0	4127	0.91	Mk.4 only
15 09 90	2.8	3498	0.17	Mk.4 only
16 09 90	3.7	4178	0.42	Mk.4 only
17 09 90	3.4	5693	0.68	Mk.3/Mk.4
18 09 90	2.7	4122	0.93	Mk.3/Mk.4
19 09 90	2.5	3071	0.19	Mk.3/Mk.4
20 09 90	2.5	3031	0.44	Mk.3/Mk.4
10 10 90	1.8	1828	0.56	Mk.4 only
11 10 90	2.7	4627	0.82	Mk.3/Mk.4
12 10 90	3.3	5970	0.08	Mk.3/Mk.4
13 10 90	3.9	6294	0.34	Mk.3/Mk.4
16 10 90	2.8	3981	0.10	Mk.3/Mk.4
17 10 90	1.4	1221	0.35	Mk.3/Mk.4
18 10 90	3.6	4402	0.61	Mk.3/Mk.4
20 10 90	1.3	2988	0.13	Mk.3/Mk.4
22 10 90	2.5	5777	0.64	Mk.3/Mk.4
23 10 90	2.5	5311	0.90	Mk.3/Mk.4
10 11 90	2.5	2240	0.50	Mk.3/Mk.4
12 11 90	4.0	3927	0.02	Mk.4 only
14 11 90	2.0	1655	0.52	Mk.4 only
17 11 90	2.0	2991	0.30	Mk.3/Mk.4
18 11 90	2.0	2828	0.55	Mk.3/Mk.4
10 01 91	2.0	1194	0.17	
18 01 91	1.9	1865	0.23	Mk.3/Mk.4
25 08 92	5.2	1952	0.59	
20 09 92	2.7	2286	0.25	
21 09 92	2.0	1452	0.50	
25 09 92	1.5	1563	0.53	
26 09 92	3.1	3527	0.79	

TABLE 8.1 (continued)

Observation Date	Duration (hours)	Events Selected	Orbital Phase at Midpoint	Notes
16 10 92	2.4	2399	0.90	
23 10 92	2.1	1525	0.69	
25 10 92	3.5	2425	0.23	
26 10 92	2.7	1860	0.49	
27 10 92	1.5	864	0.76	
TOTALS :	425.2	450098		

selection were employed. Significant differences resulted in the number of events selected here compared with the earlier work due mainly to the use of this new selection procedure.

For those observations when SMC X-1 was being monitored by both Mk.3 and 4 telescopes, the datasets from each were combined in the usual manner to avoid duplication of event records. Observations of SMC X-1 were also occasionally made using the Mk.4 telescope alone. The data from this telescope were selected on the basis of a trigger in the on-source channel alone. No relative response threshold selection was employed. In summary then, the total number of events selected in this analysis was 450 098, from 425 hours of on-source observing time.

8.1.3.3. Test Ranges in Period and Orbital Parameters

Each night's data was studied over approximately one sampling interval in period and slightly larger intervals in the orbital parameters $a\sin i$ and mid-eclipse epoch. The period appropriate to each night was predicted, as in the previous work, by extrapolation from six X-ray measurements, from SAS-3 in 1976 to Mir-KVANT in 1989 as given in Table 8.2. A least squares fit to these measurements produced the following formula:

$$P_* = 717.8401 - [1.0408 \times 10^{-3}(JD - 2\ 440\ 000)] \text{ ms} ,$$

so that for any given Julian Date the corresponding X-ray period could be found. This fit corresponded to a long-term period derivative of $-(1.205 \pm 0.009) \times 10^{-11}$ ss^{-1}, or a change of $\approx$0.01 ms in 10 days. The expected X-ray period was then calculated for each observation to 0.01 ms accuracy. Each value was valid for an interval of 10 days. The independent sampling interval for a 710 ms period in a 3.2 hr observation is ±0.044 ms. To allow for the variations in period and duration, a uniform sampling interval of ±0.05 ms was used for the 1986-1989 data. Since the 1990-1992 data were taken ≥18 months after the latest accurate X-ray measurements then known (Gilfanov et al., 1989), the interval was widened to ±0.10 ms to allow for any unexpected period

TABLE 8.2 - X-ray pulse period measurements for SMC X-1

Epoch (JD 2440000+)	Period (ms)	Reference
2836.6823	714.88585 ± 0.00004	Primini, Rappaport and Joss (1977)
3000.1562	714.7337 ± 0.0012	Davison(1977)
3986.407	713.684 ± 0.032	Darbro et al.(1977)
6942.02676	710.551 ± 0.005	Takeshima (1987)
7452	710.0972 ± 0.0022	Gilfanov et al. (1989)
7591	709.9830 ± 0.0030	

shifts.

The extent of the accretion disc believed to surround the neutron star in SMC X-1 can be represented in the 2-dimensional plane of the orbit by an ellipse with approximate principal axes from 41–66 ls in $a\sin i$ and 0.965–1.035 in phase, as derived from optical observations (Tjemkes, Zuiderwijk and van Paradijs, 1986). The extent of the accretion disc in this plane is shown in Figure 8.2. The orbital ephemeris used to calculate the position of the X-ray source was the same as that used in the previous work by Mannings (1990) and is given in Table 8.3. To allow for TeV gamma-rays to be emitted from any location in the disc, the search ranges in these two parameters were 38-80 ls and 0.95–1.05 respectively. The sampling step sizes used were 2 ls in $a\sin i$ and 0.01 in epoch shift.

8.1.3.4. Initial Results

A series of contour plots were formed which showed the chance probability of uniformity of phase in the appropriate trial pulse period interval as corrected for each assumed position of origin in the SMC X-1 system. For each resultant plot, the minimum chance probability at any orbital position over the range tested was identified and the relation of these minimum probabilities to the midpoint orbital phase of the observation is shown in Figure 8.3. At first inspection, no clear orbital phase dependence can be discerned. A tendency may be noted for the most significant results to occur in the half of the orbit after phase 0.5. A total of 66 observations (i.e. 50%) were made in each half, but for datasets showing a signal with an uncorrected chance probability lower than 10^{-3}, 2 were recorded before phase 0.5 and 8 later. The probability of this imbalance occurring by chance is 4%.

8.1.3.5. Calculation of Number of Trials

The probabilities given are uncorrected for the degrees of freedom used in the analysis. A number of factors must be taken into account to calculate the true significance of each raw chance probability. The first consideration is the total number of datasets used, 132. The lower dotted line in Figure 8.3

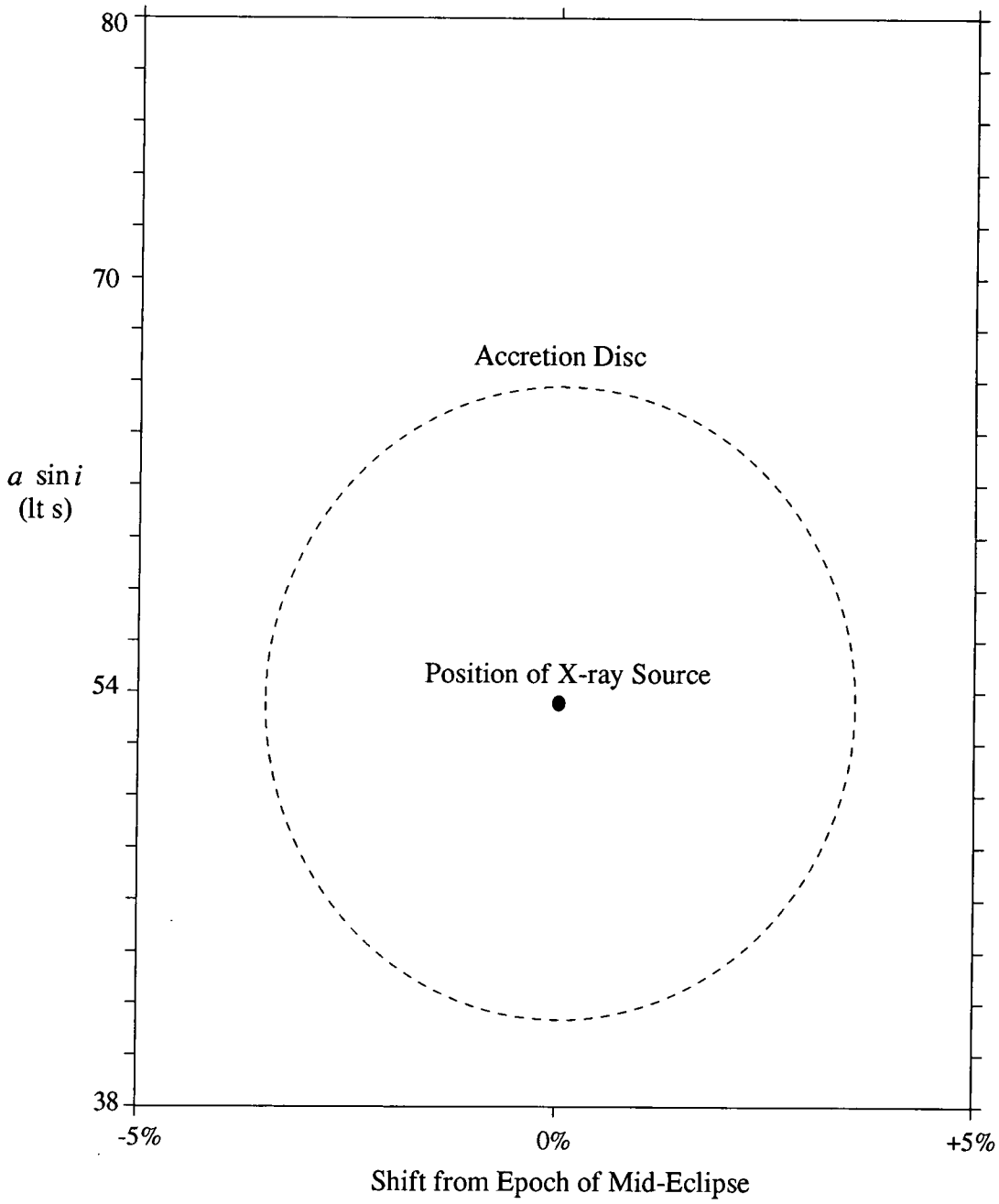

Figure 8.2 : An illustration of the extent of the accretion disc around the neutron star in the plane used for orbital searching in SMC X-1.

TABLE 8.3 - Orbital ephemeris for SMC X-1

Epoch of X-ray Mid-eclipse	:	JD 2447534.59 ± 0.01
Orbital Period	:	3.89212 ± 0.00010 d
$a \sin i$	:	53.46 ± 0.05 ls
Eccentricity	:	0 (< 0.0007)
$\dot{P}_{orb}$	:	0

(from Mannings, 1990, and references therein)

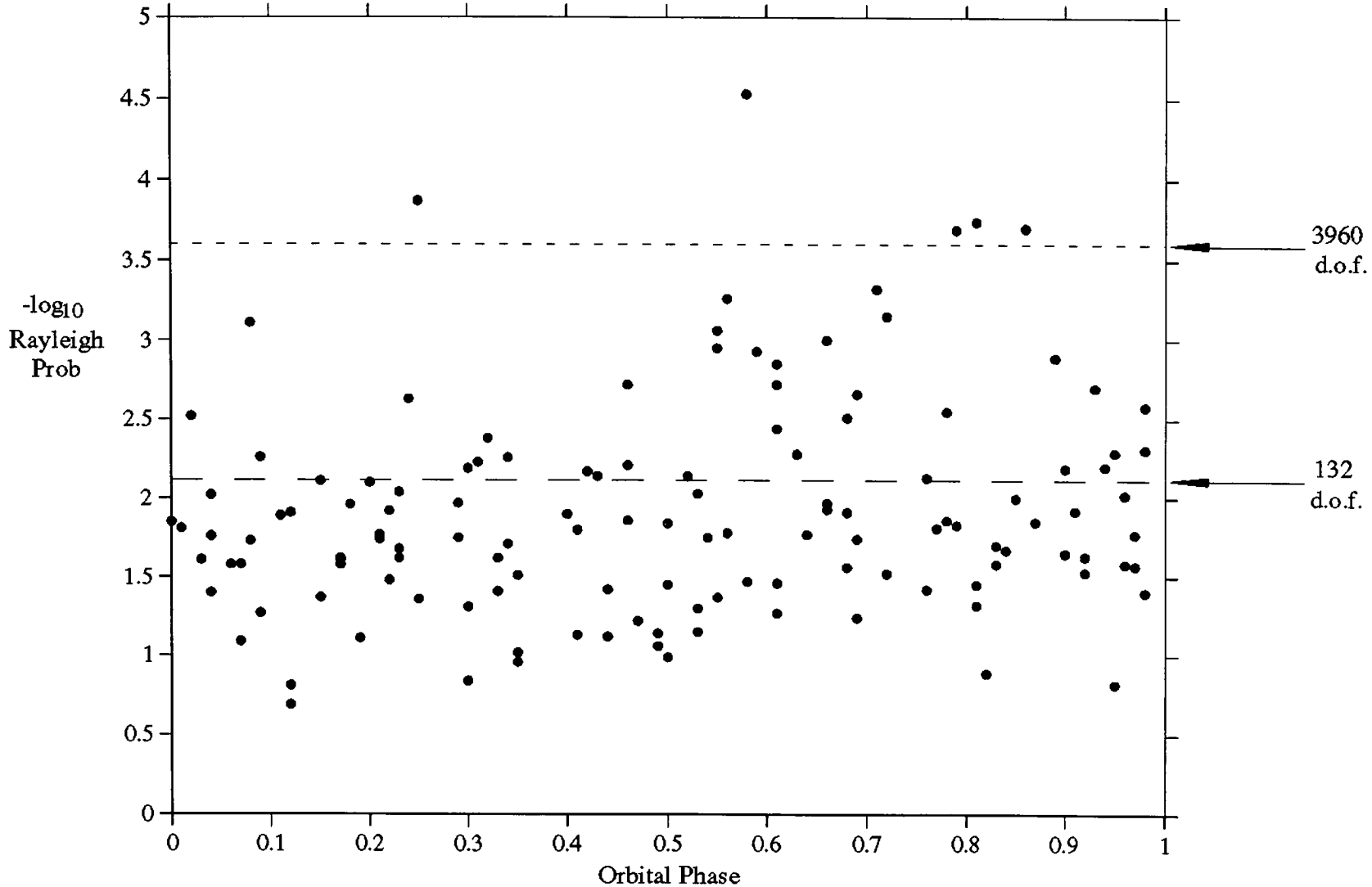

Figure 8.3 : Smallest chance probabilities of uniformity of phase at the X-ray period using the optimised orbital parameters in each of the 132 observations of SMC X-1 by the Durham group. The dashed lines show levels of chance probability of unity after allowance for degrees of freedom, as explained in the text.

corresponds to the expectation threshold below which all of the observed probabilities are consistent with a chance occurrence on this basis alone. A further factor of 3 must also be included for oversampling within the trial period range used for the Rayleigh test for uniformity of phase. However, further penalties were imposed by the use of a number of independent sampling intervals in the orbital parameters.

The method of searching over a range of values of semi-major axis and eclipse epoch was described in Chapter 4, along with an estimation of the size of independent sampling intervals in each parameter for an assumed 5-hour observation. However, the average duration of the datasets analysed here was only 3.2 hours necessitating a correction to these sampling intervals. For SMC X-1, the sampling interval in $a\sin i$ maximised at 5% at the nodes of the orbit. This interval is inversely proportional to $(\sin\theta_i - \sin\theta_f)$ where θ_i and θ_f are the angles measured from the ascending node of the initial and final orbital phase. For small angles, the difference between these sines will be directly related to the length of the observation, and therefore for a 3.2 hour dataset the sampling interval in $a\sin i$ increases to 8%. This corresponds to an average of 5 ls over the range tested, 38 - 80 ls, and hence 8 independent sampling intervals. For adjustments in eclipse epoch, the size of the sampling interval minimises at conjunction at a value of 0.6% for a 5 hour observation. The adjustment for a 3.2 hour observation is similar to that discussed for $a\sin i$ and results in a value of 1%, thus giving a total of 10 independent sampling intervals for the range used of ±0.05 in phase.

The discussion above was based on the minimisation of the sampling interval in the parameter $a\sin i$ or eclipse epoch at the nodes or at conjunction respectively. At any phase in between, the total number of intervals sampled will be the product of the number tested in $a\sin i$ and eclipse epoch independently. There is essentially no sensitivity to $a\sin i$ at conjunction and the sampling interval in eclipse epoch increases by a factor

of ≈10 at the nodes and so only one sampling interval need be allowed for. The orbital phase dependences of the size of the sampling intervals in these two parameters are 90° out of phase and both decrease sharply near their respective minima (see Chapter 4). The numbers of independent intervals tested over a constant range peak sharply in a similar fashion. As a conservative estimate averaged over the orbit, the total number of independent sampling intervals is taken as 10, i.e. the number at conjunction where the interval in eclipse epoch is smallest.

8.1.3.6. Assessment of True Significance of Results

The total number of degrees of freedom used in optimising the orbital parameters when testing for periodicity is ≈3 x 10 (30) in this treatment. Combined with the analysis of 132 separate datasets, this gives a total of 3920 degrees of freedom. The upper dotted line in Figure 8.3 shows the expectation value corresponding to this number of degrees of freedom. Only 5 observations were found to show any evidence for periodicity at a level of probability not consistent with expectation. A list of these observations is given in Table 8.4 and the probability contour diagrams are shown in Figures 8.4a-e. One of the datasets was recorded at the descending node of the orbit whilst the other four fell between phases 0.58 and 0.86, the wide region of the orbit surrounding the ascending node where temporary X-ray absorption features are often seen and thus a promising site for TeV gamma ray production via neutral pion decay.

The 5 observations were also used to produce illustrations of the variation of the chance probability contours across the full range of the orbit by using the technique of applying the Rayleigh test at a single trial period. The results are shown in Figures 8.5a,b. The small size of the independent sampling intervals in the orbital parameters is clear when compared with the similar work carried out on Centaurus X-3 in Chapter 6. It can also be seen that the favoured positions for a TeV gamma ray production site are substantially displaced from the neutron star position indicated in

TABLE 8.4 - Observations showing a weak periodic signal

Date	Phase	-log(P)	% Signal	$a \sin i$	Epoch Shift
29 07 87	0.25	3.87	7.7	55-60	0.0 - +0.05
25 11 89	0.58	4.53	6.1	69-80	-0.04
26 09 92	0.79	3.69	4.9	40-55	-0.02 - +0.05
16 09 87	0.81	3.74	5.3	75-80	-0.05 - -0.02
16 09 88	0.86	3.70	3.8	65-70	-0.04 - 0.03

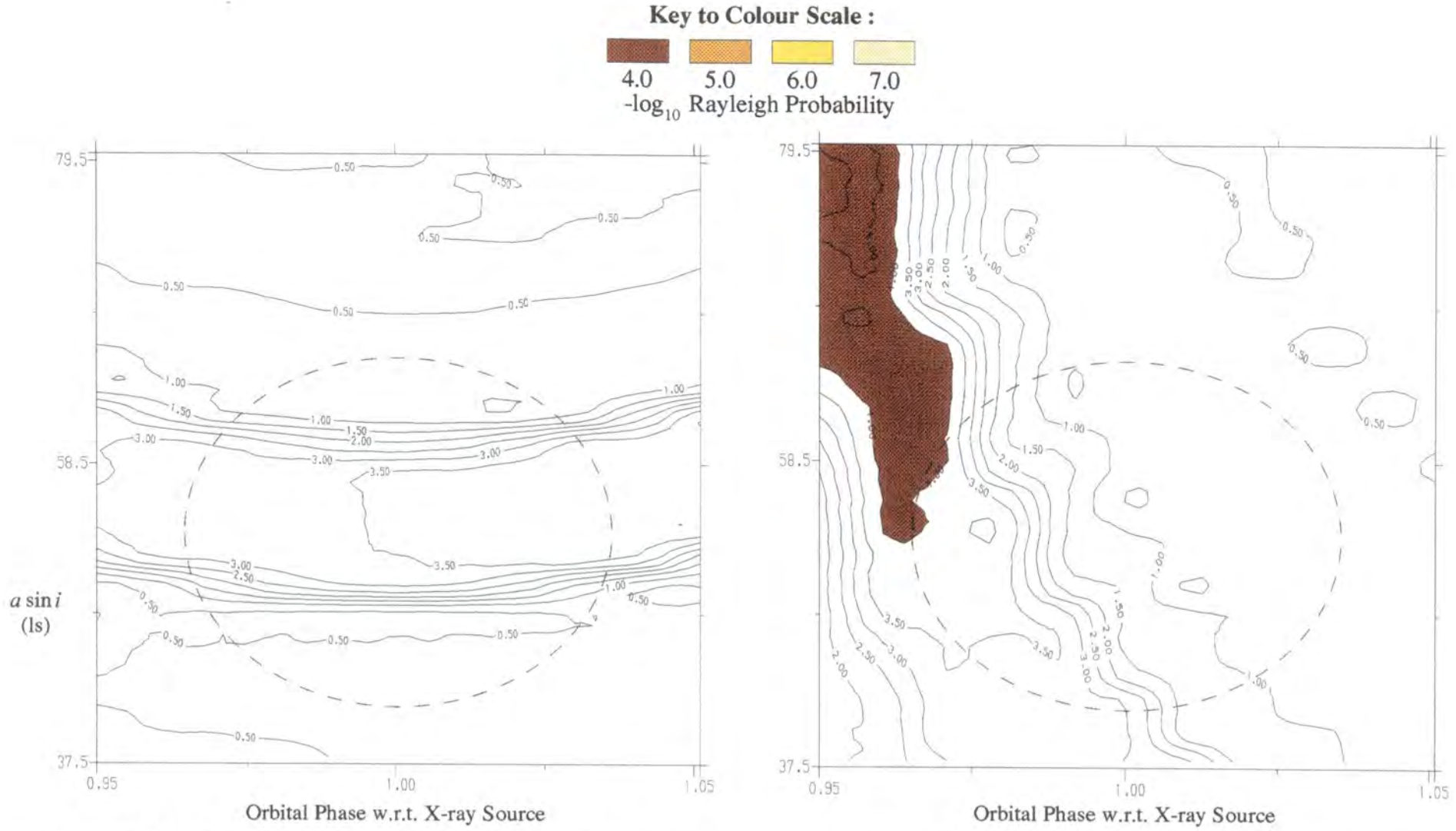

Figure 8.4a : Results of the orbital searching technique applied to the Mk.3 telescope observation of SMC X-1 on 1987 July 29 (orbital phase 0.25).

Figure 8.4b : Results of the orbital searching technique applied to the Mk.3 telescope observation of SMC X-1 on 1989 November 25 (orbital phase 0.56).

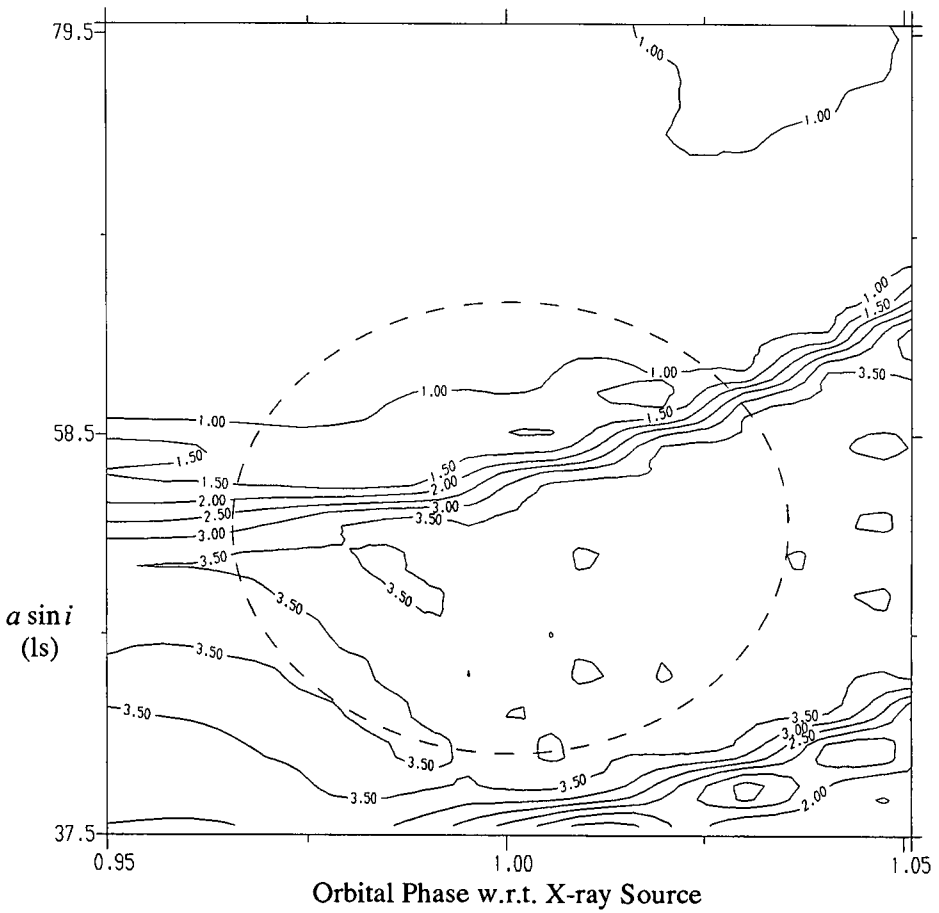

Figure 8.4c : Results of the orbital searching technique applied to the Mk.3 telescope observation of SMC X-1 on 1992 September 26 (orbital phase 0.79).

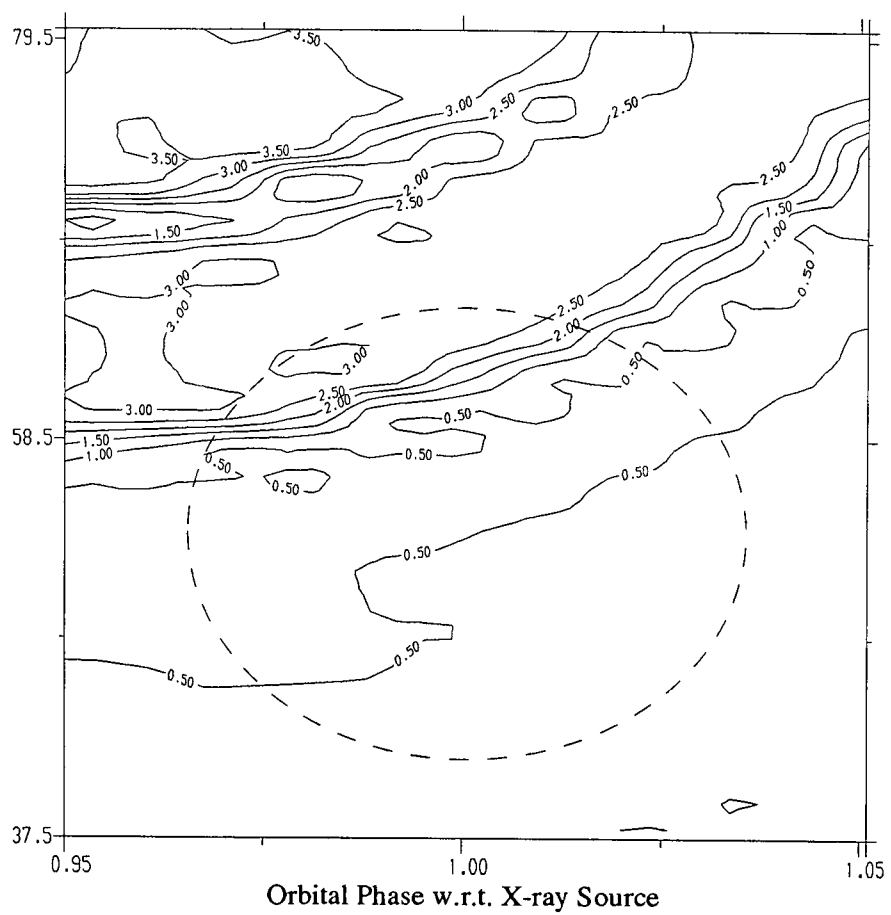

Figure 8.4d : Results of the orbital searching technique applied to the Mk.3 telescope observation of SMC X-1 on 1987 September 16 (orbital phase 0.81).

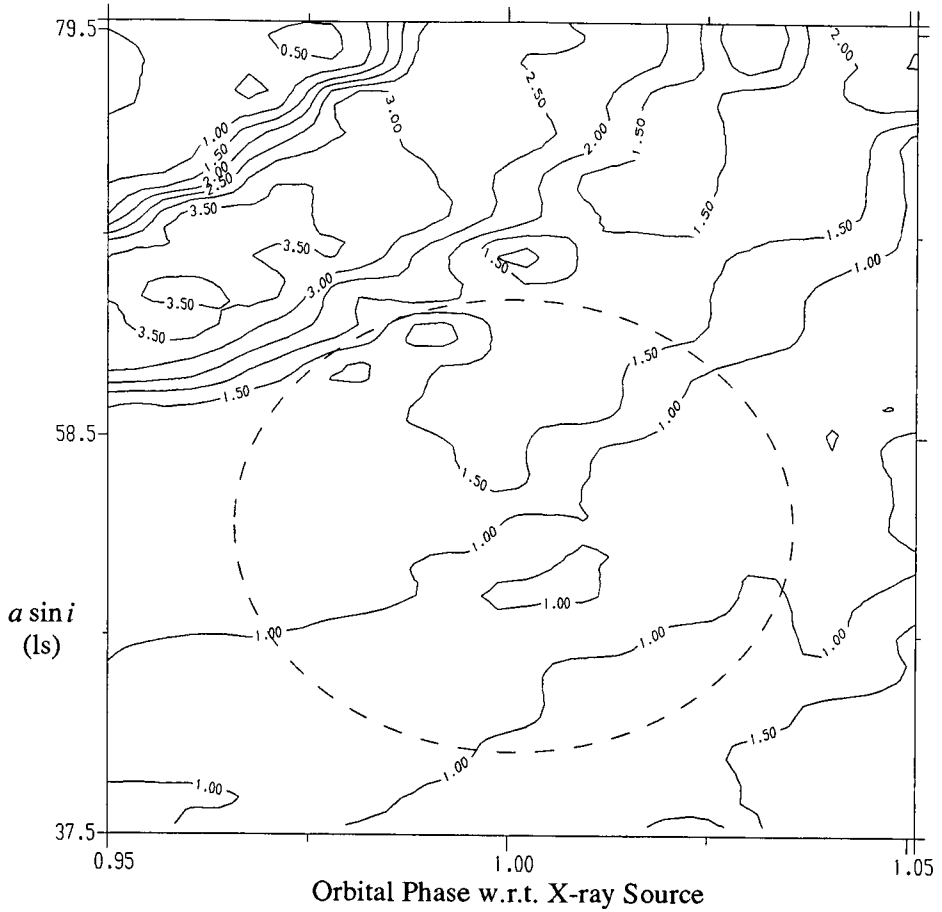

Figure 8.4e : Results of the orbital searching technique applied to the Mk.3 telescope observation of SMC X-1 on 1988 September 16 (orbital phase 0.86).

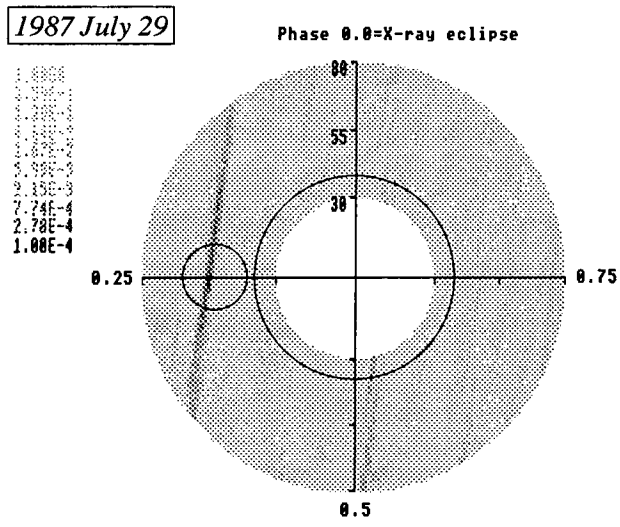

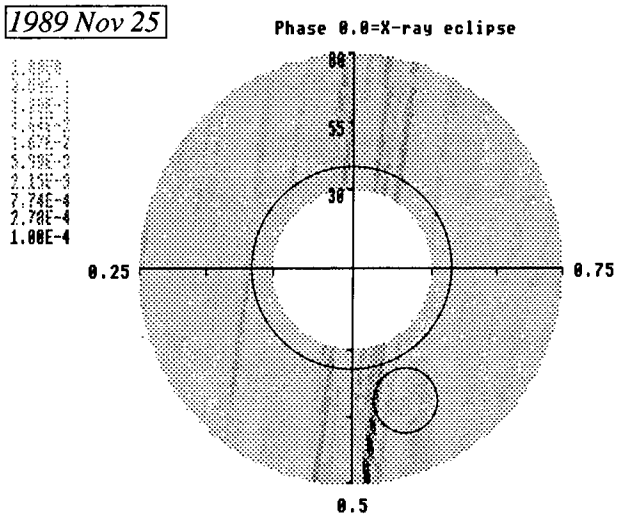

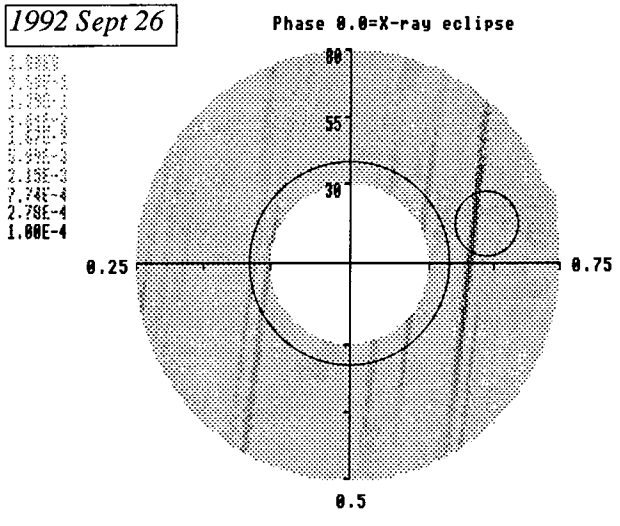

Figure 8.5a : Orbital searching applied to the SMC X-1 data from the three observations analysed in Figs. 8.4a-c.

The grey scale on the left shows the threshold chance probability in each interval. The crosshair axes show the value of $a\sin i$ in lt s.

The size of the primary star is indicated by the black circle at the centre of each diagram, and the neutron star's Roche lobe by the smaller black circle placed at the appropriate orbital phase.

1987 Sept 16

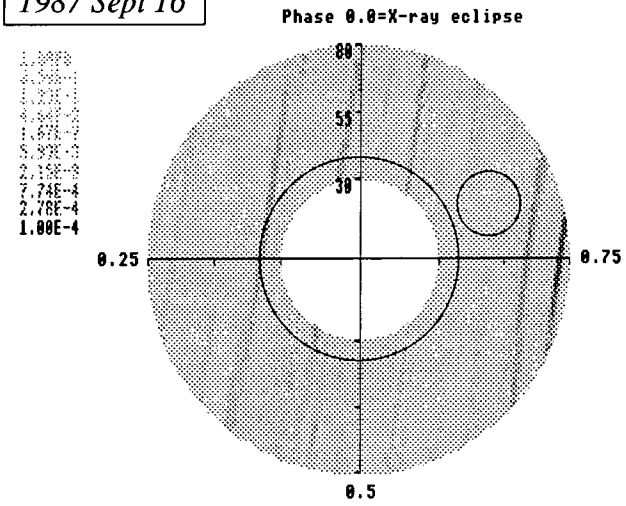

Figure 8.5b : Orbital searching applied to the SMC X-1 data from the three observations analysed in Figs. 8.4d and c.
The grey scale on the left shows the threshold chance probability in each interval. The crosshair axes show the value of $a\sin i$ in lt s.

1988 Sept 16

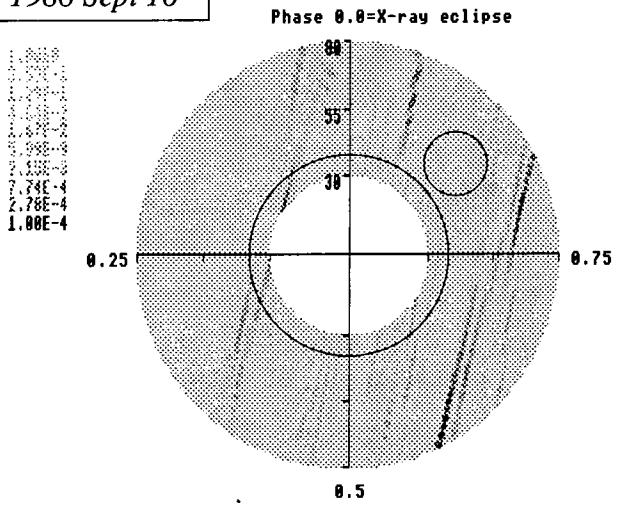

The size of the primary star is indicated by the black circle at the centre of each diagram, and the neutron star's Roche lobe by the smaller black circle placed at the appropriate orbital phase.

each (with the exception of the data from 1987 July 29).

However, even the most significant result from any dataset, that of 1989 November 25, has a corrected probability of ≈ 10% of arising purely by chance. Allowing for the degrees of freedom used in the analysis technique employed here, a 3σ detection of a periodic signal in a single dataset recorded by the Mk.3 telescope alone would require a periodic signal with an uncorrected Rayleigh chance probability of 3×10^{-7}. The average size of dataset for the Narrabri database on SMC X-1 is ≈3400 events, and such a signal in a dataset of this size would constitute 6.6% of the cosmic ray background, corresponding to a photon flux of $\approx 3 \times 10^{-10}$ cm^{-2}s^{-1} above an energy threshold of 300 GeV. No such signal was seen, and assuming a differential cosmic ray spectral index of -2.6 and a distance of 65 kpc this places an 3σ upper limit on the maximum day-to-day source luminosity of $\approx 6 \times 10^{37}$ erg s^{-1} at energies ≥300 GeV. It is worth noting that one of the observations in Table 8.4, that of 1987 July 29, displayed a periodic signal strength of 7.7%, but the small size of the dataset (1500 events) made the detection less significant. A pulsed signal of this strength would have produced a raw probability of chance occurrence of 2×10^{-8} in a dataset twice as large.

8.1.3.7. A New Orbital Ephemeris

The orbital corrections carried out in this work were made with reference to the set of parameters given in Table 8.3. Since the completion of the analysis presented here, this ephemeris has been superseded by one based on a combination of new mid-eclipse determinations by the GINGA satellite and the most precise of the similar measurements made by other experiments (Levine et al., 1993; see Table 8.5). The most important feature of this updated ephemeris is the inclusion of a rate of orbital decay, as discussed in Section 8.1.1.4. This means that the orbital period assumed when making adjustments to the epoch of mid-eclipse shows a steady decrease with time. The effect on $a\sin i$ is less certain. Whilst a full statement of the impact of this new set

TABLE 8.5 - A new orbital ephemeris for SMC X-1

Epoch of X-ray Mid-eclipse	:	JD 2442836.68277 ± 0.00020
Orbital Period	:	3.89229118 ± 0.00000048 d
asini	:	53.4876 ± 0.0004 ls
Eccentricity	:	0 (< 0.0004)
$\dot{P}_{orb}/P_{orb}$	:	$-(3.36 \pm 0.02) \times 10^{-6}$ yr^{-1}

(from Levine et al., 1993)

of parameters on the results reported here is beyond the scope of the present work, some preliminary assessments may be made.

Most importantly, the bulk of the archival X-ray data utilised by Levine et al. were also used in providing the set of parameters assumed here, so that the new ephemeris is far from independent. As an example, a comparison was made for the time of mid-eclipse on 1992 September 26, one of the latest dates of a Durham gamma ray observation and therefore one by which time any cyclic error would have accumulated to a maximum. The difference in calculation of the exact epoch of eclipse passage between the two ephemerides was 0.021 days. This corresponds to only 0.5% in orbital phase. The dataset recorded on this night was subjected to the same analysis technique as detailed in Section 8.1.3 using the new ephemeris and the comparison between this and the original contour diagram used in this work is shown in Figure 8.6. Clearly, the new ephemeris narrows the range from which emission may arise.

A more sensitive test was carried out by combining 8 observations made between 1992 September 21 and October 27 with the retention of pulse phase coherence in order to search for a periodic signal using the two different ephemerides for the correction of the 16000 recorded event times. The ephemeris of Levine et al. was found to reduce the chance probability of a signal at 709.56 ± 0.1 ms by a factor of 10 (to 3.6×10^{-4}) as compared with the result from the ephemeris previously used. No optimisation of orbital parameters was carried out. The signal strength was 2.3% of the cosmic ray background so that if genuine, a persistent pulsed photon flux of $\approx 1 \times 10^{-10}$ $cm^{-2}s^{-1}$ above 300 GeV was detected. This corresponds to a luminosity of $\approx 2 \times 10^{37}$ erg s^{-1} at these energies. The prospect of reanalysis of the Durham database using this updated ephemeris therefore holds much promise.

8.1.4. Discussion

SMC X-1 is a powerful but very distant variable X-ray source. At 65 kpc, it is at least 10 times more remote than most galactic X-ray binaries. Even if it were an order of magnitude more luminous at TeV energies as the strongest

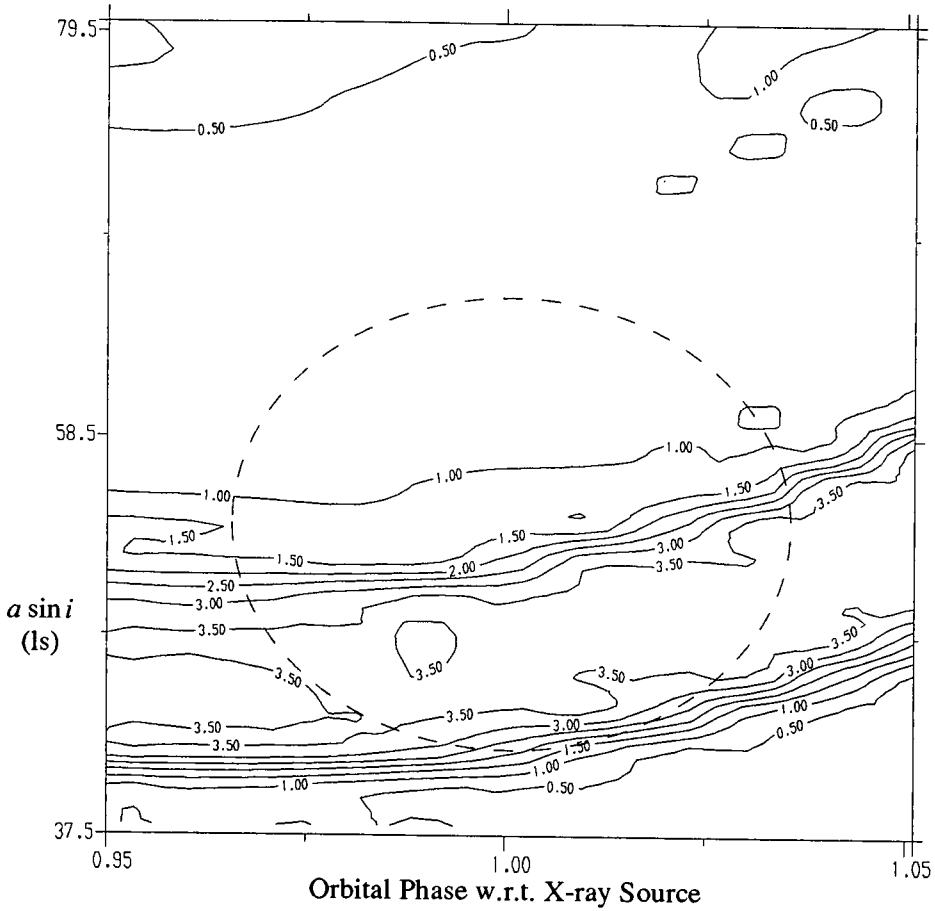

Figure 8.6 : Result of the orbital searching technique as applied to the Mk.3 telescope observation of SMC X-1 on 1992 September 26 utilising the updated ephemeris of Levine et al. (1993). This figure should be compared with Fig. 8.4c which was produced in the same manner for the same dataset using the older ephemeris given in Table 8.3.

of the local source candidates, it would still have an incident flux an order of magnitude lower. Previous analysis of the Durham TeV database could not yield significant results in the light of the the large number of degrees of freedom required. The present work, which was aimed at alleviating the problem by revealing any orbital phase dependence in the signal, has not been able to offer any improvement. Although 4 of the 5 favoured observations of the 132 analysed are at phases considered most suitable for TeV gamma ray emission they do not comprise a sufficiently strong case to make SMC X-1 a priority object for future targeted observing. However, a thorough reanalysis of the existing data using the new orbital ephemeris may allow the improvement of some of the weak signal detections reported here. If these are genuine gamma ray signals from SMC X-1, the sensitivity of this binary to the assumed orbital parameters should ensure that this new ephemeris provides much further information on a displacement of the emission site. More detailed testing for some orbital phase dependence by selecting observations grouped by phase, as was done for Cen X-3 earlier, may also be a worthwhile route.

It would seem that the best hope for gaining proof of TeV gamma ray emission would be to make a limited number of observations during an X-ray high state of the system using either a yet more refined technique of photon/proton discrimination or a telescope with a significantly lower energy threshold. For instance, a detector energy threshold of 75 GeV, as expected to be achieved by the Durham Mk.6 telescope, would allow a photon flux almost an order of magnitude lower than one at the threshold of the Mk.3 telescope to be detected, assuming an integral spectral index of -1.6. This would reduce the high upper limit previously derived for the TeV gamma ray luminosity of SMC X-1 ($\approx 10^{37}$ erg s^{-1}) to a value more in keeping with the luminosities calculated for similar sources in our galaxy. An object as elusive as SMC X-1 is clearly a spur to such advances.

8.2. TeV GAMMA RAY OBSERVATIONS OF 4U1626-67

8.2.1. 4U1626-67 : A Low Mass X-ray Binary

8.2.1.1. The 7.7 s Pulsar

The X-ray source 4U1626-67 was found to contain a 7.68 s pulsar as a result of SAS-3 observations made in 1977 (Rappaport et al., 1977). The pulsar light curve showed a broad single peak with a pulsed fraction of 7%, doubling in strength at higher energies ($\geq$ 12 keV), where a 180° phase shift was also found to occur. The pulsar period has since been monitored by various experiments and originally showed a steady spin-up rate of $\approx -5 \times 10^{-11}$ ss^{-1} (Nagase, 1989). However, a brief spin-down interval was noted by Elsner et al. (1983) and more recent observations by the Compton Observatory indicated that the source entered a spin-down phase in 1991 with an average period derivative of $+5.5 \times 10^{-11}$ ss^{-1} which was found to be stable on a timescale of at least a year (Wilson et al., 1993b). The period history is shown in Figure 8.7.

8.2.1.2. Binary Motion in 4U1626-67

No evidence for binary motion has ever been found from X-ray measurements, allowing limits to be placed on the possible size of any orbit present. The X-ray source can only have a very compact orbit with a projected semi-major axis of $\leq$0.01 ls (Levine et al., 1988; Shinoda et al., 1990). This requires the system to have a small inclination to the line of sight and the neutron star to be the more massive member of the binary pair by a factor of around 10.

The optical counterpart was identified as an 18th magnitude blue star by McClintock et al. (1977). Optical pulsations in phase with the pulsar's X-ray modulation were discovered by Ilovaisky, Motch and Chevalier (1978) and a set of detailed observations by Middleditch et al. (1981) revealed a sideband with about 25% of the strength of the main optical pulse and at a slightly longer period. The main optical pulses were interpreted as arising from X-ray reprocessing in an accretion disc within 0.5 ls of the neutron star. The secondary pulses were proposed to be due to similar reprocessing in the

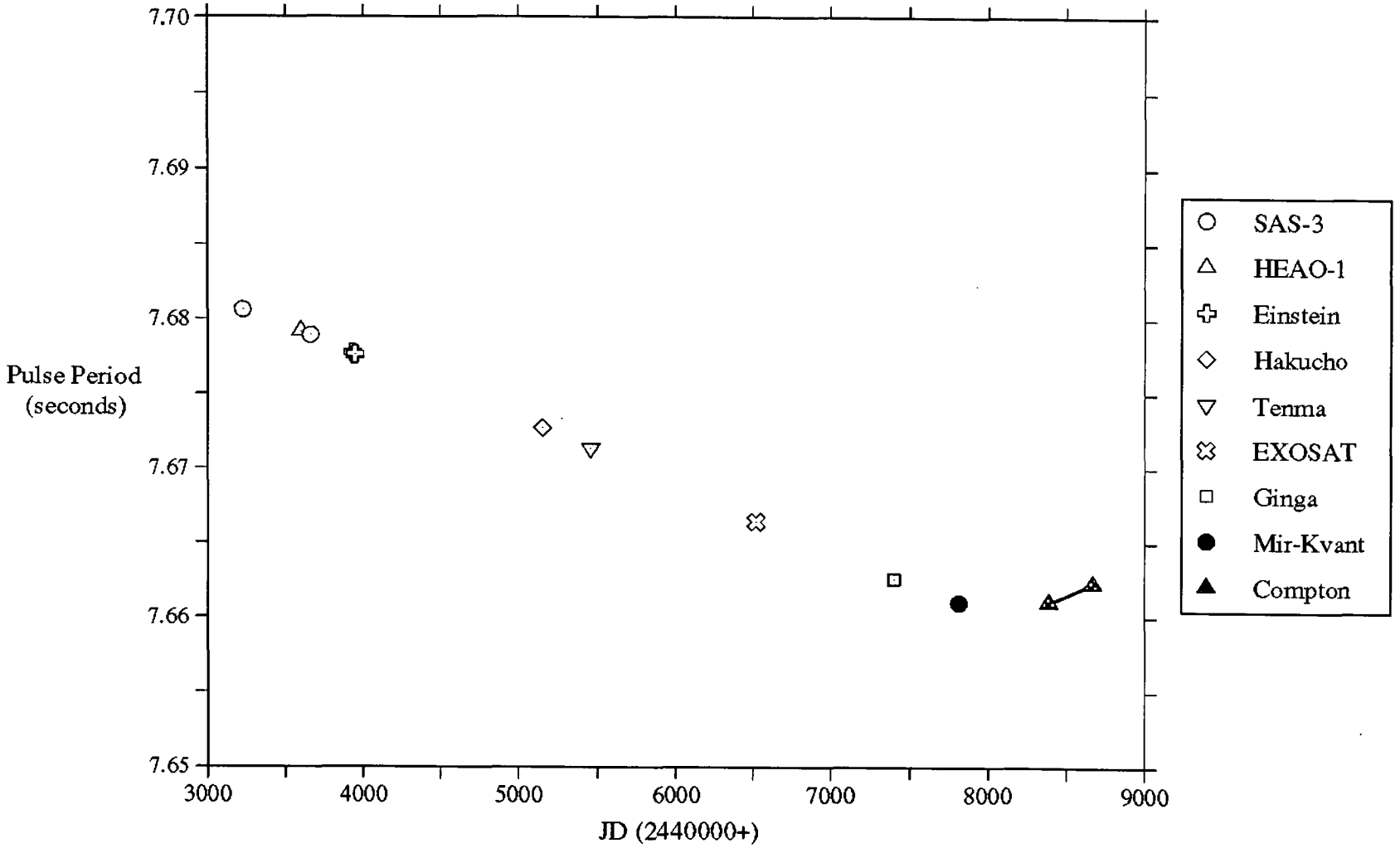

Figure 8.7 : The period history of the X-ray pulsar in 4U1626-67. (Refs. in Nagase, 1989; Gilfanov et al., 1989; Wilson et al., 1993b)

atmosphere of the orbiting non-degenerate companion star thus explaining the Doppler shift in the observed period of the resultant pulsations. The short orbital period required was uncertain but continued optical observations suggested a value near 2485 s. To explain these results the mass of the companion star must be less than 0.1 $M_\odot$, the separation of the two components only ≈1 ls and the value of $a\sin i$ for the companion star ≈0.4 ls. The resulting model of the system is shown schematically in Figure 8.8.

8.2.1.3. Further X-ray Results

The X-ray luminosity is ≈1 x 10^{37} erg s^{-1} for a source distance of 8 kpc (White et al., 1983). Cyclotron resonance features in the X-ray spectrum indicate a surface magnetic field of ≈6 x 10^{12} G (Pravdo et al., 1979). Flaring behaviour on timescales of ≈ 1000 s and Q.P.O.s at a period of ≈25 s have been observed at X-ray energies (Li et al., 1980; Shinoda et al., 1990) and these are believed to be related to phenomena within different regions of the accretion disc around the neutron star. It has been suggested that low mass X-ray binaries of similar nature to 4U1626-67 may oscillate between episodes of high X-ray luminosity, where Roche lobe overflow is driven by a stellar wind self-excited by X-ray reprocessing, and low X-ray luminosity, where mass loss causes the companion to shrink within its Roche lobe until orbital decay drives the components closer (Joss, Avni and Rappaport, 1980). Spin-down episodes may occur in the low luminosity phase due to the reduced accretion rate.

8.2.1.4. Initial TeV Gamma Ray Observations

The first observations of 4U1626-67 at TeV gamma energies were made by the Durham group (Brazier et al., 1990d). A series of datasets were recorded using the Mk.3 telescope between 1987 April and 1989 May giving a total of 110 hours on-source time. Each observation was tested for uniformity of phase at the contemporary X-ray pulsar period, and only one, 1987 June 1st, was found to show evidence for such periodicity. More interestingly, this 9 hour

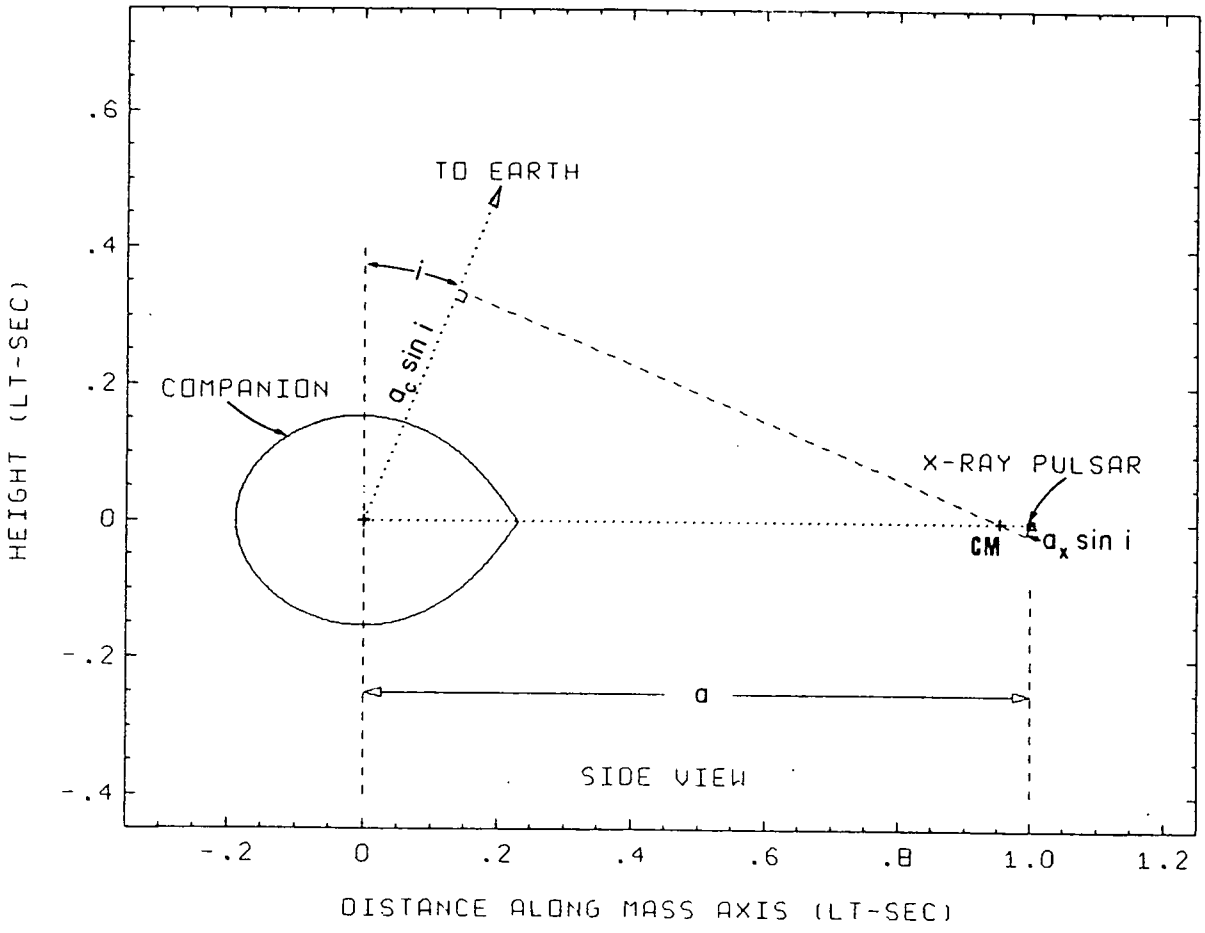

Figure 8.8 : The estimated orbital geometry of the 4U1626-67 binary system. The ratio of the mass of the companion to that of the neutron star is approximately 0.05 and the inclination 22.5°. The projected orbital radii for both stars are shown along with their separation, a.

(from Middleditch et al., 1981)

observation was divided into 621 s segments to test for modulation of the signal with the 2485 s orbital period and a preference for a single quarter of the orbit was noted with a chance probability of $\approx 10^{-5}$.

8.2.2. The 1987 Durham Dataset

8.2.2.1. Analysis of the Full Dataset

The purpose of this part of the present work was to provide a consistent reanalysis of the 1987 data in the hope of improving upon the initial promising results. Between 1987 April and July, the Mk.3 telescope recorded 20 separate datasets on 4U1626-67. The data were first studied to select only those observations made under good observing conditions, and where necessary poor segments of data within a single night were discarded. This resulted in 16 datasets being used for this work. The observations are listed in Table 8.6.

The standard data selection was applied, i.e. accepting only events which triggered the on-source channel alone, and a 45% relative response was applied to the off-source channel responses after correction for pedestal offsets. In total, 80052 events were selected from the 69 hours of observation. Each dataset was tested for periodicity using the Rayleigh test for uniformity of phase over a small range about the predicted X-ray period at this time of 7.6644 ± 0.0004 s. Only one, 1987 June 1 as identified in the original work, revealed any significant periodicity. A signal was found at 7.664 ± 0.003 ms with a chance probability of 4×10^{-5} and a strength of 3.3% of the cosmic ray background. After allowance for degrees of freedom (20 for the number of observations, and a factor of 3 for oversampling in trial period) this chance probability increased to 2.4×10^{-3}. This observation was studied in more detail, as described later.

The datasets within each dark moon interval were combined without use of relative phase information and tested for uniformity of phase at the appropriate period range. No evidence of a periodic signal was found. The data were also combined coherently and tested for uniformity of phase over the

TABLE 8.6 - Catalogue of Mk.3 telescope observations of 4U1626-27

Date	Duration (hours)	Events Selected
23 04 87	3.2	3152
26 04 87	2.4	2884
29 04 87	3.6	4022
03 05 87	4.8	6729
04 05 87	5.2	7346
01 06 87	6.1	9048
22 06 87	7.3	8892
01 07 87	1.6	1812
02 07 87	5.3	4694
03 07 87	3.0	2568
04 07 87	2.6	2599
25 07 87	6.0	7544
26 07 87	5.4	5363
28 07 87	6.3	7003
29 07 87	4.1	4280
31 07 87	2.5	2116
04 05 92	2.5	2481
05 06 92	5.2	5792
06 05 92	4.2	4342
09 05 92	1.6	2137
23 05 92	4.2	4065
24 05 92	1.8	2112
26 05 92	1.9	2838
27 05 92	6.7	8477
30 05 92	6.2	6272
03 06 92	4.0	5368
04 06 92	3.4	4915
TOTALS :	111.1	128851

period range 7664.47-7664.73 ms using a small range of period derivatives from -5.5×10^{-11} to -5.75×10^{-11} ss^{-1}. After allowing for all degrees of freedom used, no evidence was found for a persistent signal, setting a 3σ upper limit on the photon flux above 300 GeV of 6×10^{-11} cm^{-2} s^{-1} in the 1987 July data.

8.2.2.2. The Observation of 1987 June 1

The observation taken on 1987 June 1 was over 9 hours long and made under excellent observing conditions. Due to a steering fault, only the first 6.1 hours of the dataset were used for the periodic analysis. As a control check on the original event file, the off-source data were tested for evidence of a periodic signal and the results compared with those from the on-source dataset. The on-source dataset contained 10986 events which triggered the on-source channel only and showed evidence for periodicity at 7665 ± 3 ms with a chance probability of 1.1×10^{-3}. No similar effect was seen in the data recorded on any of the three off-source channels which were operating at that time (see Figure 8.9).

The combination of a long observation and a short orbital period of 2485 s meant that the 1987 June 1 dataset spanned almost 9 full binary orbits. As in the original analysis, the data were checked for orbital modulation. This was done by splitting the orbit into 621 s quarters and labelling the extracted segments 1 to 4 cyclically, with an origin at the time of the first event recorded. Due to the short duration of each section, the range of periods sampled was increased to 7.0-8.5 s. Although no single segments showed evidence for strong periodicity, there was a suggestion from the original analysis that the quarters labelled "2" contained best evidence for orbitally modulated emission. These segments were merged both with and without use of relative phase information and tested for uniformity of phase. No evidence for significant periodicity was found using either technique.

8.2.2.3. Orbital Parameter Searching

Since the previously reported analysis, the technique of optimising the

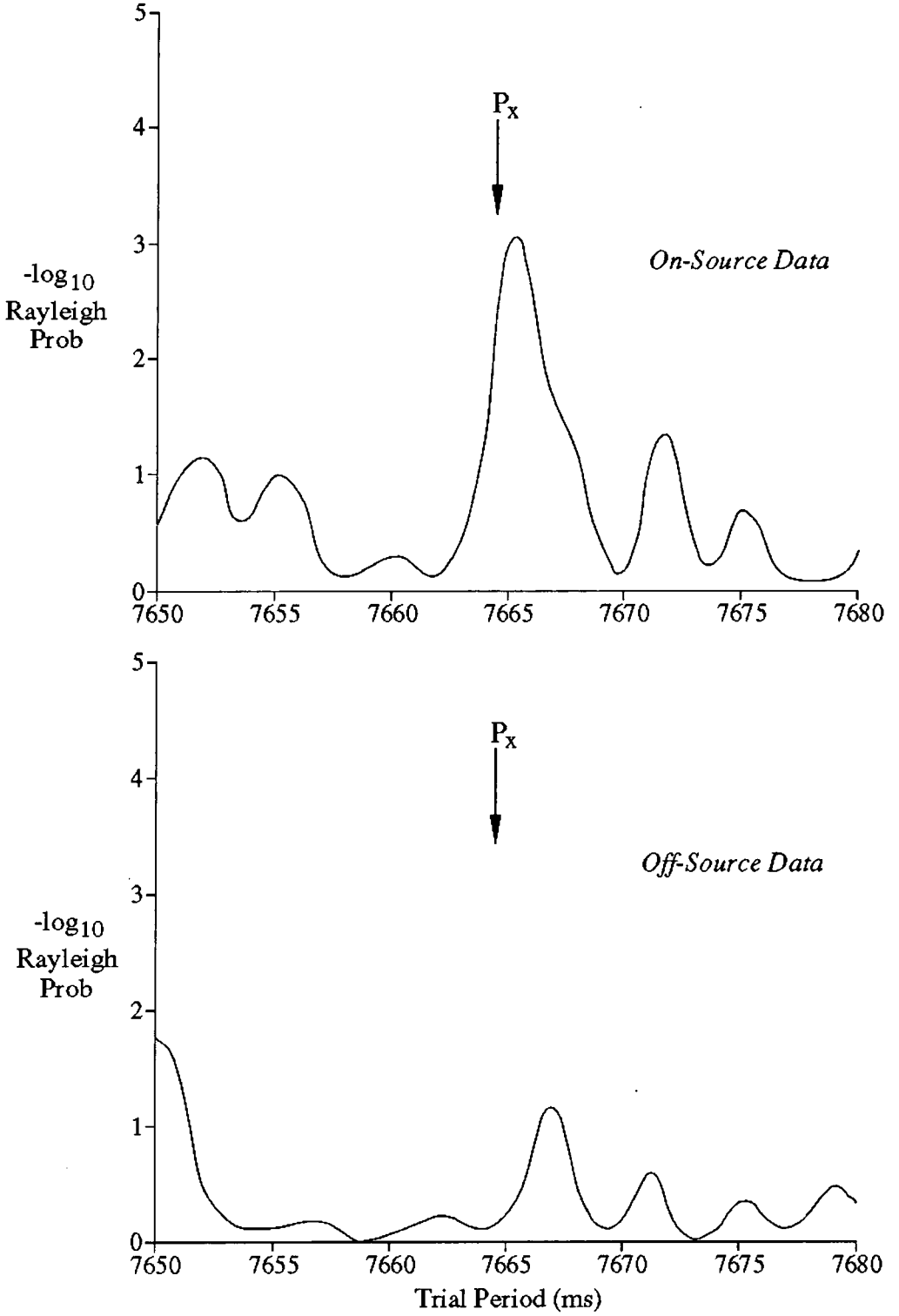

Figure 8.9 : Rayleigh probability versus trial period for the data recorded on 4U1626-67 using the Mk.3 telescope on 1987 June 1.

location of a TeV gamma ray emission site in a binary system has been developed as detailed in Chapter 4. This was applied to 4U1626-67 to test whether any improvement in the significance of the periodic signal detection was possible. Any analysis involving correction of the times by allowing for displacement to the barycentre of the binary system is difficult for this object due to its uncertain orbital characteristics, in particular the complete lack of any X-ray eclipse. Since the system is believed to be viewed almost face-on, the effect of the orbital corrections are minimal given the slow pulse period of 7.7 s. Nevertheless, knowing an approximate value of the orbital period allows an arbitrary "eclipse" epoch to be set and used as a reference time. This was defined as 12 h UT on 1987 May 31st. In all orbital searching analyses, the range in $a\sin i$ was 0.5 to 10.0 ls in 0.25 ls steps and the full range of orbital phase was covered from 0.5 to 1.5 in 0.05 steps.

The dataset for 1987 June 1 was tested for uniformity of phase at each of the orbital positions detailed above over the period range 7.660-7.670 s. The Rayleigh probability of 10^{-4} resulting from the earlier simple analysis of this dataset was recovered within $\approx$0.6 ls of the position of the X-ray source (see Figure 8.10). No further spatial resolution was possible, and no enhancement in the signal was found to be displaced from this position. The result was therefore consistent a TeV gamma ray emission site located within the accretion disc.

The set of segments corresponding to the quarters of the orbit labelled "2" as described above were combined retaining relative phase information and analysed in the same way as was the full dataset. The lowest uncorrected chance probability for uniformity of phase (3×10^{-4}) was found by correcting to $a\sin i$ of 6-8 ls. However, given the number of independent sampling intervals used, this result was not statistically significant. Even if the gamma ray production site were in the atmosphere of the companion star, the value of $a\sin i$ derived for the orbit of this star from optical work is only $\approx$0.4 ls, too small to be distinguished from the position of the X-ray source

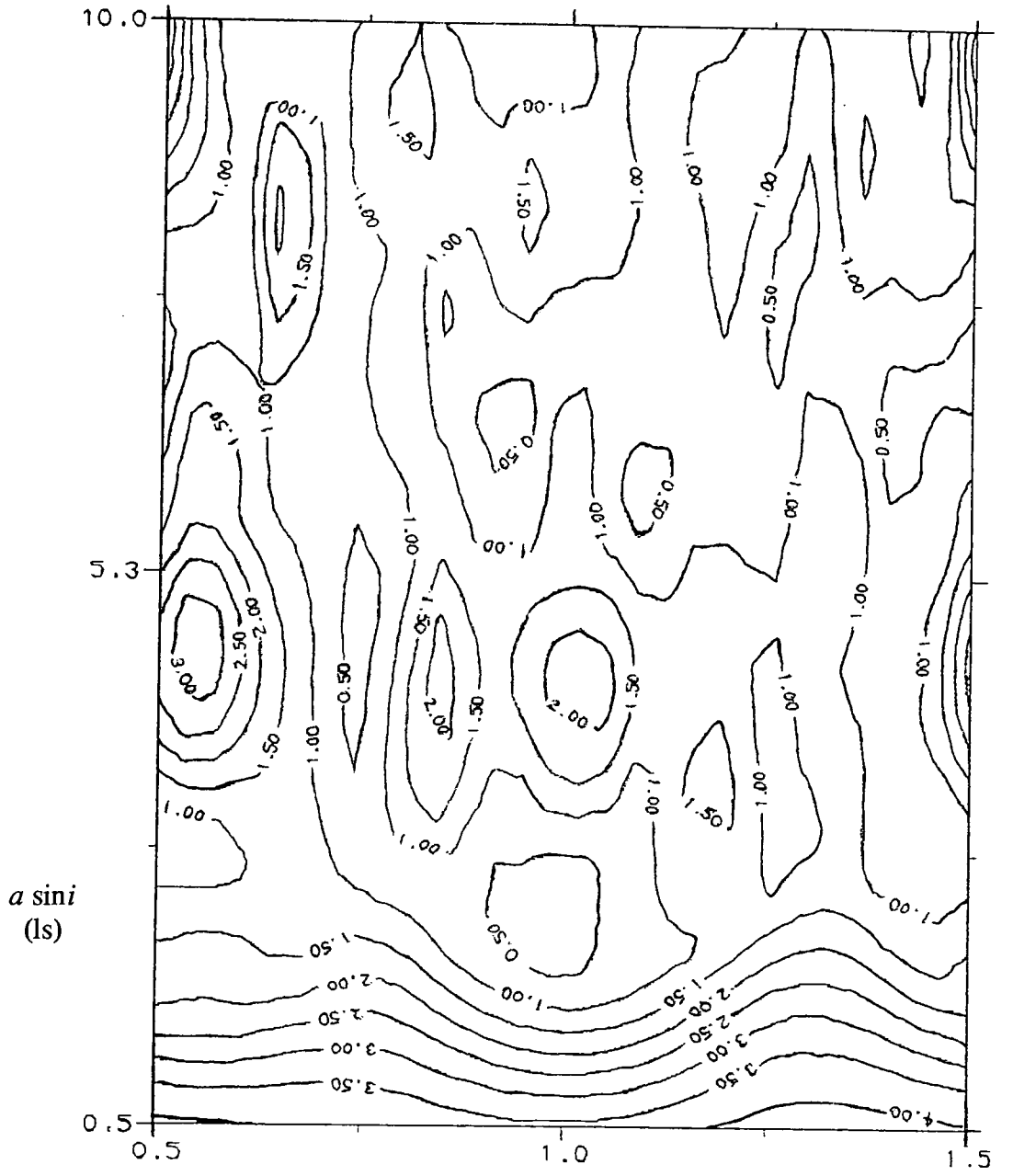

Figure 8.10 : Result of the orbital searching technique as applied to the Mk.3 telescope observation of 4U1626-67 on 1987 June 1. The Rayleigh test was applied over the period range 7660-7670 ms. The epoch shift given is with respect to an arbitrary phase origin.

using this technique. A shift of 6-8 ls in this treatment corresponds to a physical displacement in the orbital plane of ≈20 ls given an inclination of ≈20°.

8.2.3. The 1992 Durham Dataset

Interest in the observation of 4U1626-67 at TeV energies was rekindled by the Compton Observatory results outlined in Section 8.2.1.1 which showed that the 7.7 s pulsar had entered a mode of persistent pulsar spin-down for the first time since its discovery. 4U1626-67 was observed using the Mk.3 telescope during two consecutive dark-moon periods in 1992 May and June. A total of 42 hours of data were recorded; the observations are listed in Table 8.6.

Extrapolating from the period history observed by the Compton Observatory, which covered 12 months up to 1992 February, the pulsar period was predicted to be 7.6627 ms for 1992 May, increasing to 7.6629 ms for 1992 June using a spin-down rate of 5.5×10^{-11} ss^{-1}. Each of the individual observations were tested for uniformity of phase at the predicted pulsar period and no evidence for periodicity was found. In the observation carried out on 1992 May 27, a signal was found at a period of 7.657 ± 0.002 s, 50 ms shorter than the expected X-ray period, with an uncorrected chance probability of 2×10^{-4}. The orbital parameter searching technique was used to discover whether this shift could be linked with a location in the binary other than the X-ray source position. No improvement was found by correcting the event arrival times to orbital positions between $a \sin i$ of 0.2 and 3 ls and stepping through the full orbital phase range.

In addition the data from within each dark-moon interval were combined to test for persistent periodic emission. The Rayleigh test for uniformity of phase was applied to each dataset both with and without use of relative phase information and no evidence for a persistent signal at the X-ray period was found. In addition, the entire 1992 dataset spanning 30 days was combined with

phase coherence retained and tested for uniformity of phase. No evidence for periodicity was found, allowing a 3σ upper limit to be placed on the photon flux above 300 GeV of 6×10^{-11} $cm^{-2}s^{-1}$.

8.2.4. Discussion

The data analysed here have not provided evidence for the emission of TeV gamma rays from 4U1626-67. For a source distance of 8 kpc, the flux limits reported here represent an upper limit on the persistent TeV gamma ray luminosity of $\approx 6 \times 10^{35}$ erg s^{-1}. The observation of 1987 June 1st was the only single observation in which a signal modulated at the pulsar period was detected, and the significance of this detection is weakened by the number of degrees of freedom subsequently accumulated in searching through the entire dataset.

Whilst the strong magnetic field of the neutron star and the presence of a substantial amount of accreting material may make conditions favourable for the production of TeV gamma rays via neutral pion decay in the accretion disc, it is believed that we observe the system nearly face-on. This configuration makes the detection of a beam of pulsed high energy gamma rays difficult to explain if the source is in target material in the plane of the system, and would account for the failure to detect a significant flux of such photons. In addition, whilst the 1992 observations were aided by the knowledge of near contemporary X-ray period measurements, the interval of pulsar spin-down could correspond to a reduction in the accretion rate in the system, thus reducing what target material may be available as a gamma ray production site, and hence the overall gamma ray flux.

8.3. X0021-72 : A Globular Cluster X-ray Source

8.3.1. X0021-72 : Low Mass X-ray Binary or Cataclysmic Variable?

The very high number density of stars in a typical globular cluster makes for frequent interactions. Such clusters, with ageing stellar populations, are thus an ideal site for the formation of low mass X-ray binaries via

gravitational capture (Fabian, Pringle and Rees, 1975). Stellar X-ray sources discovered in nearby globular clusters have been divided into two groups on the basis of a clear partition in their typical luminosities, as shown in Figure 8.11 (Hertz and Grindlay, 1983a). The bright sources, with luminosities in the range 10^{36}-10^{38} erg s^{-1}, are generally thought to be accreting neutron stars with characteristics similar to the LMXRBs which populate the main body of our galaxy. The dim sources have luminosities from 10^{31} to 10^{34} erg s^{-1}, which are more typical of cataclysmic variables, in which material accretes onto a white dwarf. However, the very brightest of these dim sources do not sit comfortably within this classification (Charles, 1989).

One of these anomalous objects is X0021-72 situated near the core of 47 Tucanae, one of the nearest globular clusters at a distance of only 4·6 kpc (Hertz and Grindlay, 1983b). The flux from X0021-72 was found to be variable on timescales of hours to days from Einstein observations in the range 0·2-4·0 keV (Auriere, Koch-Miramand and Ortolani, 1989). The typical source luminosity varied from $\approx 7 \times 10^{33}$ to 3×10^{34} erg s^{-1}, with an average value over 4 times brighter than any galactic cataclysmic variable. However, this is still an order of magnitude below the faintest of the bright globular cluster X-ray sources. This object has been suggested to be a soft X-ray transient in quiescence (Verbunt, van Paradijs and Elson, 1984; Charles, 1989) but the identification is by no means certain.

The observations of X0021-72 by the Einstein satellite also revealed the presence of weak but significant pulsations at a period of 120·2 s in a data segment lasting 2·2 hours. A weaker but more persistent pulsation was also seen at 4·580 s. The strength and coherence of the 120 s modulation was typical of the weak periodicities seen at 10s of seconds in a number of CVs (Cordova and Mason, 1983) but the level of the steady luminosity would require such a source to be observed in semi-permanent outburst. The recent identification of a possible optical counterpart (Paresce, de Marchi and Ferraro, 1992), a faint blue variable star with a spectrum and intensity

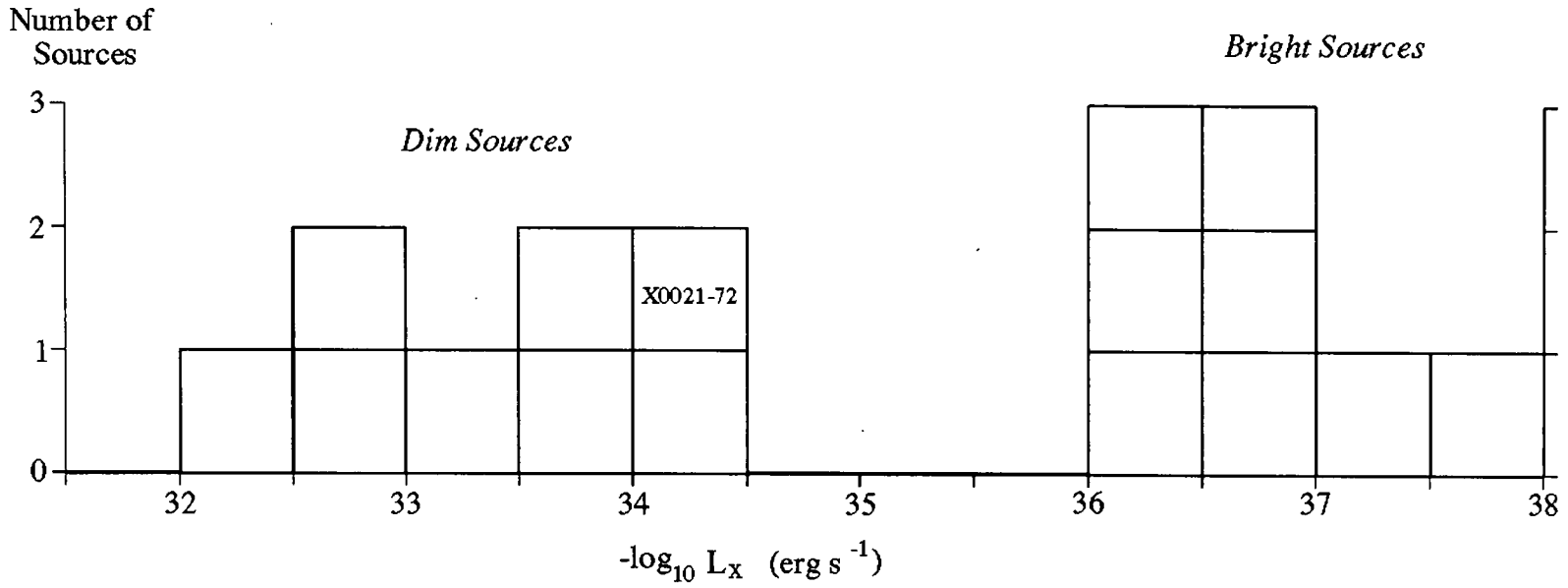

Figure 8.11 : Globular cluster X-ray sources distributed according to absolute luminosity. X0021-72 is revealed as an anomalous "dim" source.

(after Hertz and Grindlay, 1983a)

compatible with a CV accretion disc, has not fully resolved the problem. The ratio of X-ray to optical luminosity is much larger than for most CVs, though the optical brightness seems too low for even an edge-on view of a low mass X-ray binary.

8.3.2. Previous TeV Gamma Ray Observations

Shortly after the announcement of the discovery of 120 s X-ray pulsations from X0021-72, a preliminary analysis by the Potchefstroom group revealed a similar periodicity in their TeV gamma ray observations of the source (de Jager et al., 1990). Only weak evidence was found for persistent emission over 109 days of observing the source at photon energies $\geq 2{\cdot}8$ TeV, but one of the datasets was found to show evidence for uniformity of phase at $120{\cdot}1 \pm 0{\cdot}2$ s with a chance probability of $3{\cdot}7 \times 10^{-4}$. The source luminosity was estimated as 2×10^{35} erg s^{-1} above $2{\cdot}8$ TeV, a factor of 10 greater than the X-ray luminosity, which could only be achieved if the system were a low mass X-ray binary.

A previous analysis of TeV gamma ray observations of 47 Tucanae using the Durham group's Mk.3 telescope found no evidence for 120 s pulsed emission from X0021-72 (Mannings, 1990). From 33 observations, 112 hours of data were recorded and tested for uniformity of phase at 120 s. No evidence for such periodicity was found in any individual dataset and a upper limit on the persistent luminosity above $0{\cdot}4$ TeV was set at 7×10^{34} erg s^{-1}. A reanalysis of this data is presented here, involving both a more refined data selection and the inclusion of several new observations.

8.3.3. A Search for Pulsed TeV Gamma Ray Emission from X0021-72

8.3.3.1. Selection of Data from the Durham Mk.3 Telescope

The Mk.3 telescope has frequently been used to make TeV gamma ray observations of 47 Tucanae in a search for the photon flux which may arise from the large number of millisecond pulsars expected to be present in such a globular cluster (e.g. Usov, 1983; Bailyn and Grindlay, 1990). Only those

datasets recorded in the tracking mode were used in the present analysis since the 120 s periodicity of X0021-72 would be lost in the powerful artificial signal induced by the 2 minute channel-interchange interval which characterises the chopping mode. In addition to this consideration, only those datasets recorded under clear and stable weather conditions were used so as to avoid spurious periodicities being induced by external effects, with extracted segments of high quality data being selected where necessary.

The event rejection procedure used in the previous analysis of X0021-72 (Mannings, 1990) was to accept only events which triggered the on-source channel alone, and include no off-source channel responses exceeding a relative response threshold. X0021-72 is very near to SMC X-1 in the sky and is viewed over a very similar range of zenith angles. Therefore as for the reanalysis of data recorded on SMC X-1 which was reported in Section 8.1, the present work used the improved data selection detailed by Brazier (1991). This was based on a relative response threshold of 45% and the implementation of the pedestal technique (see Chapter 4). The new selection resulted in 165 544 Cerenkov events being selected from 116 hours of observations, comprising 40 individual datasets as listed in Table 8.7.

The purpose of this work was to use the Rayleigh test to search for evidence that the 120 s and 4.58 s periodicities seen at X-ray energies are also found at TeV gamma ray energies. Whilst it is highly likely that X0021-72 is in a binary system, no orbital parameters are known (although the possible optical variability on a timescale of ≈6 hrs in the star identified by Paresce, de Marchi and Ferraro (1992) would be consistent with the orbital period expected in the CV model of the source) and it is not therefore possible for the event arrival times to be corrected to the rest frame of this binary system

In a low mass binary, the orbital velocity of the X-ray source is unlikely to be much greater than $v_x \approx 10^5$ m s^{-1}, and will be less if the compact object is significantly more massive than the dwarf companion star.

TABLE 8.7 - Catalogue of Mk.3 telescope observations of X0021-72

Date	Duration (hours)	Events Selected
20 06 88	2.0	2550
21 06 88	1.9	2499
09 07 88	3.1	3246
10 07 88	2.0	1840
11 07 88	3.4	3605
12 07 88	3.3	3314
13 07 88	3.7	3185
19 07 88	3.1	5246
02 10 88	2.8	2267
03 10 88	1.6	3014
04 10 88	4.3	8773
07 10 88	3.3	6262
08 10 88	2.1	4419
09 10 88	3.5	8896
10 10 88	3.4	7608
11 10 88	3.3	3315
12 10 88	3.5	7033
13 10 88	3.8	6079
14 10 88	2.0	3124
21 10 89	3.1	4520
27 10 89	4.0	3769
28 10 89 (i)	1.5	1826
28 10 89 (ii)	1.5	1750
30 10 89	2.5	1454
01 11 89	4.5	5526
20 11 89	2.0	3137
21 11 89	3.9	5793
22 11 89	2.8	4112
27 11 89	2.5	3564
28 11 89	3.0	3922
30 11 89	2.8	3754
20 07 90	3.7	5752
21 07 90	4.1	6998
11 09 90	1.4	1617
14 09 90	4.7	5290
15 09 90	2.0	2953
16 09 90	3.2	4348
17 09 90	3.0	4498
08 11 90	3.1	3268
12 08 91	1.8	1417
TOTALS :	116.1	165544

The maximum Doppler shift of a pulsar period P which may result from orbital motion of the X-ray source is $\approx P(v_x/c)$, where c is the velocity of light. This shift may be compared with the independent period sampling interval, $\Delta P=P^2/T$, for a typical Mk.3 telescope observation lasting a time T seconds. The average value of T in the present analysis is 2·9 hours. For a 120 s period, the orbital Doppler shift expected is ≈0·04 s, whilst the independent period sampling interval is ≈1·4 s, thus making the barycentric correction unimportant. For a period of 4·58 s however, the maximum Doppler shift is of very similar size to the independent sampling interval (≈ 2 ms) so that some smearing of the pulsations could occur.

8.3.3.2. Uniformity of Phase in Individual Datasets

Each dataset was tested for uniformity of phase over the period range 115-125 s, a range of ≈ 3-8 independent sampling intervals, which allowed for a period derivative of up to $\pm 1{\cdot}5 \times 10^{-8}$ ss^{-1} to have been present since the 1979 X-ray observations. The original identification of this period actually placed a short-term upper limit of 10^{-6} ss^{-1} on the value of the period derivative, and it is unlikely that a long-term value greater than 10^{-8} ss^{-1} would be seen in such a low mass binary. No evidence for periodicity was found in any of the datasets tested in this way after allowing for the 600 degrees of freedom used (40 observations, 5 for the average number of independent sampling intervals tested and 3 for oversampling in period). A periodic signal constituting 5·6% of the cosmic ray background would have been required for a significant detection in one dataset. Given the average dataset size of 4100 events, this allowed a 3σ upper limit of 3×10^{-10} $cm^{-2}s^{-1}$ to be placed on the peak photon flux from the source on a timescale of several hours at energies above 300 GeV.

A similar procedure was followed to test for uniformity of phase at 4·580 s. The period search range was 4·575-4·585 s, spanning an average of 5 independent sampling intervals as for the periodicity search at 120 s. No

evidence was found for 4·58 s periodicity in any of the datasets tested allowing the same 3σ upper limit of 3 x 10^{-10} $cm^{-2}s^{-1}$ to be placed on the 300 GeV photon flux pulsed at this period. For a source distance of 4·6 kpc and an integral cosmic ray spectral index of -1.6, this corresponds to a 300 GeV luminosity ≤3 x 10^{35} erg s^{-1}.

A search for periodic activity on shorter timescales was also carried out by dividing each dataset into a series of 1800 s segments, with each successive segment beginning 600 s later. No significant evidence was found for short lived enhancements in the periodic emission at either 120 s or 4·58 s in any of the datasets tested.

8.3.3.3. Uniformity of Phase in the Combined Dataset

After deriving a limit on the level of the emission on short timescales, a search was made for the persistent emission of pulsed TeV gamma rays from X0021-72 on timescales of weeks and years. This task was carried out by the use of the Rayleigh test to test for uniformity of phase over a constant matrix of trial periods in every one of the 40 observations listed in Table 8.7, which span a total of 3 years. Due to the uncertainty in the orbital corrections and the possible presence of an unknown period derivative, the resultant chance probabilities at each trial period were then combined without the use of relative phase information.

This procedure was followed to search for periodic emission at both 120 s and 4·58 s. The resulting periodogram for the former test between 115 and 125 s is shown in Figure 8.12, with a peak being seen at 118 ± 1 s. The probability of this periodicity occurring by chance is 2·1 x 10^{-3} multiplied by a factor of 15 to allow for oversampling in the 5 independent trial period intervals used. The corrected probability is 3·2 x 10^{-2} and thus does not constitute a 3σ detection, but remains a tantalising indication of only a slight decrease in the period since the 1979 X-ray discovery of this periodicity (Auriere, Koch-Miramond and Ortolani, 1979). The 1989 TeV gamma ray detection by the Potchefstroom group indicated that the period had not

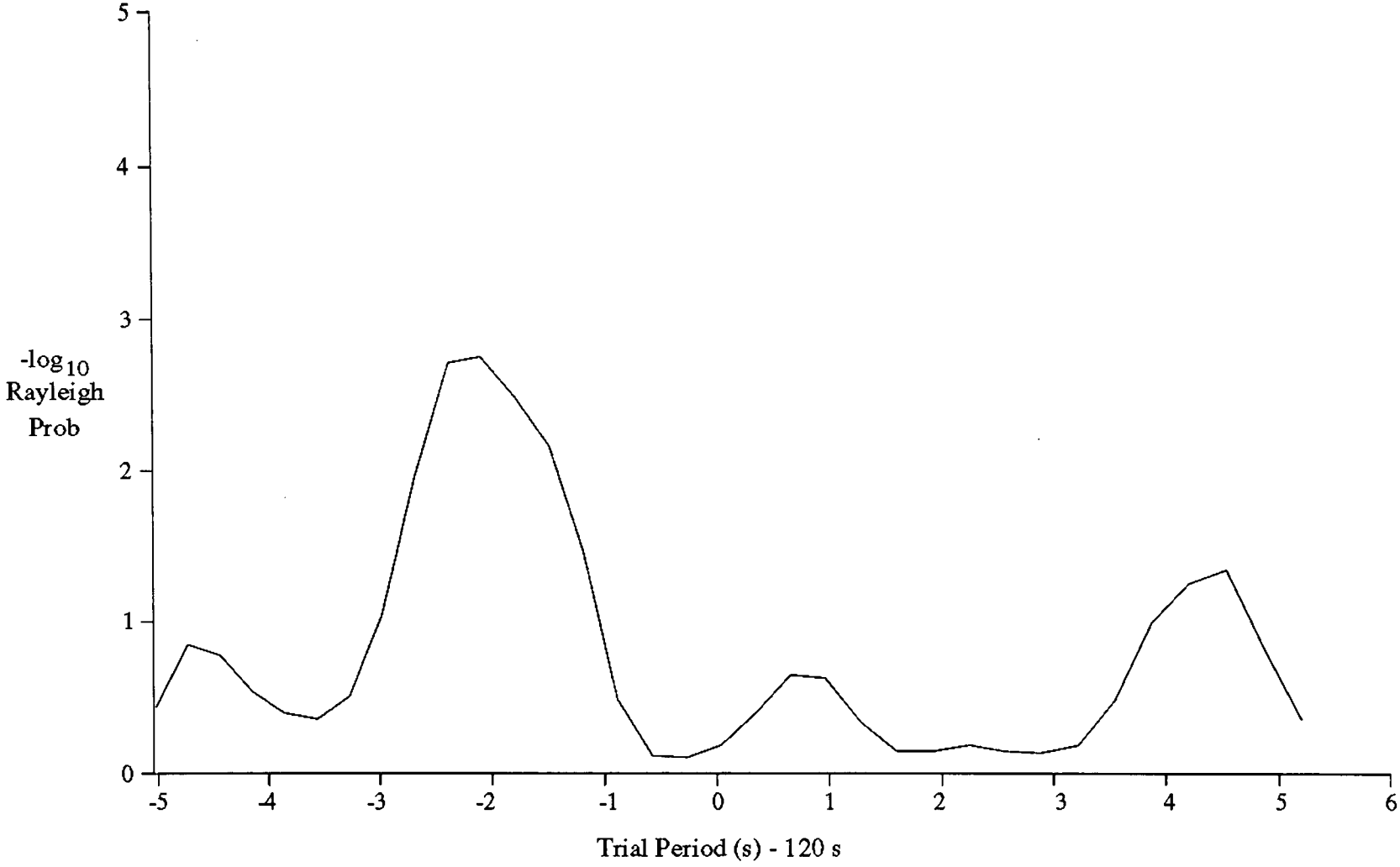

Figure 8.12 : Rayleigh probability versus trial period for an incoherent combination of all 40 Mk.3 telescope observations of X0021-72.

changed over the 10 years elapsed since the original identification, and thus contradicts the possible signal seen here. This is discussed further in section 8.3.3. The corresponding periodogram for the 4.58 s search is given in Figure 8.13. Although the most significant peak is seen at precisely 4·580 s, the probability of this signal occurring by chance is ≈0.3 ($2{\cdot}2 \times 10^{-2}$ multiplied by 15 degrees of freedom as described above) and is thus consistent with a random origin.

The value of chance probability which would have led to a 3σ detection of a pulsed flux within 5 independent sampling intervals of either of the X-ray periods tested here was $9{\cdot}0 \times 10^{-5}$. For a χ^2 probability distribution derived from a combined database of 40 independent observations and 165000 events, this level of chance probability requires a pulsed signal strength of 2·0%. This corresponds to a 3σ upper limit on the pulsed photon flux above 300 GeV within the trial period ranges tested of $\approx 1{\cdot}0 \times 10^{-10}$ $cm^{-2}s^{-1}$. For a source distance of 4.6 kpc and a differential spectral index of -2.6, this yields a time-averaged upper limit on the source luminosity above 300 GeV of 9.4×10^{34} erg s^{-1}.

The longest timespan within a dark moon period for which data has been recorded on X0021-72 is 12 days. The independent trial period sampling interval for a search at 120 s in a dataset of this duration is ≈14 ms so that pulse phase coherence may be maintained if the local period derivative does not exceed $1{\cdot}3 \times 10^{-8}$ ss^{-1}. The Rayleigh test was therefore applied to test for uniformity of phase at ≈120 s in the data from each dark moon interval with the retention of relative pulse phase information.

The strongest evidence for a periodicity in this range was found in the dataset from 1988 July, in which an uncorrected chance probability of $4{\cdot}2 \times 10^{-4}$ was found for the detection of a signal pulsed at 118·6 ± 0·2 s with a strength 2·3% of the cosmic ray background (see Figure 8.14). However the chance probability must be adjusted for the degrees of freedom used (5 for the

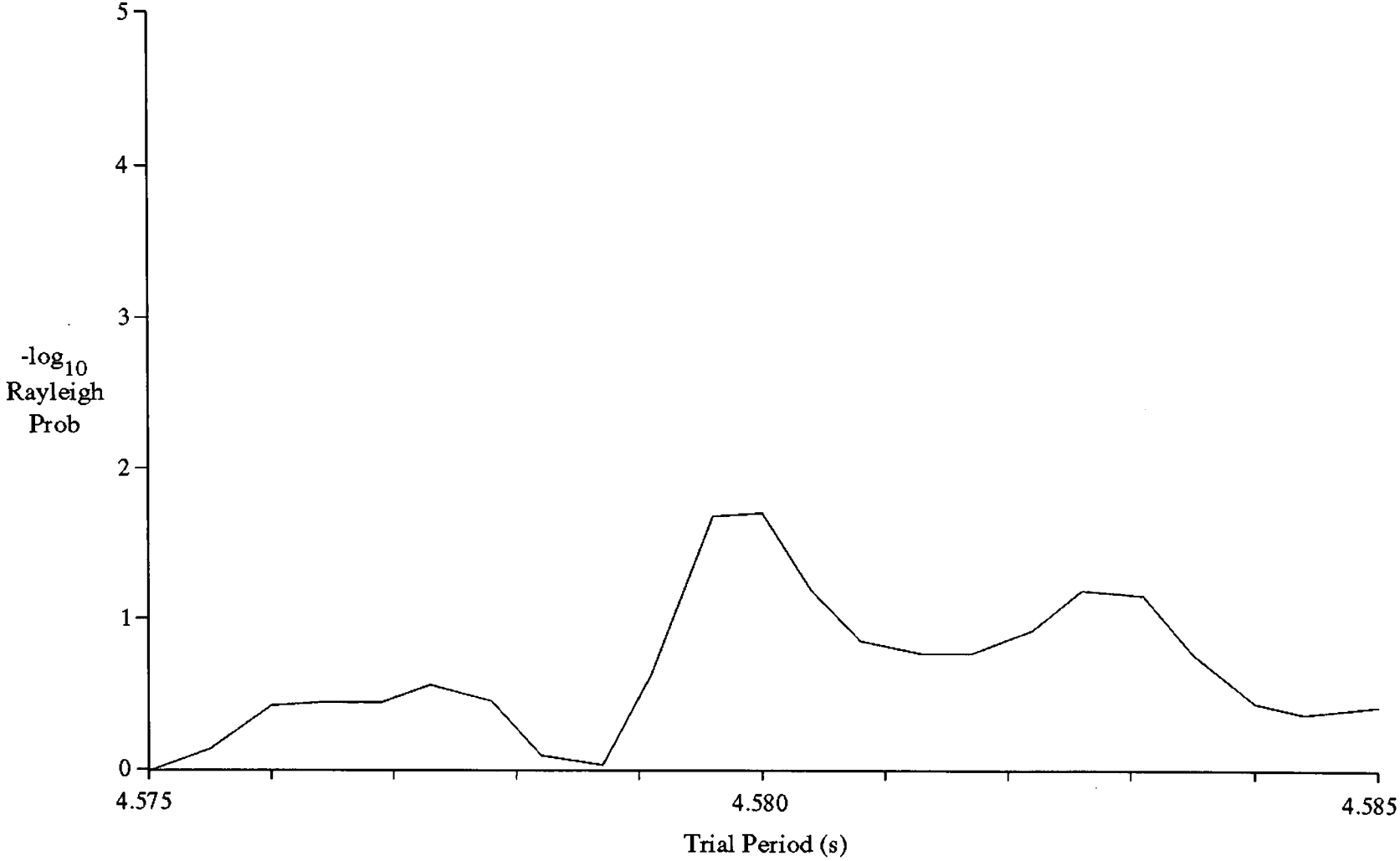

Figure 8.13 : Rayleigh probability versus trial period for an incoherent combination of all 40 Mk.3 telescope observations of X0021-72 near the possible 4.58 s X-ray period.

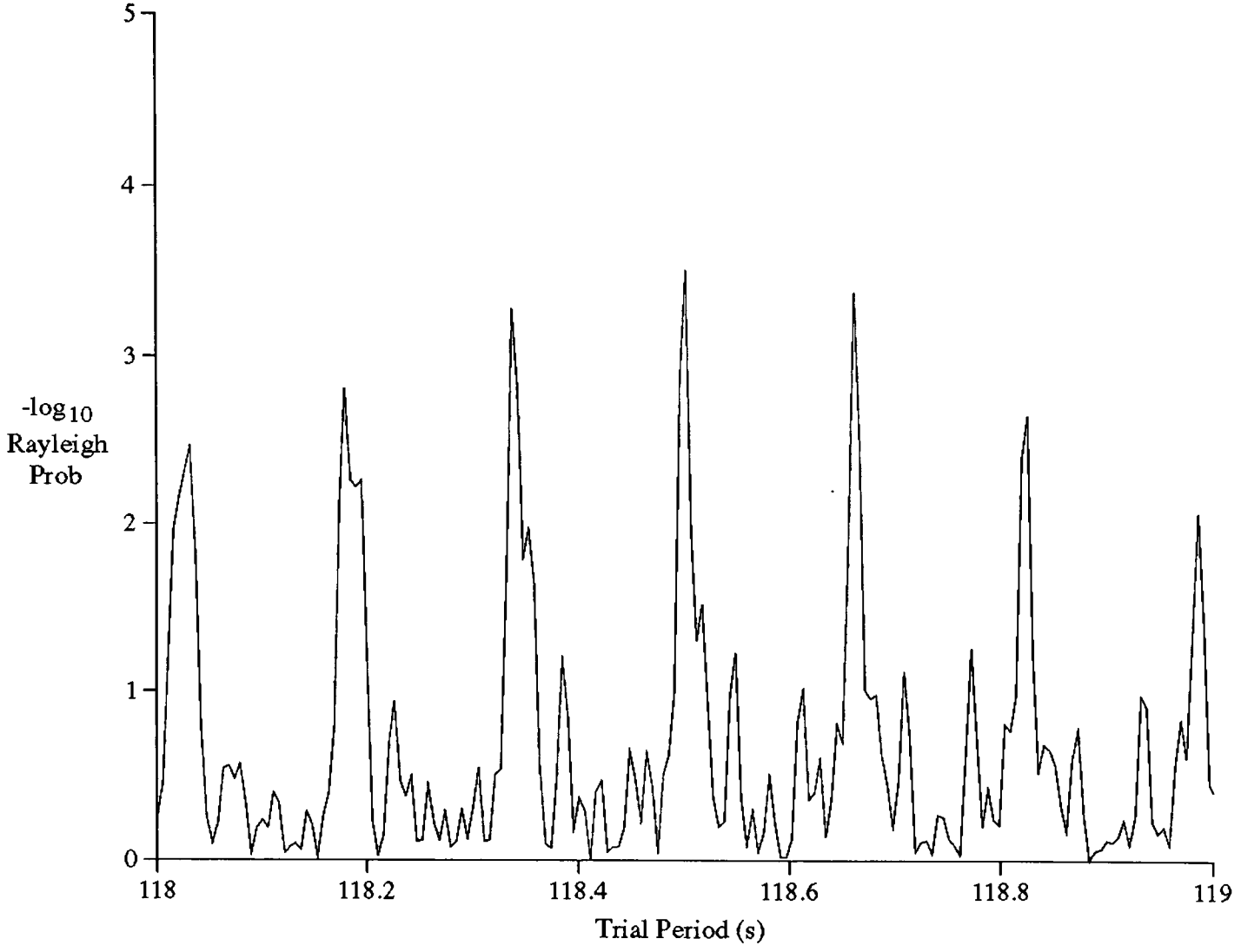

Figure 8.14 : Rayleigh probability versus trial period for a coherent combination of the 6 Mk.3 telescope observations of X0021-72 recorded in 1988 July.

number of dark moon intervals tested and 70 for the number of independent trial periods searched). The corrected probability of 0·15 is consistent with chance occurrence, and the 3σ upper limit on the flux above 300 GeV is 1.2×10^{-10} $cm^{-2}s^{-1}$.

The same procedure as above was also used to test each combined dataset for uniformity of phase between 4·577 and 4·582 s, for which pulse phase coherence could be maintained for a period derivative of $\leq 2 \times 10^{-11}$ ss^{-1}. Given the number of degrees of freedom used in this analysis, none of the data from a single dark moon interval were found to show significant evidence of periodic emission. The data recorded in 1988 October showed the lowest uncorrected chance probability of 5×10^{-4} at 4·5775 ± 0·0002 s.

8.3.4. Discussion

In summary, the many observations of 47 Tucanae made using the Mk.3 telescope have not been able to yield conclusive evidence for the observation of pulsed TeV gamma rays from X0021-72. The upper limit on the time-averaged source luminosity above 300 GeV was set at 9.5×10^{34} erg s^{-1}. The new observations included since the previous work have not been sufficient to reduce the upper limit derived from the previous work (Mannings, 1990) by a significant amount, though this new work has for the first time placed an upper limit on the TeV gamma ray flux pulsed at 4.58 s. The Potchefstroom group reported a time-averaged luminosity of 2×10^{35} erg s^{-1} for the 120 s pulsed emission above 2·8 TeV. Using an integral spectral index of -1.6, this would correspond to a source luminosity above the 300 GeV threshold of the Mk.3 telescope of 7×10^{36} erg s^{-1}, a factor of 60 above the limit reported here. A similar discrepancy was found in the maximum day-to-day pulsed luminosity.

The most interesting result reported here was the possible identification of a persistent 118 s periodicity in the TeV gamma ray flux. Whilst this was of low statistical significance, the secular spin-up rate of -5×10^{-9} ss^{-1} required to produce this period shift since the 1979 observations may be used

to speculate on the nature of the source. Assuming the average X-ray luminosity of 10^{34} erg s^{-1} is due to the accretion of material at a constant rate onto the compact object then equation 8.1 (Henrichs, 1983) may be used to predict the spin-up rate expected for a magnetised white dwarf or neutron star of one solar mass :

$$-\frac{\dot{P}}{P} = 1{\cdot}6 \times 10^{14} \cdot I_{45} \cdot (R_6.L_{37})^{-6/7} \cdot P^{-1} \qquad (8.1)$$

where P is the period in seconds, $I_{45}=I/(10^{45}$ g $cm^2)$, $R_6=R/(10^6$ cm) and $L_{37}=L/(10^{37}$ erg $s^{-1})$. Taking typical values for the radii of each class of compact object, the spin-up rate predicted for a 120 s period is $\approx 3 \times 10^{-14}$ ss^{-1} for a white dwarf and $\approx 1 \times 10^{-10}$ ss^{-1} for a neutron star. Therefore neither model is consistent with the spin-up rate derived from the present work. A much higher X-ray luminosity ($\approx 10^{36}$ erg s^{-1}) could produce the proposed spin-up for an accreting neutron star, but in a soft X-ray transient this luminosity would not be expected to persist for a sufficient amount of time (Lewin and Joss, 1983). It should also be noted that the 120 s period determined from the Einstein X-ray measurements was based on a dataset spanning only 2.2 hours and thus the accuracy of this value can only be $\pm$ 1.8 s (from equation 4.10). It is possible therefore that the present observations could be linked with the 1979 X-ray pulsar observations with the use of a much smaller period derivative.

A promising channel for future work could result from the determination of the orbital parameters by X-ray or optical observations. A confirmation of the possible 6 hour periodicity would be the first step in this direction and could enable the orbital parameter searching technique detailed in Chapter 4 to localise any site of TeV gamma ray emission. To this end, new measurements of the 120 s or 4.58 s periodicities of the source would greatly reduce the number of degrees of freedom used in testing for these uncertain periods.

9.1. Particle Acceleration Near Compact Objects

9.1.1. Requirements of Acceleration Processes

X-ray binaries have now been established as the largest category of TeV gamma ray sources in observations carried out by numerous research groups. This was an unexpected discovery and has led to the development of a number of models to explain the surprising characteristics of high energy emission from these objects, especially Cygnus X-3 and Hercules X-1. As a result of following in the wake of the observational evidence, all of the models are subject to the subsequent constraints and requirements placed on any credible explanation of the type of processes at work. A set of such considerations have been given by Hillas (1987) and Cheng et al. (1990) and are summarised as follows.

(i) To produce TeV gamma rays by neutral pion decay, the accelerated nucleons must have energies of at least $\approx 10^{15}$ eV.

(ii) The gamma ray luminosity has sometimes been found to exceed the Eddington limit on the luminosity of an accreting object. Thus if the source is powered by accretion a means must be found whereby much of the gravitational infall energy may be diverted from thermal processes.

(iii) The gamma ray luminosity comprises a significant part of the total power output in all energies, so the total energy budget of the source must be satisfactorily modified.

(iv) Any site of gamma ray production by neutral pion decay must be at a distance of least $\approx 10^6$ m from the neutron star in order to avoid absorption by pair production in its intense magnetic field.

(v) An explanation must be found for the observations of orbital phase dependence in the gamma ray signal, suggesting that the particle beam interacts with target material at only certain sites in the system. Detections of gamma ray emission during an eclipse of the X-ray source must

also be accounted for.

(vi) A gamma ray production mechanism must account for the pulsar behaviour at TeV energies with a period identical to that seen at much lower energies despite the different processes involved.

Acceleration in pulsar magnetospheres is a highly efficient means of producing high energy particles and TeV gamma rays as a result of the power available from rotational energy loss in a rapidly rotating isolated pulsar. The pulsar radiation mechanism was originally derived by Goldreich and Julian (1969) and later modifications have been made to postulate TeV gamma ray emission from millisecond pulsars (Usov, 1983). A model of TeV gamma ray production in the outer magnetospheric gaps was proposed by Cheng, Ho and Ruderman (1986) which removed the problem of the high X-ray flux which is predicted as a consequence of a production site nearer the magnetic poles. Such X-ray fluxes are not detected from typical isolated pulsars.

Goldreich and Julian considered the corotating plasma within the light cylinder of the neutron star, within which a steady state of charge separation is achieved when $E.B=0$. The charge density ρ_0 is given by

$$\rho_0 = - \frac{\Omega_* . B}{2\pi c} , \qquad (9.1)$$

where Ω_* is the angular velocity of the star and B the magnetic field, and is zero at null charge surfaces where $\Omega_* . B=0$.

The outer gaps in the magnetosphere occur where the charge-separated plasma flows along open field lines, producing plasma voids where $E.B \neq 0$ near the null charge surfaces (Cheng, Ho and Ruderman, 1986). The potential drop developed in these regions can accelerate electrons to ultrarelativistic energies with subsequent gamma ray emission and pair production maintaining the current flow.

The maximum accelerating electric potential Φ for a charged particle in the magnetic field of a pulsar spinning with angular velocity Ω is given by

$$\Phi = \frac{B_o \, R^3 \, \Omega^2}{c^2} \quad , \qquad (9.2)$$

where B_o is the surface equatorial magnetic field and R the radius of the neutron star. For typical neutron star values of 10^{12} G and 10^6 cm, the energy required for TeV gamma ray emission is simply not available in a slow X-ray binary pulsar.

The acceleration of thermionically emitted electrons by the strong electric field component parallel to the open magnetic field lines emanating from the magnetic poles was suggested to be a basis for the emission of TeV gamma rays by Cohen and Mustafa (1987). However, the absorption of such high energy photons by pair production in the magnetic field and in the hard X-ray flux from the accreting polar cap makes such a mechanism unlikely to occur without the imposition of restrictive conditions highly sensitive to the configuration of the electromagnetic fields. The role of electron acceleration in providing a contribution to the gamma ray fluxes observed from X-ray binaries seems confined to much lower photon energies.

9.1.2. Dynamo Mechanisms Derived from Accretion Processes

A possible source of the very high energy particle acceleration in an X-ray binary is the radial potential gradient induced in a rotating conducting accretion disc. Chanmugam and Brecher (1985) were responsible for a model based on a unipolar inductor mechanism, whereby the magnetic field of the neutron star penetrates its surrounding accretion disc. The differential rotation of the Keplerian disc was proposed to "wind up" and amplify the poloidal magnetic field, with a component perpendicular to the disc of $B_z(r) \propto r^{-1/2}$ where r is measured from the neutron star, resulting in a potential drop between the inner and outer edges of the disc of

$$V = - \frac{(GM)^{1/2}}{c} \, . \, B_z(r_i) \, . \, r_i^{1/2} \, . \, \ln(r_o/r_i) \quad , \qquad (9.3)$$

where M is the mass of the neutron star, and r_i and r_o (in cm) are the inner and outer radii of the disc respectively. For a magnetised neutron star with a

dipolar field aligned with its spin axis, r_i corresponds to the Alfven radius r_A of the magnetosphere :

$$r_i = r_A = 3.5 \times 10^8 \, B_{12}^{4/7} \, R_6^{10/7} \, (M/M_\odot)^{1/7} \, L_{37}^{-2/7} \, , \qquad (9.4)$$

where B_{12} is the neutron star's surface magnetic field in units of 10^{12} G, R_6 its radius in units of 10^6 cm and L_{37} its photon luminosity in units of 10^{37} erg s^{-1} resulting from conversion of gravitational potential energy at the stellar surface.

For a typical surface field of 10^{12} G, the voltage drop at r_i can be found using $B_z(r_i)=B_{12}(R/r_i)^3$. For the resultant $B_z(r_i)$ of $\approx 1.7 \times 10^5$ G, a maximum potential of 1.3×10^{15} V results for an outer disc radius of 10^{11} cm. For a dipole field described by

$$B_z(r_i).r_i^{1/2} \propto B_{12}^{-3/7} \, , \qquad (9.5)$$

it can be seen that lower surface fields will give higher potential drops in the inner regions of the disc.

This model predicts a TeV gamma ray flux originating where the particle beams interact either with the atmosphere of the primary star or with circumstellar material in the system. Pulsed emission would result if the magnetic and rotation axes are not aligned. However, the direction of particle acceleration is out of the plane of the disc where most target material for gamma ray production is expected to reside. A neutron star surface magnetic field strength of 10^{12} G makes the Alfven radius too large for a sufficient amount of accretion luminosity to be extracted before acceleration occurs to produce TeV gamma rays (Hillas, 1987). In addition, the maintenance of the full vacuum potential above the disc is unlikely in the presence of strong electric fields to draw plasma from the disc plane (Harding, 1990).

An accelerator gap model was developed by Cheng and Ruderman (1989, 1991) which differed from the model of Chanmugam and Brecher described above by considering the potential drop induced when the inner part of the accretion disc rotates faster than the neutron star magnetosphere. The null charge

region ($\Omega_*.B=0$) in this situation extends from being a surface to form a region of empty plasma where $E.B\neq0$ known as the accelerator gap. This is analogous to the outer gap model for an isolated pulsar. The acceleration process may be explained as follows.

The accretion disc is assumed to be a perfect conductor such that $E.B=0$ at all points on its surface. For the case where the disc and neutron star are in corotation with the pulsar magnetic and rotation axes aligned the magnetospheric configuration is similar to that within the light cylinder of an isolated pulsar, i.e.

$$E = \frac{\Omega \times r}{c} \times B \ . \qquad (9.6)$$

In the case where the disc spins more rapidly than the star, the magnetosphere is disrupted along the null charge surfaces and divides into three distinct charge-separated regions (see Figure 9.1). The innermost region corotates with the neutron star, whilst further out in the disc each charged particle corotates with the disc material linked by field lines which do not cross the null surfaces.

The intermediate region is composed of a plasma gap where $E.B\neq0$. With $\Omega_d>\Omega_*$ and the magnetic field lines interrupted by this gap, no current flows between the disc and the star. For an inner disc radius r_i, the potential drop developed in the limit where $\Omega_d(r_0)>>\Omega_*$ is

$$V(r) = 4 \times 10^{14}.r_8^{5/2}.B_{12}.(M/M_\odot)^{1/2}.R_6^3.(1-(r_i/r)^{5/2}) \ , \qquad (9.7)$$

where $r_8/10^8$ cm is the inner radius of the disc. $V(r)$ has a maximum value at the corotation radius r_{co} given by

$$r_{co} = (GM/\Omega_*^2)^{1/3} \ , \qquad (9.8)$$

The magnetic field lines passing through the inner disc may be pulled in by the inward flow of matter to form a small transition region beginning at r_i and ending well within r_{co} where the maximum voltage $V(r)$ is increased over the value at r_{co}.

If the current of positive ions from the star to the disc induced by this

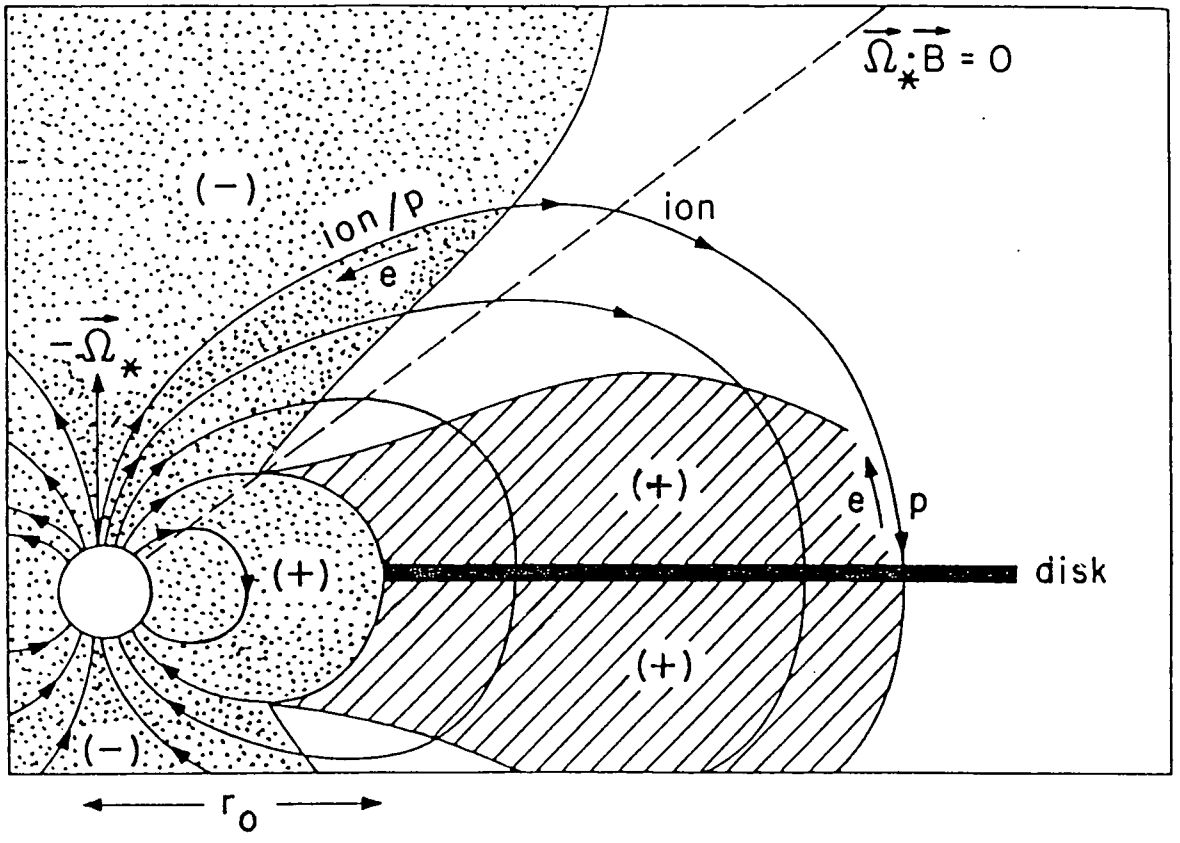

Figure 9.1 : An illustration of the three distinct regions formed in the magnetosphere of a rotating neutron star accreting from a disc in the situation where the inner disc rotates faster than the star. These are :-

(i) the innermost (dotted) region which corotates with the neutron star.

(ii) the outermost (hatched) region which corotates with the local Keplerian velocity of the disc,

(iii) the region empty of plasma (unshaded) which forms between regions (i) and (ii) where E.B=0 only at the boundaries. This is the accelerator gap where a potential drop develops parallel to the magnetic field lines.

(from Cheng and Ruderman, 1989)

potential is balanced by an equal and opposite flow of electrons from the disc, then the potential drop across the gap is steady. However, any pair production following inverse Compton scattering of soft photons emitted from the region of the neutron star causes an extra charge flow in each direction thus reducing the overall electric potential and setting a limit on its value parallel to the magnetic field lines. This limit may be relaxed if the region of the accelerator gap above the accretion flow is shielded by absorption of the X-ray flux from the neutron star (see Figure 9.2).

Since the potential drop V_g in the gap cannot reach the perfect Keplerian value of equation 9.7, an increasing current density J is induced due to the difference between the two. Ultimately the JxB torque may approach the rate of angular momentum flow into the region. A natural equilibrium is reached as the disc reduces its angular velocity $\Omega_d(r)$ from the Keplerian value until the current flow stabilises with the induced field equal to the maximum possible. The maximum acceleration voltage after allowing for pair production can be estimated as

$$V_{ppl} = 6 \times 10^{12}.L_{37}.E_x^{-1}.B_{12}^{-1/2}.R_6^{-1} \text{ Volts} , \qquad (9.9)$$

where E_x is the typical X-ray energy in units of 0.1 keV. The corresponding power is given by

$$P = 7 \times 10^{34}.\beta^{-1}.L_{37}.B_{12}^{-4/7}.(M/M_o)^{-1/7}.R_6^{-3/7} \text{ erg s}^{-1} , \qquad (9.10)$$

where $\beta = 2r_o/r_A \approx 1$. The maximum power output is unchanged if the accelerator gap is strongly shielded from the X-ray flux and its associated pair production, but the maximum voltage is increased to that achieved in a static gap situation :

$$V_{gap} = 4 \times 10^{14}.\beta^{-5/2}.(M/M_o)^{1/7}.R_6^{-4/7}.L_{37}^{5/7}.B_{12}^{-3/7} \text{ Volts.} \qquad (9.11)$$

Only protons and positive ions can be accelerated to gain the full energy eV_{gap} due to the effects on electrons of inverse Compton scattering and curvature radiation in the magnetic field. The ultra-relativistic particle beam can be directed into the disc along the magnetic field lines where TeV

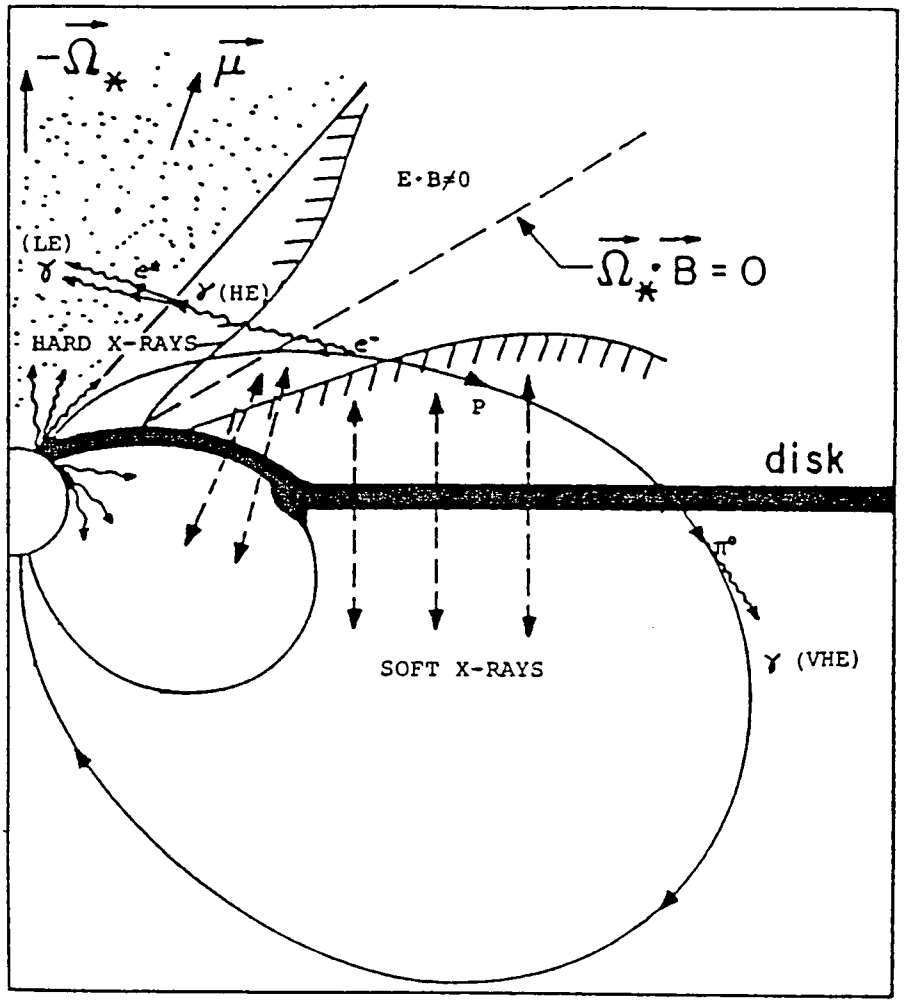

Figure 9.2 : An illustration of the "shielding" of the accelerator gaps from the hard X-ray flux emitted by the shock heating of the accretion at the magnetic poles of the neutron star. The shielding occurs due to Compton degradation of the X-ray photons as they traverse the accretion flow itself (depicted by the heavy black line). Low energy gamma ray emission may occur outside the gaps in the hard X-ray zone as a result of secondary pair production.

(from Leung, Cheng and Fung, 1993)

gamma rays may be produced either by neutral pion decay or through a partially developed electron/positron cascade.

Whilst this model is realistically limited to the production of 10^{15} eV particles, larger voltages and particle energies may be generated in a magnetic reconnection event. It was suggested by Cheng and Ruderman (1991) that neutrons produced in the photodisintegration of accelerated nuclei could allow energy to be transported further from the region of strongest magnetic field to avoid absorption of the resultant TeV gamma ray flux. A problem remains in deriving maximum acceleration potential from neutron stars with high magnetic fields and correspondingly large Alfven radii.

9.1.3. Acceleration in Accretion Shocks

Another means of extracting high energy particles from the process of accretion is by acceleration in a diffusive shock formed where the accretion flow is channelled onto the neutron star with a velocity much greater than its thermal velocity. The acceleration is most likely to occur via a Fermi mechanism, similar to that widely suggested to accelerate cosmic ray particles in the magnetic fields of the interstellar medium (e.g. Bell, 1978; Ellison and Eichler, 1985; Eichler and Vestrand, 1985). If the shock velocity may be approximated by the freefall velocity at a given distance from the stellar surface, then proton energies of $\approx 10^{16}$ eV may be reached.

To avoid the difficulty of the escape of either high energy protons or photons from a production site in the very high magnetic field near the neutron star, Kazanas and Ellison (1986) proposed that neutrons could result from nucleon collisions or photodissociation of ^{4}He nuclei to give an isotropic flux of very high energy particles. By escaping the regions of strongest magnetic field, these particles could interact to produce gamma rays in target material well outside the accretion zone.

Further problems with this scenario were pointed out by Hillas and Johnson (1989). As the accreting plasma is channelled along the narrowing field configuration towards the magnetic poles, the magnetic energy density

increases from being similar to the gas energy density at the Alfven radius to a value several orders of magnitude greater. Thus the field is too rigid to be shocked or disturbed by the accreting material, and with no small-scale deformation possible the particles cannot be reflected and Fermi acceleration to TeV energies is not possible. Only energies below a GeV may be acquired by particles whose gyroradius resonates with any small wavelike perturbations in the field caused by the infalling gas.

To achieve efficient acceleration, a region of weaker magnetic field must be found. A shock could occur further from the neutron star if a jet of protons is directed into material at the Alfven radius and elsewhere in the system. Such a model was developed by Kiraly and Meszaros (1988) who considered the formation of a relativistic particle jet ejected along the magnetic axis as a result of radiation pressure acting on the material impacting on the stellar surface. Where this jet interacts with the material collected at the magnetosphere boundary, a shock may form with subsequent acceleration of particles on the irregularities introduced into the weaker magnetic field at that radius (see Figure 9.3). If the material where the shock is formed is near corotation with the neutron star the pulse coherence of the particle beam will be retained in the gamma rays produced by decay of the beam. This is helped by the fact that photons emitted parallel to the magnetic field lines are less likely to be absorbed.

9.1.4. Other Acceleration Models

A number of other models have been proposed to attempt to circumvent some of the problems encountered by the acceleration processes described so far. These are generally based on the energy which may be directly available from magnetic instabilities, reconnection and turbulence in the accreting plasma within the neutron star magnetosphere. A typical model of this type is that suggested by Wang (1986) in which sporadic acceleration occurs when an unsteady accretion flow causes plasma instabilities at the magnetospheric

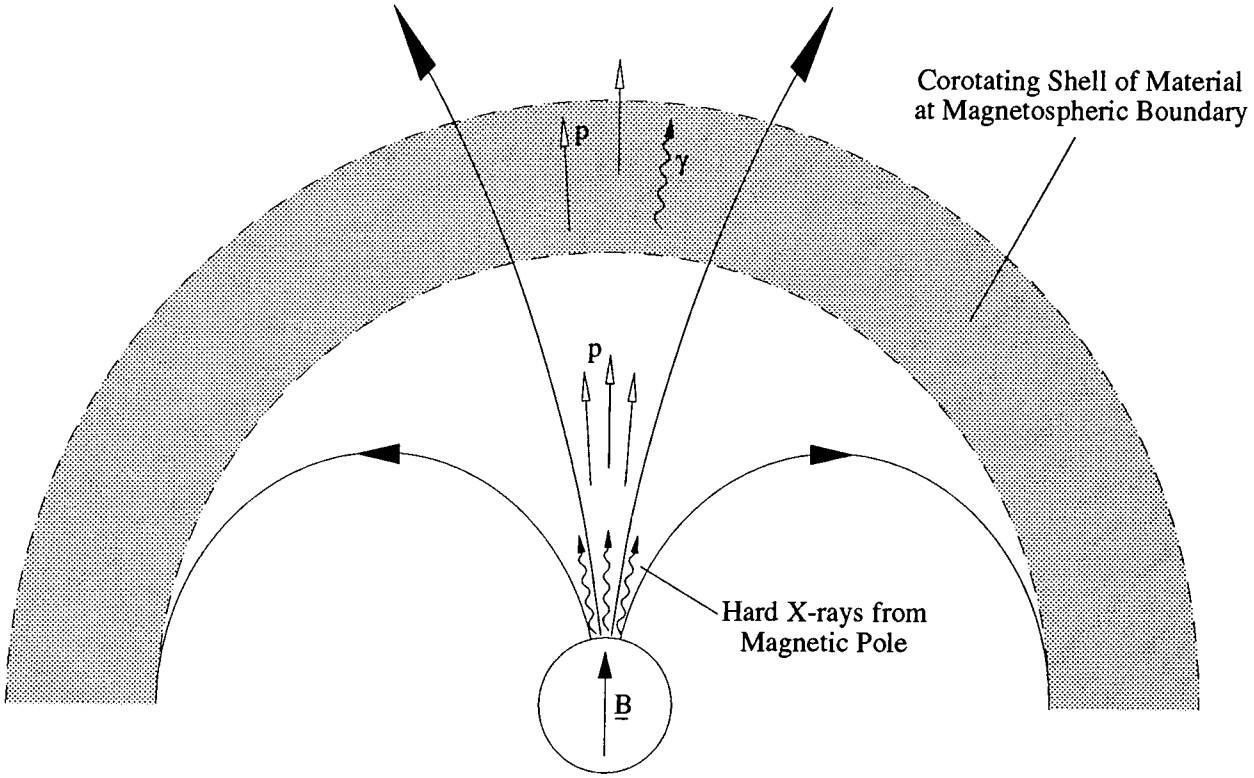

Figure 9.3 : Formation of a collisionless shock where protons ejected from the magnetic poles traverse material corotating with the neutron star at the magnetospheric boundary. The protons are accelerated by repeated coherent scattering in the corotating infalling plasma until they are of sufficient energy to escape and interact with material elsewhere in the system. This diagram shows a view where the axis of rotation is directed into the plane of the paper at a steep angle to the magnetic axis.

(after Kiraly and Meszaros, 1988)

boundary.

A detailed and attractive model was proposed by Katz and Smith (1988) which avoids some of the problems of those previously discussed. This considered protons trapped in the closed field lines near the neutron star, confined in this region by magnetic mirroring at each pole,which could be accelerated gradually with low frictional and collisional energy losses due to the low particle density as compared with the accretion flow.

Acceleration occurs due to reflection from Alfven waves propagating from two sources. The accreting plasma may cause disturbances in the open field lines on a linear scale approximately equal to the Alfven radius r_A which can thus extend as fluctuating fields throughout the closed magnetosphere. Relativistic Alfven waves may also propagate up the accretion column as a result of the "splash" of accreting material onto the neutron star surface. A TeV gamma ray flux may follow the escape of the protons from the closed magnetosphere due to a critical increase in their gyroradii on the field lines. Most of the energy of accretion could be directed into this process due the origin of the Alfven waves in plasma very near the neutron star surface. Katz and Smith also predicted that soft X-ray synchrotron emission from the accelerated protons may be detectable.

More recently, a largely qualitative variation on the disc dynamo model was described by Lamb, Hamilton and Miller (1993). They argued against the accelerator gap model proposed by Cheng and Ruderman (1989, 1991) due to the likelihood of charged particles being pulled from the accretion disc and reducing the vacuum electric potential field. Instead, the Keplerian rotation of the disc winds up the magnetic field of the slower spinning neutron star to an extent whereby magnetohydrodynamic (MHD) instabilities inject plasma from the inner disc into the magnetosphere above. The differential rotation of the disc relative to the star induces an EMF which drives electric currents in the magnetosphere deriving energy from the loss of angular momentum of the disc plasma (see Figure 9.4a). The electric potential generated is

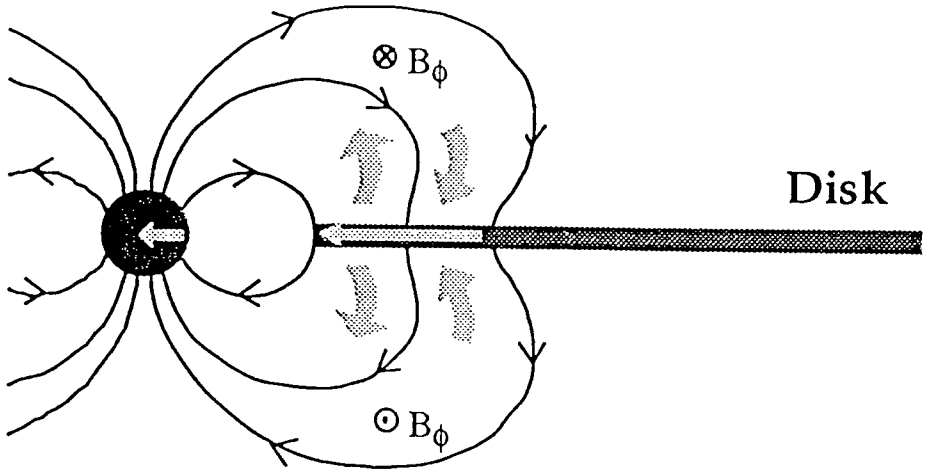

Figure 9.4a : Generation of an EMF in the inner accretion disc caused by the differential orbital motion of the plasma. The EMF gives rise to a current flow across the magnetic field within the disc and a current flow aligned with the field lines in the magnetosphere, indicated by the shaded arrows.

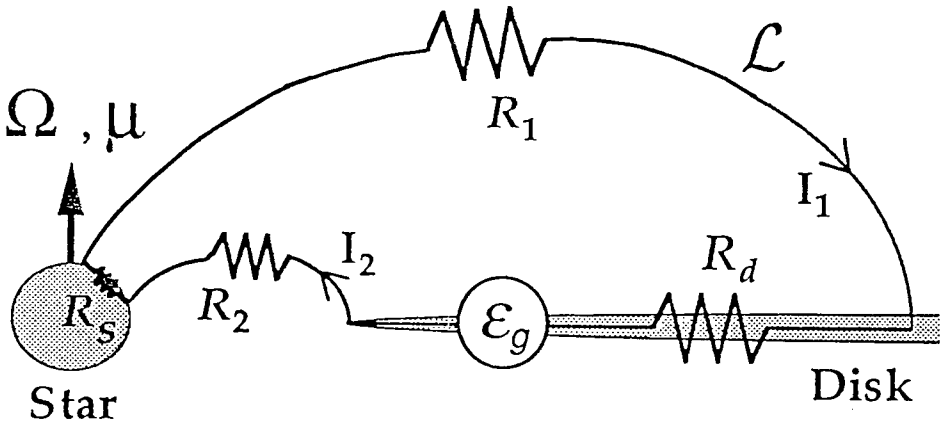

Figure 9.4b : An equivalent circuit showing the EMF generated (ε_g), the circuit inductance L, and the resistances R_d and R_s of the disc and star respectively.

(from Lamb, Hamilton and Miller, 1993)

$$E_{gen} = 10^{15}\ r_8^{-5/2}\ \mu_{30}\ (M/M_o)^{1/2}\ \text{Volts}\ , \qquad (9.12)$$

where r_8 is the magnetospheric radius in units of 10^8 cm and μ_{30} is the stellar magnetic moment in units of 10^{30} G cm^3. The current flowing in the low resistance circuit between the disc and star will grow exponentially until MHD instabilities terminate the increase (see Figure 9.4b). Rather than the E.M.F. being shorted out, particles could be accelerated by the strong currents aligned with the magnetic field due to the twisting of these flux lines. Plasma instabilities formed in the current loop may generate up to 10^{41} erg s^{-1}, with the opposing legs of the circuit accelerating both protons and electrons towards the disc where they may produce TeV gamma rays by pion decay or bremsstrahlung respectively.

9.2. Geometry for TeV Gamma Ray Production in a Binary System

9.2.1. Availability of Target Material for Proton Interaction

Once a proton beam is accelerated to energies of ≥10 TeV, it is capable of producing a substantial flux of TeV gamma rays if it can emerge from the region of the neutron star and interact with target material present in the system. Since most of the material will be confined to near the orbital plane, it is advantageous if the assumed model is capable of directing the particle beam into the region of optimal column density. A proton beam is therefore preferred as the magnetic field near the neutron star can direct the beam into the accretion disc material as shown in Figure 9.5 (Hillas and Johnson, 1991). A neutron beam produced by the photodisintegration of accelerated nuclei near the neutron star offers the advantage of maintaining pulse coherence due to its lack of dispersion in the magnetic field as compared with a proton beam containing particles with a wide range of energies.

Various accretion disc models have been developed and these can be combined with direct X-ray observations to provide values for the expected column density which would be encountered by a particle beam directed into the disc. A standard model due to Novikov and Thorne (1972) gives a value for the

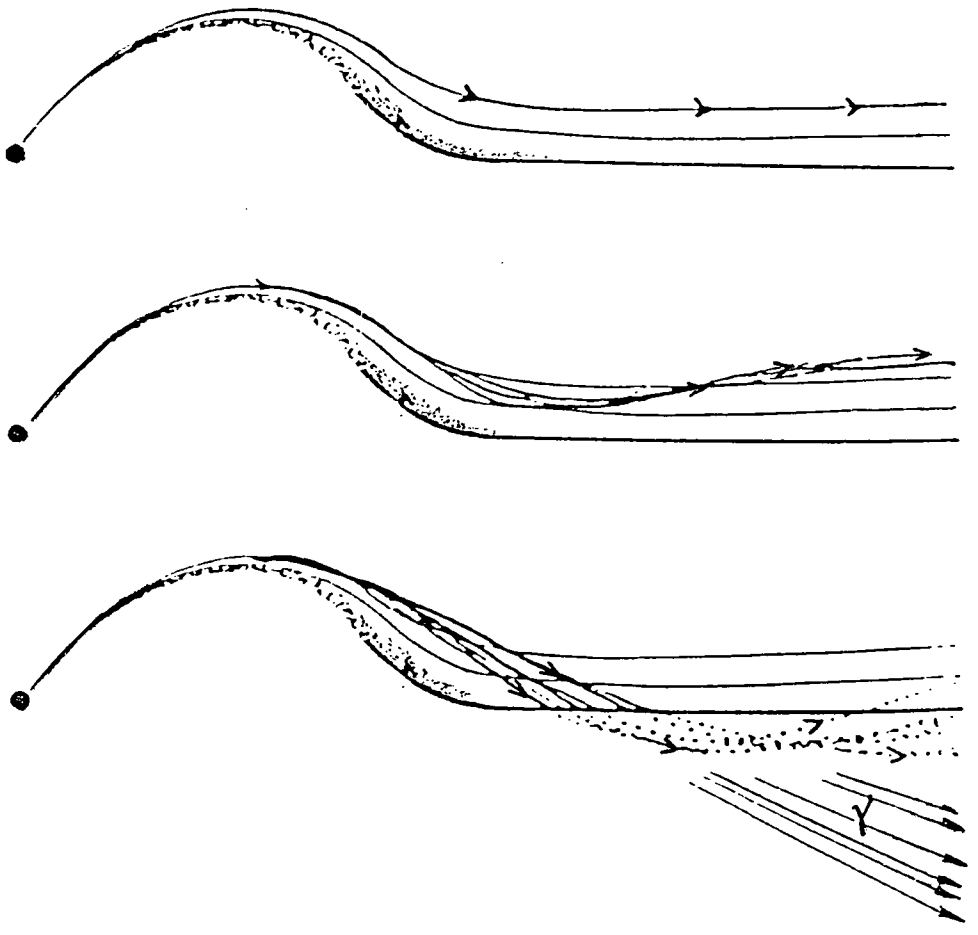

Figure 9.5 : A schematic diagram of the trajectories of protons guided in a spiral along the magnetic field lines originating at the neutron star. The magnetic field is distorted by the presence of the conducting accretion disc and accretion column (dotted region). The arrowed lines show the trajectories for protons with energy <100 TeV, 300 TeV and 1000 TeV reading from top to bottom respectively.

(from Hillas and Johnson, 1991)

column density Z in the inner regions of an accretion disc:

$$Z = 700\ \beta^{-5/2}\ L_{37}^{27/35}\ B_{12}^{-12/35}\ M_o^{-3/35}\ R_6^{-6/7}\ g\ cm^{-2}. \quad (9.13)$$

Due to the unstable nature of many accretion discs, particularly in spherically accreting systems, varying matter densities can certainly occur in the disc which may alter the column density towards the optimal value for gamma ray production of $\approx$50 g cm^{-2} (Stenger, 1984). Such behaviour would also account for the transient nature of some of the observed emission. Another target which has been frequently proposed for gamma ray production is the atmosphere of the companion star (e.g. Hillas, 1984). This is more likely in low mass X-ray binaries since the much greater photon flux from the supergiant primary stars in high mass binaries makes it more difficult for gamma ray photons to escape from the atmosphere without severe energy loss via pair production. Other production regions which have been proposed are the accretion wake which trails the neutron star in a system of unstable accretion, and bulges in the outer part of the accretion disc formed where the gas stream from the primary impacts on the edge of the disc (Protheroe and Stanev, 1987).

9.2.2. Orbital Phase Dependence of Emission

As has already been mentioned, a particle beam of energy $\geq 10^{13}$ eV which interacts with target material will produce a shower of pions and subsequent gamma rays with an angular spread of only a few milliradians. Thus to be detected by an observer, the material responsible must be very near to the line of sight, acting in effect as a giant scintillation screen. It is then clear that in the case of a target in the primary star's atmosphere or an accretion wake, which have permanent positions in the system, the strength of emission should be correlated with the orbital phase of the neutron star. The geometries for these targets are shown in Figure 9.6. For a target in the atmosphere of the companion, the phases of emission should be symmetric about mid-eclipse (though see section 9.2.3.3) and confined to that half of the

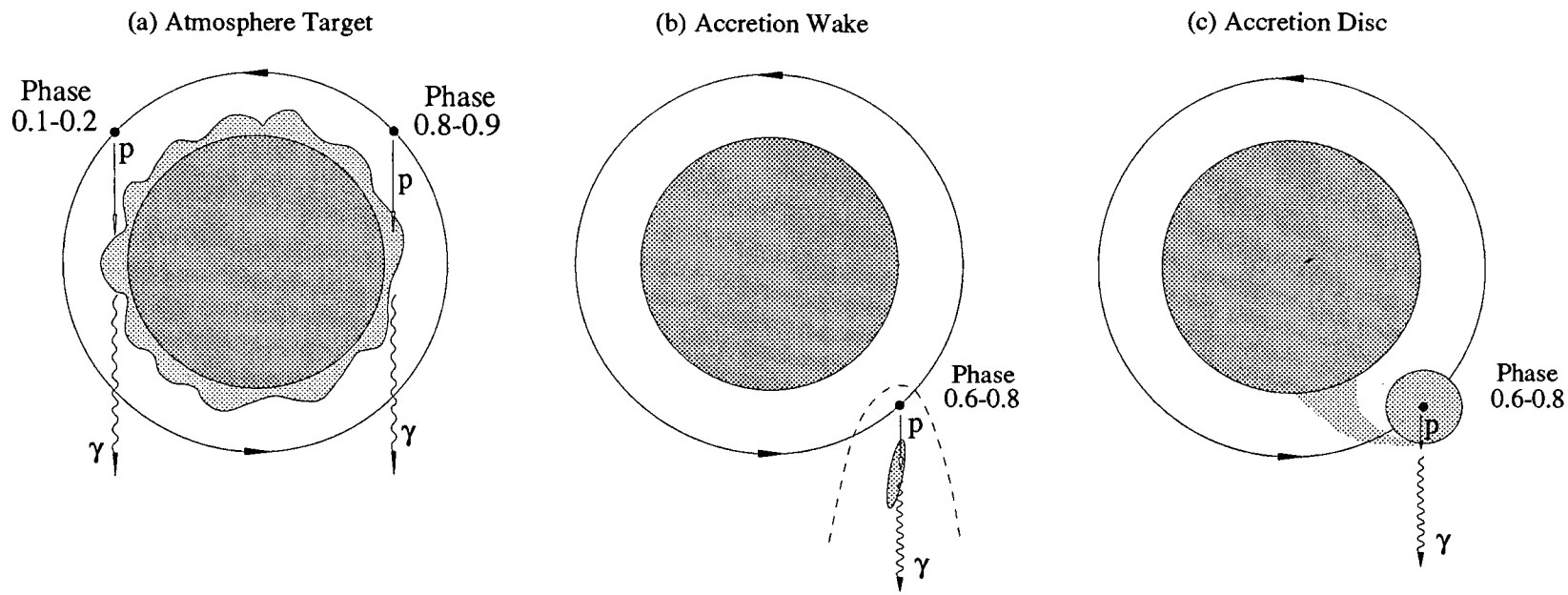

Figure 9.6 : Schematic diagrams of the targets of gas which may be present in the path of a proton beam in an X-ray binary system at a particular orbital phase. In case (a) the atmosphere of the primary star acts as the target, in case(b) the target material is in the accretion wake or shock front, and in case (c) the target is within or at the edge of the accretion disc. The phases at which observable gamma ray production is most likely in each of these targets are indicated.

(after Hillas, 1987)

orbit around the eclipse. A target in an accretion wake, gas stream or in bulges at the edge of the disc should produce gamma rays during the passage through the ascending node of the orbit, corresponding to the intervals of X-ray absorption frequently observed there. In the case of a target in the accretion disc itself, there is no reason why any phase dependence should occur, other than absorption of the signal during X-ray eclipse.

A caveat on these conclusions was provided by Moskalenko and Karakula (1993). These authors discussed the phase dependence of emission induced by absorption in the photon field of the primary star. In general it is expected that the emission will be confined to the interval where the gamma ray production region is between the observer and the luminous star (i.e. either side of inferior conjunction at phase 0.5) with the precise interval depending on the parameters of the orbit. However, these results will undoubtedly also be modified by absorption of the visible photons in the target material responsible for the gamma ray flux.

9.2.3. Particle Beam Steering

The modification of the gamma ray emission by steering of the beam of energetic charged particles in the magnetic field of the primary star has been studied by a number of authors (see below). Whilst the magnetic fields of the non-degenerate stars in X-ray binaries are not known, they may be estimated to be typically of the order of 0.01 to 1 G for early type supergiants, and up to 10^3 G for late type dwarfs. Over the path traversed by a proton outside the neutron star magnetosphere, fields of this strength are sufficient to deviate the proton trajectory by a significant amount. The weaker field present in a high mass binary is compensated by the much longer path of the proton beam in these systems.

Beam steering was originally proposed to explain the observation of bursts of gamma rays from Hercules X-1 whilst the X-ray source was in eclipse (Gorham and Learned, 1986; Gorham et al., 1987; Dowthwaite et al., 1984a) as shown in Figure 9.7. The curvature of the proton beam is given by the

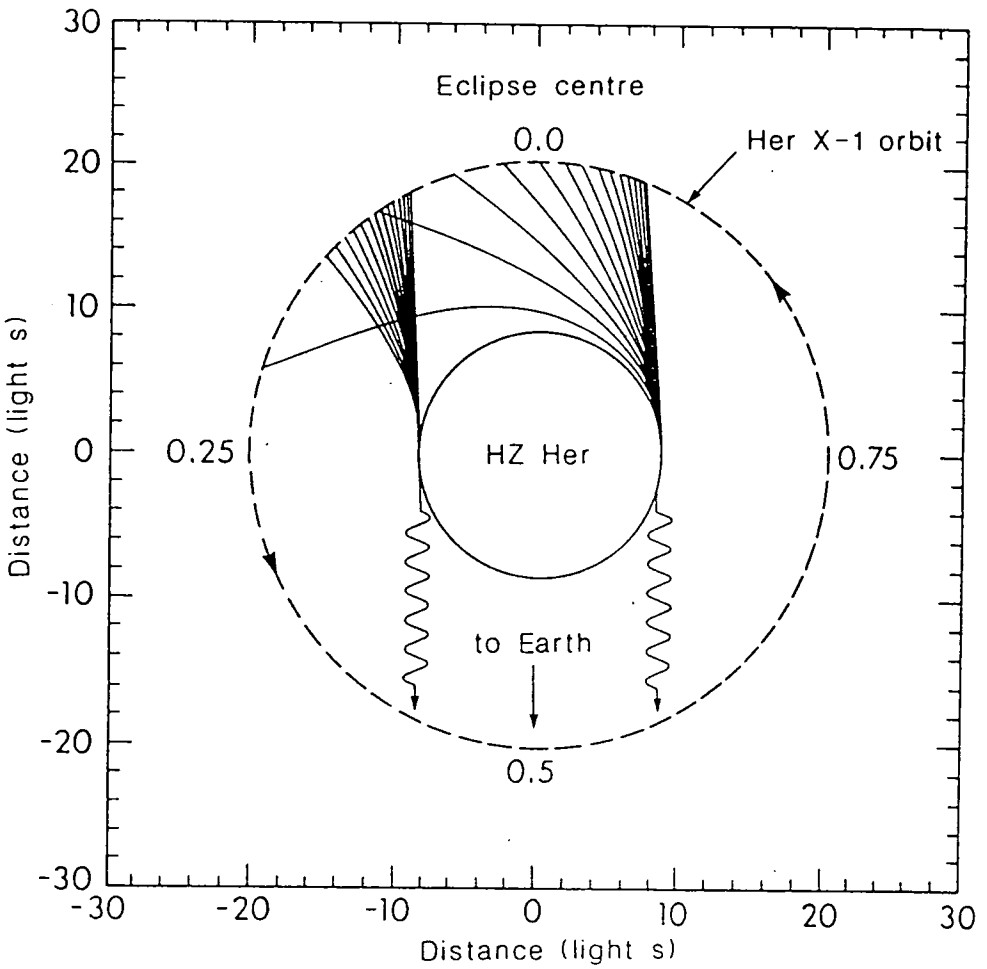

Figure 9.7 : Modified trajectories of protons steered in the magnetic field of the primary star in the Hercules X-1 binary system. The situation shown is that where the gamma rays produced at either limb of the primary star will be visible at the Earth. The protons originate at the neutron star and have energies ranging from 0.4 TeV at the left to 140 TeV at the right. The latter higher energy photons experience least deflection.

(from Gorham and Learned, 1986)

gyroradii of the particles in the dipolar field of the primary star, whilst the radial direction is given by the Lorentz force vector. The deflection experienced by a particle is inversely proportional to its energy and thus low energy particles may have their directions reversed back towards the neutron star imposing a low energy cut-off in the spectrum of gamma ray emission. In addition, a particle beam including a wide spectrum of energies may be deflected by differing amounts so that pulse phase coherence is reduced and any remaining gamma ray eclipse can become highly asymmetric. Similar considerations were applied by Mannings (1990, 1992) to explain observations of bursts from Vela X-1 around the time of eclipse (North et al., 1989).

9.3. Application to the Present Observations

9.3.1. Initial Considerations

To assess how the models of TeV gamma ray production may be applied to the X-ray binaries discussed in Chapters 6 to 8, it is necessary to determine the relevant parameters and assumptions required to perform some of the calculations involved. These considerations are given here, primarily with relevance to Centaurus X-3, Vela X-1 and SMC X-1.

It is evident from the work described in section 9.1 on theories of particle acceleration that much depends on the configuration and strength of the neutron star's magnetic field. Whilst the canonical value of 10^{12} G for the field strength provides a good starting point, direct information on the magnetic field is limited mainly to observations of cyclotron features in the X-ray spectra of these binary systems, which may be both weak and transient. A secondary method of estimating the magnitude of the field is to use the knowledge of the behaviour of the pulsar period (e.g. Henrichs, 1983; Fabbiano and Schreier, 1977). The relationship of the Alfven radius r_a and the corotation radius r_{co} was discussed in Chapter 5. Briefly, where the accretion rate is sufficient to make $r_a < r_{co}$, the accreting material inside r_{co} tends to drag the field lines along thereby increasing the spin-up rate and

eventually reducing r_{co} until an equilibrium is restored. The equilibrium state then corresponds to a near constant spin-up rate and the surface magnetic field may be estimated from combining equations 9.4 and 9.8.

The X-ray luminosity L_x derived from accretion is another important parameter and is usually a variable quantity. The mean luminosity is assumed here unless otherwise stated, as contemporary luminosity measurements are rarely available. This luminosity is assumed to result from the conversion of gravitational potential energy of the infalling material at the neutron star surface, a process with an efficiency of $\approx$10%.

Some models for the acceleration of particles via the action of a dynamo mechanism tapping energy from the inner regions of the disc require the evaluation of the inner and outer radii of the disc. Where such models are applied here, the inner radius is taken as the Alfven radius of the neutron star magnetosphere and calculated using equation 9.4. The outer radius is subject to much more uncertainty but may be reasonably estimated from the size of the Roche lobe of the neutron star, as indicated from measurements and simulations of the optical light curve (e.g. Tjemkes, Zuiderwijk and van Paradijs, 1986). The extent of the Roche lobe may be estimated using equation 5.3.

9.3.2. TeV Gamma Ray Production in Centaurus X-3

9.3.2.1 Acceleration of Particles

The observations of Centaurus X-3 described in Chapter 6 enable some speculations to be made here on the nature of high energy particle production in the system. The pulsar period behaviour has been found to show intervals of both spin-up and spin-down on short timescales within the confines of an unpredictable long term spin-up. This suggests that the neutron star is rotating at a period very near to its equilibrium value with the precise period being very sensitive to changes in the unsteady accretion rate. A natural explanation of this would be to suppose that the Alfven radius of the

magnetosphere is usually just within the corotation radius. Assuming that the average luminosity of $\approx 5 \times 10^{37}$ erg s^{-1} is the flux emitted when the accretion rate is relatively stable, the surface magnetic field required to maintain the position of the Alfven radius r_a within r_{co} is $\leq 3 \times 10^{12}$ G. A similar conclusion was reached by van der Klis, Bonnet-Bidaud and Robba (1980). A value of 3×10^{12} G is used in the calculations made here.

Other physical parameters of Cen X-3 are given in Table 9.1, the values being taken from the review by Nagase (1989) and calculated using expressions given in this chapter. Within the limits of the assumptions made, these may be used for comparison with the results of the analysis reported in Chapter 6. In particular, we seek an explanation of the gamma ray luminosity of $\approx 4 \times 10^{35}$ erg s^{-1} ($\geq$300 GeV) detected in the orbital phase range 0.77-0.81. An upper limit of 2×10^{35} erg s^{-1} above 300 GeV was placed on the persistent emission from this source. A scale diagram of the system showing the optimal phase range for gamma ray emission is shown in Figure 9.8.

Initially the possibilities for acceleration of particles to very high energies must be considered. Given the probable existence of a stable accretion disc in the system, the range of models for an accretion disc dynamo mechanism must be studied. The major requirement is to ensure that a sufficient acceleration voltage can be generated. Table 9.2 gives the maximum acceleration voltages which may be derived from the models used to provide the expressions given in equations 9.3, 9.9, 9.11 and 9.12. It is clear that all three models used are capable of producing the potential drop required, as would be expected from their design requirements given the typical parameters found in Cen X-3. The models of Chanmugam and Brecher (1985) and Cheng and Ruderman (1989, 1991) depend greatly on the maintenance of a full vacuum electric potential in the absence of thermal plasma in the accelerating region. For the conditions found at the inner regions of the disc, this is unlikely, as indicated by satellite observations of strongly pulsed Fe line emission originating in a reprocessing site within the magnetospheric boundary

TABLE 9.1 - Parameters of the Cen X-3 binary system

Eclipse Semi-angle	:	35° - 40°
Inclination	:	75° (+12°/-13°)
Stellar Separation	:	43.9 (+3.0/-2.3) ls
Companion Radius	:	28.3 (+4.6/-3.5) ls
Primary Mass	:	19.8 (+4.5/-2.7) M_o
Neutron Star Mass	:	1.06 (+0.56/-0.53) M_o
X-ray Luminosity	:	10^{37} - 10^{38} ergs s^{-1}
Corotation Radius	:	4.4 x 10^8 cm
Neutron Star Magnetic Field	:	$\approx$ 3 x 10^{12} G
Alfven Radius	:	4.2 x 10^8 cm for 5 x 10^{37} erg s^{-1}
		3.4 x 10^8 cm for 10^{38} erg s^{-1}
Roche Lobe Radius for Neutron Star	:	$\approx$ 8 ls

Values for orbital and stellar parameters are taken from Table 4 of Nagase (1989) and references therein.

The corotation radius, Alfven radius and Roche lobe radius were calculated using equations 9.10, 9.4 and 5.3.

The above also applies to Tables 9.3 and 9.5.

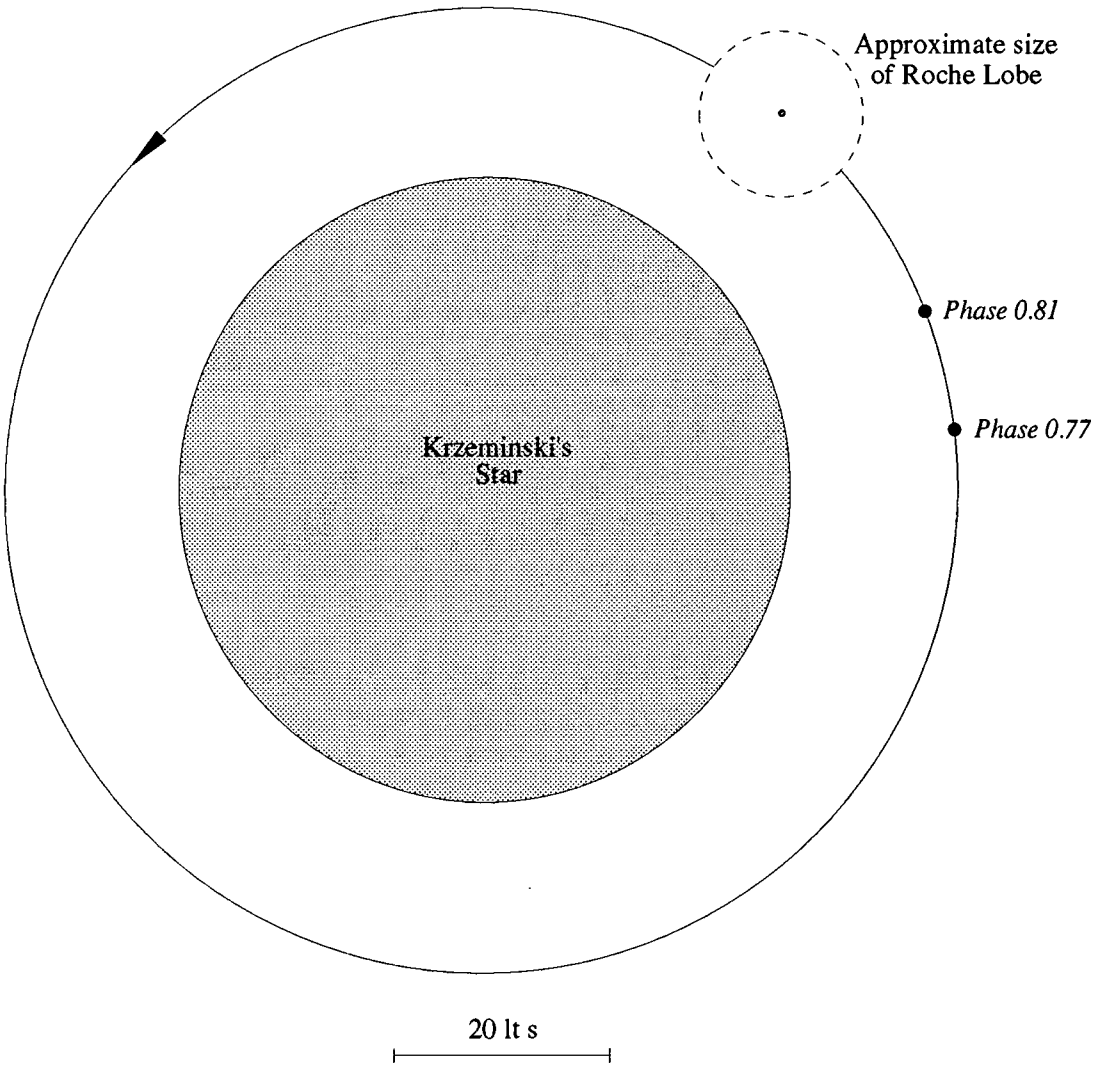

Figure 9.8 : Illustration of the Centaurus X-3 binary system showing the relative sizes of the components. The interval of strongest evidence for TeV gamma ray emission is indicated between orbital phases 0.77 and 0.81.

The size of the Roche lobe of the neutron star is calculated using the expression from Paczynski (1971) given in the text. This indicates the likely maximum extent of the accretion disc and the region around which an accretion wake or a temporary gas stream may form.

TABLE 9.2 - Particle acceleration in Centaurus X-3

(assuming 3×10^{12} G surface magnetic field)

	Low Intensity ($L_{37} = 5$)	High Intensity ($L_{37} = 10$)
Magnetic Field at r_a (Gauss)	3.8×10^4	7.6×10^4
Maximum Accretion Power at r_a (erg s^{-1})	1.2×10^{35}	2.9×10^{35}
Column Density of Accretion Disc (g cm^{-2})	1.8×10^3	3.7×10^3
Maximum Voltage in CB Model (Volts)	6.3×10^{14}	1.1×10^{15}
Maximum Voltage in CR Model (Volts)	8.0×10^{14}	1.3×10^{15}
Maximum Voltage in CR Model with Pair Production (Volts)	1.7×10^{13}	3.5×10^{13}
Maximum Power in CR Model (erg s^{-1})	2.9×10^{35}	7.2×10^{35}
Maximum Voltage in LHM Model (Volts)	8.7×10^{13}	1.4×10^{14}

Key to Abbreviations for Acceleration Models

CB : Chanmugam and Brecher, 1985

CR : Cheng and Ruderman, 1991

LHM : Lamb, Hamilton and Miller, 1993

This key is also used in Tables 9.4, 9.6, 9.8 and 9.9

(Day et al., 1993). The model of Lamb, Hamilton and Miller (1992) predicts lower voltages in the magnetospheric current loop but these are still able to give the particle energies required to generate TeV photons, especially in intervals of high X-ray luminosity.

The strong magnetic field makes shock acceleration processes unlikely. The mechanisms of Katz and Smith (1988) and Kiraly and Meszaros (1988) could be viable, provided that the configuration of the innermost magnetic field is suitable.

The observed power of 4×10^{35} erg s^{-1} in TeV gamma rays provides some problems in its explanation. It can be seen from the table that this is in excess of the maximum accretion power available at the Alfven radius, and comparable to the power produced in the accelerator gap model of Cheng and Ruderman in which the energy is released about twice as near to the stellar surface. A more detailed calculation of the Alfven radius for a disc accretor may yield a slightly lower value of r_a (e.g. Kiraly and Meszaros, 1988) and thus luminosities in excess of 10^{36} erg s^{-1} may be attainable. Nevertheless, this still causes problems for some of the models since the efficiency of photon production via pion decay is only ≈10% of the primary particle flux (e.g. Cheng and Ruderman, 1991) and electron pair cascades can rapidly degrade the photon energy below TeV energies. It is necessary to invoke either strong beaming of the emission or an acceleration zone nearer the neutron star, as suggested by Kiraly and Meszaros (1988). The latter would produce an isotropic particle flux and hence reduce the luminosity available for subsequent pion decay in target material (Hillas and Johnson, 1991).

9.3.2.2. Gamma Ray Production in Target Material

Consideration of the nature of the particle beam requires a number of points to be made. Firstly, gamma rays of energy 1 TeV must be generated at least 20 neutron star radii from the stellar surface so as to avoid pair production in the transverse magnetic field (equation 5.7). Although this

allows a production site within the magnetosphere, the hard X-ray flux from the neutron star makes this unlikely. Equation 5.9 shows that the low accelerating voltages in Cen X-3 reduce the likelihood of photopion production from the high energy protons.

The problem of the high resultant luminosity may be avoided if the particle beam is steered along the magnetic field lines into target material in the plane of the system as described by Hillas and Johnson (1991). Whilst the accelerator gap model of Cheng and Ruderman assumes a virtually undistorted field, Hillas and Johnson considered the modification by the conducting disc which steers particles almost parallel to its plane. This of course assumes that the beam is composed of protons. A neutron beam could give the advantage of reducing the problems of the production of coherent pulses and the narrow phase range in which emission is observed, both of which require a narrow beam, but would have difficulty in being directed into the disc plane unless nuclear photodisintegration should occur in transit. Given two particle beams each of solid angle Ω, the particle luminosity may be reduced by a factor $\Omega/2\pi$, and the total flux to around 10^{33} erg s^{-1} in a well-collimated beam.

As regards the likely target for gamma ray production at orbital phase 0.77-0.81, the options seem to be the accretion disc, an accretion wake or a gas stream. The geometry rules out production at the limb of the primary. There is also no support for such a production site from the spatially resolved analysis reported in Chapter 6. Table 9.2 gives the typical column density calculated for the inner accretion disc from equation 9.13. For Cen X-3 this is found to be of the order of 2000 g cm^{-2}, but allowing for the $r^{-1/2}$ dependence in this value from the standard disc model (Shakura and Sunyaev, 1973) this density is reduced to a more promising $\approx$100 g cm^{-2} in the outer regions. A gamma ray beam steered into this disc at a sufficient distance from the star would however encounter a greater thickness of material due to the inclined angle of incidence.

Ginga observations of a pre-eclipse dip (Nagase et al., 1992) showed that the absorbing material had a column density of $\approx 10^{24}$ H cm^{-2} corresponding to a grammage of ≈1-10 g cm^{-2}. The latter value could give TeV gamma ray production with an efficiency of ≈30% that of the optimal 50 g cm^{-2} (see Figure 5.6) and temporary enhancements could occur due to either an increased accretion rate or the passage of a shock front through the line of sight. However as Petterson (1978) pointed out, the absorption seen beyond phase 0.75 argues against the accretion wake model, favouring instead a gas stream as the cause of the absorption.

The width of the interval 0.77-0.81 corresponds to a projection of 3 ls perpendicular to the line of sight, or ≈6 ls allowing for the average length of an observation used in this work. Thus an unstable or uncaptured gas stream from the primary could account for the observed emission if interacting anywhere with the edge of the disc. Note also that the dips typically last for up to ≈0.05 in orbital phase and thus gamma ray emission would be expected to last throughout a single TeV gamma ray observation rather than appear as a shorter burst. Gamma ray emission may "turn on" near phase 0.75 as the material in the line of sight becomes sufficient for a detectable TeV photon flux to be generated. This assumes a somewhat unrealistic step function change in column density between a tenuous gas stream and a much denser disc. Since the state of accreting material is likely to be highly complex, material in the general region of the disc could have a range of densities between those of the stream and the disc, perhaps giving rise to weak persistent emission from material located away from the disc plane.

9.3.3. TeV Gamma Ray Production in Vela X-1

9.3.3.1. Particle Acceleration

Vela X-1 differs from Cen X-3 in a number of respects, particularly the much lower X-ray luminosity due to accretion from the stellar wind. Another factor of great relevance here is the surface magnetic field of the neutron

star. It was pointed out in Chapter 7 that direct observations have indicated that this field is somewhere in excess of 10^{13} G, and here the field is estimated for the present application.

Table 9.3 gives the range of physical parameters for Vela X-1. The long pulsar period sets the value of the corotation radius r_{co} at $\approx 8 \times 10^9$ cm. The behaviour of the pulse period suggests that the Alfven radius r_a is likely to oscillate about this value depending on the actual nature of mass accretion. Borner et al. (1987) discussed how material accreting spherically onto the magnetosphere could settle into a disc, removing angular momentum from the neutron star and thus causing a long term spin down unless disrupted by the passage of a density enhancement in the wind. Such an argument for the formation of a temporary disc in this spherically accreting system was supported by the work of Matsuda, Inuoe and Sawada (1987) and Haberl and White (1989). As seen in Table 9.3 for typical X-ray luminosities of Vela X-1, a field of $\approx 5 \times 10^{13}$ G is required to bring r_a near to r_{co}, and this value is used here. A scale diagram of the system is shown in Figure 9.9.

The bursts discussed in Chapter 7 required a photon flux above 300 GeV of $\approx 1 \times 10^{35}$ erg s^{-1} at the source, lasting for about 30 minutes. The long term emission previously reported by the Durham group corresponded to a source luminosity of $\approx 3 \times 10^{34}$ erg s^{-1}. As a disc may be present in the system, the maximum voltages generated in the disc dynamo models were calculated and are listed in Table 9.4 for two states of X-ray luminosity. It can be seen that the voltages are relatively low, two orders of magnitude below those found for Cen X-3, but may be able to produce a flux of TeV protons especially in the highest luminosity states. The pair production limit placed on the Cheng and Ruderman model rules out the maintenance of a plasma gap with a potential drop sufficient to generate TeV protons, leaving the current loop model of Lamb, Hamilton and Miller as the most plausible.

The very strong magnetic field near the neutron star makes shock acceleration processes highly unlikely. The jet model of Kiraly and Meszaros

TABLE 9.3 - Parameters of the Vela X-1 binary system

Eclipse Semi-angle	:	$33^{\circ} - 36^{\circ}$
Inclination	:	$83^{\circ} \pm 6^{\circ}$
Stellar Separation	:	122.8 (+2.1/-1.9) ls
Companion Radius	:	78.9 ± 2.5 ls
Primary Mass	:	23.0 (+1.2/-0.9) $M_{\odot}$
Neutron Star Mass	:	1.77 ± 0.21 $M_{\odot}$
X-ray Luminosity	:	$10^{35} - 10^{36}$ ergs s^{-1}
Corotation Radius	:	7.9×10^{9} cm
Neutron Star Magnetic Field	:	$\approx 5 \times 10^{13}$ G
Alfven Radius	:	8.4×10^{9} cm for 5×10^{35} erg s^{-1}
		6.9×10^{9} cm for 10^{36} erg s^{-1}
Roche Lobe Radius for Neutron Star	:	$\approx$ 24 ls

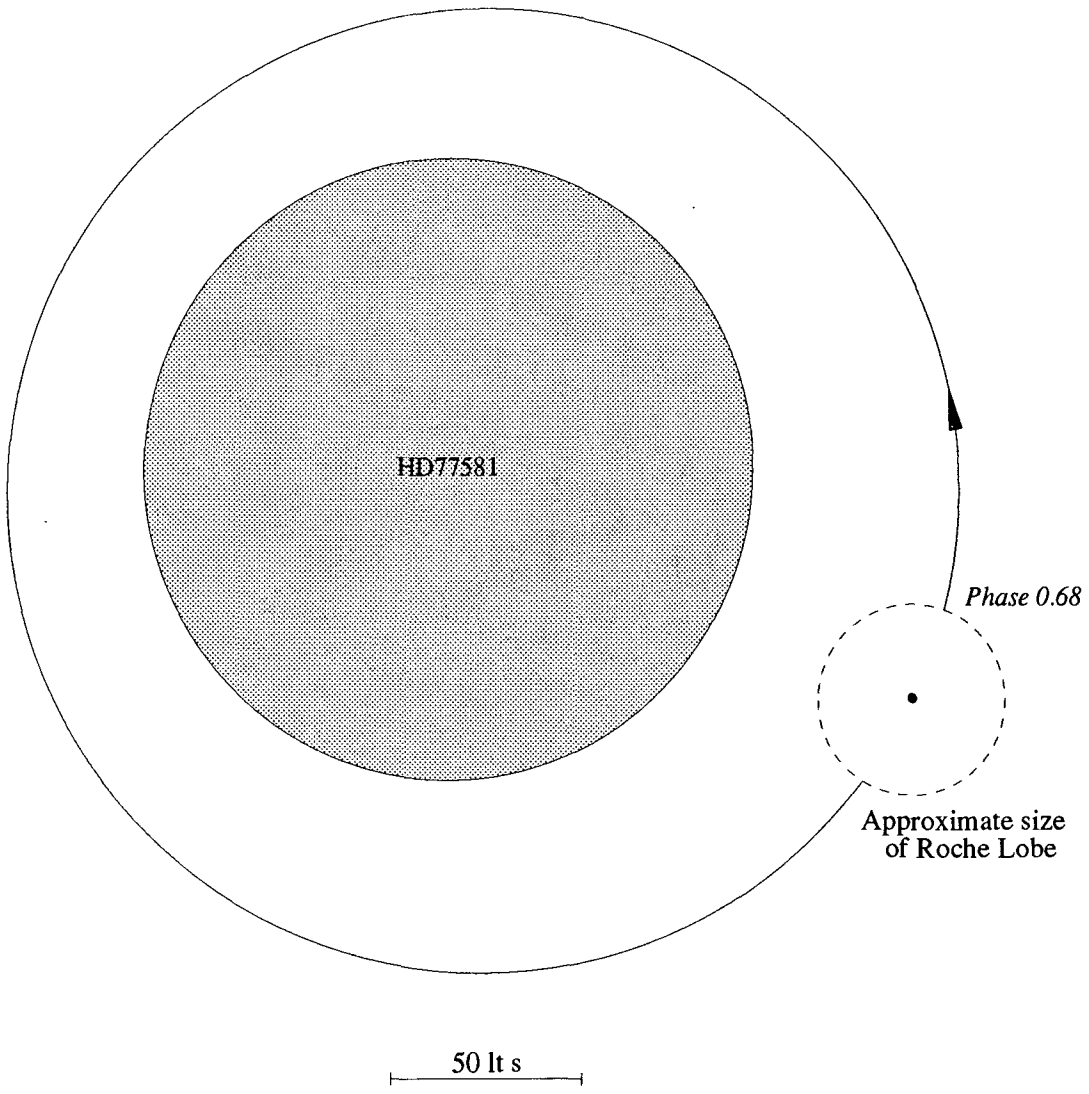

Figure 9.9 : Illustration of the Vela X-1 binary system showing the relative sizes of the components. The positions of the neutron star and its Roche lobe are shown at the orbital phase at which the bursts identified in the present work were detected.

TABLE 9.4 - Particle acceleration in Vela X-1

(assuming 5×10^{13} G surface field)

	Low Intensity ($L_{37} = 0.05$)	High Intensity ($L_{37} = 0.1$)
Magnetic Field at r_a (Gauss (Gauss)	84	150
Maximum Accretion Power at r_a (erg s^{-1})	6.0×10^{31}	1.5×10^{32}
Column Density of Accretion Disc (g cm^{-2})	6.7	13.4
Maximum Voltage in CB Model (Volts)	5.4×10^{12}	9.2×10^{12}
Maximum Voltage in CR Model (Volts)	9.6×10^{12}	1.6×10^{13}
Maximum Voltage in CR Model with Pair Production (Volts)	4.2×10^{10}	8.5×10^{10}
Maximum Power in CR Model (erg s^{-1})	1.5×10^{32}	3.6×10^{32}
Maximum Voltage in LHM Model (Volts)	1.0×10^{12}	1.7×10^{12}

requires a shell of material in corotation with the neutron star, which is difficult to maintain given the unstable accreting process. The strong field may lend support to the plasma turbulence models outlined by Katz and Smith (1988), Wang (1986) and Lamb, Hamilton and Miller (1993) due to the large amount of energy which would be available from a magnetic reconnection event, especially on short timescales.

It may be noted from Table 9.4 that the luminosities available from accretion at the Alfven radius are at least two orders of magnitude below even the lowest steady state value reported at TeV energies. Thus substantial beaming must be invoked, or an acceleration site much nearer the stellar surface. Wang (1986) demonstrated that long wavelength plasma disturbances, e.g. a Rayleigh-Taylor instability, at the magnetospheric boundary could allow plasma to penetrate much deeper than the Alfven radius and thus gain more energy for acceleration on the reconnection of current sheets in the plasma. This complex procedure may be related to the explanation of a single-peaked X-ray outburst as put forward by Borner et al. (1987) who suggested that a concentration of accreting material could be trapped over one of the magnetic poles by an azimuthal instability sustained for several pulsar rotations.

9.3.3.2. Production of TeV Photons

The site of gamma ray production in Vela X-1 should be at least ≈60 neutron star radii from the stellar surface to avoid pair production in the magnetic field (from equation 5.7). This is well within the magnetosphere so that coherent pulses could be produced here, but as for Cen X-3 the intense X-ray flux from the neutron star makes such proximity to the neutron star unlikely.

The maintenance of pulse coherence is easier for this system than most due to the period of 283 s and the long duty cycle. A proton beam should be able to produce the observed pulsation without recourse to neutral particle production. Mannings (1992) showed that TeV gamma ray observations of this

source in eclipse supported the model of a charged particle beam being steered into the limb of the primary star. As for Cen X-3 the model of Hillas and Johnson (1991) for the steering of the particle beam by the neutron star field into the orbital plane can also be applied to Vela X-1. The problem of divergence of this beam due to the energy range of the particles is reduced here since as discussed earlier, the maximum voltage available for acceleration may only be $\approx 10^{12}$ V resulting in a narrow range of energies sufficient to give high energy gamma ray production. This argument also favours gamma ray production directly from pion decay rather than through an electromagnetic cascade which would rapidly degrade the photon energies.

Possible targets for gamma ray production in this system are as normally postulated for X-ray binaries. As can be seen from Table 9.4 the column density of the inner disc in the high luminosity state is ≈ 20 g cm^{-2}. Allowing for the inclined path of the proton beam, required to direct TeV photons into the line of sight, a column density approaching the optimal 50 g cm^{-2} may easily be achieved. As pointed out by Cheng and Ruderman (1991) this indicates that Vela X-1 could be a persistent source of gamma ray emission, as seen by the Potchefstroom and Durham groups, for as long as an accretion disc exists. The bursts seen by the Potchefstroom groups could be explained by the passage of the proton beam through a low energy window in the disc and into the limb of the primary.

To explain the transient high luminosity bursts reported here requires a more transient target. At a phase of 0.68, a target in a gas stream, shock front or a bulge in the outer disc would all be possible. The orbital searching technique applied in this work is unable to achieve sufficient spatial resolution to determine the precise site of emission. Very high absorbing densities of 10^{24}-10^{25} H cm^{-2} (grammages of 2-20 g cm^{-2}) have been postulated to account for the dips seen around the region of the ascending node (e.g. Staubert et al., 1980; Nagase et al., 1984a; Lapshov et al., 1992) and would be acceptable as a target for TeV gamma ray production by pion

decay. Whilst these dips may also arise from a quenching of the accreting material by a reduction in the stellar wind flow, without measurements of an accompanying decrease in the pulse period, neither of the two possibilities can be discounted. The variable low energy X-ray cut-off in Vela X-1 tends to support an absorber as the cause (Staubert et al., 1980). A GRANAT observation of a severe intensity dip lasting for several hours on 1991 January 9 was made at an orbital phase of ≈0.73, only 4 orbital cycles before the first of the bursts reported here, suggesting that a quasi-stable absorber may have been present in this interval for at least ≈40 days.

It may also be noted that the orbital phase 0.68 corresponds almost exactly to the time of passage of the neutron star through apastron (its most distant position from the primary star). Given the low eccentricity of 0.08, some kind of tidal resonance effect, whilst an interesting channel for further investigation, would seem difficult to demonstrate.

9.3.4. TeV Gamma Ray Production in SMC X-1

The steady spin-up of the SMC X-1 pulsar period since its discovery suggests that the neutron star is revolving in its equilibrium state with a good balance of r_a and r_{co} being maintained at the magnetospheric boundary. The high average X-ray luminosity of $\approx 5 \times 10^{38}$ erg s^{-1} is attributed to the efficient transfer of material through the disc onto the neutron star. Combining this value of L_x with the balance of r_a and r_{co} yields a surface magnetic field for the neutron star very near the canonical 10^{12} G. The high density of the inner disc may affect the process of restoration of equilibrium rotation. A value of 1×10^{12} G is used in this treatment. The other physical parameters given in Table 9.5 are from Nagase (1989) and the equations given in this chapter.

Unlike Cen X-3 and Vela X-1, no significant flux of TeV gamma rays has been detected from SMC X-1. In this work a limit of $\approx 6 \times 10^{37}$ erg s^{-1} was placed on the photon luminosity above 300 GeV observed in any of the 132

TABLE 9.5 - Parameters of the SMC X-1 binary system

Eclipse Semi-angle	:	26.5^{o} - 29^{o}
Inclination	:	65^{o} ($+12^{o}/-9^{o}$)
Stellar Separation	:	62.9 (+4.9/-4.7) ls
Companion Radius	:	37.8 (+7.8/-8.0) ls
Primary Mass	:	16.8 (+4.2/-3.5) M_{o}
Neutron Star Mass	:	1.06 (+0.33/-0.31) M_{o}
X-ray Luminosity	:	10^{38} - 10^{39} ergs s^{-1}
Corotation Radius	:	1.2×10^{8} cm
Neutron Star Magnetic Field	:	$\approx 1 \times 10^{12}$ G
Alfven Radius	:	1.1×10^{8} cm for 5×10^{38} erg s^{-1}
Roche Lobe Radius for Neutron Star	:	$\approx$ 12 ls

observations made. The earlier work by Mannings (1990) placed a limit of 1.5 x 10^{37} erg s^{-1} on the flux recorded on a timescale of ≈10 days. Due to the remoteness of this object these limits are an order of magnitude or more greater than the fluxes detected at the Earth from any galactic TeV gamma ray sources, but in neither limit is the X-ray luminosity exceeded. It is therefore interesting to calculate the fluxes predicted by the production models described in this chapter. Table 9.6 lists the accelerating voltages which are predicted by the accretion based models. It is apparent that all, even the pair production limited voltage from Cheng and Ruderman (1991), are capable of producing protons with the required energy. Allowing for the efficiency of photon production via pion decay, gamma ray energies of around 10 TeV can be reached.

The accretion luminosity available at the Alfven radius is ≈5 x 10^{36} erg s^{-1}, increasing to ≈10^{37} erg s^{-1} in the model of Cheng and Ruderman, which is below the limits derived by TeV gamma ray observations. Again, beaming of the gamma ray flux could reduce the actual luminosities required. Allowing for the distance to SMC X-1, the actual photon flux at the Earth would be somewhat lower than that expected from Cen X-3 (at a distance of 8 kpc compared with the 65 kpc of SMC X-1).

A site for TeV gamma ray production must be well removed from the inner regions of the accretion disc due to the intense X-ray flux from the neutron star and the high column density of the material in the inner disc (≥10^4 g cm^{-2}). Even at the outer regions of the 10 ls disc, the density is only reduced to ≈300 g cm^{-2}. A particle beam could therefore only produce a detectable flux of gamma rays if directed into material of lower density well out of the disc plane. In high X-ray intensity states of this system, absorption dips are not seen (e.g. Bonnet-Bidaud and van der Klis, 1981). Therefore the column density of material in the system may not often be suitable for TeV gamma ray production.

The pulse period of 0.71 s is one of the shortest in any X-ray binary

TABLE 9.6 - Particle acceleration in SMC X-1

(assuming 1×10^{12} G surface field)

	$L_{37} = 50$
Magnetic Field at r_a (Gauss)	7.5×10^5
Maximum Accretion Power at r_a (erg s^{-1})	4.6×10^{36}
Column Density of Accretion Disc (g cm^{-2})	1.4×10^4
Maximum Voltage in CB Model (Volts)	7.3×10^{15}
Maximum Voltage in CR Model (Volts)	6.6×10^{15}
Maximum Voltage in CR Model with Pair Production (Volts)	3.0×10^{14}
Maximum Power in CR Model (erg s^{-1})	1.1×10^{37}
Maximum Voltage in LHM Model (Volts)	8.1×10^{14}

system and if this is to remain as a coherent pulse at TeV energies the divergence of the proton beam must be minimised. The divergence of the beam will increase with the distance from the neutron star and hence a neutron beam would be a more favourable option in this system. The high X-ray flux would assist in this respect by enabling more efficient photodisintegration of the accelerated nuclei.

9.3.5. TeV Gamma Ray Production in Low Mass X-ray Binaries

9.3.5.1. 4U1626-67

In the case of 4U1626-67, direct observations of the X-ray spectra and pulse profiles have suggested that this system contains a neutron star with a surface field of $\approx 5 \times 10^{12}$ G (Kii et al., 1986; Pravdo et al., 1979). Measurements of the pulse period behaviour of this object suggest that the interaction of the accreting material with the magnetosphere is well-balanced The assumption of a neutron star surface field of 5×10^{12} G allows the near balance of r_{co} and r_a expected in such circumstances if the source luminosity is taken to be 3×10^{37} erg s^{-1}. The orbital parameters of this system are poorly defined, and the values related to the optical determination of the orbital period (Middleditch et al., 1981) are given in Table 9.7. The accretion disc radius is that estimated by McClintock et al. (1980) from optical reprocessing of the X-ray pulse.

The accelerating voltages possible for the accretion driven acceleration processes are given in Table 9.8. Proton energies of more than $\approx 10^{13}$ eV can be reached in all of these models giving the possibility of TeV gamma ray production in optimal circumstances. The long term upper limit on the power emitted at photon energies above 300 GeV was set at 1×10^{35} erg s^{-1} in Chapter 8. It can be seen from Table 9.8 that this is comfortably higher than the maximum power attainable from accretion at the Alfven radius or from the accelerator gaps, so that a more sensitive observation would be required to detect an isotropic gamma ray flux. Since the magnetosphere is likely to be

TABLE 9.7 - Parameters of the 4U1626-67 binary system

Inclination	:	18^{o} $(+18^{o}/-7^{o})$
Stellar Separation	:	1.14 ± 40 ls
Neutron Star Mass	:	$\approx 1.4\ M_{o}$
Companion Star Mass	:	$\approx 0.08\ M_{o}$ (if main sequence dwarf)
X-ray Luminosity	:	$\approx 3 \times 10^{37}$ ergs s^{-1}
Corotation Radius	:	6.4×10^{8} cm
Neutron Star Magnetic Field	:	$\approx 5 \times 10^{12}$ G
Alfven Radius	:	6.7×10^{8} cm for 3×10^{37} erg s^{-1}
Accretion Disc Radius	:	≈0.5 ls

Values for orbital and stellar parameters are taken from Model 1 of Middleditch et al. (1981).

The corotation radius and Alfven radius were calculated using equations 9.10, 9.4 and 5.3.

The accretion disc radius is that estimated by McClintock et al. (1980).

TABLE 9.8 - Particle acceleration in 4U1626-67

(assuming 5×10^{12} G surface magnetic field)

	$L_{37} = 3$
Magnetic Field at r_a (Gauss)	1.6×10^{4}
Maximum Accretion Power at r_a (erg s^{-1})	4.5×10^{34}
Column Density of Accretion Disc (g cm^{-2})	900
Maximum Voltage in CB Model (Volts)	1.8×10^{14}
Maximum Voltage in CR Model (Volts)	4.6×10^{14}
Maximum Voltage in CR Model with Pair Production (Volts)	8.0×10^{12}
Maximum Power in CR Model (erg s^{-1})	1.1×10^{35}
Maximum Voltage in LHM Model (Volts)	5.0×10^{13}

near to corotation with the pulsar, the model of Kiraly and Meszaros (1988) could be invoked to produce a jet of accelerated protons to interact with material at the magnetospheric boundary. Such a model would also have the advantage of directing the gamma rays out of the plane of the system, which is inclined at ≥70° to our line of sight.

This high inclination also rules out gamma ray production in a gas stream, the limb of the companion or any other material present in the plane of the system. The accretion disc would be a possible production site were the proton beam to be incident at a steep angle. It is likely that only the highest energy protons would achieve this (Hillas and Johnson, 1991). The column density of the inner disc is 500-1000 g cm^{-2}, and hence TeV gamma ray production could only occur near the edge of the disc where the column density drops to ≈20% of this value. Given the high inclination such a production site would have a projected distance of only 0.1 ls from the neutron star and thus the shift would not be detectable using the orbital searching technique.

9.3.5.2. X0021-72

Given the lack of knowledge of any of the precise physical parameters of the X0021-72 system, as well as the lack of a positive signal detection at TeV photon energies, the application of gamma ray production models to this object can only be speculative. As was discussed in Chapter 8, it is not clear whether this anomalous source is a cataclysmic variable, a low mass X-ray binary or a soft X-ray transient. The suggestion of a spin-up of the 120s pulsar between the 1979 X-ray observations and the TeV gamma ray observations reported here could only be explained by a neutron star accreting from a stable disc. The spin-up rate is subject to considerable uncertainty, and optical observations suggest that a strongly magnetised white dwarf is a better candidate for the accreting object.

Therefore, as for the other objects studied in this chapter, a range of models were applied to this system but assuming three different compact object candidates, each of mass 1.4 M_o - (a) a neutron star with a 10^{12} G surface

field, (b) a neutron star with a 10^8 G surface field, and (c) a white dwarf with a 10^7 G surface field. The results are listed in Table 9.9. Briefly, it can be seen that the model best capable of producing high energy protons is case (a), i.e. a low mass X-ray binary containing a 10^8 G neutron star. In this case, all of the accretion driven models predict that proton energies of around 10 TeV are attainable. Thus a weak flux of TeV gamma rays could be detected if directed into an accretion disc, which has a column density of $\approx$40 g cm^{-2} in this situation thereby being suitable for gamma ray production via pion decay.

Case (c) pertaining to a white dwarf in a cataclysmic binary is another possibility, but gives maximum proton energies an order of magnitude lower than found for case (b). The luminosities in each are in the region of 10^{33} erg s^{-1}, and therefore significant beaming would be required to give a signal detection at the level of the upper limit of $\approx 10^{35}$ erg s^{-1} imposed by the TeV gamma ray observations given here. It may also be noted that some of the shock acceleration models could be feasible in the accretion column of a white dwarf where the magnetic energy density may be low enough to allow the formation of shocks in the flow of material onto the polar cap.

TABLE 9.9 - Particle acceleration in X0021-72

	Case A	Case B	Case C
Maximum Accretion Power at r_a (erg s^{-1})	1.6×10^{31}	3.0×10^{33}	5.8×10^{32}
Column Density of Accretion Disc (g cm^{-2})	1.6	37	0.22
Maximum Voltage in CB Model (Volts)	3.2×10^{12}	3.9×10^{14}	1.2×10^{12}
Maximum Voltage in CR Model (Volts)	6.6×10^{12}	3.4×10^{14}	1.7×10^{13}
Maximum Voltage in CR Model with Pair Production (Volts)	1.8×10^{10}	1.8×10^{12}	5.7×10^{9}
Maximum Power in CR Model (erg s^{-1})	3.8×10^{31}	7.3×10^{33}	1.4×10^{33}
Maximum Voltage in LHM Model (Volts)	7.2×10^{11}	3.7×10^{13}	1.9×10^{12}

Case A : Neutron star, mass 1.4 M_o, B-field 10^{12} G

Case B : Neutron star, mass 1.4 M_o, B-field 10^{8} G

Case C : White dwarf, mass 1.4 M_o, B-field 10^{7} G

CHAPTER 10 - DISCUSSION AND FUTURE WORK

10.1. The Status of X-ray Binaries as TeV Gamma Ray Sources

This thesis has provided updated analyses of TeV gamma ray observations of five X-ray binaries. Centaurus X-3 and Vela X-1 have been found to show significant evidence for pulsed emission at a specific orbital phase, near the ascending node in each case. These two binary systems join the three discussed in Chapter 5 (Cyg X-3, Her X-1 and 4U0115+63) to form the group of X-ray binaries for which a substantial amount of evidence for TeV gamma ray emission has been accumulated. The three other systems analysed in Chapter 8 have not been found to show evidence for such emission, but the discussion in Chapter 9 has put forward some explanations as to why emission may be weaker or more difficult to detect from these objects.

Four of the five candidate X-ray binary TeV gamma ray sources show some orbital phase dependence in the strength of their gamma ray signal. The exception is 4U0115+63, which is a much wider Be binary for which the detected signal has been steady over a timescale of $\approx$10 days (only a limited sample of the 24 day orbital period). Interaction of an accelerated proton beam with spherically accreting target material in this system will be much less dependent on the orbital phase than in the other more compact binary systems. Both Cen X-3 and Vela X-1 have been found to show some evidence for weaker persistent emission, and both are believed to accrete from both a stellar wind and Roche lobe overflow. The most compact of the systems, Cyg X-3 and Her X-1, show gamma ray signals very strongly modulated with orbital phase. Promising recent results from the cataclysmic variable AE Aquarii (Bowden et al., 1992; Meintjes et al., 1993) suggest that such compact binaries may become important targets in a search for sporadic TeV gamma ray emission.

The observation of a sporadic gamma ray signal should not be taken as an indication of a spurious origin. Measurements using the Compton Observatory have demonstrated that high energy astrophysical phenomena are often transient

in nature. As discussed by Hillas and Johnson (1991) the probable beaming of a high energy proton flux into a target in a binary system will produce a narrow gamma ray beam. This photon beam will be transiently detected when the target material is present in the line of sight. Any wandering or precession of the neutron star magnetic poles, as is believed to occur in Her X-1, could further reduce the chance of detection.

The utility of the analysis technique which investigates the possibility of weak periodic emission from various sites in a binary system has been amply illustrated in this work. The resolution presently attainable is sufficient to discriminate between a gamma ray production site in the gas stream, accretion disc or the limb of the companion star in some systems. This technique may also remove the apparent problem posed by shifting of the observed period from the X-ray period reported for some observations (e.g. Her X-1). The continued use of this tool by the Durham group should provide further valuable results in the future. It is inevitable that searching in period and orbital parameters, as is necessary for X-ray binaries (as opposed to searching in period only for isolated pulsars), will use many degrees of freedom. This results in the true significance of any detection being much less than that of the uncorrected value. Knowledge of accurate contemporary pulse periods (e.g. from BATSE monitoring) reduces this effect and if a displaced emission site is identified in one dataset, the hypothesis that this site is responsible for emission in others should be adhered to so as to further reduce the searching.

10.2. Implications for Future Work

The most obvious route to rapid progress in the field of TeV gamma ray studies of X-ray binaries with existing techniques would seem to be the targeting of future observations at preselected intervals in orbital phase. The results could either confirm the present suspicion of phase dependence in the emission from a number of sources or perhaps demonstrate that the theories put forward to date to explain the emission are not correct. The nature of

such targeted observing would vary from source to source. For example, work carried out on Cygnus X-3 has suggested that only a very narrow phase interval should be selected to search the data for a 12.59 ms pulsar signal; such a precise prediction may not be possible for other systems.

If the phase dependence of the emission at TeV energies is indeed due to the presence of varying amounts of target material then X-ray observations may provide the key. These have shown that the brief intervals of absorption in most systems vary in phase between 0.5 and 0.8 and, if present at all, only maintain their position over a few orbits. Therefore only a general definition of an optimum interval can generally be made, especially in systems where the precise nature of accretion is uncertain. For example, observations of Cen X-3 reported here show that a likely site for gamma ray production is in a bulge at the edge of the accretion disc and therefore the specification of the phase interval 0.77-0.81 is viable. Despite the success of the prediction made here of a detectable pulsed signal from Vela X-1 at phase 0.68, this could not have been achieved on the basis of the X-ray data alone. For this source, X-ray absorption is seen anywhere between phases 0.5 and 0.9 but careful monitoring could reveal the most likely position of the densest absorbing material.

It would also help greatly if these targeted observations could be carried out simultaneously by independent TeV gamma ray groups, although experience has shown that differences in weather and longitude at various sites make such projects difficult. The simultaneous, albeit fortuitous, detection of a burst of pulsed gamma rays from Her X-1 in by two groups in 1985 (see Chapter 5) showed the promise of such a coordinated effort.

Further assistance in assessing the likelihood of gamma ray emission from X-ray binaries should come from satellite results. The close monitoring of pulsar behaviour by the Compton Observatory's BATSE instrument has already provided valuable knowledge for studies of Cen X-3 and 4U1626-67 and more will surely follow. The EGRET instrument is capable of detecting the synchrotron

radiation at MeV-GeV energies which is predicted as a consequence of the model of Katz and Smith (1988) for example. Failure to detect any such emission would allow more refined limits to be placed on acceleration models. Non-thermal radiation from the accelerator gaps was predicted by Leung, Cheng and Fung (1993). A photon excess may occur at very low and medium X-ray energies ($\leq$300 eV and $\geq$30 keV for Cen X-3) which could be detected by ROSAT.

Apart from these considerations, further improvements to the sensitivity of ground-based techniques are the key to more and better source detections in this field. Contemporary progress in instrumentation and analysis will be discussed in the final two sections.

10.3. Recent Advances in Ground Based Gamma Ray Astronomy

10.3.1. Gamma Ray Selection using Cerenkov Shower Imaging

The technique of imaging Cerenkov air showers could be said to have come of age in the last five years. Its success has pointed the way to the design of the next generation of Cerenkov telescopes. The preliminary work in this area was briefly discussed in Chapter 2. Computer simulations played a pivotal role in establishing this technique. The most influential simulations with regard to Cerenkov imaging techniques were those carried out by Hillas (1985). The effort was directed into testing the characteristics of air showers produced by TeV protons and photons and the response their radiation would generate in the Mt. Hopkins 10 m Cerenkov telescope (Cawley et al., 1989).

Given the approximately elliptical shape of the shower images for gamma rays a set of parameters was defined, associated with the projected shape of the shower, and hence its angular extent and orientation with respect to the centre of the field of view. The most important of these "Hillas parameters" are depicted in Figure 10.1. A discriminant approach to the pattern recognition of the images drawn from the two populations of primary particles was utilised. It was shown that a high level of discrimination should be attainable, corresponding to a 98% rejection of the proton background and a

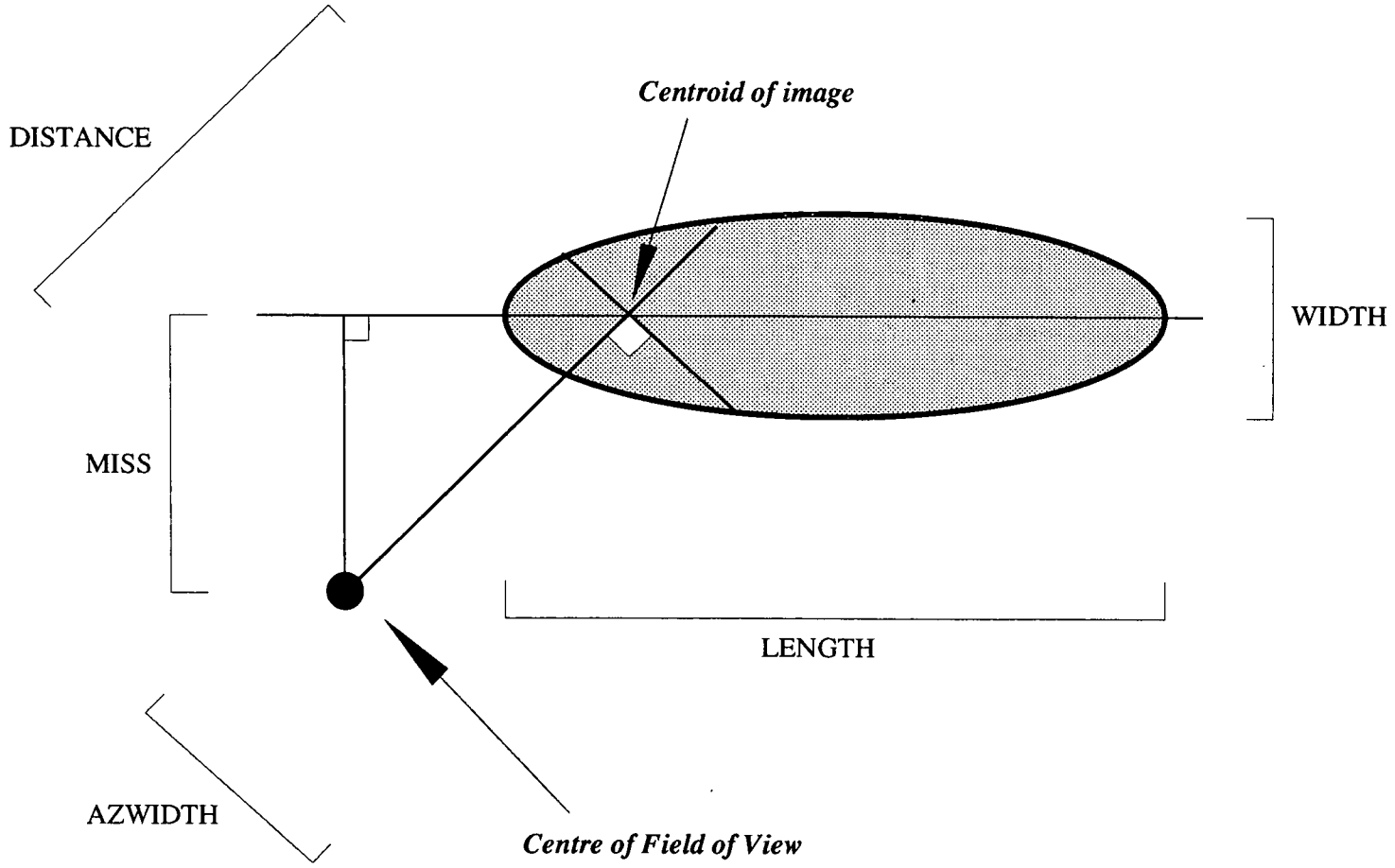

Figure 10.1 : A schematic diagram showing the principal parameters used to measure the shape and orientation of a Cerenkov shower image in the focal plane of a detector. The parametrisation was developed by Hillas (1985).

(after Fegan, 1992)

60-70% retention of gamma rays from a source at the centre of the field of view of an imaging telescope.

10.3.2. A Telescope Incorporating a Cerenkov Imaging Camera

The detector package placed at the focus of the 10 m reflector at the Whipple Observatory contains a hexagonally close-packed array of photomultiplier tubes, defining a set of pixels. This "camera" package originally contained 37 tubes of 0.5° aperture, as used in Hillas' original simulations, but has since been upgraded to consist of 109 smaller tubes of 0.25° aperture (Cawley et al., 1989). In operation, the source region and an off-source control region are viewed in the 10 square degree full field for alternate 28-minute intervals.

Before analysis of the data, the signals recorded in each tube for each event are compensated to allow for the characteristic response of each tube and the offset or pedestal value inherent to each digitiser. The corrected spatially resolved image of each Cerenkov shower in the focal plane is used to calculate a set of Hillas parameters and enable gamma ray selection.

10.3.3. TeV Gamma Ray Sources Observed using Shower Imaging

10.3.3.1. The Crab Nebula

After many years of observation by various groups, the unambiguous detection of a TeV gamma ray flux from the Crab Nebula by the Whipple collaboration has established this object as possibly the first 'standard candle' of TeV gamma ray astronomy. The imaging technique was successful in detecting a d.c. signal from the Crab Nebula at a significance of 9σ using the original 37-element Whipple camera (Weekes et al., 1989). This initial detection resulted solely from the use of the simple Azwidth parameter (see Figure 10.1) to preferentially select gamma ray induced showers. The same technique was used to analyse the 1988-89 dataset recorded using the improved 109-element camera. A 20σ detection resulted, which corresponded to a d.c. flux of 7×10^{-11} cm^{-2} s^{-1} above 400 GeV (Vacanti et al., 1991). The strength of this signal was sufficient to warrant optimisation of the data preparation

as applied to the Crab Nebula dataset (Punch et al., 1991). The resultant 'Supercut' procedure resulted in a 34σ detection for the 1988-89 data, and a 45σ detection for the full 1988-91 dataset (Lang et al., 1991). Both of these significances are somewhat overstated due to their containing the dataset from which the extended selection was derived.

Some support for the d.c. signal from the Crab Nebula has come from results with considerably lower statistical significance reported by other research groups (Weekes, 1993). The spectrum of high energy gamma ray emission from the Crab Nebula including these results is shown in Figure 10.2.

Despite the strong evidence for TeV gamma ray emission from the Crab Nebula, no evidence for emission pulsed at the 33 ms period of the Crab Pulsar has been found in the Whipple dataset. An upper limit for the pulsed emission above 400 GeV was $1{\cdot}4 \times 10^{-12}$ cm^{-2} s^{-1}, less than 2% of the d.c. signal (Vacanti et al., 1991). The strongest evidence for pulsed emission at TeV photon energies came from the Durham group who detected a signal precisely in phase with the radio and optical main pulse (Dowthwaite et al., 1984b).This result was based on over 100 hours of observations and the estimated photon flux was $(7{\cdot}9 \pm 0{\cdot}8) \times 10^{-12}$ cm^{-2} s^{-1} above 1000 GeV. Pulsed TeV gamma ray emission at a significance of 4.3σ was recently reported in a preliminary analysis of 40 hours of observations by the Tata Institute group (Acharya et al., 1993). The resolution of the d.c. and pulsed proportions of the TeV gamma ray signal is an important and outstanding problem.

10.3.3.2. Markarian 421

The detection of the giant elliptical BL Lac galaxy Markarian 421 has made it the first extragalactic TeV gamma ray source, and only the second in all, to be discovered via the Cerenkov imaging method (Punch et al., 1992). Using the same selection procedure successfully applied to the Crab Nebula, a d.c. signal was found from Mkn 421 at a significance of 6·3σ, giving a flux of $1{\cdot}5 \times 10^{-11}$ cm^{-2} s^{-1} above 500 GeV. Mkn 421 is the nearest active galaxy

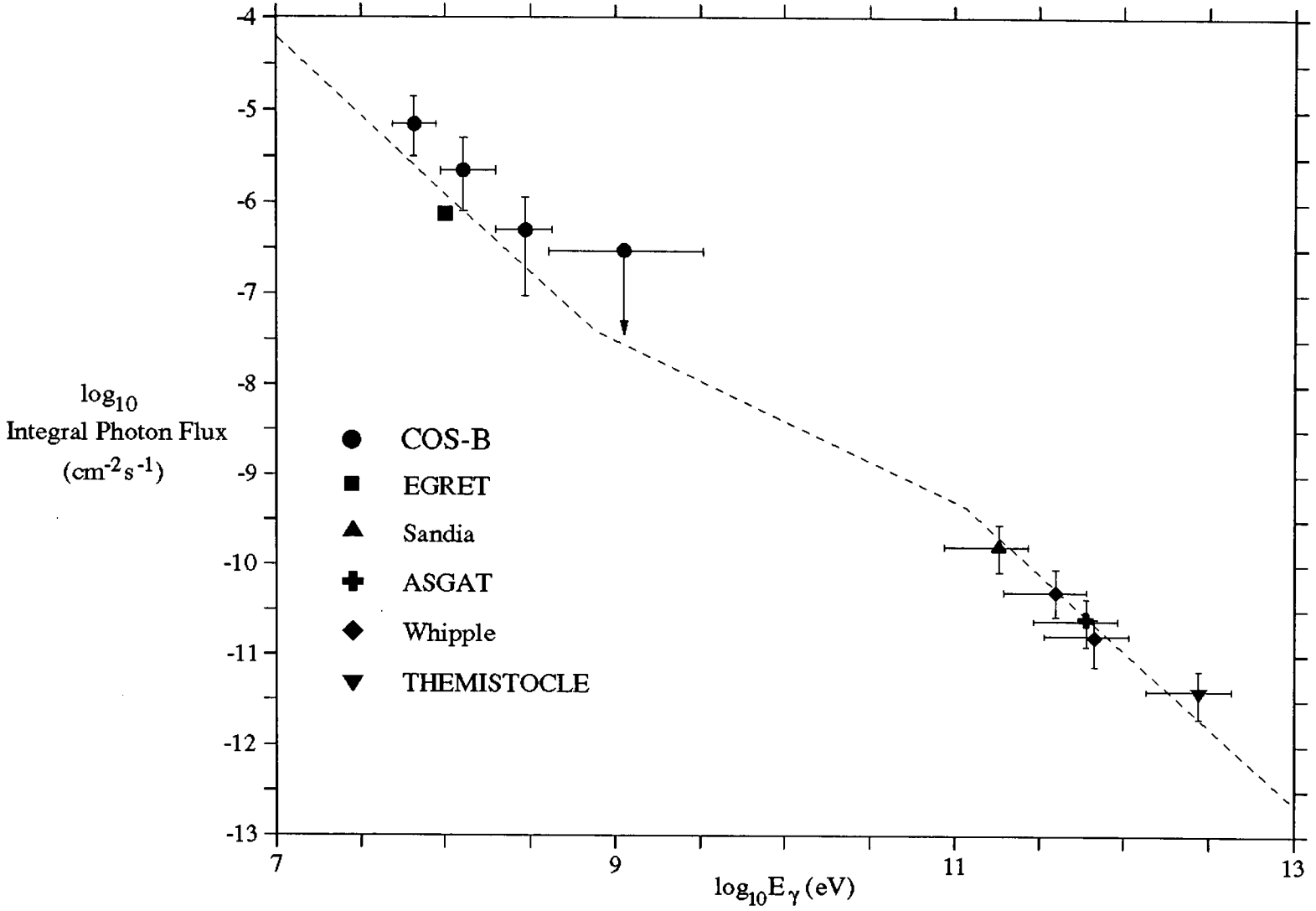

Figure 10.2 : The high energy gamma ray spectrum of the unpulsed emission from the Crab Nebula. This figure is based on Lamb (1992) with EGRET data from Nolan et al. (1993). The dashed line shows the model spectrum produced by de Jager and Harding (1992).

(z=0.031) to have been detected by the Compton Observatory's EGRET experiment (Lin et al., 1992), and is thus least affected by absorption of TeV photons on the cosmic infra-red background (Stecker, de Jager and Salamon, 1992).

10.4. Future Work

10.4.1. Linking Space-Based and Ground-Based Observations

A number of ground-based projects are currently under development and the current state of progress in the techniques of the field may be gauged from reports presented at the 23rd ICRC at Calgary (1993) and at the Palaiseau and Calgary workshops (Vacanti and Fleury, 1993). A major objective of future work in high energy gamma ray astronomy must be the bridging of the gap in energy threshold between observations made using satellites and those made from the ground using the atmospheric Cerenkov technique. At present the EGRET instrument on the Compton Observatory measures the highest photon energies yet detected by spark chamber experiments of ≈50 GeV. The flux of photons at this energy detected by this technique is vanishingly small, and is unlikely to be increased by technical advances in the foreseeable future. Therefore the onus rests on lowering the energy threshold of atmospheric Cerenkov installations.

As event selection procedures in many projects become more complex, the energy threshold is not greatly reduced due to limitations on the counting rate for even an optimised signal. Most of the proposed experiments involve refined imaging techniques operating at ≥1 TeV. The single most important requirement to reduce the threshold is to increase the effective collecting mirror area, i.e. the "brute force" approach. A particularly useful aspect complementing the move to lower energies comes from the decreasing proportion of hadronic showers which are detected at energies below ≈100 GeV (Weekes and Turver, 1977). As outlined in Chapter 2, the use of a single large dish is less effective than the sharing of the reflector area over two or three dishes operated in fast coincidence. The Durham group have demonstrated the effectiveness of a three-fold coincidence system over a long period of time,

and this has provided the lowest energy threshold reached to date (≈200 GeV for the Mk.3a and 5a telescopes)

10.4.2. Stereoscopic Observations

With the establishment of high resolution shower imaging as a valuable tool in Cerenkov astronomy, much attention is being paid to the extraction of maximum information from each detected event. One promising and novel approach is the use of two or more telescopes in tandem to record simultaneous simple images of a Cerenkov flash from different locations in the light pool at the ground. This procedure is being developed by the Durham group and will require a great deal of investigation and refinement.

10.4.3. The Durham Programme for the 1990s

10.4.3.1. The Mark 3a/Mark 5a Stereo Pair

The current plans of the Durham group for future instrumentation utilise both of the options for improvement discussed in the previous section in order to achieve the goal of a gamma ray observatory capable of carrying out a detailed study of Cerenkov events over the range 50-2000 GeV (Bowden et al., 1993). The first stage in this new project was the construction of the Mk.5 telescope for simple imaging (see Chapter 3). A second key part of the operation is also in place following the recent refurbishing of the Mk.3 telescope. In 1993 April the central 11m^2 tesselated reflector was replaced by a 10m^2 parabolic dish identical to those used in the Mk.5 telescope. The array of 7 photomultiplier tubes viewing the central dish was replaced by a package of 31 closely packed tubes of 0.5° aperture, once again identical to that viewing the centre dish in the Mk.5 telescope. As a result, the modified Mk.3a and Mk.5a telescopes now possess identical performance including modest imaging capabilities. The pair of telescopes are shown in Figure 10.3. The triple fast coincidence triggering system has been measured to give a total count rate of ≈300 minute^{-1} at the zenith suggesting an estimate of 250 GeV for the threshold energy.

A key aspect of the operation of the two imaging telescopes in tandem is

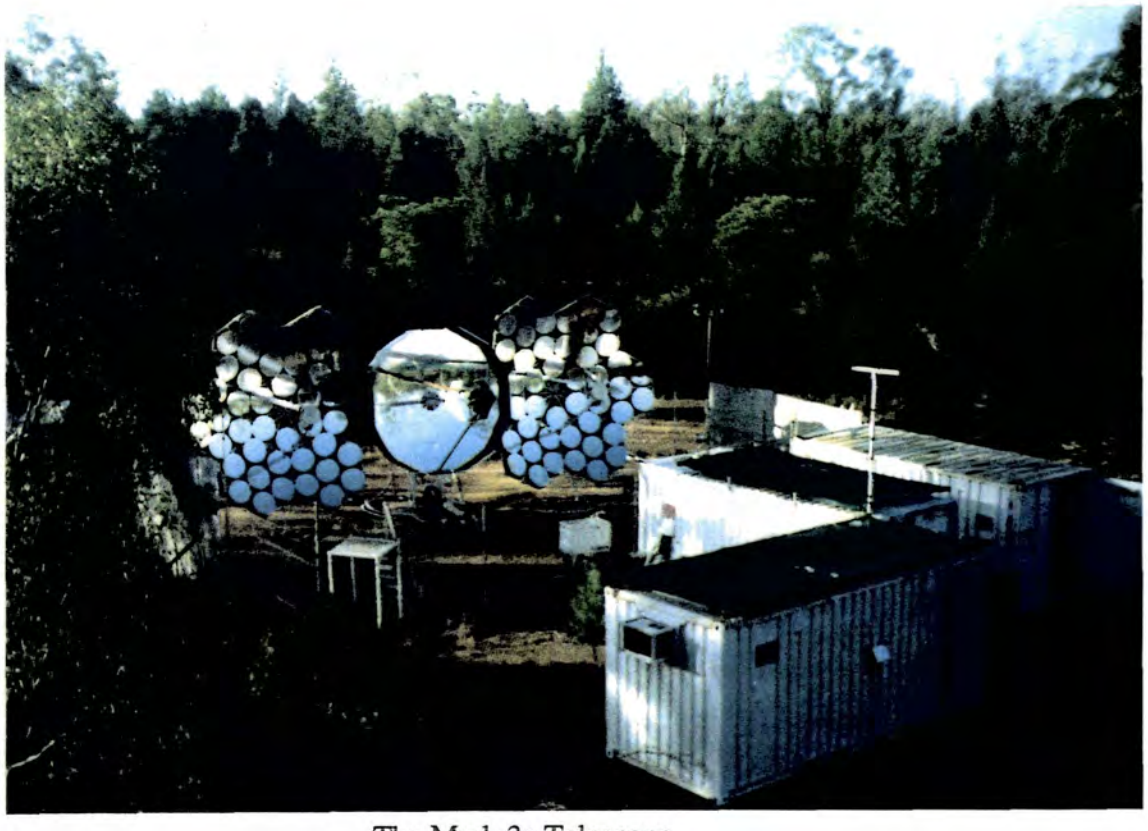

The Mark 3a Telescope

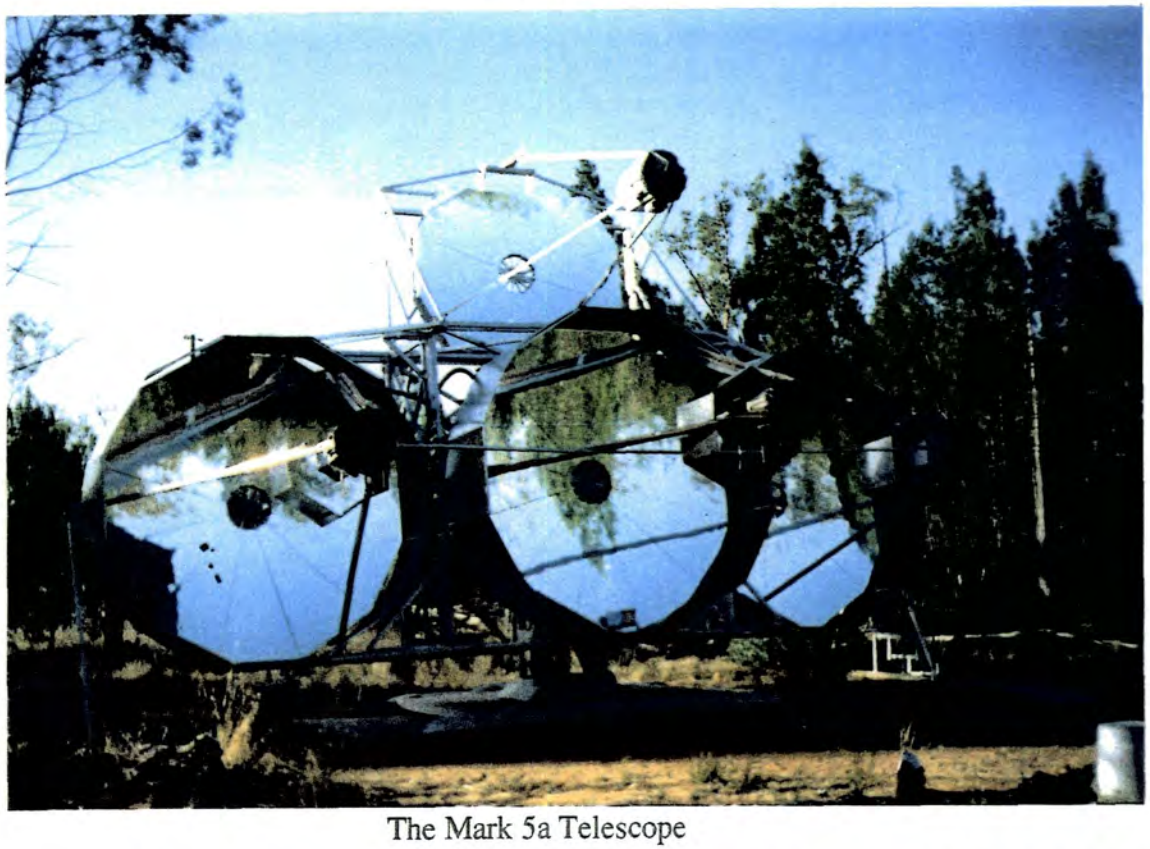

The Mark 5a Telescope

Figure 10.3 : The stereo imaging pair of atmospheric Cerenkov telescopes operated by the Durham group at Narrabri since 1993 April.

the identification of common events, which comprise ≈45% of the total number when the telescopes are operating in the zenith. For this subset of stereo data, information is extracted on the lower moments of the light signal, i.e. the brightness of the light flash, the position of the image centroid and the r.m.s. spread of the light in the focal plane. For a gamma ray induced shower, a good correlation is predicted between the brightness, point of impact on the ground, depth of production in the atmosphere and angular spread as measured by both telescopes. This information can be derived even if only a small number of the pixels in the imaging camera are triggered and hence a low energy threshold can be retained; ≈350 GeV for an observation in the zenith. Simulations followed by initial studies of the proton background have indicated that up to 99% rejection of the proton background should be possible while retaining the majority of the gamma rays. This gives a 3σ sensitivity of 2.5×10^{-11} $cm^{-2}s^{-1}$ for the flux above 350 GeV in a 30 hour observation of a d.c. source (or 1.5×10^{-11} $cm^{-2}s^{-1}$ for a typical pulsed source). Both telescopes can also operate as stand-alone simple imaging cameras to carry out efficient 31 pixel imaging of Cerenkov showers above a threshold of ≈250 GeV.

10.4.3.2. The Mark 6 Telescope

In addition to the facility described above, a major effort is underway to construct a new large telescope. This will be identical in mechanical design to the Mk.5 but doubled in size, giving 4 times the mirror collecting area. Each parabolic dish has an area of 42 m^2 and is constructed of 24 segments, giving a FWHM image size specified as ≈0.1°. To assist the reduction of the energy threshold, measures will be taken to increase the light directed into the photomultiplier tubes by the use of Winston cones and to eliminate scattered light from the sky and ground by the use of shielding about each dish and detector package parallel to the optic axis.

The two outer dishes will be viewed by clusters of 19 0.5° aperture photomultiplier tubes, corresponding pairs of which are used to define an

event trigger in conjunction with a response in a 109 pixel (0.25°) camera viewing the centre dish. Investigation of the performance of a range of telescopes of ever increasing size have shown that under optimal conditions, a threshold of ≤75 GeV should be reached. For a 30 hour observation of a d.c. source, the 3σ flux limit will be 5 x 10^{-10} $cm^{-2}s^{-1}$ above 75 GeV (3 x 10^{-10} $cm^{-2}s^{-1}$ for a pulsed flux) even before any event selection is applied. The central high resolution camera will also be used to trigger independently, as is the case for telescope comprising a single 60 m^2 dish and a 109 pixel camera used by the Whipple group. The threshold for this method of high resolution imaging is estimated to be ≈500 GeV giving a 3σ d.c. flux limit of 2 x 10^{-11} $cm^{-2}s^{-1}$ for a 30 hour observation. If construction and deployment proceed as planned, the installation at Narrabri will be completed in mid-1994 and will contain a telescope at the cutting edge of new techniques in atmospheric Cerenkov astronomy.

10.4.3.3. The Expected Performance of the System

As an example of the predicted capabilities of this improved system, Figure 10.4 shows the threshold detection limits appropriate to the instruments described above as compared with the flux expected from extrapolation of the spectrum of the quasar 3C279 as detected by EGRET (Hartman et al., 1992). It is clear that the new Durham telescopes will provide valuable information on the nature of the high energy emission from this class of object. The use of the new instruments will also allow substantial improvement to observations of X-ray binaries. Considering Cen X-3 for example, at a distance of 8 kpc, the current limit on the persistent pulsed luminosity above 300 GeV is ≈3 x 10^{35} erg s^{-1} from over 300 hours of on-source time. The stereo imaging capability of the Mk.3a/5a stereo pair will enable this upper limit to be reached from only 30 hours of viewing.

10.5. Final Words

The current plans for the expansion of atmospheric Cerenkov facilities

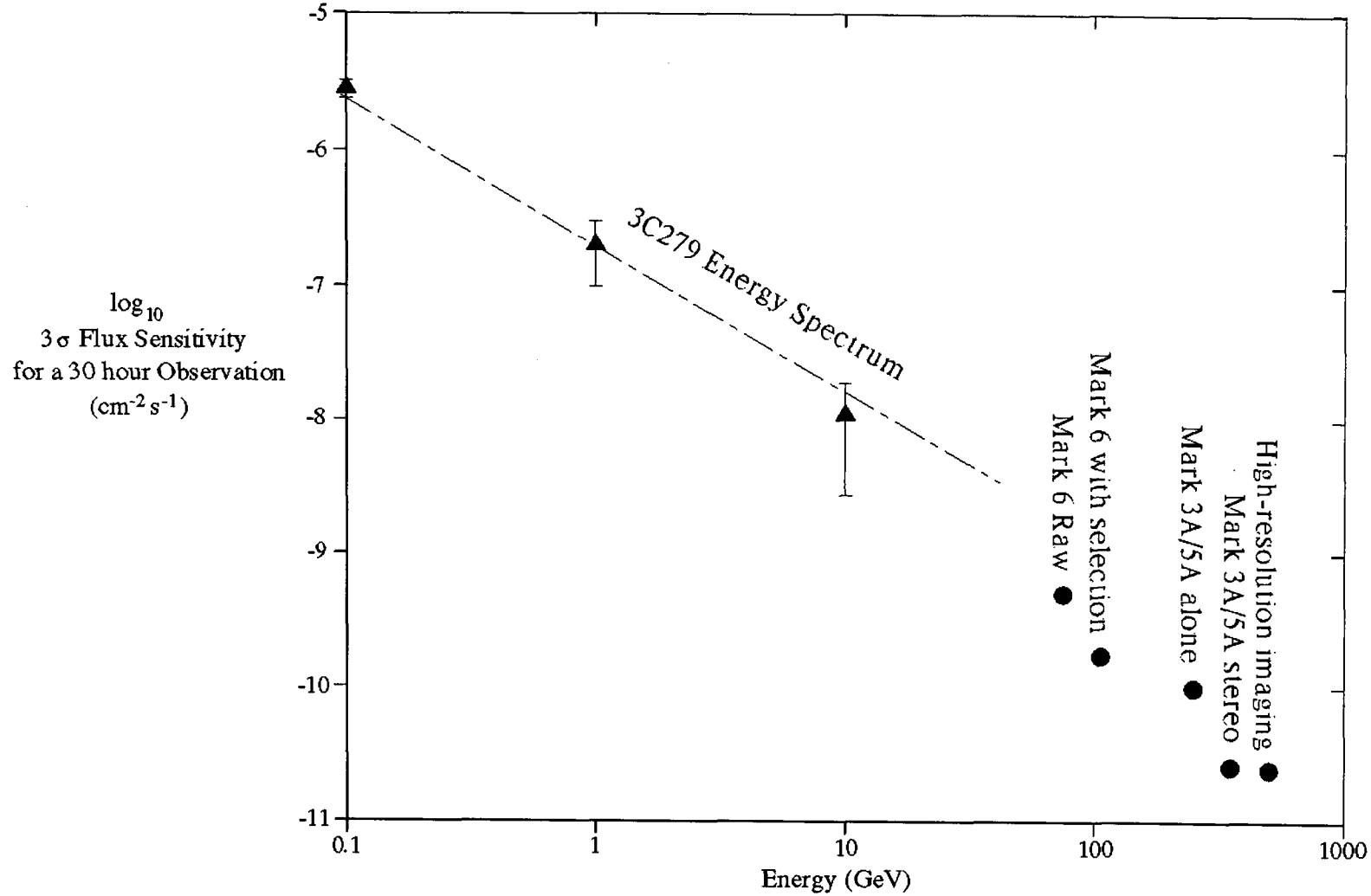

Figure 10.4 : The estimated sensitivity for each of the four operational modes of the Durham telescopes at Narrabri. The fluxes are based on a 30 hour dataset recorded on a DC source. The integrated energy spectrum of 3C279 as measured by EGRET is extrapolated as an indication of the ability of the new installations. (from Bowden et al., 1993)

are more ambitious than ever before. At such stages in the development of an observational field, the reporting of new results on sources inevitably takes a back seat to measurements and predictions of the capabilities of the new techniques. With the skill and enthusiasm being directed into this area by so many research groups, the next 2-3 years should provide a rich harvest of experimental information, new observational data and consequent advances in the interpretation of the results. In regard to the present work on X-ray binaries, it is to be hoped that increased awareness of the importance of TeV gamma ray observations will encourage theoretical work to progress and make quantifiable predictions on the nature of the high energy emission.

It has also frequently been found that unexpected discoveries dominate as techniques in a research field progress rapidly. The detection of Mkn 421 by the Whipple group and the exciting results from other active galactic nuclei gained by measurements using the Compton Observatory suggest that this class of source may hold many interesting discoveries in store. The propagation of TeV photons from active galaxies across intergalactic space may be a test of the strength of the cosmic infra-red background, since a cut-off is predicted in the energy spectra of such sources at $\approx$0.1-10 TeV (Stecker, de Jager and Salamon, 1992). This is an area where ground-based observations could make a significant contribution to the wider field of astrophysics, possibly even leading to a new measurement of Hubble's constant. The observing programme planned by the Durham group will place some emphasis on measurements of TeV gamma ray emission from active galactic nuclei and investigation of the cosmological implications.

The opportunity for a link with the impressive amount of high energy measurements by the Compton Observatory must be used to its full advantage. As a result the field of TeV gamma ray astronomy should be deservedly recognised as an invaluable contribution to the understanding of the highest energy radiation processes in astrophysics.

REFERENCES

Acharya, B.S., Bhat, P.N., Krishna Swamy, M.R., Mondal, N.K., Ramana Murthy, P.V., Rao, M.V.S., Sathyanarayana, G.P. and Vishwanath, P.R., 1993, Proc.23rd ICRC (Calgary), 1, 263

Aharonian, F.A., Akhperjanian, A.G., Kankanian, A.S., Mirzoyan, R.G., Stepanian, A.A., Muller, N., Samorski, M., Stamm, W., Bott-Bodenhausen, M., Lorenz, E. and Sawallisch, P., 1991, Proc.22nd ICRC (Dublin), 2, 615

Ajne, B., 1968, Biometrika, 55, 343

Akerlof, C.W., Cawley, M.F., Fegan, D.J., Hillas, A.M., Lamb, R.C., Lewis, D.A., Meyer, D.I. and Weekes, T.C., 1990, Nucl.Phys.B, 14A, 237

Akerlof, C.W., Cawley, M.F., Chantell, M., Fegan, D.J., Lamb, R.C., Lawrence, M.A., Lang, M.J., Lewis, D.A., Meyer, D.I.,Mohanti, G., O'Flaherty, K.S., Punch, M., Reynolds, P.T., Schubnell, M.S., Weekes, T.C. and Whitaker, T., 1991, Proc.22nd ICRC (Dublin), 1, 324

Allen, W.H., Bond, I.A., Budding, E., Conway, M.J., Daniel, A., Fenton, K.B., Fujii, H., Fujii, Z., Hayashida, N., Hibino, K., Honda, M., Humble, J.E., Kabe, S., Kasahara, K., Kifune, T., Lythe, G.D., Masaike, A., Matsubara, Y., Mitsui, K., Miura, Y., Mori, M., Muraki, Y., Nagano, M., Nakamura, T., Nishizawa, M., Norris, P.M., Ogio, S., Saito, To., Sakata, M., Sato, H., Shimizu, H.M., Spencer, M., Storey, J.R., Tanimori, T., Teshima, M., Torii, S., Wadsworth, A., Watase, Y., Woodhams, M.D., Yamamoto, Y., Yock, P.C.M. and Yuda, T., 1993, Ap.J., 405, 554

Angelini, L., 1989, Proc.23rd ESLAB Symposium on Two Topics in X-ray Astronomy (Bologna), 1, 81

Anzer, U., and Borner, G., 1983, Astron.Ap., 122, 73

Auriere, M., Koch-Miramond, L. and Ortolani, S., 1989, Astron.Ap., 214, 113

Austin, R., Camerini, U., Finley, J., Fry, W., Gaidos, J, Hudson, J., Jacobsen, J., Jennings, J., Kelley, L., Kenter, A., Kertzman, M., Learned, J.G., Loeffler, F., Loveless, R., March, R., Morse, R., Palfrey, T., Reeder, D., Resvanis, L.K., Sembroski, G., Sinnis, C., Skinner, M., Slane, P.,Szentgyorgyi, A., Weeks, D., Wilson, C. and Zernstein, G., 1990, Proc.21st ICRC (Adelaide), 2, 110

Avni, Y. and Bahcall, J., 1974, Ap.J., 192, L139

Baillon, P., Behr, L., Danagoulian, S., Dudelzak, B., Eschstruth, P., Espigat, P., Fabre, B., Fontaine, G., George, R., Ghesquiere, C., Kovacs, F., Meynadier, C., Pons, Y., Riskalla, R., Rivoal, M., Roy, P., Schune, P., Socroun, T., Touchard, A.M. and Vrana, J., 1991, Proc. 22nd ICRC (Dublin), 1, 220

Bailyn, C.D. and Grindlay, J.E., 1990, Ap.J., 353, 159

Baity, W.A., Ulmer, M.P., Wheaton, W.A. and Peterson, L.E., 1974, Ap.J., 187, 341

Batschelet, E., 1981, "Circular Statistics in Biology" (London:Acad.Press)

Becker, R.H., Rothchild, R.E., Boldt, E.A., Holt, S.S., Pravdo, S.H., Serlemitsos, P.J. and Swank, J.H., 1978, Ap.J., 221, 912

Bell, A.R., 1978, MNRAS, 182, 147

Bennett, K., Bignami, G.F., Hermsen, W., Mayer-Hasselwander, H.A.,Paul, J.A. and Scarsi, L., 1977, Astron.Ap., 59, 273

Bennett, K., Busetta, M., Buccheri, R., Carraminana, A., Connors, A., Diehl, R., Hermsen, W., Kuiper, L., Lichti, G., Ryan, J., Schonfelder, V. and Strong, A., 1993, Proc.23rd ICRC (Calgary), 1, 172

Bertsch, D.L., Brazier, K.T.S., Fichtel., C.E., Hartman, R.C., Hunter, S.D., Kanbach, G., Kniffen, D.A., Kwok, P.W., Lin, Y.C., Mattox, J.R., Mayer-Hasselwander, H.A., Montigny, C.v., Michelson, P.F., Nolan, P.L., Pinkau, K., Rothermel, H., Schneid, E.J., Sommer, M., Sreekumar, P. and Thompson, D.J., 1992, Nature, 357, 306

Bhat, P.N., Gupta, S.K., Ramanamurthy, P.V., Sreekantan, B.V., Tonwar, S.C. and Vishwanath, P.R., 1987, in "Very High Energy Gamma Ray Astronomy", ed. K.E. Turver (Reidel:Dordrecht), pp 143-146

Bignami, G.F., 1984, La Rivista del Nuovo Cimento, 7, 10

Bignami, G.F. and Caraveo, P.A., 1992, Nature, 357, 287

Bignami, G.F., Caraveo, P.A. and Lamb, R.C., 1984, Ap.J., 272, L9

Blackett, P.M.S., 1948, Report of the Gassiot Committee of the Royal Society, 34

Boley, F.I., 1964, Rev.Mod.Phys., 36, 792

Bonnet-Bidaud, J-M, and Chardin, G., 1988, Phys.Rep., 170, 325

Bonnet-Bidaud, J.M. and van der Klis, M., 1981, Astron.Ap., 97, 134

Borner, G., Hayakawa, S., Nagase, F. and Anzer, U., 1987, Astron.Ap., 182, 63

Bowden, C.C.G., Bradbury, S.M., Brazier, K.T.S., Carraminana, A., Chadwick, P.M., Cottle, P., Dipper, N.A., Edwards, P.J., Hogg, T.W., Hilton, S.E., Lincoln, E.W., McComb, T.J.L., Orford, K.J., Rayner, S.M., Robertshaw, M., Tindale, K. and Turver, K.E., 1991a, Proc.22nd ICRC (Dublin), 2, 626

Bowden, C.C.G., Bradbury, S.M., Brazier, K.T.S., Carraminana, A., Chadwick, P.M., Dipper, N.A., Edwards, P.J., Lincoln, E.W., Mannings, V.G., McComb, T.J.L., Orford, K.J., Rayner, S.M. and Turver, K.E., 1991b, Proc.22nd ICRC (Dublin), 1, 321

Bowden, C.C.G., Bradbury, S.M., Brazier, K.T.S., Carraminana, A., Chadwick, P.M., Dipper, N.A., Edwards, P.J., Lincoln, E.W., McComb, T.J.L., Orford, K.J., Rayner, S.M. and Turver, K.E., 1991c, Proc.22nd ICRC (Dublin), 1, 332

Bowden, C.C.G., Bradbury, S.M., Chadwick, P.M., Dickinson, J.E., Dipper, N.A., Edwards, P.J., Lincoln, E.W., McComb, T.J.L., Orford, K.J., Rayner, S.M. and Turver, K.E., 1992a, J.Phys. G, 18, L55

Bowden, C.C.G., Bradbury, S.M., Chadwick, P.M., Dickinson, J.E., Dipper, N.A., Edwards, P.J., Lincoln, E.W., McComb, T.J.L., Orford, K.J., Rayner, S.M. and Turver, K.E., 1992b, Astroparticle Physics, 1, 47

Bowden, C.C.G., Bradbury, S.M., Brazier, K.T.S, Carraminana, A., Chadwick, P.M., Dipper, N.A., Edwards, P.J., Lincoln, E.W., Mannings, V.G., McComb, T.J.L., Orford, D.J., Orford, K.J., Rayner, S.M. and Turver, K.E., 1992c, J.Phys. G, 18, 413

Bowden, C.C.G., Bradbury, S.M., Chadwick, P.M., Dickinson, J.E., Dipper, N.A., McComb, T.J.L., Orford, K.J., Rayner, S.M. and Turver, K.E., 1992d, J.Phys.G, 18, L127

Bowden, C.C.G., Bradbury, S.M., Chadwick, P.M., Cottle, P., Dickinson, J.E., Dipper, N.A., Dye, S., Hilton, S.E., Hogg, W., Lincoln, E.W., McComb, T.J.L., Orford, K.J., Osborne, J.L., Parkin, K., Rayner, S.M., Robertshaw, M., Roff, D.G., Tindale, K. and Turver, K.E., 1993, paper presented at "Towards a Major Atmospheric Cerenkov Detector II" (Calgary workshop)

Boynton, P.E., Deeter, J.E., Lamb, F.K. and Zylstra, G., 1986, Ap.J., 307, 545

Brazier, K.T.S., 1991, Ph.D. Thesis, University of Durham

Brazier, K.T.S., Carraminana, A., Chadwick, P.M., Currell, T.R., Dipper, N.A., Lincoln, E.W., Mannings, V.G., McComb, T.J.L., Orford, K.J., Rayner, S.M. and Turver, K.E., 1989, Experimental Astronomy, 1, 77

Brazier, K.T.S., Carraminana, A., Chadwick, P.M., Dipper, N.A., Lincoln, E.W., Mannings, V.G., McComb, T.J.L., Orford, K.J., Rayner, S.M. and Turver, K.E., 1990a, Proc.21st ICRC (Adelaide), 2, 91

Brazier, K.T.S., Carraminana, A., Chadwick, P.M., Dipper, N.A., Lincoln, E.W., Mannings, V.G., McComb, T.J.L., Orford, K.J., Rayner, S.M. and Turver, K.E., 1990b, Proc.21st ICRC (Adelaide), 2, 379

Brazier, K.T.S., Carraminana, A., Chadwick, P.M., Dipper, N.A., Lincoln, E.W., Mannings, V.G., McComb, T.J.L., Orford, K.J., Rayner, S.M., Turver, K.E. and Williams, D.G., 1990c, Proc. 21st ICRC (Adelaide), 2, 296

Brazier, K.T.S., Carraminana, A., Chadwick, P.M., Dipper, N.A., Lincoln, E.W., Mannings, V.G., McComb, T.J.L., Orford, K.J., Rayner, S.M., Turver, K.E. and Williams, D.G., 1990d, Proc. 21st ICRC (Adelaide), 2, 292

Browning, R. and Turver, K.E., 1977, Nuovo Cimento, 38A, 223

Buccheri, R., Bennett, K., Bignami, G.F., Bloemen, J.B.G.M., Boriakoff, V., Caraveo, P.A., Hermsen, W., Kanbach, G., Manchester, R.N., Masnou, J.L., Mayer-Hasselwander, H.A., Ozel, M.E., Paul, J.A., Sacco, B., Scarsi, L. and Strong, A.W., 1983, Astron.Ap., 128, 245

Caraveo, P.A., Bignami, G.F., Vigroux, L. and Paul, J.A., 1984, Ap.J., 276, L45

Carraminana, A., Chadwick, P.M., Dipper, N.A., Lincoln, E.W., Mannings, V.G., McComb, T.J.L., Orford, K.J., Rayner, S.M., Turver, K.E. and Williams, D.G., 1989a, in "Timing Neutron Stars", eds. H. Ogelman and E.P.J. van den Heuvel (Dordrecht:Kluwer), pp 369-374

Carraminana, A., Chadwick, P.M., Dipper, N.A, Lincoln, E.W., Mannings, V.G., McComb, T.J.L., Orford, K.J., Rayner, S.M, Turver, K,E and Williams, D.G., 1989b, Ap.J., 346, 967

Carraminana, A., Chadwick, P.M.,, Dipper, N.A., Lincoln, E.W., Mannings, V.G., McComb, T.J.L., Orford, K.J., Rayner, S.M. and Turver, K.E., 1990, Astron.Ap., 228, 327

Castagnoli, C., Dardo, M. and Penengo, P., 1967, Phys. Rev., 160, 1186

Castagnoli, C., Picchi, P. and Locci, M.A., 1972, Nuovo Cimento, 9B, 213

Cerenkov, P.A., 1937, Phys.Rev., 52, 378

Chadwick, P.M., 1987, Ph.D. Thesis, University of Durham

Chadwick, P.M., Dipper,N.A., Dowthwaite, J.C., Gibson, A.C., Harrison, A.B., Kirkman, I.W., Lotts, A.P., Macrae, J.H., McComb, T.J.L., Orford, K.J., Turver, K.E. and Walmsley, M., 1985, Nature, 318, 642

Chadwick, P.M., Dipper,N.A., Kirkman, I.W., McComb, T.J.L., Orford, K.J. and Turver, K.E., 1987, in "Very High Energy Gamma Ray Astronomy", ed. K.E. Turver (Dordrecht:Reidel), pp 121-123

Chadwick, P.M., McComb, T.J.L. and Turver, K.E., 1990, J.Phys.G, 16, 1773

Chanmugam, G. and Brecher, K., 1985, Nature, 313, 767

Charles, P.A., 1989, Proc.23rd ESLAB Symposium on Two Topics in X-ray Astronomy (Bologna), 1, 129

Charles, P.A., Mason, K.O., White, N.E., Culhane, J.E., Sanford, P.W. and Moffat, A.F.J., 1978, MNRAS, 183, 813

Cheng, K.S., Cheung, T., de Jager, O.C., Lau, M.M. and Yu, K.N., 1990, Proc.21st ICRC (Adelaide), 2, 374

Cheng, K.S., Ho., C. and Ruderman, M., 1986, Ap.J., 300, 521

Cheng, K.S. and Ruderman, M., 1989, Ap.J., 337, L77

Cheng, K.S. and Ruderman, M., 1991, Ap.J., 373, 187

Chodil, G., Mark, H., Rodrigues, R., Seward, F., Swift, C.D., Hiltner, W.A., Wallerstein, G. and Mannery, E.J., 1967a, Phys.Rev.Lett., 19, 681

Chodil, G., Mark, H., Rodrigues, R., Seward, F.D. and Swift, C.D., 1967b, Ap.J., 150, 57

Chudakov, A.E., Zatsepin, V.I., Nesterova, N.M. and Dadykin, V.L., 1965, J.Phys.Soc.Japan (Suppl. AIII), 106

Clear, J., Bennett, K., Buccheri, R., Grenier, I.A., Hermsen, W., Mayer-Hasselwander, H.A. and Sacco, B., 1987, Astron.Ap., 174, 85

Cohen, J.M., and Mustafa, E., 1987, Ap.J., 319, 930

Cordova, F.A. and Mason, K.O., 1983, in "Accretion-driven Stellar X-ray Sources", eds. W.H.G. Lewin and E.P.J. van den Heuvel (Cambridge:C.U.P.), pp 147-188

Cox, R.T., 1944, Phys.Rev., 66, 106

Craig, M.A.B., 1984, Ph.D. Thesis, University of Durham

Cranshaw, T.E. and Galbraith, W., 1954, Phil.Mag., 45, 1109

Crawford, J.A. and Kraft, R.P., 1956, Ap.J., 123, 44

Cressie, N., 1977, J.Appl.Prob., 14, 272

Darbro, W., Ghosh, P., Elsner, R.F., Weisskopf, M.C., Sutherland, P.G. and Grindlay, J.E., 1981, Ap.J., 246, 231

Davison, P.J.N., 1977, MNRAS, 179, 15p

Day, C.S.R., Nagase, F., Asai, K. and Takeshima, T., 1993, Ap.J., 408, 656

Deeter, J.E., Boynton, P.E., Shibazaki, N., Hayakawa, S., Nagase, F. and Sato, N., 1987, Astron.J., 93, 877

Deeter, J.E., Boynton, P.E., Miyamoto, S., Kitamoto, S., Nagase, F. and Kawai, N., 1991, Ap.J., 323, 424

de Jager, H.I., de Jager, O.C., North, A.R., Raubenheimer, B.C., van der Walt, D.J. and van Urk, G., 1986, South African J.Phys., 9, 107

de Jager, O.C. and Harding, A.K., 1992, Ap.J., 396, 161

de Jager, O.C., Meintjes, P.J., Brink, C., Nel, H.I., North, A.R., Raubenheimer, B.C., van der Walt, D.J. and Waanders, F.B., 1990, submitted to Astron.Ap. (preprint)

Dickinson, J.E., Ph.D. Thesis, University of Durham (in preparation)

Dowthwaite, J.C., 1987, Ph.D. Thesis, University of Durham

Dowthwaite, J.C., Harrison, A.B., Kirkman, I.W., Macrae, J.H., Orford, K.J., Turver, K.E. and Walmsley, M., 1984a, Nature, 309, 691

Dowthwaite, J.C., Harrison, A.B., Kirkman, I.W., Macrae, J.H., McComb, T.J.L., Orford, K.J., Turver, K.E. and Walmsley, M., 1984b, Ap.J., 286, L35

Eadie, W.T., Drijard, D., James, F.E., Roos, M. and Sadoulet, B., 1971, "Statistical Methods in Experimental Physics" (Amsterdam:North-Holland)

Eadie, G., Peacock, A., Pounds, K.A., Watson, M., Jackson, J.C. and Hunt, R., 1975, MNRAS, 172, 35p

Ebisuzaki, S., Edwards, P.G., Fujii, H., Fujimoto, M., Gregory, A.G., Hara, T., Hayashida, N., Kabe, S., Kakimoto, F., Kifune, T., Kobayakawa, K., Masaike, A., Matsubara, Y., Mizumoto, Y., Muraki, Y., Oda, H., Ogio, S., Ohno, Y., Patterson, J.R., Roberts, M.D., Rowell, G.P., Smith, N.I., Suda, T., Tanimori, T., Teshima, M., Thornton, G.J., Watase, Y. and Wild, N., 1991, Proc.22nd ICRC (Dublin), 2, 611

Eichler, D. and Vestrand, W.T., 1985, Nature, 318, 745

Ellison, D.C. and Eichler, D., Phys.Rev.Lett., 55, 2735

Elsner, R.F., Darbro, W., Leahy, D., Weisskopf, M.C., Sutherland, P.G., Kahn, S.M. and Grindlay, J.E., 1983, Ap.J., 266, 769

Fabbiano, G. and Schreier, E.J., 1977, Ap.J., 214, 235

Fabian, A.C., Pringle, J.E. and Rees, M.J., 1975, MNRAS, 172, 15p

Fazio, G.G., 1970, Nature, 225, 905

Fegan, D.J., 1992, "Towards a Major Atmospheric Cerenkov Detector" (Palaiseau), eds. P. Fleury and G. Vacanti (Gif-sur-Yvette:Editions Frontieres), pp 3-41

Fegan, D.J., McBreen, B., O'Mongain, E., Porter, N.A. and Slevin, P.J., 1968, Canadian J.Phys., 46, S433

Felten, J.E. and Morrison, P., 1963, Phys.Rev.Lett., 10, 453

Fichtel, C.E., Thompson, D.J. and Lamb, R.C., 1987, Ap.J., 319, 682

Finger, M.H., Wilson, R.B., Meegan, C.A., Paciesas, W.S. and Fishman, G.J., 1992, The Compton Observatory Science Workshop (St. Louis), NASA Conf. Publ. 3137, 185

Finger, M.H., Wilson, R.B., Harmon, B.A., Fishman, G.J., Meegan, C.A. and Paciesas, W.S., 1993, in "Compton Gamma Ray Observatory" (St.Louis), AIP Conf.Proc. 280, eds. M. Friedlander, N.Gehrels and D.J. Macomb (New York:AIP Press), pp386-390

Fisher, R.A., 1954, "Statistical Methods for Research Workers" , 12th edition (Edinburgh:Oliver and Boyd)

Forman, W., Jones, C., Tananbaum, H., Gursky, H., Kellogg, E. and Giacconi, R., 1973, Ap.J., 182, L103

Frank, I.M. and Tamm, Ig., 1937, Dokl.Akad.Nauk., 14, 109

Fruin, J.H., Jelley, J.V., Long, C.D., Porter, N.A. and Weekes, T:C., 1964, Phys.Lett., 10, 176

Galbraith, W. and Jelley, J.V., 1953, Nature, 171, 349

Galbraith, W. and Jelley, J.V., 1955, J.Atmos.Terr.Phys., 6, 250, 304

Garmire, G. and Kraushaar, W.L., 1965, Sp. Sci. Rev., 4, 123

Gehrels, N., Chipman, E. and Kniffen, D.A., 1993, in "Compton Gamma Ray Observatory" (St.Louis), AIP Conf.Proc. 280, eds. M. Friedlander, N.Gehrels and D.J. Macomb (New York:AIP Press), pp 3-17

Ghosh, P., and Lamb, F.K., 1978, Ap.J., 223, L83

Ghosh, P., and Lamb, F.K., 1979a, Ap.J., 232, 259

Ghosh, P., and Lamb, F.K., 1979b, Ap.J., 234, 296

Giacconi, R., Gursky, H., Kellogg, E., Schreier, E., Tananbaum, H., 1971, Ap.J., 167, L67

Gilfanov, M., Sunyaev, R., Churazov, E., Loznikov, V., Efremov, V., Kaniovskiy, A., Kuznetsov, A., Yamburenko, N., Melioranskiy, A., Skinner, G.K., Al-Emam, O., Patterson, T.G., Willmore, A.P., Brinkman, A.C., Heise, J., in't Zand, J.J.M., Jager, R., Pietsch, W., Doebereiner, S., Englhauser, J., Reppin, C., Truemper, J., Voges, W., Kendziorra, E., Maisack, M., Mony, B., Staubert, R., Parmar, A.N. and Smith, A., 1989, Proc.23rd ESLAB Symposium on Two Topics in X-ray Astronomy (Bologna), 1, 71

Goldreich, P. and Julian, W.H., 1969, Ap.J., 157, 869

Goret, P., Grenier, I., Petrou, N., Raviart, A., Tabary, A., Tregeur, L. and Vacanti, G., 1991, Proc.21st ICRC, 2, 630

Gorham, P.W. and Learned, 1986, Nature, 323, 422

Gorham, P.W., Cawley, M.F., Fegan, D.J., Gibbs, K.G., Lamb, R.C., Porter, N.A., Stenger, V.J. and Weekes, T.C., 1987, in "Very High Energy Gamma Ray Astronomy", ed. K.E. Turver (Dordrecht:Reidel), pp 125-130

Gregory, A.A., Patterson, J.R., Roberts, M.D., Smith, N.I. and Thornton, G.J., 1990, Astron.Ap., 237, L5

Grindlay, J.E., 1971, Nuovo Cimento, 2B, 119

Grindlay, J.E., Helmken, H.K., Hanbury Brown, R., Davis, J. and Allen, L.R., 1975, Ap.J., 201, 82

Grindlay, J.E., Helmken, H.F. and Weekes, T.C., 1976, Ap.J., 209, 592

Gruber, D.E. and Rothschild, R.E., 1984, Ap.J., 283, 546

Gursky, H. and Schreier, E., 1975, in "Neutron Stars, Black Holes and Binary X-ray Sources", eds. H. Gursky and R. Ruffini (Dordrecht:Reidel), pp 175-180

Haberl, F., 1989, Proc.23rd ESLAB Symposium on Two Topics in X-ray Astronomy (Bologna), 1, 31

Halpern, J.P. and Holt, S.S., 1992, Nature, 357, 222

Hardee, P.E., 1977, Ap.J., 216, 873

Harding, A.K., 1990, Nucl.Phys.B (Proc.Suppl.), 14A, 3

Harding, A.K., Meszaros, P., Kirk, J.G. and Galloway, D.J., 1984, Ap.J., 278, 369

Hartman, R.C., Bertsch, D.L., Fichtel., C.E., Hunter, S.D., Kanbach, G., Kniffen, D.A., Kwok, P.W., Lin, Y.C., Mattox, J.R., Mayer-Hasselwander, H.A., Michelson, P.F., Montigny, C.v., Nel, H.I., Nolan, P.L., Pinkau, K., Rothermel, H., Schneid, E., Sommer, M., Sreekumar, P. and Thompson, D.J., 1992, Ap.J., 385, L1

Hayakawa, S. and Nagase, F., 1982, in "Accreting Neutron Stars", eds. W.Brinkmann and J.Trumper (Garching:MPI), pp 14-20

Henrichs, H.P., 1983, in "Accretion-driven Stellar X-ray Sources", eds. W.H.G. Lewin and E.P.J. van den Heuvel (Cambridge:C.U.P.), pp 393-429

Henry, P. and Schreier, E., 1977, Ap.J., 212, L16

Hertz, P. and Grindlay, J.E., 1983a, Ap.J., 267, 283

Hertz, P. and Grindlay, J.E., 1983b, Ap.J., 275, 105

Hess, V., 1912, Physik. Zeitschr., 13, 1084

Hill, D.A. and Porter, N.A., 1961, Nature, 191, 690

Hillas, A.M., 1984, Nature, 312, 50

Hillas, A.M., 1985, Proc.19th ICRC (La Jolla), 3, 445

Hillas, A.M., 1987, in "Very High Energy Gamma Ray Astronomy" ed. K.E.Turver (Dordrecht:Reidel), pp 71-80

Hillas, A.M. and Johnson, P.A., 1989, Proc.Int.Workshop on VHEGRA (Crimea), pp 96-99

Hillas, A.M. and Johnson, P.A., 1991, Proc.22nd ICRC (Dublin), 2, 452

Hodges, J.L., 1955, Ann.Math.Stats., 26, 523

Howe, S.K., Primini, F.A., Bautz, M.W., Lang, F.L., Levine, A.M. and Lewin, W.H.G., 1983, Ap.J., 272, 678

Illarionov, A.F. and Sunyaev, R.A., 1975, Astron.Ap., 39, 185

Ilovaisky ,S.A., Motch, C. and Chevalier, C, 1978, Astron.Ap., 70, L19

Jelley, J.V., 1967, Progress in Elementary Particle and Cosmic Ray Physics Vol.9, eds. J.G. Wilson and S.A. Woutheysen (Amsterdam:North-Holland), pp 41-159

Jelley, J.V., 1987, in "Very High Energy Gamma Ray Astronomy" ed. K.E.Turver (Dordrecht:Reidel), pp 27-37

Joss, P.C., Avni, Y. and Rappaport, S., 1980, Ap.J., 221, 645

Kanbach, G., Bennett, K., Bignami, G.F., Buccheri, R., Caraveo, P., D'Amico, N., Hermsen, W., Lichti, G.G., Masnou, J.L., Mayer-Hasselwander, H.A., Paul, J.A., Sacco, B., Swanenburg, J.N. and Wills, R.D., 1980, Astron.Ap., 90, 163

Kanbach, G., Bertsch, D.L., Favale, A., Fichtel., C.E., Hartman, R.C., Hofstadter, R., Hughes, E.B., Hunter, S.D., Hughlock, B.W., Kniffen, D.A., Lin, Y.C., Mattox, J.R., Mayer-Hasselwander, H.A., Montigny, C.v., Nolan, P.L., Pinkau, K., Rothermel, H., Schneid, E.J., Sommer, M., Thompson, D.J. and Walker, A.H., 1990 (preprint)

Katz, J.I. and Smith, I.A., 1988, Ap.J., 326, 733

Kazanas, D. and Ellison, D.C., 1986, Nature, 319, 380

Kelley, R.L., Rappaport, S., Clark, G.W. and Petro, L.D., 1983, Ap.J., 268, 790

King, A.R. and Shaviv, G., 1984, Nature, 308, 519

Kiraly, P. and Meszaros, P., 1988, Ap.J., 333, 719

Kniffen, D.A., Fichtel, C.E., Hartman, R.C., Lamb, R.C. and Thompson, D.J., 1977, Proc.12th ESLAB Symp.(Frascati), pp 47-53

Konapelko, A.K., Plyasheshnikov, A.V. and Shmidt, A.A., 1991, Proc.22nd ICRC (Dublin), 1, 484

Kraushaar, W., Clark, G.W., Garmire, G., Helmken, H., Higbie, P. and Agogino, M., 1965, Ap.J., 141, 845

Kraushaar, W.L., Clark, G.W., Garmire, G., Borken, R., Higbie, P., Leong, C. and Thorsos, T., 1972, Ap.J., 177, 341

Krzeminski, W., 1974, Ap.J.(Lett.), 192, L135

Lamb, F.K., Hamilton, R.J. and Miller, M.C., 1993, in "Isolated Pulsars" (Taos), eds. K.A. van Riper, R. Epstein and C. Ho (Cambridge:C.U.P.), pp 364-371

Lamb, R.C., 1992, in "Towards a Major Atmospheric Cerenkov Detector" (Palaiseau), eds. P. Fleury and G. Vacanti (Gif-sur-Yvette:Editions Frontieres), pp 43-52

Lamb, R.C. and Weekes, T.C., 1986, Ap.J.Lett., 206, L29

Lamb, R.C., Cawley, M.F., Fegan, D.J., Gibbs, K.G., Gregory, A.A., Gorham, P.W., Lewis, D.A., Porter, N.A., Stenger, V.J. and Weekes, T.C., 1987, in "Very High Energy Gamma Ray Astronomy", ed. K.E. Turver (Dordrecht:Reidel), pp 139-142

Lambert, A., Lloyd-Evans, J., Perrett, J.C. and Smith, N.C.T., 1987, in "Very High Energy Gamma Ray Astronomy" ed. K.E.Turver (Dordrecht:Reidel), pp 255-290

Lamers, H.G.J.L.M., van den Heuvel, E.P.J. and Petterson, J.A., 1976, Astron.Ap, 49, 327

Lang, F.L., Levine, A.M., Bautz, M., Hauskins, S., Howe, S., Primini, F.A., Lewin, W.H.G., Baity, F.A., Knight, F.K., Rothschild, R.E. and Petterson, J.A., 1981, Ap.J., 246, L21

Lang, M.J., Akerlof, C.W., Cawley, M.F., Colombo, E., Fegan, D.J., Hillas, A.M., Kwok, P.W., Lamb, R.C., Lawrence, M.A., Lewis, D.A., Macomb, D., Meyer, D.I., O'Flaherty, K.S., Punch, M., Reynolds, P.T., Schubnell, M.S., Vacanti, G., Weekes, T.C., 1991, Proc.21st ICRC (Dublin), 1, 204

Lapshov, I.Yu., Syunyaev, R.A., Chichkov, M.A., Dremin, V.V., Brandt, S. and Lund, N., 1992, Sov.Astron.Lett., 1992, 18, 16

Lasker, B., 1974, Nature, 250, 308

Leahy, D.A., Elaner, R.F. and Weisskopf, M.C., 1983, Ap.J., 272, 256

Leung, P.P., Cheng, K.S. and Fung, P.C.W., 1993, Ap.J., 410, 309

Levine, A., Ma, C.P., McClintock, J., Rappaport, S., van der Klis, M. and Verbunt, F., 1988, Ap.J., 327, 732

Levine, A., Rappaport, S., Deeter, J.E., Boynton, P.E. and Nagase, F., 1993, Ap.J., 410, 328

Lewis, D.A., Cawley, M.F., Fegan, D.J., Hillas, A.M., Kwok, P.W., Lamb, R.C., Reynolds, P.T., Porter, N.A. and Weekes, T.C., 1991, Ap.J., 369, 379

Lewis, W., Rappaport, S., Levine, A. and Nagase, F., 1992, Ap.J., 389, 665

Lewin, W.H.G. and Joss, P.C., 1983, in "Accretion-driven Stellar X-ray Sources", eds. W.H.G. Lewin and E.P.J. van den Heuvel (Cambridge:C.U.P.), pp 41-116

Li, F.K., Joss, P.C., McClintock, J.E., Rappaport, S. and Wright, E.L., 1980, Ap.J., 240, 628

Li, T-P and Wu, M, 1989, Astron.Ap., 346, 391

Liebert, J., 1980, Ann.Rev.Astron.Ap., 18, 363

Lin, Y.C., Bertsch, D.L., Chiang, J., Fichtel., C.E., Hartman, R.C., Hunter, S.D., Kanbach, G., Kniffen, D.A., Kwok, P.W., Mattox, J.R., Mayer-Hasselwander, H.A., Michelson, P.F., Montigny, C.v., Nolan, P.L., Pinkau, K., Schneid, E., Sreekumar, P. and Thompson, D.J., 1992, Ap.J., 401, L61

Longair, M.S., 1992, "High Energy Astrophysics" Vol.1 (Cambridge:C.U.P.), pp 120-122 and 146-151

Loznikov, V.M., Konorkina, E.E. and Melioranskii, A.S., 1992, Sov.Astron.Lett., 18, 233

Lucke, R., Yentis, D., Friedman, H., Fritz, G. and Shulman, S., 1976, Ap.J., 206, L25

Macrae, J.H.K., 1985, Ph.D. Thesis, University of Durham

Mannings, V.G., 1990, Ph.D.Thesis, University of Durham

Mannings, V., 1992, Astron.Ap., 258, 335

Mardia, K.V., 1972, "Statistics of Directional Data" (London:Acad.Press)

Mastichiadis, A., 1986, Astron.Ap., 169, 373

Matsuda, T., Inoue, M. and Sawada, K., 1987, MNRAS, 226, 785

Mattox, J.R., Bertsch, D.L., Fichtel, C.E., Hartman, R.C., Kniffen, D.A. and Thompson, D.J., 1992, Ap.J., 401, L23

McClintock, J.E., Rappaport, S., Joss, P.C., Bradt, H., Buff, J., Clark, G.W., Hearn, D., Lewin, W.H.G., Matilsky, T., Mayer, W. and Primini, F., 1976, Ap.J., 206, L99

McClintock, J.E., Canizares, C.R., Bradt, H.V., Doxsey, R.E., Jernigan, J.G. and Hiltner, W.A., 1977, Nature, 270, 320

McClintock, J.E., Canizares, C.R., Li, F.K. and Grindlay, J.E., 1980, Ap.J., 235, L81

Meegan, C.A., Fishman, G.J., Wilson, R.B., Paciesas, W.S., Brock, M.W., Horack, J.M., Pendleton, G.N. and Kouvelioutou, C., 1992, IAU Circular 5478

Meintjes, P.J., de Jager, O.C., Raubenheimer, B.C., Brink, C., Nel, H.I., North, A.R. and Visser, B., 1993, Proc.23rd ICRC (Calgary), 1, 338

Meszaros, P. and Bonazzola, S., 1981, Ap.J., 251, 695

Michelson, P.F., Bertsch, D.L., Chiang, J., Fichtel, C.E., Hartman, R.C., Hunter, S.D., Kanbach, G., Kniffen, D.A., Kwok, P.W., Lin, Y.C., Mattox, J.R., Mayer-Hasselwander, H.A., Nolan, P.L., Pinkau, K., Rothermel, H., Schneid, E., Sommer, M., Sreekumar, P., Thompson, D.J. and von Montigny, C., 1992, IAU Circ. 5470

Middleditch, J., Mason, K.O., Nelson, J.E. and White, N.E., 1981, Ap.J., 244, 1001

Molteni, D., Rapisarda, M., Re, S. and Robba, N.R., 1982, Astron.Ap., 111, 365

Morrison, P., 1958, Nuovo Cimento, 7, 858

Moskalenko, I.V. and Karakula, S., 1993, Proc.23rd ICRC (Calgary), 2, 459

Murukami, T., Inoue, H., Kawai., N., Koyama., K., Makishima, K., Matsuoka, M., Oda, M., Ogawara, Y., Ohashi, T., Shibazaki, N., Tanaka, Y., Hayakawa, S., Kunieda, H., Makino, F., Masai, K., Nagase, F., Taware, Y., Miyamoto, S., Tsunemi, H., Yamashita, K. and Kondo, I., 1983, Ap.J., 264, 563

Nagase, F., 1989, P.A.S.J., 41, 1

Nagase, F., Hayakawa, S., Kunieda, H., Makino, F., Masai, K., Tawara, Y., Inoue, H., Koyama, K., Makishima, K., Matsuoka, M., Murukami, T., Oda, M., Ogawara, Y., Ohashi, T., Shibazaki, N., Tanaka, Y., Kondo, I., Miyamoto, S., Tsunemi, H. and Yamashita, K., 1981, Nature, 290, 572

Nagase, F., Hayakawa, S., Kunieda, H., Masai, K., Sato, N., Tawara, Y., Inoue, H., Koyama, K., Makino, F., Makishima, K., Matsuoka, M., Murukami, T., Oda, M., Ogawara, Y., Ohashi, T., Shibazaki, N., Tanaka, Y., Miyamoto, S., Tsunemi, H., Yamashita, K. and Kondo, I., 1984a, Ap.J., 280, 259

Nagase, F., Hayakawa, S., Kii, T., Sato, N., Ikegami, T., Kawai, N., Makishima, K., Matsuoka, M., Mitani, K., Murakami, T., Oda, M., Ohasi, T., Tanaki, Y and Kitamoto, S., 1984b, P.A.S.J., 36, 667

Nagase, F., Corbet, R.F.D., Day, C.S.R., Inoue, H., Takeshima, T. and Yoshida, K., 1992, Ap.J., 396, 147

Neshpor, Yu.I. and Zyskin, Yu.L., 1986, Bull.Crimean Ap.Obs., pp 122-125

North, A.R., Raubenheimer, B.C., de Jager, O.C., van Tonder, A.J. and van Urk, G., 1987, Nature, 326, 567

North, A.R., Brink, C., Cheng, K.S., de Jager, O.C., Nel, H.I. and Raubenheimer, B.C., 1990, Proc.21st ICRC (Adelaide), 2, 275

North, A.R., Raubenheimer, B.C., Brink, C., de Jager, O.C., Meintjes, P.J., Nel, H.I., van Urk, G. and Visser, B., 1991a, Proc.22nd ICRC (Dublin), 2, 340

North, A.R., Raubenheimer, B.C., Brink, C., de Jager, O.C., Meintjes, P.J., Nel, H.I., van Urk, G. and Visser, B., 1991b, Proc. 22nd ICRC (Dublin), 1, 328

Novokov, I.D. and Thorne, K.S., 1972, in "Black Holes" eds. C. de Witt and B. de Witt, (New York:Gordon and Breach), p.343

Ogelman, H., 1989, in "Timing Neutron Stars", eds. H. Ogelman and E.P.J. van den Heuvel (Dordrecht:Kluwer), pp 169-190

Ogelman, H., Beuermann, K.P., Kanbach, G., Mayer- Hasselwander, H.A., Capozzi, D., Fiordilino, E. and Molteni, D., 1977, Astron.Ap., 58, 385

Orford, K.J. and Turver, K.E., 1976, 264, 722

Paczynski, B., 1971, Ann.Rev.Astron.Ap., 9, 183

Paresce, F., de Marchi, G. and Ferraro, F.R., 1992, Nature, 360, 46

Petterson, J.A., 1978, Ap.J., 224, 625

Petterson, J.A., 1983, in "Accretion-driven Stellar X-ray Sources", eds. W.H.G. Lewin and E.P.J. van den Heuvel (Cambridge:C.U.P.), pp 367-391

Plyasheshnikov, A.V. and Bignami, G.F., 1985, Nuovo Cimento, 8C, 39

Porter, N.A., 1973, Nuovo Cimento Lett., 8, 481

Porter, N.A. and Weekes, T.C., 1978, Smithsonian Astrophysical Observatory Special Report 381

Pounds, K.A., Cooke, B.A., Ricketts, M.J., Turner, M.J. and Elvis, M., 1975, MNRAS, 172, 473

Pravdo S.H., White, N.E., Boldt, E.A., Holt, S.S., Serlemitsos, P.J., Swank, J.H., Szymkowiak, A.E., Tuohy, I. and Garmire, G., 1979, Ap.J., 231, 912

Price, R.E., Groves, D.J., Rodrigues, R.M., Seward, F., Swift, C.D. and Toor, A., 1971, Ap.J., 168, L7

Primini, Rappaport, S. and Joss, P.C., 1977, Ap.J., 217, 543

Pringle, J.E., 1976, MNRAS, 177,65

Pringle, J.E. and Rees, M.J., 1972, Astron.Ap., 21,1

Pringle, J.E. and Wade, R.A., 1985, "Interacting Binary Stars" (Cambridge:C.U.P)

Protheroe, R.J., 1987, Proc.20th ICRC (Moscow), 8, 21

Protheroe, R.J. and Clay, R.W., 1985, Nature, 315, 205

Protheroe, R.J., Clay, R.W. and Gerhardy, P.R., 1984, 280, L47

Protheroe, R.J. and Stanev, T., 1987, Nature, 328, 136

Punch, M., Akerlof., C.W., Cawley, M.F., Fegan, D.J., Lamb, R.C., Lawrence, M.A., Lang, M.J., Lewis, D.A., Meyer, D.I., O'Flaherty, K.S., Reynolds, P.T. and Schubnell, M.S., 1991, Proc.22nd ICRC (Dublin), 1, 465

Punch, M., Akerlof., C.W., Cawley, M.F., Chantell, M., Fegan, D.J., Fennell, S., Gaidos, J.A., Hagan, J., Hillas, A.M., Jiang, Y., Kerrick, A.D., Lamb, R.C., Lawrence, M.A., Lewis, D.A., Meyer, D.I., Mohanty, G., O'Flaherty, K.S., Reynolds, P.T., Rovero, A.C., Schubnell, M.S., Sembroski, G., Weekes, T.C., Whitaker, T. and Wilson, C., 1992, Nature, 358, 477

Ramana Murthy, P.V. and Wolfendale, A.W., 1986, "Gamma Ray Astronomy" (Cambridge:C.U.P.)

Rappaport, S. and Joss, P.C., 1977, Nature, 266, 683

Rappaport, S.A. and Joss, P.C., 1983, in "Accretion-driven Stellar X-ray Sources", eds. W.H.G. Lewin and E.P.J. van den Heuvel (Cambridge:C.U.P.), pp 1-40

Rappaport ,S., Markert, T., Li., F.K., Clark, G.W., Jernigan, J.G. and McClintock, J.E., 1977, Ap.J., 217, L29

Rappaport, S., Clark, G.W., Cominsky, L., Joss, P.C. and Li, F., 1978, Ap.J., 224, L1

Raubenheimer, B.C., 1990, Astron.Ap., 234, 172

Raubenheimer, B.C., North, A.R., de Jager, O.C. and Nel, H.I., 1989, Ap.J., 336, 394

Raubenheimer, B.C. and Ogelman, H., 1990, Astron.Ap., 230, 73

Resvanis, L.K., Learned, J.G., Stenger, V., Weeks, D., Gaidos,J., Loeffler, F., Olson, J., Palfrey, T., Sembroski, G., Wilson, C., Camerini, U., Finley, J., Fry, W., Jaworski, M., Jennings, J., Kenter, A., Koepsel, R., Lomperski, M., Loveless, R., March, R., Matthews, J., Morse, R., Reeder, D., Sandler, P., Slane, P. and Szentgyorgyi, A., 1987,in "Very High Energy Gamma Ray Astronomy", ed. K.E. Turver (Dordrecht:Reidel), pp 135-138

Rieke, G.H., 1969, Proc.11th ICRC (Budapest), 3, 601

Riffert, H. and Meszaros, P., 1988, Ap.J., 325, 207

Roberts, M.D., Thornton, G.J., Edwards, P.G., Patterson, J.R. and Rowell, G.P., 1993, Proc.23rd ICRC (Calgary), 1, 322
Rossi, B. and Greisen, K., 1941, Rev.Mod.Phys., 13, 240

Savonije, G.J., 1983, in "Accretion-driven Stellar X-ray Sources", eds. W.H.G. Lewin and E.P.J. van den Heuvel (Cambridge:C.U.P.), pp 344-366

Schonfelder, V., 1989, in "Cosmic Gamma Rays, Neutrinos and Related Astrophysics" eds. M.M. Shapiro and J.P. Wefel (Dordrecht:Kluwer), pp 401-422

Schreier, E., Giacconi, R., Gursky, H., Kellogg, E. and Tananbaum, H., 1972a, Ap.J., 172, L71

Schreier, E., Levinson, R., Gursky, H., Kellogg, E., Tananbaum, H. and Giacconi, R., 1972b, Ap.J., 178, L79

Schreier, E.J., Swartz, K., Giacconi, R., Fabbiano, G. and Morin, J., 1976, Ap.J., 204, 539

Sitte, K., 1962, Nuovo Cimento, 24, 86

Shinoda ,K., Kii, T., Mitsuda, K., Nagase, F. and Tanaka, Y., 1990, PASJ, 42, L27

Shklovskii, I., 1967, Sov.Astron., 11, 749

Sparks, W.M., 1975, Ap.J., 199, 462

Standish, E.M., 1982, Astron.Ap., 114, 297

Staubert, R., Kendziorra, E., Pietsch, W., Reppin, C., Trumper, J. and Voges, W., 1980, Ap.J., 239,1010

Stecker, F.W., de Jager, O.C. and Salamon, M.H., 1992, Ap.J., 390, L49

Stenger, V.J., 1984, Ap.J., 284, 810

Stepanian, A.A., Vladimirsky, B.M. and Fomin, V.P., 1972, Nature Phys.Sci., 239, 40

Stepanian, A.A., Vladimirsky, B.M., Neshpor, Yu.I. and Fomin, V.P., 1975, Ap.Sp.Sci., 38, 267

Sturrock, P.A., 1971, Ap.J., 164, 529

Takeshima, 1987, private communication

Tanaka, Y., 1984, Adv.Sp.Res., 3, 509

Thompson, D.J., Fichtel, C.E., Hartman, R.C., Kniffen, D.A. and Lamb, R.C., 1977, Ap.J., 213, 252

Thompson, D.J., Arzoumanian, Z., Bertsch, D.L., Brazier, K.T.S., D'Amico, N., Fichtel, C.E., Fierro, J.M., Hartman, R.C., Hunter, S.D., Johnston, S., Kanbach, G., Kaspi, V.M., Kniffen, D.A., Lin, Y.C., Lyne, A.G., Manchester, R.N., Mattox, J.R., Mayer-Hasselwander, H.A., Michelson, P.F., Montigny, C.v., Nel, H.I., Nice, D., Nolan, P.L., Pinkau, K., Rothermel, H., Schneid, G.J., Sommer, M., Sreekumar, P. and Taylor, J.H., 1992, Nature, 359, 615

Thornton, G.J., Edwards, P.G., Gregory, A.G., Patterson, J.R., Roberts, M.D., Rowell, G.P. and Smith, N.I., 1991, Proc.22nd ICRC (Dublin), 2, 336

Tumer, O.T., Hammond, J.S., White, R.S. and Zych, A.D., 1990, Proc.21st ICRC (Adelaide), 2, 155

Tuohy, I.R., 1976, MNRAS, 174, 45p

Tuohy, I.R. and Rapley, C.G., 1975, Ap.J., 198. L69

Turver, K.E. and Weekes, T.C., 1978, Nuovo Cimento, 45B, 99

Ulmer, M.P., 1976, Ap.J., 204, 548

Ulmer, M.P., Baity, W.A., Wheaton, W.A. and Peterson, L.E., 1972, Ap.J., 178, L121

Usov, V.V., 1983, Nature, 305, 409

Vacanti, G., Cawley, M.F., Fegan, D.J., Gibbs, K.G., Hillas, A.M., Kwok, P., Lamb, R.C., Lewis, D.A., Macomb, D., Porter, N.A., Reynolds, P.T. and Weekes, T.C., 1991, Ap.J., 377, 467

van der Klis, M. and Bonnet-Bidaud, J.M., 1984, Astron.Ap., 135, 155

van Paradijs, J., 1989, in "Timing Neutron Stars", eds. H. Ogelman and E.P.J. van den Heuvel (Dordrecht:Kluwer), pp 191-208

van Paradijs, J. and Zuiderwijk, E., 1977, Astron.Ap., 61, L19

van Paradijs, J., Zuiderwijk, E.J., Takens, R.J., Hammerschlag- Hensberge, G., van den Heuvel, E.P.J. and de Loore, C., 1977, Astron.Ap.(Suppl.Ser.), 30, 195

van der Klis, M., Bonnet-Bidaud J.M. and Robba, N.R., 1980, Astron.Ap., 88, 8

Verbunt, F., van Paradijs, J. and Elson, R., 1984, MNRAS, 210, 899

Vidal, N.V., Wickramasinghe, D.T. and Peterson, B.A., 1973, Ap.J., 182, L77

Vladimirsky, B.M, Stepanian, A.A. and Fomin, V.P., 1973, Proc. 13th ICRC (Denver), 1, 456

Wang, Y.-M., 1986, Ap.Sp.Sci., 121, 193

Wang, Y.-M., 1987, Astron. Ap., 183, 257

Wang, Y.-M. and Frank, J., 1981, Astron.Ap., 93, 255

Webster, B.L., Martin, W.L., Feast, M.W. and Andrews, P.J., 1972, Nature Phys.Sci., 240, 183

Weekes, T.C., 1985, in Proc.New Particles 85 (Madison), eds. V. Barger, D. Cline and F. Halzen, (Singapore:World Scientific), 338

Weekes, T.C., 1988, Physics Reports, 160(1 and 2), pp 1-121

Weekes, T.C., 1992, Sp.Sci.Rev., 59, 315

Weekes, T.C., 1993, paper presented at "Towards a Major Atmospheric Cerenkov Detector II" (Calgary workshop)

Weekes, T.C. and Turver, K.E., 1977, Proc.12th ESLAB Symposium (Frascati), pp 279-285

Weekes, T.C., Cawley, M.F., Fegan, D.J., Gibbs, K.G., Hillas, A.M., Kwok, P.W., Lamb, R.C., Lewis, D.A., Macomb, D., Porter, N.A., Reynolds, P.T. and Vacanti, G., 1989, Ap.J., 342, 379

White, N.E., Swank, J.H, and Holt, S.S., 1983, Ap.J., 270, 711

Wilson, R.B., Finger, M.H., Pendleton, G.N., Fishman G.J., Meegan, C.A. and Paciesas, W.S., 1993a, in "Isolated Pulsars" (Taos), eds. K.A. van Riper, R. Epstein and C. Ho (Cambridge:C.U.P.), pp 257-263

Wilson, R.B., Fishman, G.J., Finger, M.H., Pendleton, G.N., Prince, T.A. and Chakrabarty, D., 1993b, in "Compton Gamma Ray Observatory" (St.Louis), AIP Conf.Proc. 280, eds. M. Friedlander, N.Gehrels and D.J. Macomb (New York:AIP Press), pp 291-302

Yodh, G.B., 1992, "High Energy Neutrino Astrophysics" (Hawaii workshop), (preprint)

Zatsepin, V.I. and Chudakov, A.E., 1962, Sov.Phys.JETP, 15, 1126

Zhang, F.J. and Baath, L.B., 1990, Astron.Ap., 236, 47

UNIV DUNELM